

Diastereomeric Piperidinium Salts: Their Preparation, Study, and Use in Synthesis

by

Christine Rachel Dunbar

A thesis submitted in partial fulfillment of the requirements for the degree of

Doctor of Philosophy

Department of Chemistry

University of Alberta

© Christine Rachel Dunbar, 2015

Abstract

Diastereomeric piperidinium salts were prepared as substrates for the Stevens [1,2]-rearrangement of ammonium ylides, the key step in a proposed synthetic route towards lysergic acid, a valuable compound in medicinal and synthetic chemistry. Because of unexpected reactivity seen in the alkylation of substituted piperidine derivatives to form the piperidinium salts, an analysis of the previous literature in this field was undertaken; literature experimental data was subjected to computational analysis to more fully understand the complexities of this reaction, as well as to find and demonstrate the utility of a suitable computational approach to this reaction. In addition to analyzing previously-reported data, new alkylation experiments were undertaken to broaden the known substrate scope of this reaction and to provide more recent data for computational analysis. This computational analysis was also applied to the formation of piperidinium salts in the original route towards lysergic acid, showing its applicability to known problems in synthesis. During the course of this computational research, many interesting mechanistic questions arose in other projects in the group; computational mechanistic work was undertaken in the context of an unusual interrupted Nazarov reaction, as well as in the nascent field of the reactivity of six-membered cyclic allenes.

Preface

Chapter 3 of this thesis has been published as C. R. Dunbar and F. G. West, “Diastereoselective N-Quaternization of Piperidines,” *Canadian Journal of Chemistry*, **2014**, *Accepted*. I was responsible for the computational work and the manuscript composition. F. G. West was the supervisory author and was involved with concept formation and manuscript composition.

Part of Chapter 4 of this thesis will soon be published as C. R. Dunbar, L. J. Miedema, and F. G. West, “Diastereoselectivity in the *N*-Alkylation of 3-Hydroxy-*N*-alkylpiperidines,” *Organic Letters*, **2014**, *Manuscript in preparation*. I was responsible for the computational work, some experimental work and characterization of compounds, and the manuscript composition. L. J. Miedema performed most of the experimental work. F. G. West was the supervisory author and was involved with concept formation and manuscript composition.

Part of Chapter 5 of this thesis has been published as Y.-K. Wu, C. R. Dunbar, R. MacDonald, M. J. Ferguson, and F. G. West, “Experimental and Computational Studies on the Interrupted Nazarov Reactions: Exploration of Umpolung Reactivity at the α -Carbon of Cyclopentanones,” *Journal of the American Chemical Society*, **2014**, *136*, 14903-14911. Y.-K. Wu was responsible for the experimental work, characterization of compounds, and most of the manuscript composition. I was responsible for the computational work and some of the manuscript composition. R. MacDonald provided X-ray data for compounds **13**, **14a**, and **18**. M. J. Ferguson provided X-ray data for compounds **6a** and **16c** (numbering from paper). F. G. West was the supervisory author and was involved with concept formation and manuscript composition.

The experimental work in Chapter 6 of this thesis was performed by V. A. Lofstrand; it is included here with his permission.

Dedication

For my mother, who always believed I could do anything.

Acknowledgements

I would like to thank my supervisor, Frederick G. West, for supporting me through the strange path this project took. I would like to thank my supervisory committee – Jeffrey Stryker, Julianne Gibbs-Davis, Todd Lowary, and Jack Tuszynski – for good discussions and interesting ideas; in particular, Julianne Gibbs-Davis planted the idea of computational research in my mind. Other University of Alberta professors I would like to acknowledge are Mariusz Klobukowski and Alex Brown for computational chemistry advice. I would like to thank the entire West group, past and present members, for support, encouragement, ideas, and fun times. I would like to single out Verner Lofstrand as one of my best friends and a great collaborator, Yonghoon Kwon for always making me laugh, and Yen-Ku Wu for being the first of my colleagues to trust his experimental work to my computational abilities. I would like to thank Hayley Wan for encouraging my teaching and computational chemistry aspirations and Nada Djokic for being my counselor, both in teaching and life in general. I would like to thank Katie Nizio and Jeffrey Bunquin for being loyal friends and supporters. I would like to thank Cassandra Churchill for some good computational discussions. Although there are too many to mention individually, there were many more colleagues in the University of Alberta Department of Chemistry who added positivity and laughter to my time here. I would like to thank my undergraduate supervisors – Marco Ciufolini, Glenn Sammis, and Laurel Schafer – for encouraging me to pursue graduate research and providing me with the research experience and knowledge to get a head start in the PhD program. I would finally like to thank my family, especially my mom, dad, and brother, as well as my cats, Mew Mew and Ceres, and, last but not least, my husband, Michael Deo, for being my best friend, teammate, and favourite person in the world.

Table of Contents

Abstract.....	ii
Preface.....	iii
Dedication.....	v
Acknowledgements.....	vi
List of Tables.....	xii
List of Figures.....	xv
List of Schemes.....	xxiii
List of Symbols and Abbreviations.....	xxvii
Chapter 1: Introduction.....	1
Section 1.1: Overview.....	1
Section 1.2: Structural Features and Properties of Lysergic Acid and its Derivatives.....	2
Section 1.3: Previous Syntheses of Lysergic Acid.....	3
Section 1.4: The Stevens [1,2]-Rearrangement and its Use in Synthesis.....	16
Section 1.5: Two Proposed Synthetic Routes to Lysergic Acid Using the Stevens [1,2]-Rearrangement of Ammonium Ylides.....	21
Chapter 2: Towards the Synthesis of Lysergic Acid.....	24
Section 2.1: Introduction.....	24
Section 2.2: Choosing an Intermediate in the Synthesis of Piperidine Derivative 75	24
Section 2.2.1: Synthesis of Enone 86	25
Section 2.2.2: Synthesis of Encarbamate 87	28
Section 2.2.3: Synthesis of Acyclic Imine 88	29
Section 2.3: Synthesis of Piperidine 75 from Enone 86	30

Section 2.4: Alternate Route to Obtain Piperidine Derivative 147	37
Section 2.5: Summary and Future Plans	39
Section 2.6: Experimental.....	40
Section 2.6.1: General Methods.....	40
Section 2.6.2: Experimental Procedures	42
Chapter 3: Diastereoselective Alkylation of <i>N</i> -Substituted Piperidines	70
Section 3.1: Introduction.....	70
Section 3.2: Literature Review and Analysis.....	71
Section 3.2.1: Methylation of <i>N</i> -Alkylpiperidine Derivatives.....	73
Section 3.2.2: Ethylation of <i>N</i> -Alkylpiperidine Derivatives.....	75
Section 3.2.3: Benzylation of <i>N</i> -Alkylpiperidine Derivatives	75
Section 3.2.4: Other Alkylating Agents in the Quaternization of <i>N</i> -Alkylpiperidine Derivatives	76
Section 3.2.5: Alkylation of Conformationally Mobile Piperidine Systems	77
Section 3.2.6: Explanations Offered For Trends in <i>N</i> -Alkylation	79
Section 3.3: Case Studies.....	80
Section 3.3.1: Computational Details	80
Section 3.3.2: House, 1972 – Methylation of 4- <i>tert</i> -butyl-1-ethylpiperidine.....	81
Section 3.3.3: Katritzky, 1973 – Benzylation of 1-methyl-4-phenylpiperidine	85
Section 3.3.4: Smith, 1973 – Reaction of 1,2-, 1,3-, and 1,4-dimethylpiperidine with 2- chloro-1-phenylethanone	90
Section 3.4: Summary and Future Plans	99
Chapter 4: New <i>N</i> -Alkylation Experiments and their Computational Analysis.....	102

Section 4.1: Introduction.....	102
Section 4.2: Design and Execution of New <i>N</i> -Alkylation Experiments.....	102
Section 4.3: Diastereomer Assignment Using Simulated NMR Chemical Shifts	106
Section 4.3.1: Computational Details	106
Section 4.3.2: Hydroxyl-substituted Piperidinium Salt 164	107
Section 4.3.3: <i>tert</i> -Butyldiphenylsiloxy-substituted Piperidinium Salt 167	109
Section 4.4: Computational Analysis of New Alkylation Experiments	111
Section 4.4.1: Computational Details	112
Section 4.4.2: Alkylation Reactions to form Piperidinium Salt 164	113
Section 4.4.3: Alkylation Reactions to form Piperidinium Salt 167	117
Section 4.5: Further Study of the Alkylation of Lysergic Acid Synthesis Intermediate 147 .	121
Section 4.5.1: New Alkylation Experiments on Piperidine 147	121
Section 4.5.2: Assignment of Diastereomeric Piperidinium Salts 148-D1 and 148-D2	122
Section 4.5.3: Computational Analysis of the Alkylation of Piperidine 147	124
Section 4.6: Summary and Future Plans	126
Section 4.6: Experimental.....	129
Section 4.6.1: General Methods.....	129
Section 4.6.2: Experimental Procedures	130
Chapter 5: The Computational Mechanistic Study of an Interrupted Nazarov Reaction	139
Section 5.1: The Nazarov and Interrupted Nazarov Reactions.....	139
Section 5.2: Experimental Findings in the Interrupted Nazarov Reaction with Furan	140
Section 5.3: Computational Findings in the Interrupted Nazarov Reaction with Furan.....	143
Section 5.3.1: Computational Details	143

Section 5.3.2: Regarding the Stereochemistry of 181	144
Section 5.3.3: Regarding the Formation of 181 versus 182	147
Section 5.4: Summary and Future Plans.....	167
Chapter 6: Computational Mechanistic Studies of Cycloadditions between 1,2-Cyclohexadiene and Various Dipolar Compounds.....	169
Section 6.1: Introduction.....	169
Section 6.2: Computational Study of 1,2-Cyclohexadiene Dimerization.....	170
Section 6.2.1: Computational Details.....	171
Section 6.2.2: Computational Results.....	172
Section 6.3: Reactions of Cycloallenes with Nitrile Oxides.....	174
Section 6.3.1: Computational Details.....	175
Section 6.3.2: Computational Results.....	176
Section 6.4: Reactions of Cycloallenes with Azomethine Imines.....	179
Section 6.4.1: Computational Details.....	180
Section 6.4.2: Computational Results.....	181
Section 6.5: Reactions of Cycloallenes with Nitrones.....	186
Section 6.5.1: Computational Details.....	186
Section 6.5.2: Computational Results.....	187
Section 6.6: Identification of an Unusual Cycloallene Cycloaddition Product via Simulated ¹ H NMR Chemical Shifts.....	191
Section 6.6.1: Computational Details.....	192
Section 6.6.2: Computational Results.....	192
Section 6.7: Summary and Future Plans.....	194

References..... 197

List of Tables

Table 1. Literature examples of diastereoselective <i>N</i> -methylation of <i>N</i> -alkylpiperidines.....	74
Table 2. Literature examples of diastereoselective <i>N</i> -ethylation of <i>N</i> -alkylpiperidine derivatives	75
Table 3. Literature examples of diastereoselective <i>N</i> -benzylation of <i>N</i> -alkylpiperidine derivatives.....	76
Table 4. Literature examples of diastereoselective <i>N</i> -alkylation of <i>N</i> -alkylpiperidine derivatives	77
Table 5. Literature examples of diastereoselective <i>N</i> -alkylation of <i>N</i> -alkylpiperidine systems capable of ring inversion.....	78
Table 6. Transition state energies and the corresponding product ratios for each methylation reaction of 4- <i>tert</i> -butyl-1-ethylpiperidine 150 to form diastereomeric salts 151-D1 and 151-D2	84
Table 7. Relative transition state Gibbs free energies (kcal/mol) and the corresponding product ratios (%) for each benzylation reaction; “152” refers to the reaction of 1-methyl-4- phenylpiperidine 152 , “D1” refers to the formation of axial alkylation product 153-D1 , 154-D1 , or 155-D1 , “ax1” refers to the first axial alkylation transition state, “O” refers to the use of <i>p</i> - methoxybenzyl chloride as the alkylating agent.	88
Table 8. Relative transition state Gibbs free energies (kcal/mol) and the corresponding product ratios (%) for the alkylation of 1,2-dimethylpiperidine 156 . Note that only transition states within 3 kcal/mol from the lowest energy transition state are included.	96

Table 9. Relative transition state Gibbs free energies (kcal/mol) and the corresponding product ratios (%) for the alkylation of 1,3-dimethylpiperidine 158 . Note that only transition states within 3 kcal/mol from the lowest energy transition state are included.	97
Table 10. Relative transition state Gibbs free energies (kcal/mol) and the corresponding product ratios (%) for the alkylation of 1,4-dimethylpiperidine 160 . Note that most transition states above 3 kcal/mol from the lowest energy transition state are excluded with some exceptions.	98
Table 11. Benzylation of <i>N</i> -methylpiperidines 162 and 165 . Reactions were performed at room temperature, and the diastereomeric ratio was determined via integration of the appropriate ¹ H NMR signals (see text for further information).	104
Table 12. Methylation of <i>N</i> -benzylpiperidine derivatives 163 and 166 . Reactions were performed at room temperature, and the diastereomeric ratio was determined via integration of the appropriate ¹ H NMR signals (see text for further information).	104
Table 13. Experimental and calculated product ratios in the reaction of 3-hydroxy-1-methylpiperidine 162 with benzyl chloride in DCM.	114
Table 14. Experimental and calculated product ratios in the reaction of 1-benzyl-3-hydroxypiperidine 163 with methyl iodide in DCM.	115
Table 15. Calculated product ratios in the reaction of 1-methyl-3-(trimethylsiloxy)piperidine 168 with benzyl chloride in DCM compared with the experimental ratio for the benzylation of 3-(<i>tert</i> -butyldiphenylsiloxy)-1-methylpiperidine 165	118
Table 16. Calculated product ratios in the reaction of 1-benzyl-3-(trimethylsiloxy)piperidine 169 with methyl iodide in DCM compared with the experimental ratio for the methylation of 1-benzyl-3-(<i>tert</i> -butyldiphenylsiloxy)piperidine 166	119
Table 17. Benzylation of <i>N</i> -methylpiperidine derivative 147	121

Table 18. Calculated product ratios in the reaction of piperidine 172 with benzyl bromide in DCM compared with the experimental ratio for the benzylation of piperidine 147 . Only transition states within 3 kcal/mol of the lowest energy transitions state are included.	125
Table 19. Relative ΔG s (kcal/mol) of singlet intermediates and transition states in the cycloaddition of cycloallene 187a and azomethine imine 192 at the B3LYP/6-31+G(d)/PCM(MeCN) level. “Path 1” refers to the reaction pathway that forms (an intermediate on the way to) the “ <i>endo</i> ” product (where the hydrogens on the two stereocentres are <i>cis</i> to one another), and “Path 2” refers to the eventual formation of the “ <i>exo</i> ” product.....	185
Table 20. Comparison of the experimental ^1H NMR chemical shifts for 199 and the computed chemical shifts for diastereomers D1-D4	193

List of Figures

Figure 1. Lysergic acid and derivatives. Changes to the lysergic acid skeleton are shown in blue.	2
Figure 2. Ammonium ylides in Ghigo's study of the Stevens [1,2]-rearrangement mechanism.	19
Figure 3. The first boundary condition of the Curtin-Hammett Principle illustrated by piperidine protonation.	72
Figure 4. The second boundary condition of the Curtin-Hammett Principle illustrated by piperidine alkylation.	72
Figure 5. Transition structures in the reaction of 4- <i>tert</i> -butyl-1-ethylpiperidine 150 with methyl chloride; “TS” refers to transition structure, “150” refers to the reaction of 150 , “D1” refers to formation of the axial alkylation product 151-D1 vs. “2” forming the equatorial alkylation product D2 , “ax” refers to axial alkylation vs. “eq” as equatorial alkylation, and “Cl” refers to the methylating agent used.	83
Figure 6. Transition structures in the reaction of 1-methyl-4-phenylpiperidine 152 with benzyl chloride to form diastereomeric salts 154-D1 and 154-D2	87
Figure 7. The lowest energy transition structures for the benzylation of 1-methyl-4-phenylpiperidine 152 with each alkylating agent.	89
Figure 8. IRC plots of forming N-C bond distance (Å) versus ΔG (kcal/mol) for the benzylation of 1-methyl-4-phenylpiperidine 152 via transition states TS152-D1-ax2	90
Figure 9. The main conformers of 1,2-, 1,3-, and 1,4-dimethylpiperidine with 3D structures and relative Gibbs free energies in kcal/mol calculated at B3LYP/6-31+G(d)/PCM(MeCN). Note that the 3D structures of 156-3 , 156-4 , 158-3 , and 158-4 are the enantiomers of the line drawing shown.	92

Figure 10. Transition states in the alkylation of 1,3-dimethylpiperidine conformer 158-4 . Gibbs free energies in kcal/mol at B3LYP/6-31+G(d)/PCM(MeCN) relative to the lowest energy transition state in this system (TS158-D2-eq3) are given in parentheses.	93
Figure 11. Transition states in the alkylation of 1,4-dimethylpiperidine conformer 160-1 . Gibbs free energies in kcal/mol at B3LYP/6-31+G(d)/PCM(MeCN) relative to the lowest energy transition state in this system (TS160-D2-eq1) are given in parentheses.	93
Figure 12. The lowest energy transition structures in the alkylation of 1,2-, 1,3-, and 1,4-dimethylpiperidine.	95
Figure 13. Identifying ¹ H NMR chemical shifts of 164-D1 and 164-D2 . Structures optimized at B3LYP/6-31+G(d,p), NMR calculations at mPW1PW91/6-311+G(2d,p)/SMD(CHCl ₃). Calculated chemical shifts reflect a weighted average of contributions of all conformers with a >1% contribution to the population, though only the lowest energy conformer of each diastereomer is shown. Experimental chemical shifts are reported in CDCl ₃	108
Figure 14. Hydrogen bonding of the alcohol oxygen with a proton on the axial methyl or benzyl group of diastereomeric piperidinium salts 164	109
Figure 15. Identifying ¹ H NMR chemical shifts of 170-D1 and 170-D2 . Structures optimized at B3LYP/6-31+G(d,p), NMR calculations at mPW1PW91/6-311+G(2d,p)/SMD(CHCl ₃). Calculated chemical shifts reflect a weighted average of contributions of all conformers with a >1% contribution to the population, though only the lowest energy conformer of each diastereomer is shown. Experimental chemical shifts are reported in CDCl ₃	111
Figure 16. Lowest energy transition states in the reaction of 3-hydroxy-1-methylpiperidine 162 with benzyl chloride in DCM. Structures optimized at B3LYP/6-31+G(d)/PCM(DCM) with	

single point energies at M06-2x/6-311+G(d,p)/PCM(DCM) (relative Gibbs free energies in kcal/mol shown in parentheses). 116

Figure 17. Lowest energy transition states in the reaction of 1-benzyl-3-hydroxypiperidine **163** with methyl iodide in DCM. Structures optimized at B3LYP/6-31+G(d)/PCM(DCM) with single point energies at M06-2x/6-311+G(d,p)/PCM(DCM) (relative Gibbs free energies in kcal/mol shown in parentheses). 117

Figure 18. Lowest energy transition states in the reaction of 1-methyl-3-trimethylsilylpiperidine **168** with benzyl chloride in DCM. Structures optimized at B3LYP/6-31+G(d)/PCM(DCM) with single point energies at M06-2x/6-311+G(d,p)/PCM(DCM) (relative Gibbs free energies in kcal/mol shown in parentheses). 120

Figure 19. Lowest energy transition states in the reaction of 1-benzyl-3-trimethylsilylpiperidine **169** with methyl iodide in DCM. Structures optimized at B3LYP/6-31+G(d)/PCM(DCM) with single point energies at M06-2x/6-311+G(d,p)/PCM(DCM) (relative Gibbs free energies in kcal/mol shown in parentheses). 120

Figure 20. ORTEP diagram of piperidinium salt **171-D1**. 122

Figure 21. Identifying ¹H NMR chemical shifts of **173-D1** and **173-D2**. Structures optimized at B3LYP/6-31+G(d,p), NMR calculations at mPW1PW91/6-311+G(2d,p)/SMD(CHCl₃). Calculated chemical shifts reflect a weighted average of contributions of all conformers with a >1% contribution to the population, though only the lowest energy conformer of each diastereomer is shown. Experimental chemical shifts are reported in CDCl₃. 123

Figure 22. Lowest energy transition states in the reaction of **172** with benzyl bromide in DCM. Structures optimized at B3LYP/6-31+G(d)/PCM(DCM) with single point energies at M06-2x/6-311+G(d,p)/PCM(DCM) (relative Gibbs free energies in kcal/mol shown in parentheses). 126

Figure 23. ORTEP diagrams of interrupted Nazarov products 181 and 182.....	142
Figure 24. ORTEP diagram of adduct 183.	143
Figure 25. B3LYP/6-311+G(d,p) gas phase geometries of the eight isomeric transition states of furan capture of the oxyallyl cation activated by TMS. Values in parentheses are relative energies in kcal/mol obtained from single point energies in M06-2x/6-311+G(d,p)/PCM(DCM) with thermal contributions to the Gibbs free energy from the gas phase B3LYP/6-311+G(d,p) calculations. Indicated distances are in Angstroms. The gray lines indicate the forming bond distance, the green lines indicate CH- π interaction distances, and the blue lines indicate p-orbital interaction (non-bond forming) distances.....	145
Figure 26. B3LYP/6-311+G(d,p)/PCM(DCM) geometries of the eight isomeric transition states of furan capture of the oxyallyl cation activated by BF ₃ . Values in parentheses are relative energies in kcal/mol obtained from single point energies in M06-2x/6-311+G(d,p)/PCM(DCM) with thermal contributions to the Gibbs free energy from the B3LYP/6-311+G(d,p)/PCM(DCM) calculations. Indicated distances are in Angstroms. The gray lines indicate the forming bond distance, the green lines indicate CH- π interaction distances, and the blue lines indicate p-orbital interaction (non-bond forming) distances.....	146
Figure 27. Torsional steering in the reaction of furan with TMS-activated oxyallyl cation 180a . Only the relevant sections of TS-TMS-7 and TS-TMS-3 are presented for clarity. The values indicated are the dihedral angles between the adjacent methyl and phenyl groups.....	147
Figure 28. Stationary points in the reaction of TMS-activated oxyallyl cation 180a with furan via TS-TMS-1 . Values in parentheses are relative energies in kcal/mol obtained from single point energies in M06-2x/6-311+G(d,p)/PCM(DCM) with thermal contributions to the Gibbs free energy from the B3LYP/6-311+G(d,p) calculations.....	149

Figure 29. Stationary points in the reaction of TMS-activated oxyallyl cation **180a** with furan via **TS-TMS-2**. Values in parentheses are relative energies in kcal/mol obtained from single point energies in M06-2x/6-311+G(d,p)/PCM(DCM) with thermal contributions to the Gibbs free energy from the B3LYP/6-311+G(d,p) calculations..... 150

Figure 30. Stationary points in the reaction of TMS-activated oxyallyl cation **180a** with furan via **TS-TMS-3**. Values in parentheses are relative energies in kcal/mol obtained from single point energies in M06-2x/6-311+G(d,p)/PCM(DCM) with thermal contributions to the Gibbs free energy from the B3LYP/6-311+G(d,p) calculations..... 151

Figure 31. Stationary points in the reaction of TMS-activated oxyallyl cation **180a** with furan via **TS-TMS-4**. Values in parentheses are relative energies in kcal/mol obtained from single point energies in M06-2x/6-311+G(d,p)/PCM(DCM) with thermal contributions to the Gibbs free energy from the B3LYP/6-311+G(d,p) calculations..... 152

Figure 32. Stationary points in the reaction of TMS-activated oxyallyl cation **180a** with furan via **TS-TMS-5**. Values in parentheses are relative energies in kcal/mol obtained from single point energies in M06-2x/6-311+G(d,p)/PCM(DCM) with thermal contributions to the Gibbs free energy from the B3LYP/6-311+G(d,p) calculations..... 153

Figure 33. Stationary points in the reaction of TMS-activated oxyallyl cation **180a** with furan via **TS-TMS-6**. Values in parentheses are relative energies in kcal/mol obtained from single point energies in M06-2x/6-311+G(d,p)/PCM(DCM) with thermal contributions to the Gibbs free energy from the B3LYP/6-311+G(d,p) calculations..... 154

Figure 34. Stationary points in the reaction of TMS-activated oxyallyl cation **180a** with furan via **TS-TMS-7**. Values in parentheses are relative energies in kcal/mol obtained from single

point energies in M06-2x/6-311+G(d,p)/PCM(DCM) with thermal contributions to the Gibbs free energy from the B3LYP/6-311+G(d,p) calculations..... 155

Figure 35. Stationary points in the reaction of TMS-activated oxyallyl cation **180a** with furan via **TS-TMS-8**. Values in parentheses are relative energies in kcal/mol obtained from single point energies in M06-2x/6-311+G(d,p)/PCM(DCM) with thermal contributions to the Gibbs free energy from the B3LYP/6-311+G(d,p) calculations..... 156

Figure 36. Stationary points in the reaction of BF₃-activated oxyallyl cation **180a** with furan via **TS-BF₃-1**. Values in parentheses are relative energies in kcal/mol obtained from single point energies in M06-2x/6-311+G(d,p)/PCM(DCM) with thermal contributions to the Gibbs free energy from the B3LYP/6-311+G(d,p)/PCM(DCM) calculations..... 157

Figure 37. Stationary points in the reaction of BF₃-activated oxyallyl cation **180a** with furan via **TS-BF₃-2**. Values in parentheses are relative energies in kcal/mol obtained from single point energies in M06-2x/6-311+G(d,p)/PCM(DCM) with thermal contributions to the Gibbs free energy from the B3LYP/6-311+G(d,p)/PCM(DCM) calculations..... 158

Figure 38. Stationary points in the reaction of BF₃-activated oxyallyl cation **180a** with furan via **TS-BF₃-3**. Values in parentheses are relative energies in kcal/mol obtained from single point energies in M06-2x/6-311+G(d,p)/PCM(DCM) with thermal contributions to the Gibbs free energy from the B3LYP/6-311+G(d,p)/PCM(DCM) calculations..... 159

Figure 39. Stationary points in the reaction of BF₃-activated oxyallyl cation **180a** with furan via **TS-BF₃-4**. Values in parentheses are relative energies in kcal/mol obtained from single point energies in M06-2x/6-311+G(d,p)/PCM(DCM) with thermal contributions to the Gibbs free energy from the B3LYP/6-311+G(d,p)/PCM(DCM) calculations..... 160

Figure 40. Stationary points in the reaction of BF ₃ -activated oxyallyl cation 180a with furan via TS-BF ₃ -5. Values in parentheses are relative energies in kcal/mol obtained from single point energies in M06-2x/6-311+G(d,p)/PCM(DCM) with thermal contributions to the Gibbs free energy from the B3LYP/6-311+G(d,p)/PCM(DCM) calculations.....	161
Figure 41. Stationary points in the reaction of BF ₃ -activated oxyallyl cation 180a with furan via TS-BF ₃ -6. Values in parentheses are relative energies in kcal/mol obtained from single point energies in M06-2x/6-311+G(d,p)/PCM(DCM) with thermal contributions to the Gibbs free energy from the B3LYP/6-311+G(d,p)/PCM(DCM) calculations.....	162
Figure 42. Stationary points in the reaction of BF ₃ -activated oxyallyl cation 180a with furan via TS-BF ₃ -7. Values in parentheses are relative energies in kcal/mol obtained from single point energies in M06-2x/6-311+G(d,p)/PCM(DCM) with thermal contributions to the Gibbs free energy from the B3LYP/6-311+G(d,p)/PCM(DCM) calculations.....	163
Figure 43. Stationary points in the reaction of BF ₃ -activated oxyallyl cation 180a with furan via TS-BF ₃ -8. Values in parentheses are relative energies in kcal/mol obtained from single point energies in M06-2x/6-311+G(d,p)/PCM(DCM) with thermal contributions to the Gibbs free energy from the B3LYP/6-311+G(d,p)/PCM(DCM) calculations.....	164
Figure 44. The frontier molecular orbitals of TS-BF ₃ -7". The blue circle highlights the area of high electron density between the carbons undergoing bond formation.	166
Figure 45. The frontier molecular orbitals of TS-TMS-7". The blue circle highlights the lack of electron density between the carbons undergoing bond formation.	167
Figure 46. Gas phase mechanisms of 1,2-cyclohexadiene dimerization.	173
Figure 47. Dimerization mechanisms of 1,2-cyclohexadiene in acetonitrile.....	174

Figure 48. Calculated mechanisms of cycloaddition between 1,2-cyclohexadiene 187a and nitrile oxide 188	177
Figure 49. Calculated mechanisms of cycloaddition between 1,2-cyclohexadiene 187b and nitrile oxide 188	178
Figure 50. Singlet diradical mechanism for cycloaddition in the gas phase.....	179
Figure 51. The mechanism of cycloaddition of 1,2-cyclohexadiene 187a and azomethine imine 190	182
Figure 52. The mechanism of cycloaddition of 1,2-cyclohexadiene 187b and azomethine imine 190	183
Figure 53. The mechanism of cycloaddition of cycloallene 187a and azomethine imine 192 ..	184
Figure 54. Diastereomeric concerted and singlet diradical transition structures in the reaction of cycloallene 187a with azomethine imine 192 at the B3LYP/6-31+G(d)/PCM(MeCN) level. “TS1” refers to the transition state in the reaction pathway that forms (an intermediate on the way to) the “ <i>endo</i> ” product (where the hydrogens on the two stereocentres are <i>cis</i> to one another), and “TS2” refers to the eventual formation of the “ <i>exo</i> ” product.	185
Figure 55. Mechanisms of cycloaddition of cycloallene 187a with nitrene 194	188
Figure 56. Mechanisms of cycloaddition of cycloallene 187b with nitrene 194	189
Figure 57. Mechanisms of cycloaddition of cycloallene 187a with nitrene 196	190
Figure 58. The four possible diastereomers of 2:1 adduct 199	191
Figure 59. The lowest energy conformer of each diastereomer of 199 at the B3LYP/6-31+G(d,p) level.....	194

List of Schemes

Scheme 1. Woodward's 1956 total synthesis of lysergic acid.....	4
Scheme 2. Julia's 1969 formal synthesis of lysergic acid.....	5
Scheme 3. Oppolzer's 1981 synthesis of lysergic acid.....	6
Scheme 4. Ramage's formal synthesis of lysergic acid.....	7
Scheme 5. Ninomiya's 1982 formal synthesis of lysergic acid.....	7
Scheme 6. Rebek's 1983 synthesis of the lysergic acid methyl ester.....	8
Scheme 7. Saá and Vollhardt's 1994 synthesis of LSD.....	9
Scheme 8. Hendrickson's 2004 total synthesis of lysergic acid.....	9
Scheme 9. Fujii and Ohno's 2008 synthesis of lysergic acid.....	10
Scheme 10. Asymmetric synthesis of the lysergic acid methyl ester by Fukuyama.....	12
Scheme 11. Fujii and Ohno's 2011 asymmetric synthesis of lysergic acid.....	13
Scheme 12. Jia's synthesis of (+)-lysergic acid.....	14
Scheme 13. Fukuyama's 2013 asymmetric synthesis of lysergic acid.....	15
Scheme 14. (a) The first Stevens [1,2]-rearrangement, (b) the corresponding Stevens [2,3]-rearrangement.....	16
Scheme 15. The Stevens [1,2]-rearrangement starting from an amine-tethered diazoketone. “ML _n ” refers to a metal (usually copper or rhodium) with any number of ligands.....	17
Scheme 16. Proposed mechanisms for the Stevens [1,2]-rearrangement: (a) ionic, (b) pericyclic, and (c) diradical.....	18
Scheme 17. Examples of the use of the Stevens [1,2]-rearrangement in natural product synthesis.....	20
Scheme 18. First proposed retrosynthesis of lysergic acid using the Stevens rearrangement.....	22

Scheme 19. Second proposed synthetic route towards lysergic acid using the Stevens [1,2]-rearrangement.	23
Scheme 20. Three possible intermediate targets in the synthesis of piperidine 75	25
Scheme 21. Modified synthesis of enone 86 from tetrahydropyridine 89	25
Scheme 22. Alternate synthesis of intermediate 90	26
Scheme 23. Attempted allylic oxidation of protected tetrahydropyridine 90	26
Scheme 24. Attempted synthesis of bromide 103 and synthesis of amine 105 in order to form CBz-protected enone 86 via ring-closing metathesis.	27
Scheme 25. Attempted synthesis of enone 86 via dehydrogenation of ketone 109	27
Scheme 26. Planned synthesis of piperidine 75 from intermediate 87	28
Scheme 27. Attempted synthesis of intermediate 80	28
Scheme 28. De Kimpe's piperidinone synthesis.	29
Scheme 29. Attempt to cyclize imine 88 to pyrrolidine 122	30
Scheme 30. Targeted conjugate addition products from enone 79	31
Scheme 31. Unsuccessful attempts at conjugate addition into enone 86 using cuprate reagents.	31
Scheme 32. Synthesis of methyl-substituted ketone 123	31
Scheme 33. Synthesis of phenyl- and vinyl-substituted ketones 124 and 125	32
Scheme 34. Phenyl- and vinylthienylcuprate addition to cyclohexenone 129	32
Scheme 35. Conjugate addition of lithium dithiane to enone 86 and cyclohexenone 129	33
Scheme 36. Synthesis of ketone 127	33
Scheme 37. Synthesis of piperidine 75 from enone 86	34
Scheme 38. Synthesis of indole derivative 74	35
Scheme 39. Alkylation of piperidine 75	35

Scheme 40. Failed deprotection attempts on piperidinium salt 141	36
Scheme 41. Failed deprotection attempts on piperidine 75	37
Scheme 42. Synthesis of Stevens rearrangement precursor 143 via alkene-protected piperidine derivative 147	38
Scheme 43. Synthesis of phenyl-substituted alkene 149	38
Scheme 44. Methylation of 4- <i>tert</i> -butyl-1-ethylpiperidine 150	82
Scheme 45. Benzylation of 1-methyl-4-phenylpiperidine 152	86
Scheme 46. Selectivity in the reactions of 1,2-, 1,3-, and 1,4-dimethylpiperidine with 2-chloro-1-phenylethanone.	91
Scheme 47. Alkylation of piperidine derivative 174 to obtain drug candidate 175	101
Scheme 48. Alkylation of piperidine derivatives 162 , 163 , 165 , and 166	103
Scheme 49. Benzylation of the four main conformers of 3-hydroxy-1-methylpiperidine 162 to form two diastereomeric products 164-D1 and 164-D2	106
Scheme 50. Alkylation of the model TMS-protected piperidines 168 and 169	118
Scheme 51. Benzylation of piperidine 147	121
Scheme 52. Salt metathesis on piperidinium salt 148	122
Scheme 53. The computationally-studied benzylation of piperidine 172 with benzyl bromide.	124
Scheme 54. The Nazarov reaction.....	139
Scheme 55. The interrupted Nazarov reaction.	140
Scheme 56. Divergent reactivity in the Nazarov reaction of divinyl ketone 180 interrupted by furan.	141
Scheme 57. Reaction of cycloadduct 182 with trimethylsilyl triflate.	142

Scheme 58. The Nazarov cyclization of divinyl ketone 180 followed by trapping of the oxyallyl cation with allyl silanes and allyl stannanes.	168
Scheme 59. Examples of the preparation and reactivity of 1,2-cyclohexadiene.....	169
Scheme 60. Examples of cycloadditions between 1,2-cyclohexadienes and 1,3-dipoles.	170
Scheme 61. The dimerization of allene as reported by Johnson.	170
Scheme 62. The dimerization of 1,2-cyclohexadiene.	171
Scheme 63. Trapping of the diradical intermediate in the dimerization of 1,2-cyclohexadienes.	171
Scheme 64. Reaction of 1,2-cyclohexadienes with nitrile oxide 188	175
Scheme 65. Cycloadditions between 1,2-cyclohexadienes and azomethine imines.	180
Scheme 66. Cycloadditions between 1,2-cyclohexadienes and nitrones.	186
Scheme 67. Reaction of 1,2-cyclohexadiene 187a with azide 198 to form 2:1 adduct 199	191
Scheme 68. Dimerization of 1-acetoxy-1,2-cyclohexadiene.....	196

List of Symbols and Abbreviations

^1H	proton (spectral)
^{13}C	carbon 13 (spectral)
3D	three dimensional (computational)
6-31+G(d)	Pople basis set (computational)
6-311+G(d,p)	Pople basis set (computational)
6-311+G(2d,p)	“
A	unspecified acid (Brønsted or Lewis)
Å	Angstrom(s)
Ac	acetyl
acac	acetylacetonate
app	apparent (spectral)
APT	attached proton test (spectral)
aq	aqueous
Ar	aryl
atm	atmosphere(s)
avg	average
ax	axial
B3LYP	DFT hybrid functional ⁸²
Boc	<i>tert</i> -butoxycarbonyl
Bn	benzyl
br	broad (spectral)
<i>n</i> -Bu	butyl (linear)

<i>s</i> -Bu	<i>sec</i> -butyl
<i>t</i> -Bu	<i>tert</i> -butyl
Bz	benzoyl
°C	degrees Celsius
calc	calculated
cat	used in a catalytic amount
CBz	carboxybenzyl
cc-pVTZ	correlation-consistent basis set ⁸⁹
CCSD	coupled cluster (post-Hartree Fock <i>ab initio</i> method)
CIDNP	chemically induced dynamic nuclear polarization
cm ⁻¹	wave numbers
CMAD	corrected mean absolute deviation
conc	concentrated
<i>m</i> CPBA	<i>meta</i> -chloroperbenzoic acid
Cy	cyclohexyl
D	diastereomer or deuterium
d	doublet (spectral)
D3	Grimme's dispersion correction model ¹²⁵
DBU	1,8-diazabicyclo[5.4.0]undec-7-ene
DCM	dichloromethane
dd	doublet of doublets (spectral)
ddd	doublet of doublets of doublets (spectral)
DFT	density functional theory

DIBAL	diisobutylaluminum hydride
DMAP	4-dimethylaminopyridine
DME	1,2-dimethoxyethane
DMF	<i>N,N</i> -dimethylformamide
DMP	Dess-Martin Periodinane or 3,5-dimethylpyrazole (with CrO ₃)
DMPU	1,3-Dimethyl-3,4,5,6-tetrahydro-2(1H)-pyrimidinone
DMSO	dimethylsulfoxide
<i>dr</i>	diastereomeric ratio
dt	doublet of triplets (spectral)
ECP	effective core potential (computational)
<i>ee</i>	enantiomeric excess
EI	electron impact (mass spectrometry)
ent	enantiomer
eq	equatorial
equiv	equivalents
ESI	electrospray ionization (mass spectrometry)
Et	ethyl
EtOAc	ethyl acetate
EWG	electron-withdrawing group
exptl	experimental
FMO	frontier molecular orbital
G	Gibbs free energy
g	grams

GIAO	gauge-independent atomic orbital (computational)
h	hours
HMPA	hexamethylphosphoramide
HOMO	highest occupied molecular orbital
HRMS	high resolution mass spectrometry
HSQC	heteronuclear single quantum coherence (spectral)
Hz	Hertz
IBX	2-iodoxybenzoic acid
IR	infrared
IRC	intrinsic reaction coordinate (computational)
J	Joule(s)
<i>J</i>	coupling constant
K	Kelvin
kcal	kilocalories
L	litres or unspecified ligand
L*	unspecified chiral ligand
LA	Lewis acid
LDA	lithium diisopropylamide
LSA	lysergic acid
LSD	lysergic acid diethylamide
LUMO	lowest unoccupied molecular orbital
M	molar or unspecified metal
m	multiplet (spectral)

M ⁺	molecular ion (mass spectrometry)
Me	methyl
MHz	megahertz
min	minute(s)
mL	millilitre(s)
MMFF94	Merck molecular force field
mmol	millimole(s)
mol	mole(s)
M06-2x	DFT hybrid functional ⁸³
MP2	post-Hartee-Fock <i>ab initio</i> method ⁸⁶
mPW1PW91	DFT hybrid functional ⁸⁴
MS	molecular sieves or mass spectrometry
Ms	methanesulfonyl
m/z	mass-to-charge ratio
n	unspecified number
NIS	<i>N</i> -iodosuccinimide
NMO	<i>N</i> -methyldmorpholine- <i>N</i> -oxide
NMR	nuclear magnetic resonance
nOe	nuclear Overhauser effect
Ns	2- or 4-nitrobenzenesulfonyl
Nu	unspecified nucleophile
ORTEP	Oak Ridge thermal ellipsoid plot
P	product

<i>p</i>	para
PCM	polarizable continuum model (computational)
pdt	product
PG	protecting group
Ph	phenyl
Piv	pivaloyl
PNB	<i>para</i> -nitrobenzyl
ppm	parts per million
PPTS	pyridinium <i>para</i> -toluenesulfonate
<i>i</i> -Pr	isopropyl
<i>n</i> -Pr	propyl (linear)
Pyr	pyridine
q	quartet (spectral)
quant	quantitative
R	unspecified alkyl group or gas constant
R _f	retention factor (chromatography)
rt	room temperature
s	singlet (spectral)
SDB	Stuttgart-Dresden-Bonn relativistic effective core potential (computational)
[Si]	unspecified silyl group
SMD	Truhlar's universal solvation model ⁹⁷
S _N 2	bimolecular nucleophilic substitution
sp ²	hybrid orbital from combining one s and two p orbitals

T	temperature
t	triplet (spectral)
TBDPS	<i>tert</i> -butyldiphenylsilyl
TBS	<i>tert</i> -butyldimethylsilyl
TES	triethylsilyl
Tf	trifluoromethanesulfonyl
THF	tetrahydrofuran
TIPS	triisopropylsilyl
TLC	thin layer chromatography
TMEDA	<i>N,N,N',N'</i> -tetramethylethylenediamine
TMS	trimethylsilyl
TS	transition state or transition structure
Ts	<i>para</i> -toluenesulfonyl
X	unspecified group (usually leaving group)
Y	unspecified atom/group
Z	unspecified atom/group
°	degrees (angle)
‡	transition state/structure
δ	chemical shift (spectral)
Δ	difference or heat
π	pi (bond/system of orbitals)

Chapter 1: Introduction

Section 1.1: Overview

This thesis covers a wide range of topics, from synthesis to computational studies, and from nitrogen heterocycles to the Nazarov reaction to cycloallene chemistry. The common thread throughout this thesis is the desire to dig deeper and more fully understand organic chemistry at the molecular level. We began with the desire to synthesize lysergic acid, a complex alkaloid natural product used in medicinal chemistry, utilizing chemistry well-developed by the West group – the Stevens [1,2]-rearrangement of ammonium ylides. This unique and promising reaction has thus far been only used in the synthesis of fairly small, simple natural products, despite being known for over 80 years. Chapter 2 details the synthetic work undertaken towards lysergic acid, including the surprising results that lead to a more detailed study of piperidine alkylation. Chapter 3 introduces the concept of diastereoselective alkylation of substituted piperidine derivatives in the form of a literature review and analysis, as well as a computational analysis of experimental results found in the literature. To complement this retrospective analysis, Chapter 4 details experimental alkylation studies, computational analyses, and identification of diastereomeric products via comparison of experimental and computed ^1H NMR chemical shifts. As the application of computational chemistry to piperidine alkylation was explored, other interesting results in different projects within the West group led to computational mechanistic studies outside of the scope of the original lysergic acid synthesis project. Chapter 5 discusses computational insights into an unusual interrupted Nazarov reaction performed by Dr. Yen-Ku Wu, and Chapter 6 discusses ongoing computational studies of cycloallene reactions performed by Verner Lofstrand. The rest of this chapter will

introduce the original synthetic project, discussing lysergic acid (including the previous synthetic efforts towards this molecule) and the Stevens rearrangement of ammonium ylides.

Section 1.2: Structural Features and Properties of Lysergic Acid and its Derivatives

(+)-Lysergic acid was isolated in 1934 as the hydrolysis product of ergot, a mixture of alkaloids produced by *Claviceps purpurea*, a fungus that grows on grains such as rye and barley.¹ The ergot alkaloids have a long history; in the Middle Ages, people who consumed grains contaminated with this fungus developed a gangrenous disease called St. Anthony's Fire, which was later found to be caused by the ergot alkaloids produced by this fungus.² More recently, however, ergot alkaloids and other derivatives of lysergic acid have found medicinal uses such as the treatment of migraines, Parkinson's disease, and tumours; Figure 1 shows some examples of medicinally-important lysergic acid derivatives.³

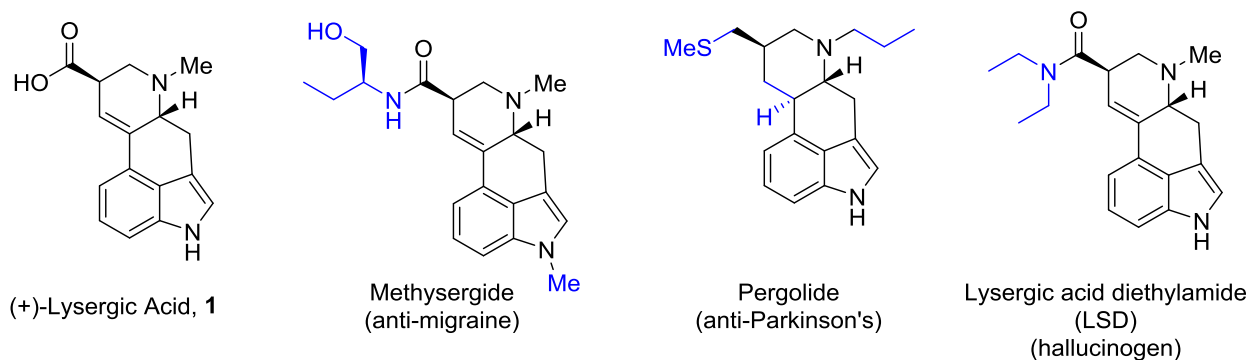


Figure 1. Lysergic acid and derivatives. Changes to the lysergic acid skeleton are shown in blue.

In addition to its medicinal value, lysergic acid has been studied extensively in organic synthesis due to its unique structure. In addition to having a tetracyclic skeleton with two stereocentres, the presence of a tertiary amine and an indole moiety adds a great deal of challenge to the synthesis of lysergic acid; both of these functional groups are highly

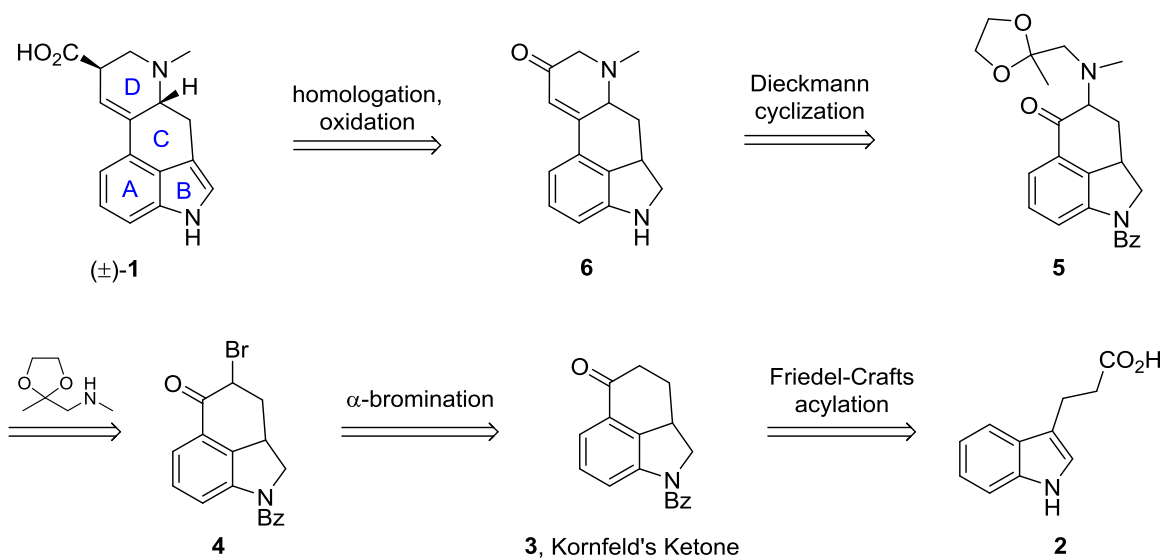
nucleophilic and can participate in a large number of side reactions. Additionally, the basicity of the tertiary amine makes both synthesis and purification difficult.

Section 1.3: Previous Syntheses of Lysergic Acid

There have been eight total syntheses and eight formal syntheses of lysergic acid (reaching an intermediate only one or two steps away from lysergic acid), as well as a few syntheses of key intermediates, reported in the literature.^{4,5,6} Despite the large number of syntheses, many of the earlier syntheses used similar strategies, and only five are enantioselective.

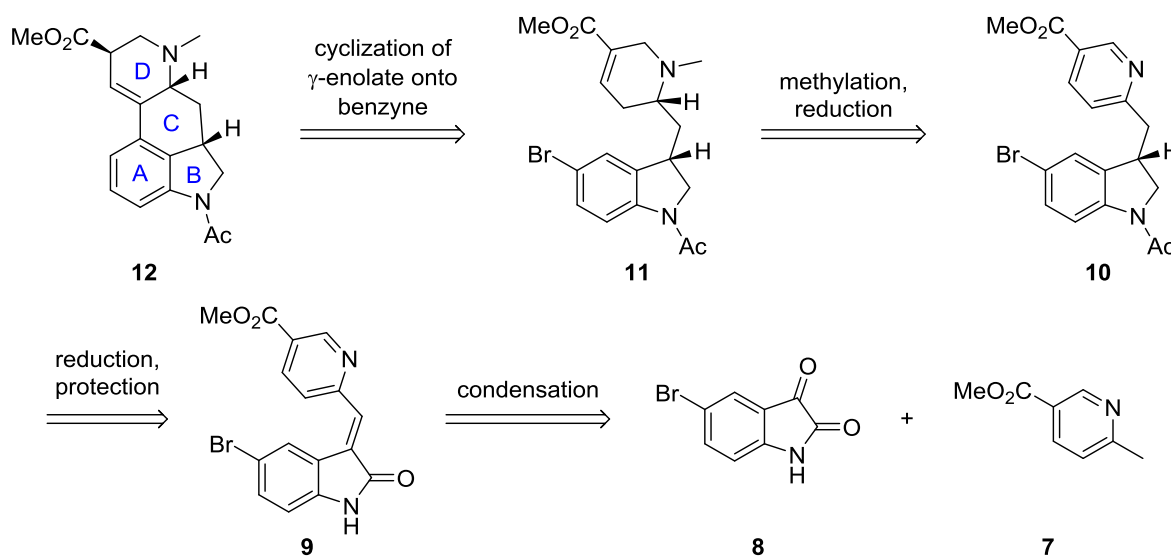
The first total synthesis of lysergic acid (**1**) was reported by the Woodward group in 1956 (retrosynthesis shown in Scheme 1).^{4a} This pioneering work produced racemic lysergic acid in 15 steps with a 1.0% yield overall. The first key step was a Friedel-Crafts acylation to form the tricyclic Kornfeld's ketone (**3**), a key intermediate used in many subsequent syntheses. Note that the starting indole (**2**) had to be hydrogenated first to prevent it from acting as a nucleophile in subsequent reactions. After bromination α to the ketone to form **4**, the next step that caused difficulty was the displacement of the bromide with the amine nucleophile to form **5**. Fortunately, after searching various work-arounds for this step, it was discovered that the simple displacement occurred well in a non-polar solvent. The acetal was deprotected, and a Dieckmann cyclization formed the D ring to afford **6**. Reduction of the enone to the allyl alcohol was achieved readily, and then treatment of the corresponding chloride with sodium cyanide in liquid hydrogen cyanide produced the homologated product; the nitrile was hydrolyzed to the acid in conditions that also removed the benzoyl group on the indoline nitrogen. The last step was dehydrogenation with Raney nickel to re-form the indole and produce racemic lysergic acid.

Although this synthesis was plagued with difficulties, it was an enormous accomplishment back in the 1950s.



Scheme 1. Woodward's 1956 total synthesis of lysergic acid.

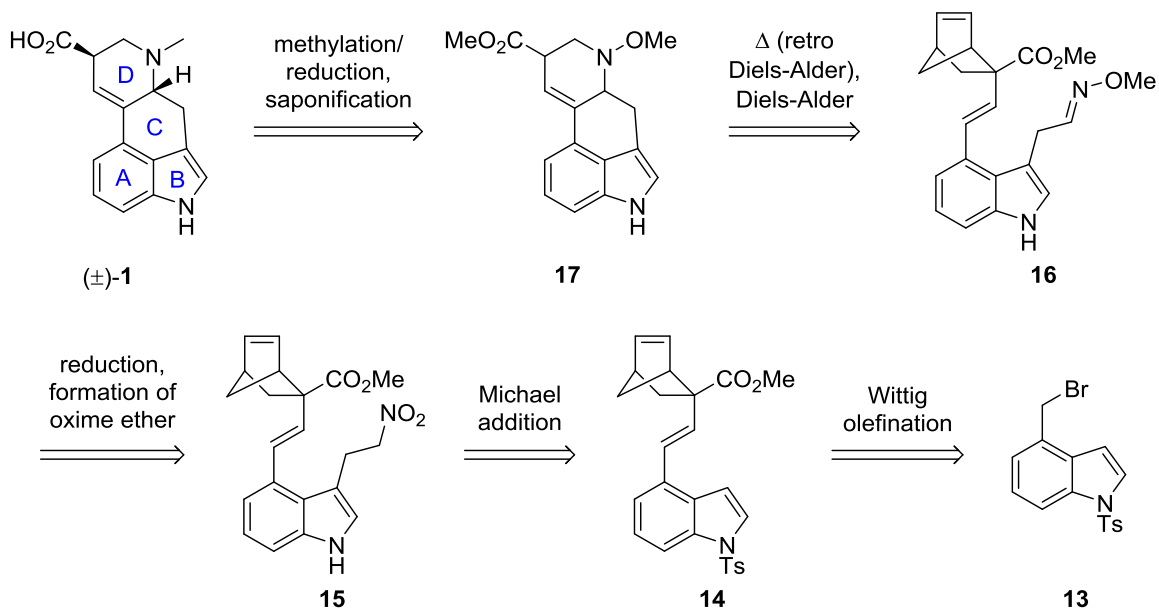
In 1969, Julia and coworkers published a formal synthesis of lysergic acid.^{5a} The main differences in Julia's synthesis versus Woodward's were the introduction of the D ring as a pyridine that would later be hydrogenated to the tetrahydropyridine (**10** → **11**), as well as aryne formation to induce cyclization to form the C ring (**11** → **12**) (Scheme 2). Notably, this synthesis was quite step-efficient, allowing formation of **12** in just 7 steps from commercially-available starting materials **7** and **8** (9 steps to lysergic acid using Woodward's deprotection/dehydrogenation end game).



Scheme 2. Julia's 1969 formal synthesis of lysergic acid.

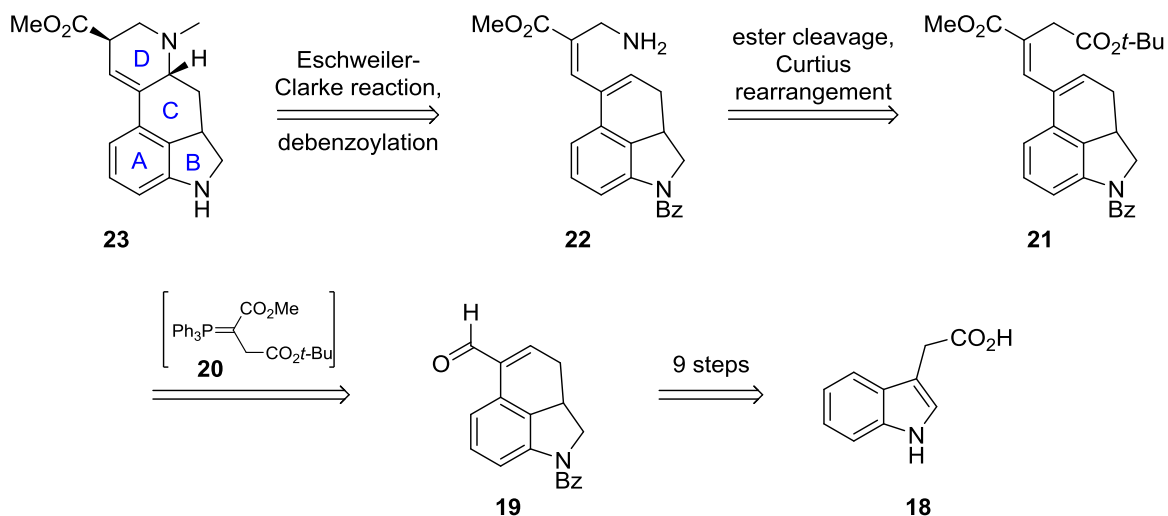
The second total synthesis of lysergic acid was performed 25 years later in 1981 by the Oppolzer group (Scheme 3).^{4b} This synthesis was carried out while keeping the indole intact and, for the most part, unprotected, unlike Woodward's. In fact, the nucleophilicity of the indole was exploited in order to perform a conjugate addition into nitroethylene to form intermediate **15**. The C and D rings were formed in one step using an intramolecular Diels-Alder reaction between the oxime ether and tethered diene (unveiled in the retro Diels-Alder reaction of the

bicyclo[2.2.1]heptene) of intermediate **16**. Lysergic acid was then obtained from intermediate **17** by replacing the methoxy group on the amine with a methyl group and saponifying the methyl ester. While not as efficient or straightforward as Woodward's synthesis, Oppolzer's synthesis was a unique and elegant approach to lysergic acid.



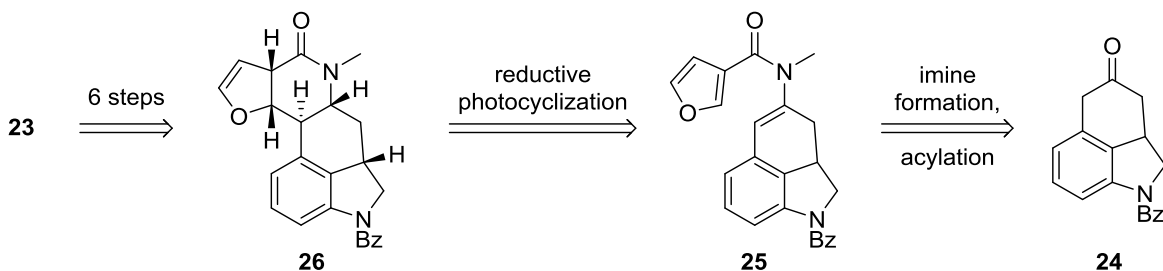
Scheme 3. Oppolzer's 1981 synthesis of lysergic acid.

Oppolzer's synthesis was followed by five more formal syntheses of lysergic acid in the 1980s; the first of these was Ramage's synthesis, also in 1981 (Scheme 4).^{5b} The starting point for this synthesis was one of Woodward's discarded intermediates, **19**, which Ramage synthesized from commercially-available indole derivative **18** in nine steps. A Wittig olefination with **20** provided the rest of the carbons for the D ring, and then the *tert*-butyl ester of **21** was transformed into the primary amine with the help of a Curtius rearrangement. An Eschweiler-Clarke reaction was employed to install the *N*-methyl group and form the D ring. Debenzoylation gave intermediate **23**, two steps from lysergic acid using Woodward's endgame.



Scheme 4. Ramage's formal synthesis of lysergic acid.

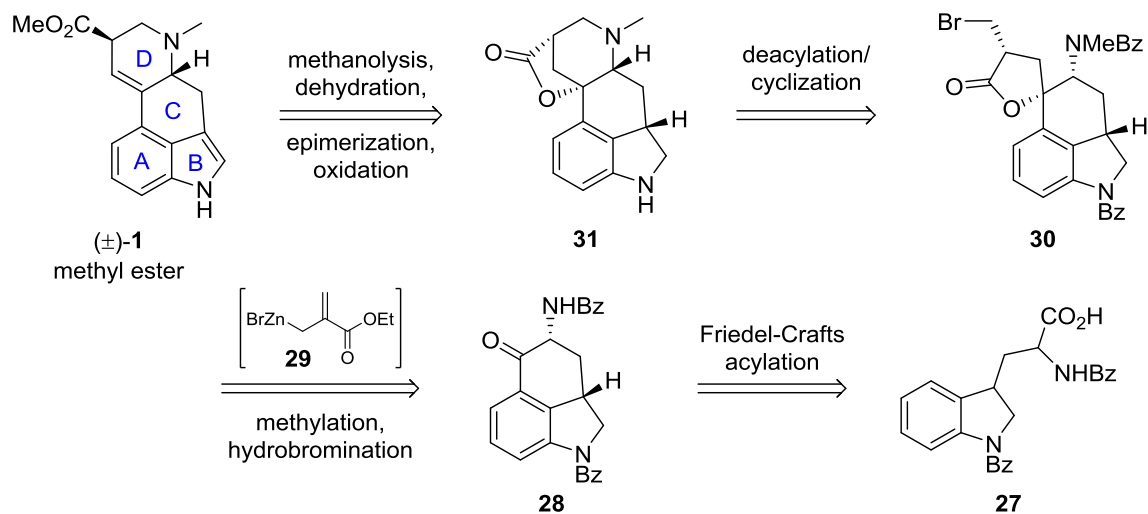
In 1982, the Ninomiya group published a synthesis of lysergic acid intermediate **23** starting from another of Woodward's dead-end intermediates, **24**, via a reductive cyclization of tricyclic intermediate **25** (Scheme 5).^{5c} Six more steps from **26**, including oxidative cleavage and elimination to form the unsaturation in the D ring, gave intermediate **23**.



Scheme 5. Ninomiya's 1982 formal synthesis of lysergic acid.

In 1983, Rebek published a total synthesis of the lysergic acid methyl ester that followed a similar strategy to Woodward's synthesis, though starting from tryptophan derivative **27** to

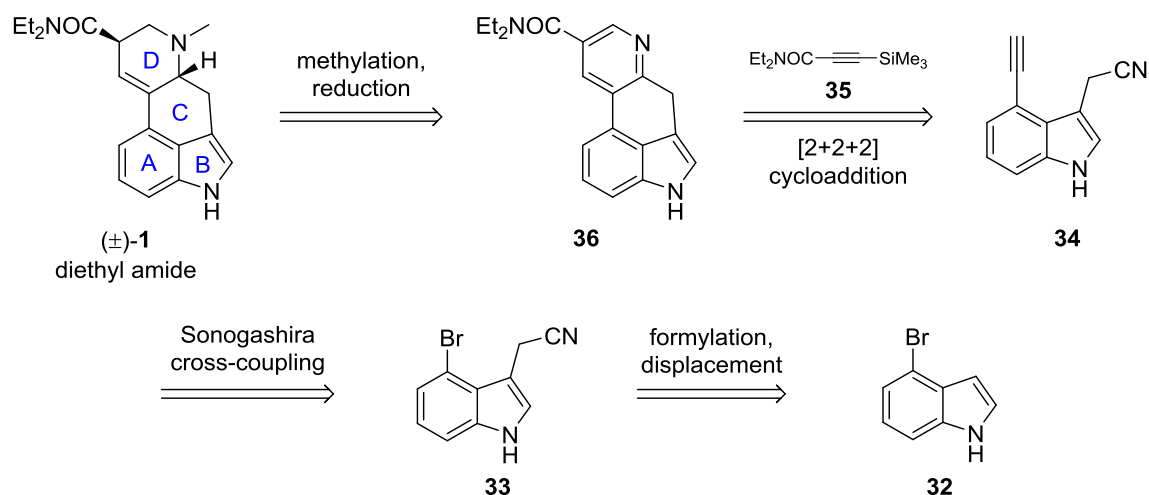
avoid installing the amine later (Scheme 6).^{5d} An amine alkylation was used instead to form the D ring.



Scheme 6. Rebek's 1983 synthesis of the lysergic acid methyl ester.

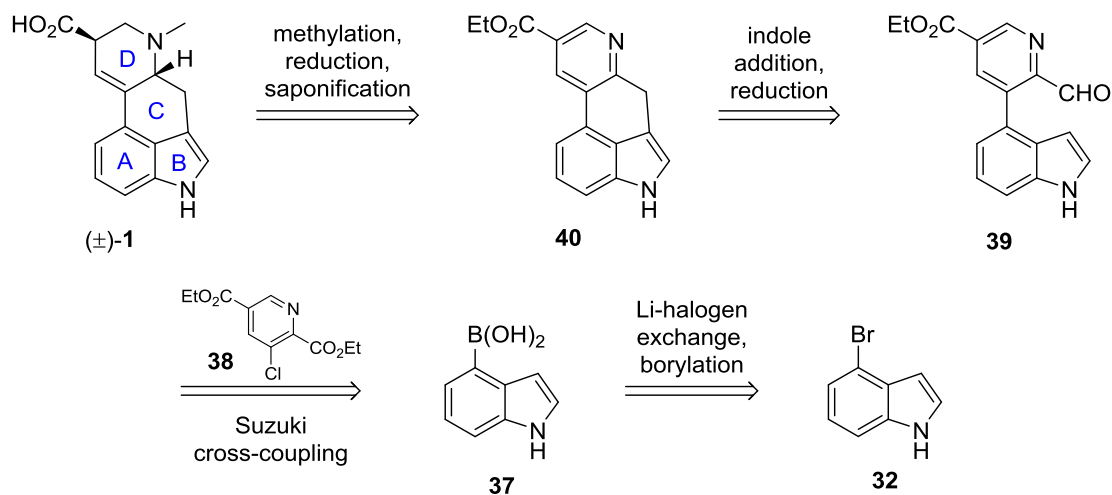
The final two formal syntheses in the 1980s by Kurihara in 1986^{5e} and Ortar in 1988^{5f} started from Woodward's intermediate **3**, Kornfeld's ketone, and intercepted intermediate **23** (as Ramage and Ninomiya did). Both syntheses used a very similar strategy to Ramage's.

The next synthesis of lysergic acid was a total synthesis of lysergic acid diethylamide (LSD), one of the first synthetic ergot alkaloids,⁷ published in 1994 by Saá and Vollhardt (Scheme 7).^{5g} The key step was a Co-catalyzed [2+2+2] cycloaddition to form the D ring as a pyridine (as well as forming the C ring in the process). This was then methylated and reduced to form the tetrahydropyridine. Notably, this synthesis required no protecting group for the indole, which was carried through intact. This elegant synthesis took only 7 steps to form LSD from commercially-available indole derivative **32**.



Scheme 7. Saá and Vollhardt's 1994 synthesis of LSD.

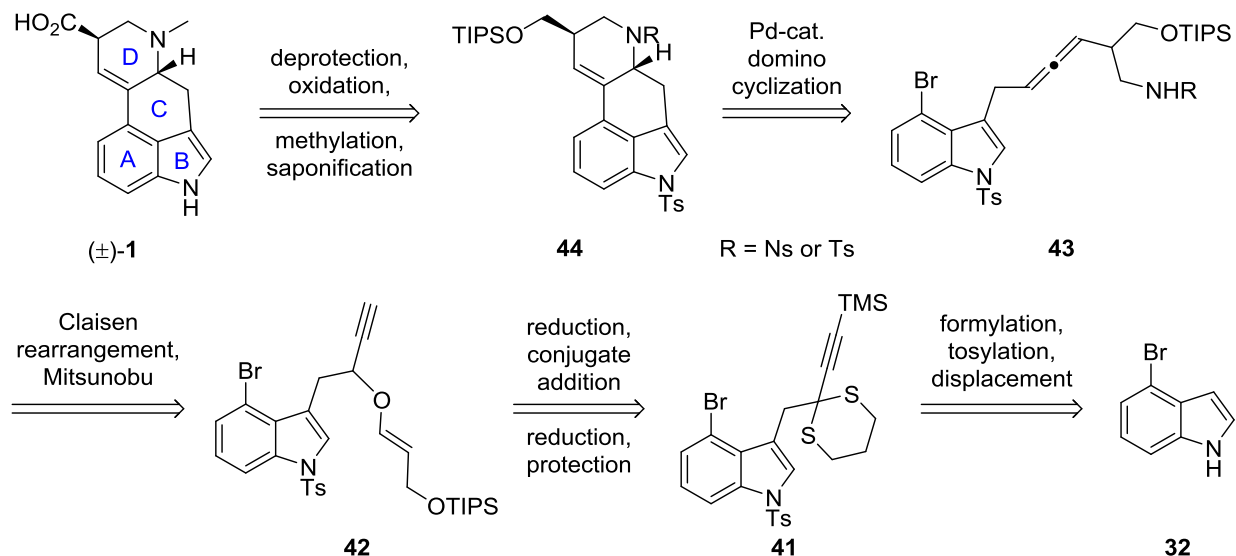
Using a similar approach, Hendrickson reported the total synthesis of lysergic acid in 2004 (Scheme 8).^{4c} Starting from the same commercially-available compound **32** that Saá and Vollhardt used, the D ring as a pyridine was connected to the indole first followed by formation of the C ring via nucleophilic addition of the indole into an aldehyde.



Scheme 8. Hendrickson's 2004 total synthesis of lysergic acid.

The first asymmetric total synthesis of lysergic acid was also reported in 2004 by the Szántay group.^{4d} While an important milestone in the lysergic acid story, this synthesis followed Woodward's original synthesis almost to the letter; the only differences were the use of a pivaloyl protecting group on the indole (which was kept intact) and a chiral resolution after the Dieckmann cyclization to obtain enantioenrichment.

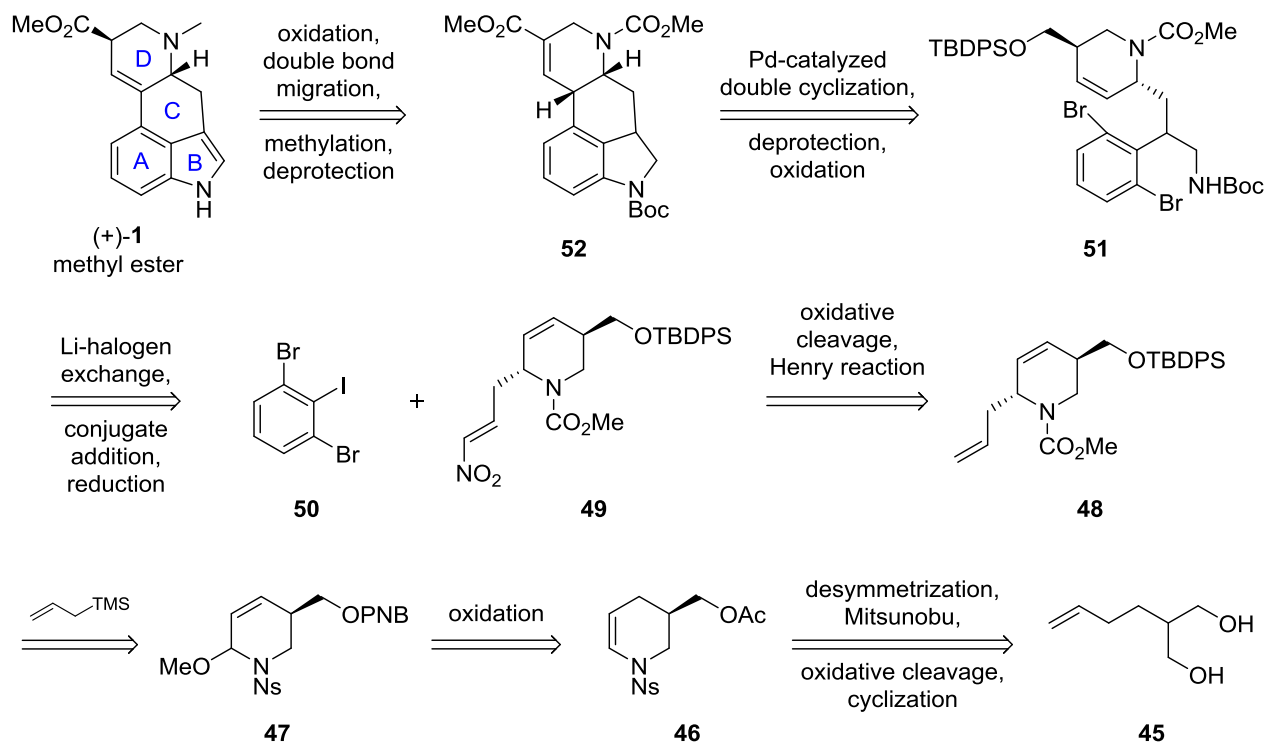
In 2008, Fujii and Ohno reported a total synthesis of lysergic acid starting from the same bromoindole **32** that Saá, Vollhardt, and Hendrickson started from (Scheme 9).^{4e} Although quite a lengthy synthesis at 21 steps, the use of a gold-catalyzed Claisen rearrangement to form allene **43** and subsequent palladium-catalyzed domino cyclization to form **44** is a unique approach to the formation of the C and D rings in one transformation.



Scheme 9. Fujii and Ohno's 2008 synthesis of lysergic acid.

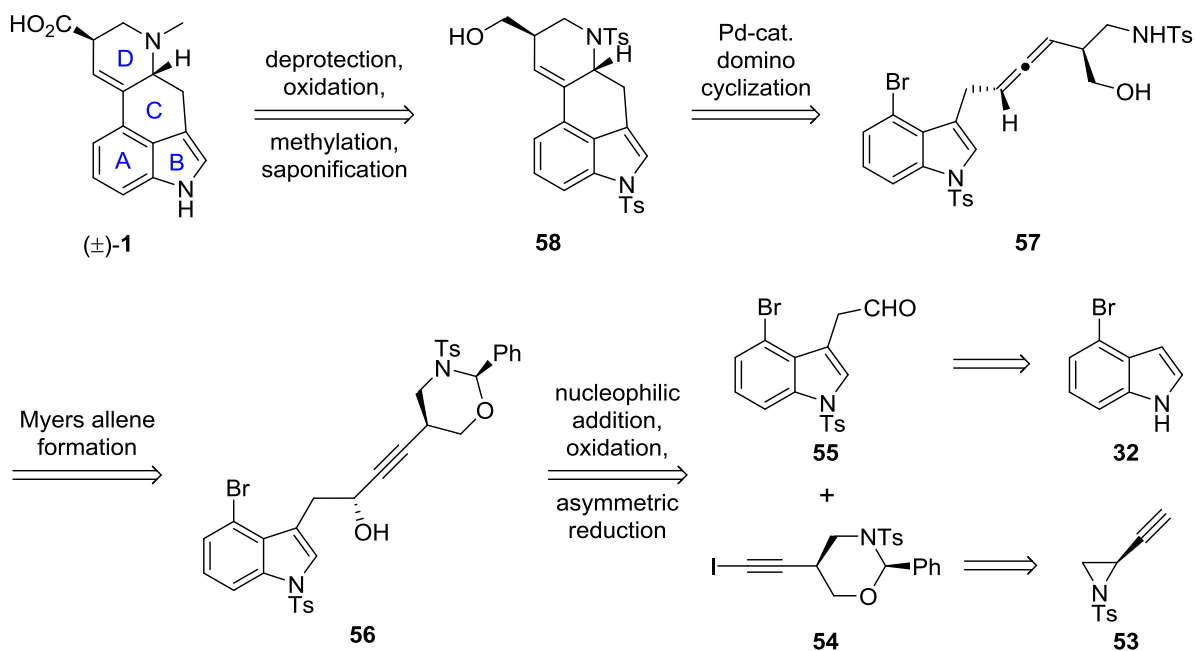
In 2009, the Fukuyama group published the asymmetric synthesis of the lysergic acid methyl ester (Scheme 10).^{5h} The first stereocentre was formed enantioselectively via a lipase-

mediated desymmetrization of diol **45**. This then became the D ring, tetrahydropyridine **46**. Oxidation with *N*-iodosuccinimide (NIS) caused migration of the double bond and added a methoxy group next to the nitrogen to form intermediate **47**. This allowed introduction of an allyl group next to the nitrogen, giving compound **48**. Oxidative cleavage of the double bond followed by Henry reaction gave intermediate **49**. Lithium-halogen exchange on **50** provided a nucleophile for conjugate addition to introduce the A ring. Palladium-catalyzed double cyclization on **51** formed both the B and C rings. A series of functional group manipulations provided the lysergic acid methyl ester. This is by far the longest synthesis of a lysergic acid intermediate at 33 steps. Although lacking efficiency, it did provide an enantioenriched product (only the second synthesis to do so), and the approach to the lysergic acid skeleton was unique, starting with formation of the D ring rather than starting with the A and B rings in the form of an indole derivative like all other previous syntheses.



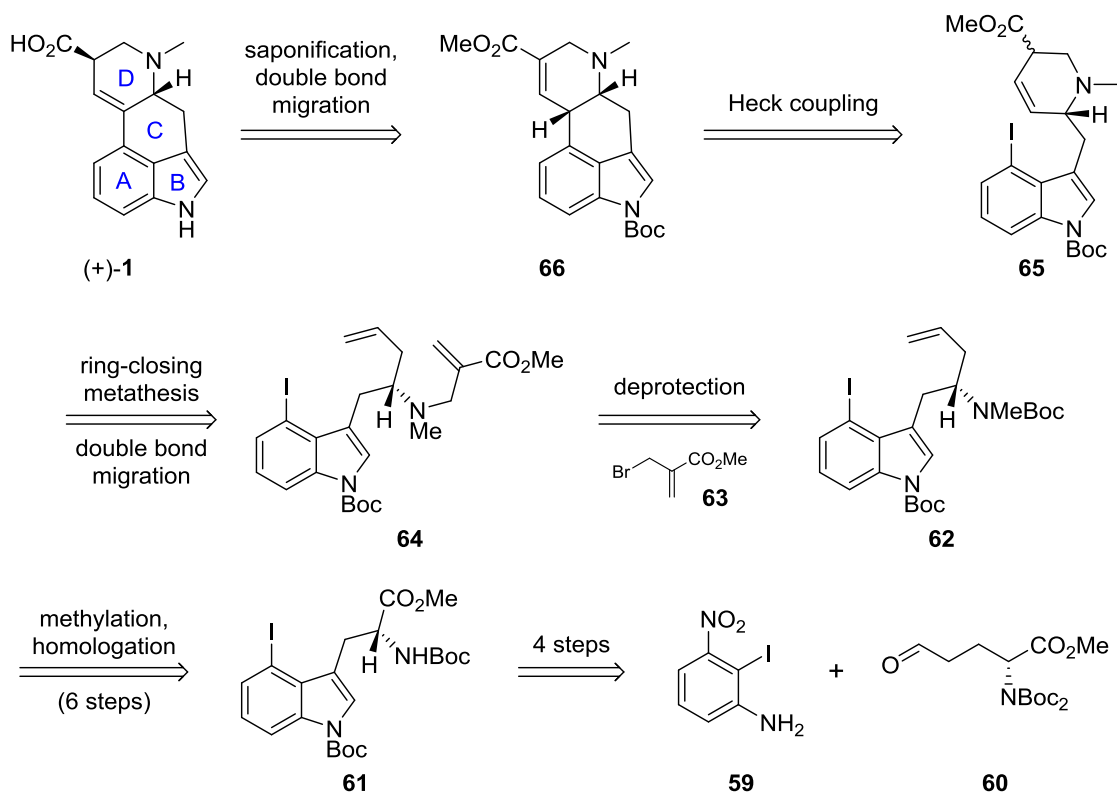
Scheme 10. Asymmetric synthesis of the lysergic acid methyl ester by Fukuyama.

In 2011, Fujii and Ohno presented a second total synthesis of lysergic acid, this time an asymmetric synthesis (Scheme 11).^{4f} They used the same approach as their previous synthesis – a palladium-catalyzed domino cyclization to form the C and D rings simultaneously – as well as a similar rearrangement invented by Myers⁸ to form the allene required for the cyclization. The main difference was the use of enantioenriched alkynyl aziridine **53** as the starting material, which is reported to come from L-serine in eight steps. Aziridine **53** was used to produce alkynyl iodide **54** via a palladium-catalyzed reductive coupling with formaldehyde followed by cyclization/hemiaminal formation and iodination.



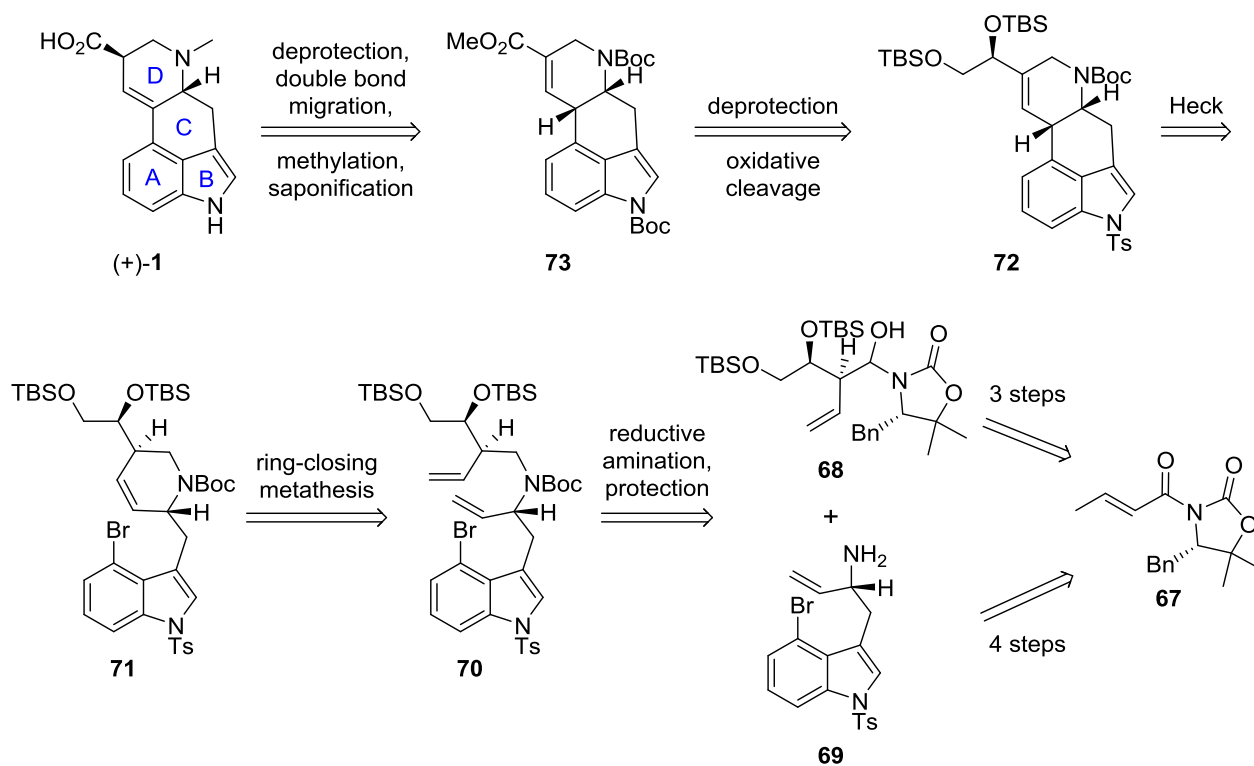
Scheme 11. Fujii and Ohno's 2011 asymmetric synthesis of lysergic acid.

A second asymmetric synthesis of lysergic acid in 2011 by Jia and coworkers employed a ring-closing metathesis reaction to form the D ring followed by a Heck cross-coupling reaction to close the C ring (Scheme 12).^{4g} The starting material for the synthesis is intermediate **61**, though they report the synthesis of *ent*-**61** from “known chiral aldehyde” *ent*-**60** in a previous publication.⁹ The implication is that intermediate **61** could come from the unnatural enantiomer of glutamic acid.



Scheme 12. Jia's synthesis of (+)-lysergic acid.

The latest total synthesis was another asymmetric synthesis from the Fukuyama group in 2013 (Scheme 13).^{4h} The approach was very similar to Jia's, employing an olefin metathesis to form the D ring and a Heck coupling to form the C ring. The stereocentres in this case, however, each came from aldol reactions using an Evans oxazolidinone as a chiral auxiliary.

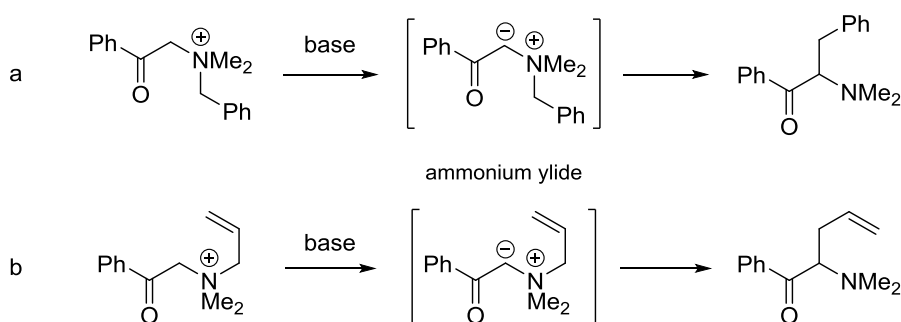


Scheme 13. Fukuyama's 2013 asymmetric synthesis of lysergic acid.

While there is a large number of varying approaches to the lysergic acid skeleton, the starting point generally involves having the indole portion of the skeleton (the A and B rings) already intact. Typically, the indole is protected with an electron-withdrawing group on the nitrogen and/or by reducing the indole to an indoline. Additionally, the amine is usually protected with an electron-withdrawing group in order to be carried through many steps in the synthesis. It has been found to be straightforward to obtain the correct diastereomer of lysergic acid, as epimerization of the stereocentre next to the acid under thermodynamic conditions leads to the correct stereochemistry of the product. However, obtaining the first stereocentre is quite a challenge, as noted in the five asymmetric syntheses. Chiral resolution, desymmetrization of a prochiral starting material, starting with a natural or unnatural amino acid, and using chiral auxiliaries are all the methods used to achieve enantioenrichment of the final product. Most

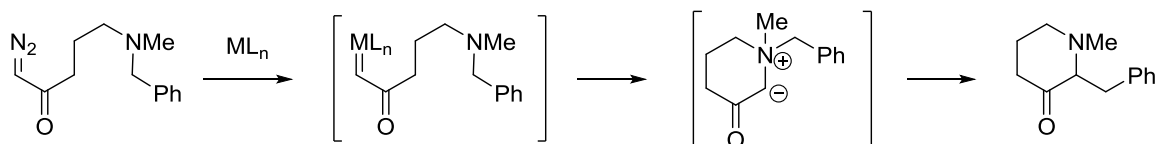
notable is the lack of catalytic asymmetric reactions applied to the synthesis of (+)-lysergic acid. This, as well as the large number of steps required to synthesize lysergic acid (especially in the case of asymmetric syntheses), shows that there is still a lot of room for improvement in designing a synthetic route towards lysergic acid and its derivatives.

Section 1.4: The Stevens [1,2]-Rearrangement and its Use in Synthesis



Scheme 14. (a) The first Stevens [1,2]-rearrangement, (b) the corresponding Stevens [2,3]-rearrangement.

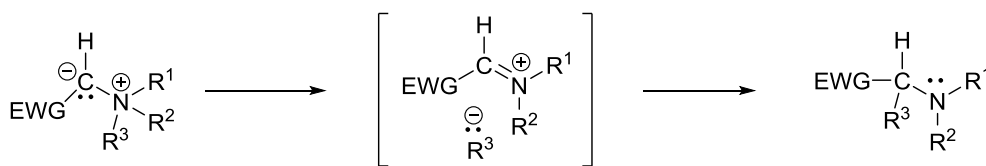
The Stevens [1,2]-rearrangement was discovered in 1928 during an attempted benzyl deprotection (Scheme 14a).¹⁰ Since its discovery, the Stevens rearrangement has also been shown to occur in a [2,3] fashion with allylic substituents on the starting ammonium salt (Scheme 14b); additionally, this rearrangement can occur on substrates in which the nitrogen is replaced with sulfur or oxygen, that is, via sulfonium and oxonium ylides.¹¹ In addition to formation via deprotonation of an ammonium salt, the ammonium ylide intermediate can also be formed via attack of an amine on a metallocarbene derived from a diazoketone (Scheme 15);¹² sulfonium and oxonium ylides can be formed in a similar manner.



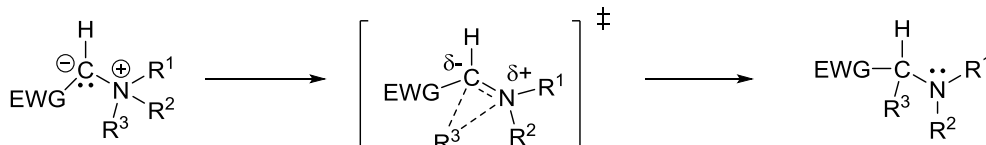
Scheme 15. The Stevens [1,2]-rearrangement starting from an amine-tethered diazoketone. “ML_n” refers to a metal (usually copper or rhodium) with any number of ligands.

Despite being an important, well-known reaction, the mechanism of the Stevens rearrangement has remained somewhat mysterious. Initially, after some crossover experiments by Stevens and coworkers that showed the reaction to proceed intramolecularly, an ionic mechanism was proposed (Scheme 16a).¹³ Further experiments such as CIDNP and solvent viscosity studies suggested a radical pair mechanism (Scheme 16c).¹⁴ It was noted, however, that the migrating group retained its stereochemical configuration, which was more consistent with a concerted, albeit symmetry forbidden, rearrangement (Scheme 16b).¹⁵

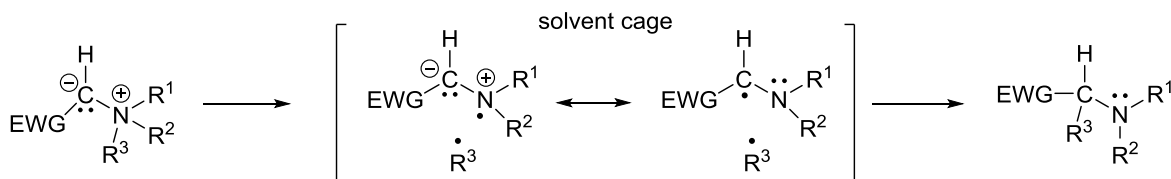
(a) Ionic Mechanism:



(b) Pericyclic Mechanism:



(c) Diradical Mechanism:



EWG = electron-withdrawing group, such as a ketone, ester, or aromatic group

R¹⁻³ = alkyl groups

Scheme 16. Proposed mechanisms for the Stevens [1,2]-rearrangement: (a) ionic, (b) pericyclic, and (c) diradical.

The first theoretical investigation of the mechanism of the Stevens rearrangement in 1974 by Dewar suggested that, due to the high exothermicity of the shift, a concerted mechanism may be possible via the breakdown of the Woodward-Hoffman rules.¹⁶ This first study could not, however, rule out a diradical mechanism. In the 1990s, Yates published several theoretical studies of the mechanism of the Stevens [1,2]-shift, finding that, for a few simple systems, including ammonium ylides stabilized by a carbonyl group, the radical pair mechanism was favoured to a large degree over a concerted or ionic mechanism; these studies were also the first to include the effects of solvation in the calculations.¹⁷ In 2000, Dai and coworkers used semi-

empirical calculations to support their theory that the Stevens rearrangement goes through a concerted “ π -complex transition state” in order to explain the retention of configuration of a chiral migrating group and other intramolecular properties of the reaction.¹⁸ An in-depth study of the Stevens rearrangement mechanism in many (albeit simple, Figure 2) systems by Ghigo in 2010 echoed Yates’ findings, though the migration of a phenyl group was found to proceed via a concerted mechanism.¹⁹ Ghigo’s study was also the first to try to explain the experimentally-observed retention of configuration of a chiral migrating group in a quantitative manner. The most recent study of the Stevens rearrangement by Singleton sought to understand why the Stevens [1,2]-rearrangement occurs often as a side reaction in the Stevens [2,3]-rearrangement.²⁰ Using both conventional computational methods and dynamic trajectory studies on a simple allyl-substituted system, they found that the [1,2]-shift may occur via the same transition state as the [2,3]-shift. While interesting, for this study, it was assumed that the [1,2]-shift occurs through a diradical mechanism and the [2,3]-shift occurs through a concerted mechanism; no other mechanisms for either of these reactions were considered.

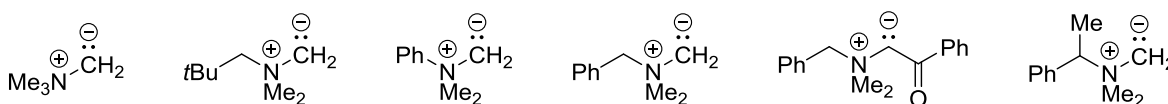
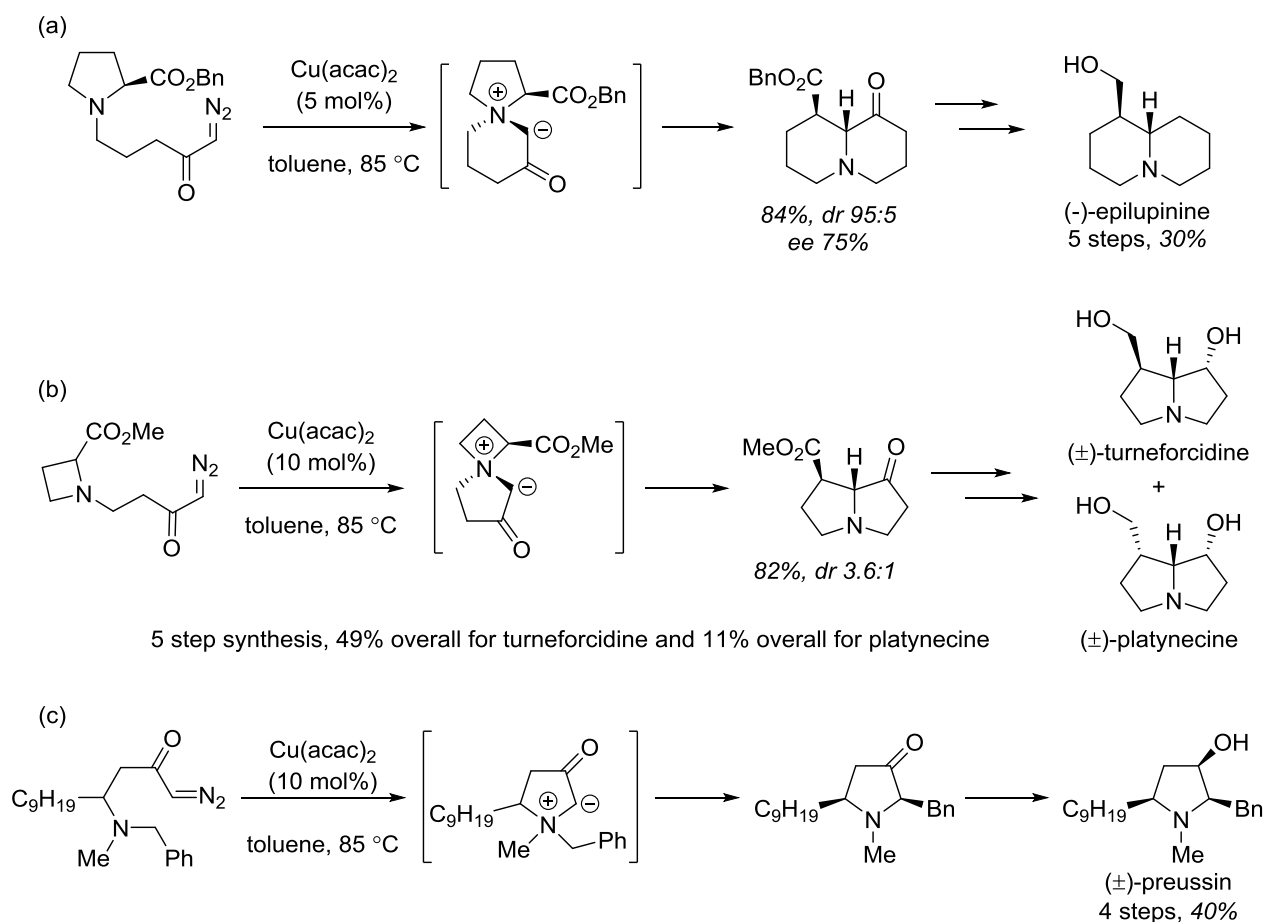


Figure 2. Ammonium ylides in Ghigo's study of the Stevens [1,2]-rearrangement mechanism.

Although the reaction mechanism is still somewhat controversial, the Stevens [1,2]-rearrangement has been found to be useful for small molecule synthesis.^{11,21} In terms of alkaloid natural product synthesis, the asymmetric total synthesis of (-)-epilupinine and the racemic total syntheses of turneforcidine and platynecine were achieved by the West group using the Stevens rearrangement as the key step (Scheme 17a,b).²² More recently, Burtoloso published the three-

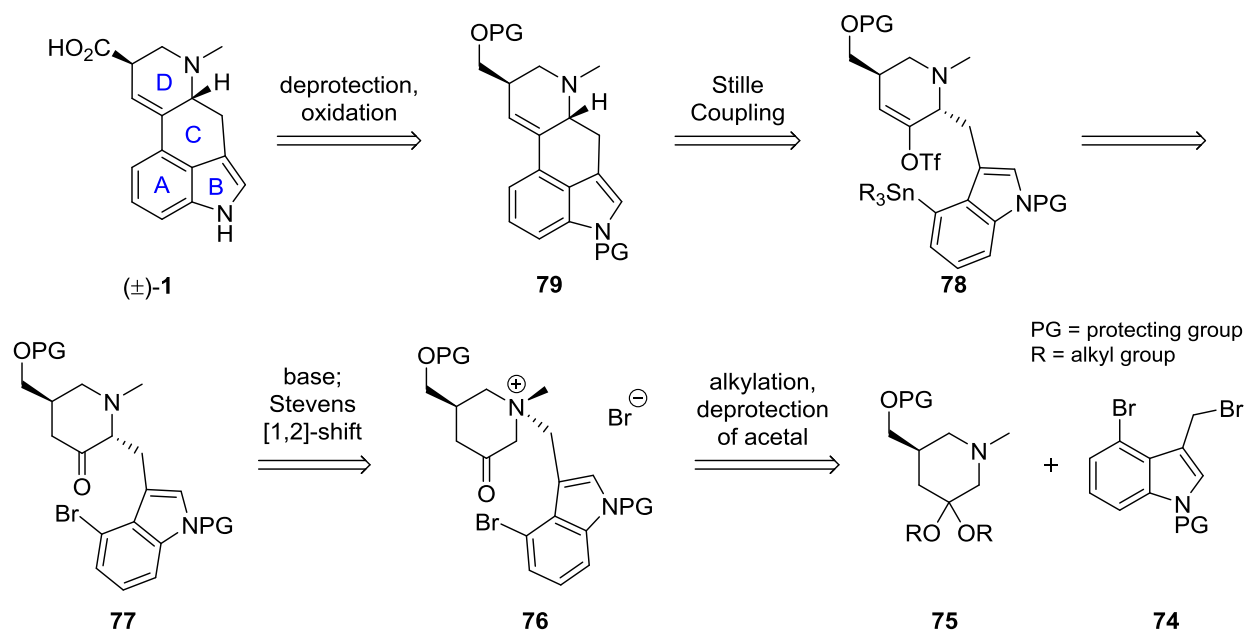
step racemic synthesis of preussin using the Stevens rearrangement (Scheme 17c).²³ While these are elegant syntheses of natural products with interesting structural features and medicinal importance, the complexity of these compounds is low. In order to show the usefulness of the Stevens [1,2]-rearrangement in complex natural product synthesis, as well as to probe its mechanism in a more complex setting, we proposed its use as the key step in two complementary syntheses of lysergic acid.



Scheme 17. Examples of the use of the Stevens [1,2]-rearrangement in natural product synthesis.

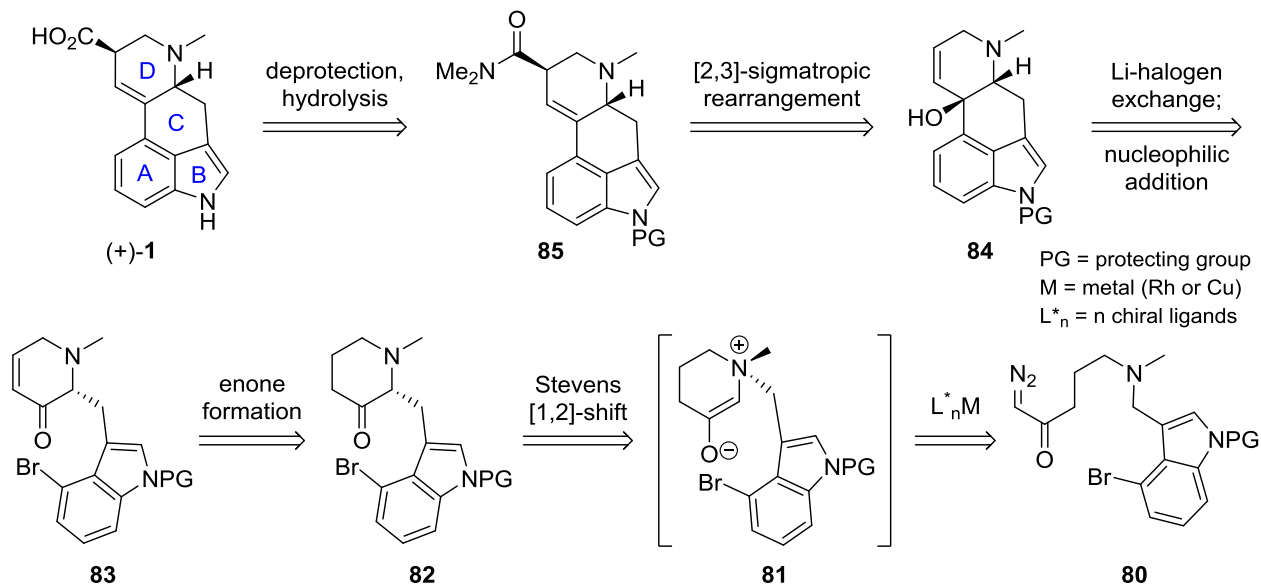
Section 1.5: Two Proposed Synthetic Routes to Lysergic Acid Using the Stevens [1,2]-Rearrangement of Ammonium Ylides

The first route we envisioned to synthesize lysergic acid utilizes the traditional method of ylide generation – deprotonation of a quaternary ammonium salt (Scheme 18). We planned to start with A, B, and D rings intact; we proposed the diastereoselective alkylation of piperidine derivative **75** (D ring) with known indole derivative **74** (A and B rings). Notably, if piperidine **75** could be made enantiopure, we could achieve one of the few asymmetric synthesis of lysergic acid. After removal of the acetal to reveal a ketone, ammonium salt **76** could be treated with base to form an ylide that would undergo a Stevens [1,2]-rearrangement. Based on previous work in pyrrolidine systems,²⁴ we presumed that the Stevens rearrangement would occur along the same face of the ring, setting the second of the two carbon stereocentres in the lysergic acid skeleton. From Stevens rearrangement product **77**, formation of the enol triflate and transformation of the aryl bromide into an organotin species would give intermediate **78**, which would then undergo a Stille coupling to close the C ring. Simple deprotection and oxidation of **79** would provide us with lysergic acid.



Scheme 18. First proposed retrosynthesis of lysergic acid using the Stevens rearrangement.

The second synthetic route we proposed using the Stevens [1,2]-rearrangement involves the more contemporary method of ylide generation – attack of an amine on a metallocarbene formed from a diazoketone (Scheme 19). The reaction to form a piperidone from a diazoketone tethered amine is known (in a racemic fashion) with a simple benzyl group (rather than an indole derivative as in intermediate **80**).¹² Our idea was to use an organometallic catalyst with chiral ligands to effect an asymmetric ylide formation/Stevens rearrangement; this would be quite a challenge, as an asymmetric Stevens [1,2]-rearrangement on an ammonium ylide has not yet been reported. With piperidone **82** in hand, a dehydrogenation would be performed to form **83**. A lithium-halogen exchange on the bromide followed by nucleophilic addition into the enone would close the C ring. An allylic transposition via a [2,3]-sigmatropic rearrangement of the allyl alcohol derivatized by the dimethylformamide dimethyl acetal would provide the dimethyl amide in the correct position with the correct stereochemistry. A simple deprotection and hydrolysis of the amide to the acid would give (+)-lysergic acid.



Scheme 19. Second proposed synthetic route towards lysergic acid using the Stevens [1,2]-rearrangement.

We chose to start with route 1, as the stepwise formation of the ammonium salt followed by base-induced ylide formation would allow us to isolate and fully characterize the ammonium salt, giving us a better idea of the identity of the species undergoing the Stevens rearrangement. This synthetic work is described in Chapter Two.

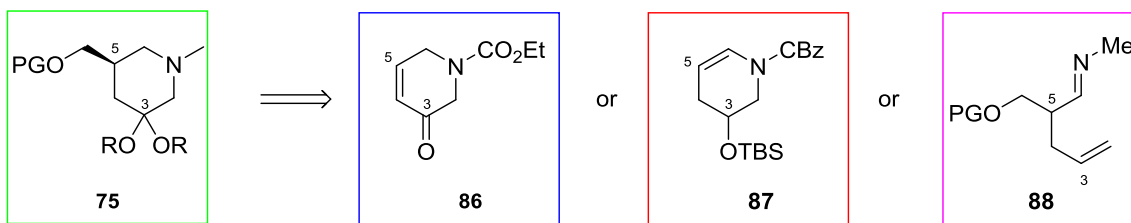
Chapter 2: Towards the Synthesis of Lysergic Acid

Section 2.1: Introduction

In order to demonstrate the utility of the Stevens [1,2]-rearrangement of ammonium ylides in complex natural product synthesis, we devised two syntheses of lysergic acid; one started with a chiral piperidine derivative, and one began with an acyclic diazoketone (Chapter 1, Section 1.5, Scheme 18 and Scheme 19). We chose our first route as a starting point due to the ability to isolate and characterize the intermediate ammonium salt, which we felt would provide us with more mechanistic insight into the Stevens rearrangement. The first task, then, was to synthesize the chiral piperidine derivative **75**.

Section 2.2: Choosing an Intermediate in the Synthesis of Piperidine Derivative 75

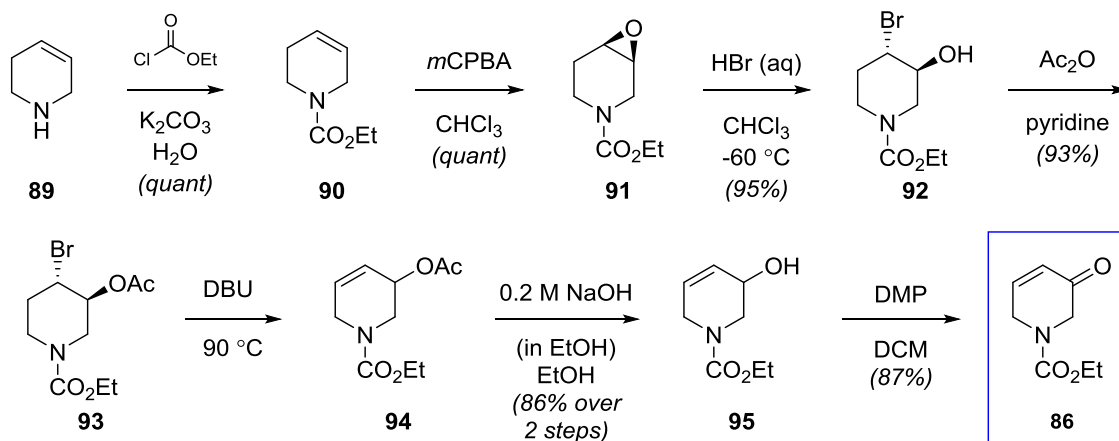
A literature search revealed three possible approaches to synthesizing piperidine **75** via intermediates **86**, **87**, and **88** (Scheme 20). The first two intermediates, enone **86** and enecarbamate **87**, were especially appealing due to the ability to easily create analogues of **75** with different substituents at the 5-position of the piperidine ring, a sought-after synthetic feature in drug development. Additionally, due to a large number of reports of asymmetric conjugate addition processes,²⁵ intermediate **86** could potentially allow an asymmetric synthesis of **75** (and its analogues) and, thus, an asymmetric synthesis of lysergic acid.



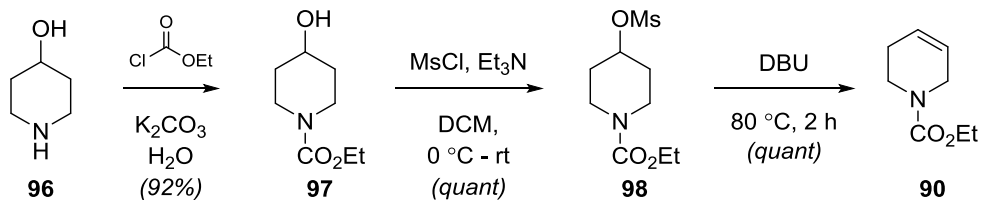
Scheme 20. Three possible intermediate targets in the synthesis of piperidine **75**.

Section 2.2.1: Synthesis of Enone **86**

The first intermediate studied was enone **86**. The synthesis of this compound was reported in 1982 by Imanishi and coworkers.²⁶ We modified their route slightly, using a DMP oxidation rather than a Jones oxidation to obtain the enone (Scheme 21). Additionally, as tetrahydropyridine **89** is very expensive, we opted to make intermediate **90** from 4-hydroxypiperidine **96** instead (Scheme 22). This unfortunately added two steps to an already lengthy route.

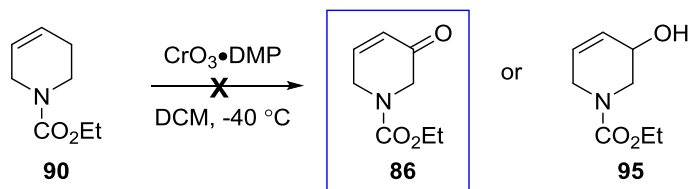


Scheme 21. Modified synthesis of enone **86** from tetrahydropyridine **89**.



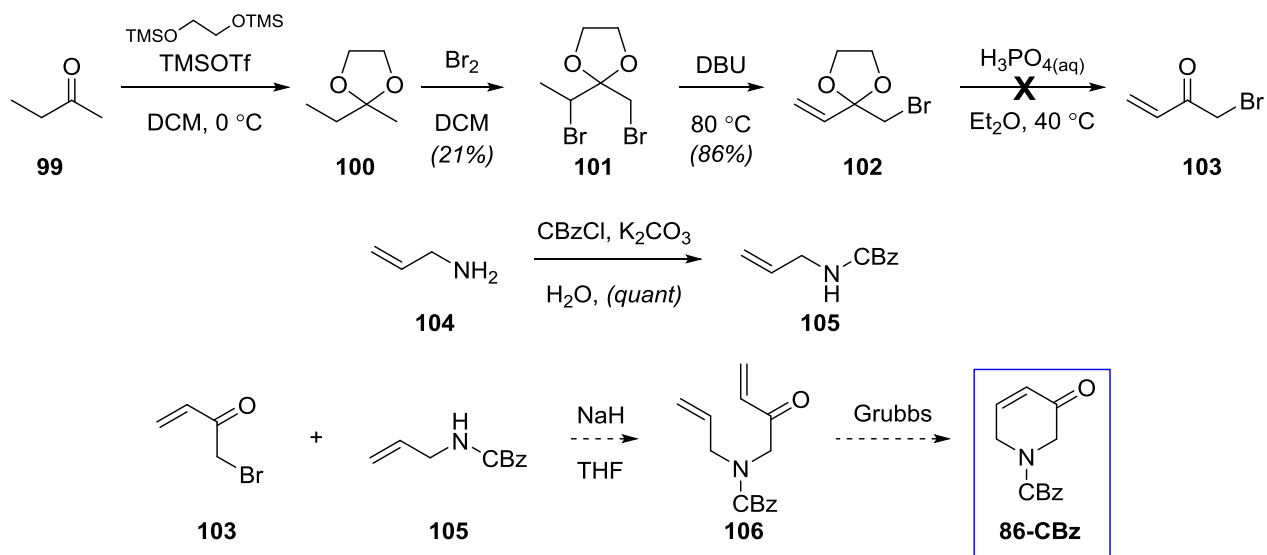
Scheme 22. Alternate synthesis of intermediate **90**.

In an attempt to shorten the synthesis of enone **86**, we first attempted an allylic oxidation on **90** to get to the allylic alcohol **95** or the enone directly using a method reported by Salmond,²⁷ but this reaction failed (Scheme 23). We realized quickly that there were many possible unproductive pathways through which tetrahydropyridine **90** could react, including aromatization or oxidation at the other allylic position, so no other allylic oxidations were attempted.



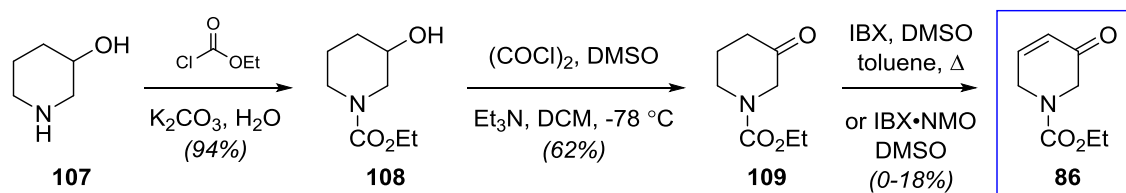
Scheme 23. Attempted allylic oxidation of protected tetrahydropyridine **90**.

We considered synthesizing **86-CBz** via a ring-closing metathesis reaction (Scheme 24). Unfortunately, while the synthesis of the CBz-protected allyl amine **105** was successful, the last step in the literature procedure²⁸ to form bromide **103** produced only an intractable mixture with no product visible in the crude ¹H NMR spectrum, so this route was abandoned.



Scheme 24. Attempted synthesis of bromide **103** and synthesis of amine **105** in order to form CBz-protected enone **86** via ring-closing metathesis.

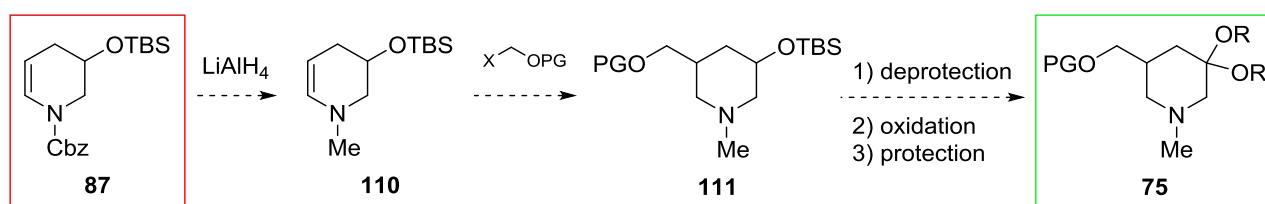
Our last attempt to shorten the route to enone **86** involved starting the protection and Swern oxidation of 3-hydroxypiperidine **107** to ketone **109** followed by a dehydrogenation to the enone (Scheme 25). Two different dehydrogenation reagents were tried: an IBX•DMSO complex and an IBX•NMO complex.²⁹ The IBX•DMSO complex gave us 18% yield once, but all subsequent attempts at this reaction resulted in only trace amounts of product. The IBX•NMO complex gave us none of the desired product. Thus, this route also had to be abandoned.



Scheme 25. Attempted synthesis of enone **86** via dehydrogenation of ketone **109**.

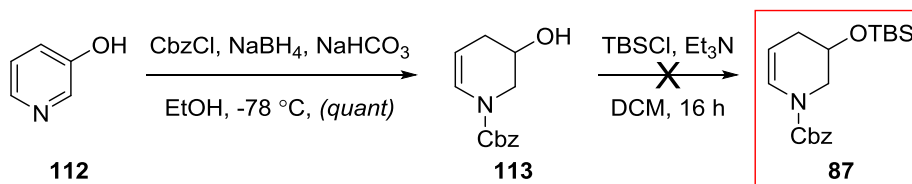
Section 2.2.2: Synthesis of Enecarbamate **87**

Because of the length of the route to reach enone **86**, we also looked at the possibility of synthesizing our piperidine intermediate via intermediate **87**. Our idea was to reduce the Cbz group to a methyl group, and then use enamine **110** as a nucleophile to add in our CH₂OPG group via the appropriate electrophilic reagent; then, deprotection followed by oxidation and acetal formation would get us to **75** (Scheme 26).



Scheme 26. Planned synthesis of piperidine **75** from intermediate **87**.

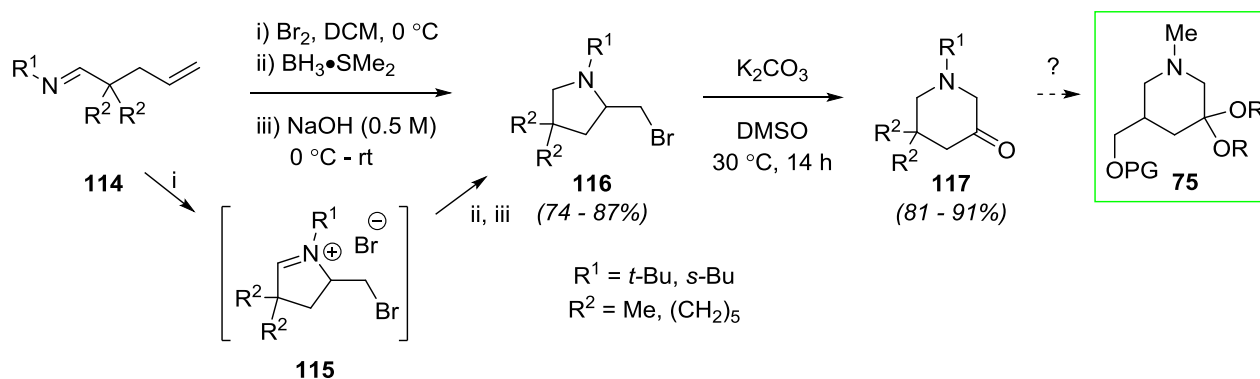
While the synthesis of intermediate **113** was successful, following a literature procedure by Ogasawara³⁰ to reduce 3-hydroxypyridine (**112**), TBS protection was unfortunately unsuccessful (Scheme 27). It is unclear as to whether or not the enecarbamate underwent side reactions or if the alcohol was eliminated to form the conjugated diene. Thus, this route was abandoned.



Scheme 27. Attempted synthesis of intermediate **80**.

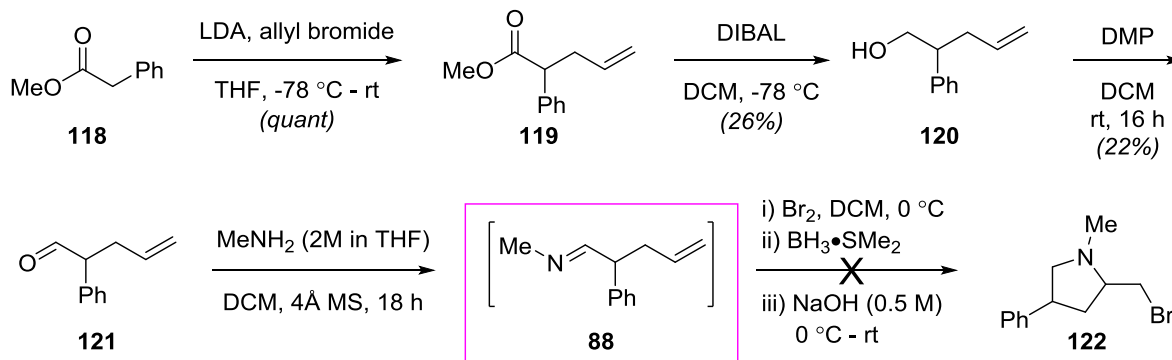
Section 2.2.3: Synthesis of Acyclic Imine **88**

Our last alternate intermediate for forming piperidine **75** was acyclic precursor **88**. This idea came about due to the literature report from the De Kimpe group on the synthesis of piperidinones **117** from imines **114** (Scheme 28).³¹ The structural similarities between **117** and our target **75** inspired us to pursue this strategy.



Scheme 28. De Kimpe's piperidinone synthesis.

We envisioned that it might be possible to enact a similar synthetic route with $R^1 =$ methyl and $R^2 =$ phenyl/hydrogen to get to a derivative of piperidine **75** with the CH_2OPG group replaced with phenyl. Unfortunately, the cyclization did not occur with these substituents (Scheme 29). We attribute this to the small substituent on the nitrogen (methyl vs. *tert*-butyl), as well as the lack of quaternary centre in the carbon chain. In light of this, it was unlikely that we were going to be able to synthesize piperidine **75** using such a route.

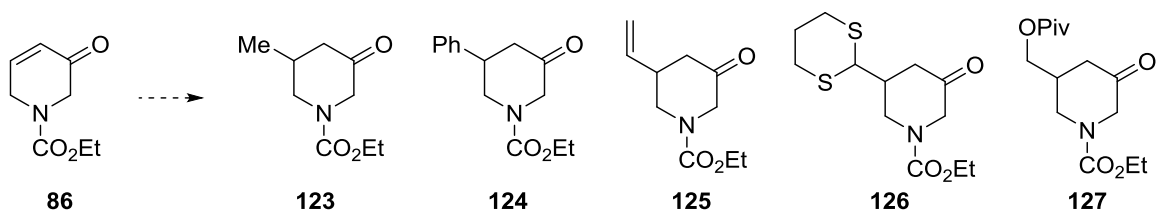


Scheme 29. Attempt to cyclize imine **88** to pyrrolidine **122**.

In the end, enone **86** was chosen as the intermediate with which to perform the synthesis of piperidine **75**, despite its inconveniently long synthetic route.

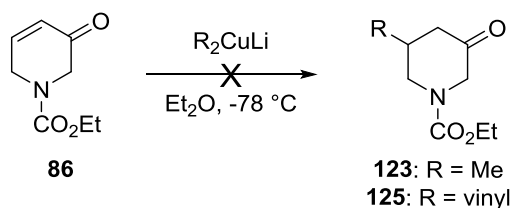
Section 2.3: Synthesis of Piperidine **75** from Enone **86**

As mentioned in the previous section, enone **86** was an appealing intermediate due to the ability to add in different substituents via conjugate addition to make different analogues of piperidine **75** and, thus, lysergic acid (see Chapter 1, Section 1.5, Scheme 18 for the planned retrosynthesis). Additionally, we also wanted to study how different substituents affect the diastereoselectivity of the subsequent Stevens rearrangement. The substituents targeted include methyl, phenyl, vinyl, dithiyl, and pivalomethyl (Scheme 30); the last four substituents were doubly important in that they could be converted to the acid in the lysergic acid endgame using simple transformations, such as oxidative cleavage in the case of **124** and **125** and deprotection/oxidation in the case of **126** and **127**.

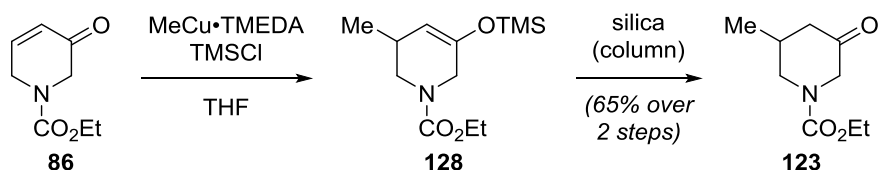


Scheme 30. Targeted conjugate addition products from enone **79**.

Dialkyl/alkenylcuprates were found to be unsuccessful in introducing alkyl or alkenyl groups to enone **86** (Scheme 31); this was likely due to difficulties forming these reagents and keeping them from decomposing before having a chance to react. However, a technique by Johnson³² using a milder, more stable organocopper reagent complexed with TMEDA allowed synthesis of methyl-substituted ketone **123** from enone **86** in good yield (Scheme 32).



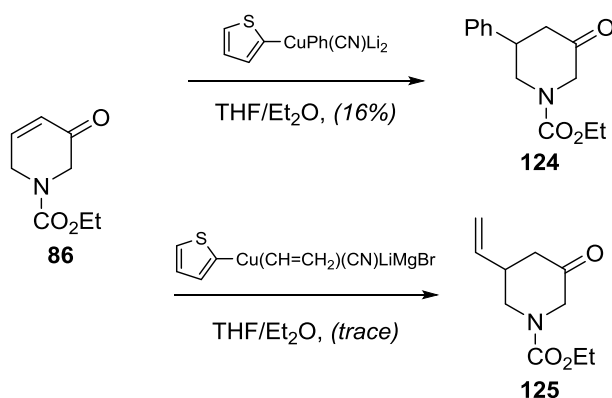
Scheme 31. Unsuccessful attempts at conjugate addition into enone **86** using cuprate reagents.



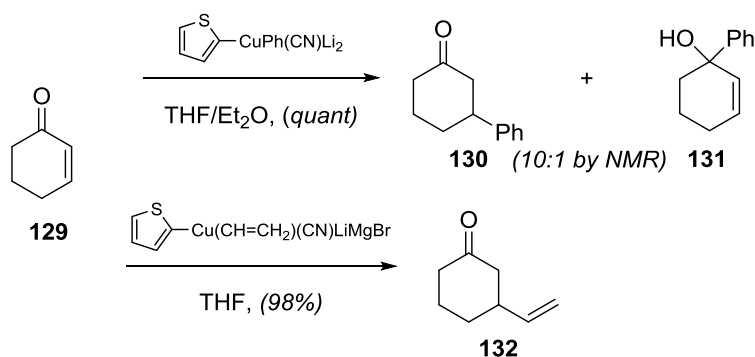
Scheme 32. Synthesis of methyl-substituted ketone **123**.

Due to the lack of success with dialkylcuprates, thienylcyanocuprate reagents were used to introduce phenyl and vinyl substituents, producing ketones **124** and **125** (Scheme 33).

Unfortunately, the yields were very low; in order to see if it was a problem with how the cuprate was made, this reaction was performed on cyclohexenone **120**. These reactions went in almost quantitative yield (Scheme 34), leading us to believe that the carbamate has a detrimental effect on the reactivity of **79** in conjugate additions; although we currently have no explanation for this effect, we feel that this would be worth looking into both experimentally and computationally.



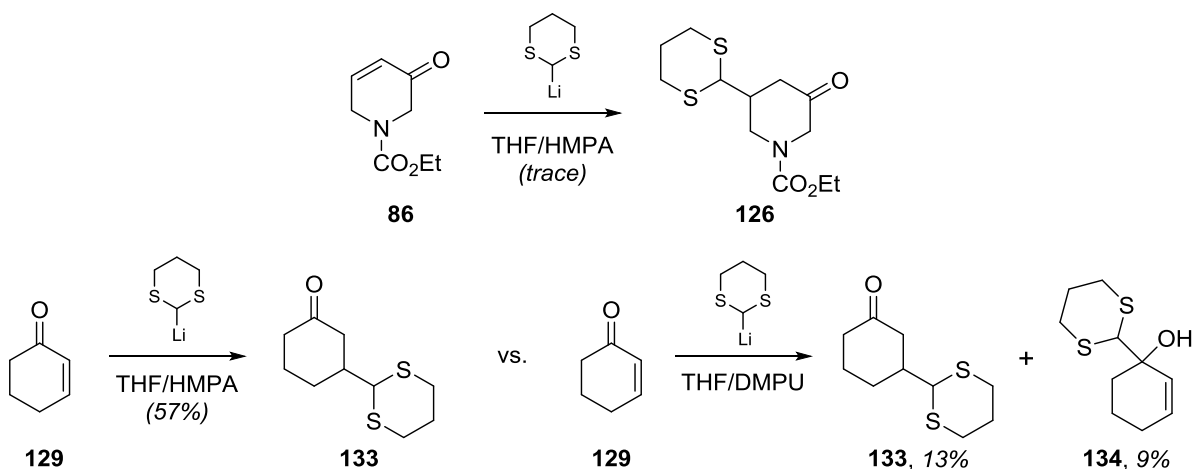
Scheme 33. Synthesis of phenyl- and vinyl-substituted ketones **124** and **125**.



Scheme 34. Phenyl- and vinylthienylcuprate addition to cyclohexenone **129**.

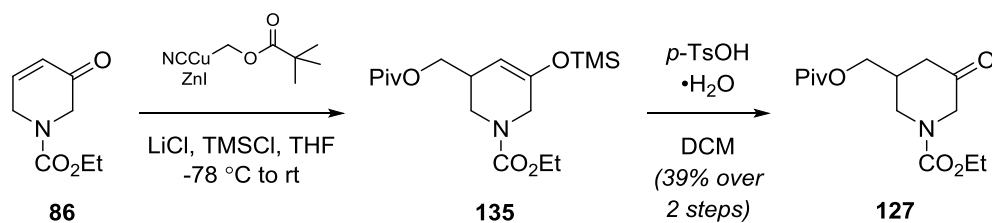
Similarly, a low yield of dithane-substituted ketone **126** prompted a test of the reaction conditions³³ on cyclohexenone **129**; once again, it was made clear that the carbamate of enone **86**

was hampering reactivity (Scheme 35). Note that, while the literature conditions include DMPU as the cosolvent, we found HMPA to give superior yields and selectivities.



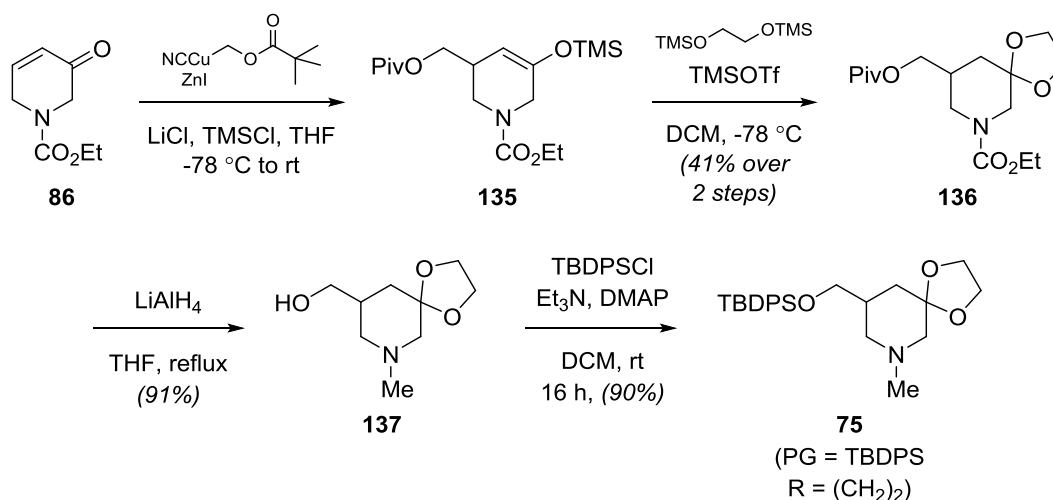
Scheme 35. Conjugate addition of lithium dithiane to enone **86** and cyclohexeneone **129**.

Knochel and coworkers found that an organozinc reagent containing an alpha heteroatom could be prepared; this milder zinc reagent then could be used to form an organocopper reagent that could perform conjugate additions on enones activated by TMSCl.³⁴ This conjugate addition procedure followed by acid-catalyzed hydrolysis of the resulting silyl enol ether allowed us to synthesize pivalomethyl-substituted ketone **127** quite readily (Scheme 36).



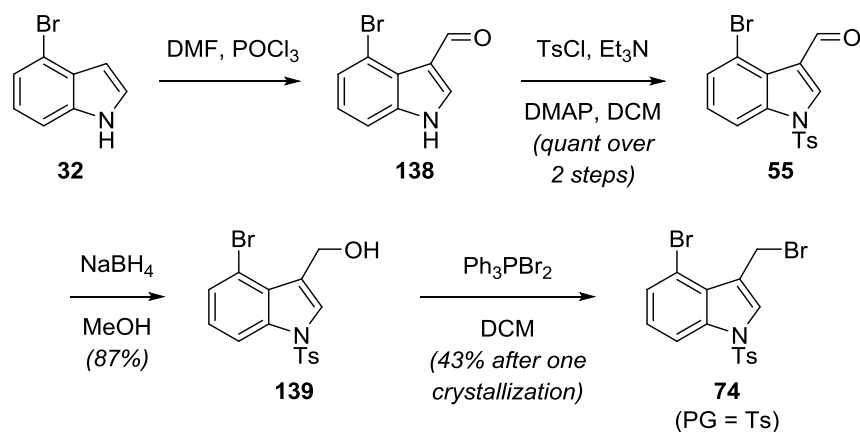
Scheme 36. Synthesis of ketone **127**.

Because of the presence of a protected primary alcohol in the correct position, silyl enol ether **135** was chosen to continue the synthetic route towards piperidine **75** (Scheme 37). It was discovered that cyclic acetal **136** could be formed directly from silyl enol ether **135** using Noyori's conditions³⁵ without having to transform it to ketone **127** first, providing a better yield and reducing the number of steps. A lithium aluminum hydride reduction removed the pivalate and reduced the carbamate to the desired *N*-methyl group. The alcohol was then protected as the *tert*-butyldiphenylsilyl ether to give piperidine derivative **75**.



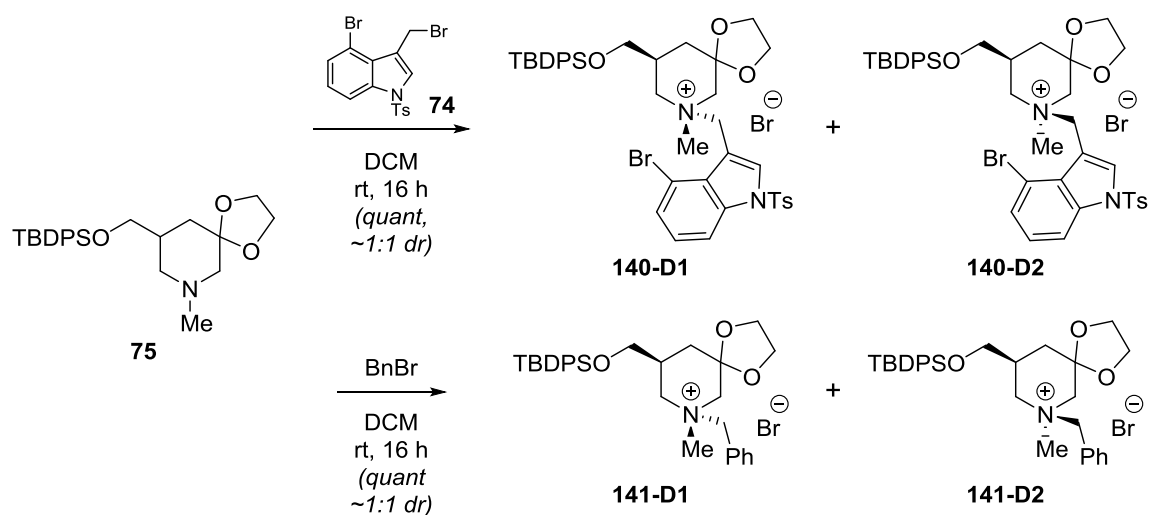
Scheme 37. Synthesis of piperidine **75** from enone **86**.

With piperidine **75** in hand, the next step was to perform the *N*-alkylation to form an ammonium salt that could undergo the Stevens rearrangement. The indole derivative necessary for the lysergic acid synthesis was synthesized in a reasonable yield using Fujii and Ohno's (Chapter 1, Section 1.3, Scheme 9) procedure with a *p*-toluenesulfonyl group as the protecting group on the nitrogen (Scheme 38).^{4f}



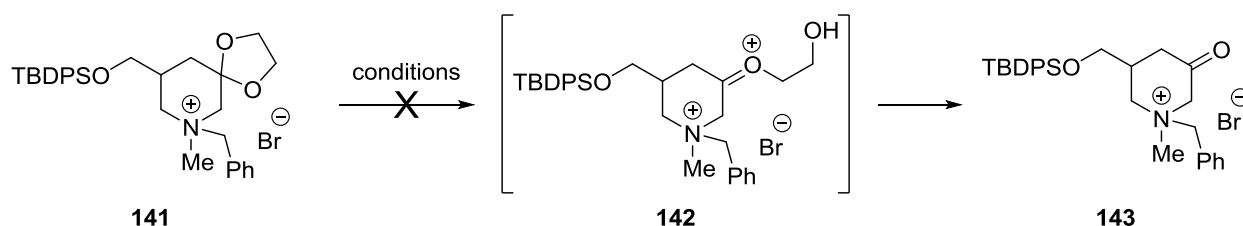
Scheme 38. Synthesis of indole derivative **74**.

The alkylation of piperidine **75** with indole derivative **74** proceeded in quantitative yield, but, unfortunately, with very little diastereoselectivity; using benzyl bromide rather than the piperidine derivative gave the same result (Scheme 39). Diastereomeric ratio was determined using ^1H NMR data. For both **140** and **141**, the two diastereomeric signals associated with the benzylic methylene on the nitrogen were well-resolved, so integration of these peaks was used to calculate *dr*.



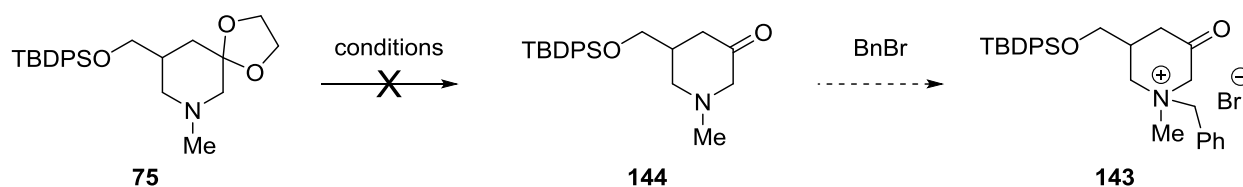
Scheme 39. Alkylation of piperidine **75**.

Despite this setback, we still wanted to observe what happens in the Stevens rearrangement. Unfortunately, no matter which conditions we tried on the benzylated piperidine **141**, the acetal could not be deprotected to provide the ketone necessary for the Stevens rearrangement; we suspect this may be due to unfavourable oxocarbenium ion formation adjacent to an already positively-charged nitrogen centre (Scheme 40). Deprotection conditions tried include: 1 M HCl in THF or acetone,³⁶ cerium(III) chloride heptahydrate and sodium iodide in refluxing acetonitrile,³⁷ thiourea in refluxing ethanol/water,³⁸ PPTS in refluxing acetone/water,³⁹ 80% acetic acid in water at 65 °C,⁴⁰ sodium periodate and sulfuric acid in dioxane,⁴¹ triphenylcarbenium tetrafluoroborate in DCM,⁴² titanium tetrachloride in ether,⁴³ triphenylphosphine and carbon tetrabromide in THF,⁴⁴ and variations thereof.



Scheme 40. Failed deprotection attempts on piperidinium salt **141**.

Due to the failure to deprotect our acetal, we had to come up with a different strategy to synthesize our Stevens rearrangement precursor. The attempt was made to deprotect first and then alkylate (Scheme 41), but this was likewise unsuccessful, this time likely due to the inherent instability of 3-piperidones; it was noted previously in the West group that treatment with HCl gas to form an ammonium salt was necessary to prevent decomposition long enough to get an elemental analysis on Stevens rearrangement products containing a 3-piperidone moiety.¹² A new protection scheme was sought for our piperidine precursor.



Scheme 41. Failed deprotection attempts on piperidine **75**.

Section 2.4: Alternate Route to Obtain Piperidine Derivative 147

Instead of protecting the ketone of our Stevens rearrangement precursor analogue **143** as an acetal, we thought we could transform the ketone of conjugate addition product **127** into an alkene; this way, we could perform an oxidative cleavage to obtain ketone **143**. Although the yield on the initial Wittig reaction to obtain alkene **145** was a bit low, the rest of the steps were quite successful to get to piperidinium salt **148** (Scheme 42). Initially, a two step sequence of osmium tetroxide-mediated dihydroxylation of alkene **148** followed by sodium periodate cleavage to ketone **143** was attempted, but this approach was unsuccessful; thus, ozonolysis was employed. This did, unfortunately, give us a mixture of desired ketone **143**, hydrate **143a**, and hemiacetal **143b**. A Stevens rearrangement was attempted on this mixture using potassium *tert*-butoxide at 0 °C in THF, but no product could be isolated; a Stevens rearrangement has yet to be attempted on the pure ketone **143**.

Section 2.5: Summary and Future Plans

We have made significant progress towards lysergic acid via our first proposed synthetic route (Chapter 1, Scheme 18). We have successfully synthesized an analogue of the key Stevens rearrangement precursor **75**, piperidinium salt **143** (Scheme 42). Additionally, our conjugate addition approach to synthesizing piperidines **75** and **147** (Scheme 42) allows for creation of many analogues with different substituents at the 5-position, as demonstrated in the synthesis of conjugate addition products **123** to **127** (Scheme 30) and phenyl-substituted alkene **149**, as well as the potential for the synthesis of enantioenriched intermediates via asymmetric conjugate addition reactions.

In the course of these synthetic studies, we have discovered a deficiency in the chemical literature; that is, our current knowledge of the stereochemical course of piperidine alkylation provides little insight into our quest to form only one diastereomer of piperidinium salt **148**. Consequently, we opted to study this reaction much more in depth; this is the subject of Chapters 3 and 4 of this thesis. With more knowledge about this reaction, we can hopefully find reaction conditions that will allow us to synthesize our intermediate ammonium salt with greater diastereoselectivity. This discovery emphasizes the importance of natural product synthesis not just as a means to an end but also as an arena for the study of chemical reactivity.

An additional setback encountered during the course of these synthetic studies was the difficulty in installing the ketone in the piperidine ring; oxidative cleavage could only be effected using ozonolysis, but this gave us a mixture of ketone, hydrate, and methoxy hemiacetal that failed to provide the Stevens rearrangement product. If we can figure out how to produce only ketone in the reaction, isolate just the ketone, or convert the hydrate and hemiacetal back to the

ketone, we can hopefully perform a successful Stevens rearrangement and continue with our synthesis.

Once we have tested the rest of the reactions in this route, piperidine **147** will be made in an enantioselective fashion using an asymmetric conjugate addition to enone **86**. This way, our first route can be transformed into one of the few enantioselective syntheses of lysergic acid, and the only one that, rather than starting with a key stereocentre or performing a chiral resolution, uses an asymmetric reaction to install the first stereocentre.

Progress towards lysergic acid via our second proposed route (Chapter 1, Scheme 19) has consisted mainly of the repetition of a literature reaction, namely, that shown in Chapter 1, Scheme 15. Although we have not made significant progress, this route remains the most promising in terms of providing a short, asymmetric synthesis of lysergic acid. Many chiral catalysts and varying reaction conditions will need to be screened; however, if we can find the right conditions, we will have succeeded in achieving an asymmetric Stevens [1,2]-rearrangement of an ammonium ylide, which is still unprecedented in the literature. Study of this reaction has the potential to add significantly to the state of knowledge in organic synthesis and physical organic chemistry.

Section 2.6: Experimental

Section 2.6.1: General Methods

All chemicals were purchased from Sigma-Aldrich, Fluka, Caledon, or Alfa Aesar and used as received unless stated otherwise. For flash chromatography, technical grade solvents were used without further purification. For reactions, dichloromethane was distilled from

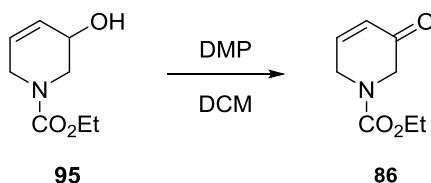
calcium hydride under an atmosphere of argon. Diethyl ether and tetrahydrofuran were distilled from sodium/benzophenone under an atmosphere of argon.

Reactions were magnetically stirred and monitored by TLC unless otherwise stated. Chromatographic purification was performed as flash chromatography (Silicycle SiliFlash® F60 silica gel) using the solvents indicated as eluent with 0.3-0.5 bar pressure. Thin layer chromatography (TLC) was performed on Merck silica gel 60 F254 TLC glass plates and visualized with UV light and potassium permanganate stain. The yields given refer to purified compounds unless otherwise stated.

^1H and ^{13}C NMR spectra were recorded on Agilent/Varian DD2 MR (400 MHz), Agilent/Varian Inova (300 MHz, 400 MHz, or 500 MHz), Agilent/Varian Mercury (400 MHz), or Agilent/Varian VNMRS (500 MHz) spectrometers in the solvents indicated. All signals are reported in ppm relative to the internal chloroform signal at 7.26 ppm or 77.0 ppm or the internal methanol signal at 3.31 ppm or 49.0 ppm as standard. The data are being reported as (s=singlet, d=doublet, t=triplet, q=quadruplet, m=multiplet or unresolved, br=broad signal, app = apparent, coupling constant(s) in Hz, integration). Infrared spectra were recorded on a Matteson Galaxy Series FT-IR 300 spectrophotometer as thin films. Absorptions are given in wavenumbers (cm^{-1}). Mass spectrometric measurements were performed as high resolution ESI measurements on an Agilent Technologies 6220 oaTOF high-resolution mass spectrometer or high resolution EI measurements on an Agilent Technologies 5975C MSD high-resolution mass spectrometer.

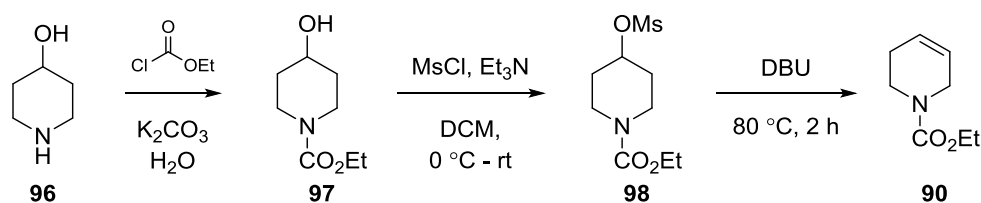
Section 2.6.2: Experimental Procedures

DMP oxidation of allyl alcohol **95** to enone **86**:



Freshly-prepared⁴⁵ Dess-Martin Periodinane (DMP) (1.128 g, 2.66 mmol) was added to a 100 mL round bottom flask fitted with Teflon stir bar, septum, and argon inlet. Dichloromethane (26.4 mL, 0.10 M) was added to the flask and stirred to form a slurry of DMP. Allyl alcohol **95** (0.310 g, 1.81 mmol; prepared as per Imanishi's procedure²⁶) was dissolved in dichloromethane (11.7 mL, 0.15 M) and transferred via cannula into the DMP slurry. The flask was covered with aluminum foil to prevent decomposition of the enone and stirred overnight at room temperature. Saturated aqueous sodium bicarbonate solution (40 mL) was added and the organic layer separated. The aqueous layer was extracted twice more with dichloromethane (2 x 40 mL), and the combined organic layers were dried over anhydrous magnesium sulfate, filtered, and the solvent removed *in vacuo* to give a red-orange oil. The crude oil was then purified via column chromatography using 30% ethyl acetate:hexanes (the enone has an R_f of 0.33 in 50% ethyl acetate:hexanes) to give enone **86** as a colourless oil (0.266 g, 87%). Characterization data matched that previously reported.²⁶

Protection of 4-hydroxypiperidine, mesylation, and elimination to give protected tetrahydropyridine **83**:



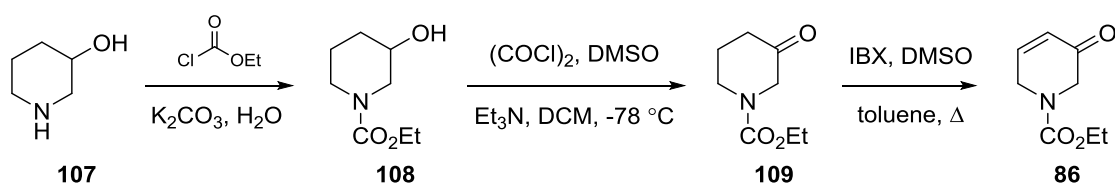
4-Hydroxypiperidine (5.105 g, 50.5 mmol; purchased from Sigma-Aldrich) was dissolved in water (11 mL, 4.7 M) in a 50 mL round bottom flask equipped with a stir bar. The flask was placed in a 0 °C ice bath, and ethyl chloroformate (5.2 mL, 54.4 mmol) was added dropwise while rapidly stirring the reaction mixture. Potassium carbonate (7.540 g, 54.6 mmol) was then added portionwise to this mixture over 5 min, and the ice bath was removed. After 1.5 h, diethyl ether (20 mL) was added to the reaction mixture. The organic and aqueous layers were separated, and the aqueous layer was extracted twice more with ether (2 x 20 mL). The combined organic layers were then dried over anhydrous magnesium sulfate, filtered, and the solvent removed *in vacuo* to give alcohol **97** as a colourless oil (8.066 g, 92%); further purification was deemed unnecessary based on the crude ¹H NMR spectrum.

Alcohol **97** (8.066 g, 46.6 mmol) was dissolved in dichloromethane (47 mL, 1.0 M) in a 250 mL round bottom flask equipped with a stir bar, septum, and argon inlet. Triethylamine (10 mL, 72 mmol) was added, and the reaction flask was placed in a 0 °C ice bath. Methanesulfonyl chloride (4.0 mL, 52 mmol) was added dropwise and the ice bath removed. The reaction mixture was stirred overnight, followed by addition of saturated aqueous sodium bicarbonate solution (50 mL). The organic and aqueous layers were separated, and the aqueous layer was extracted two more times with dichloromethane (2 x 50 mL). The combined organic layers were washed with saturated sodium chloride solution (150 mL), dried over anhydrous magnesium sulfate, filtered,

and the solvent removed *in vacuo* to give mesylate **98** as an orange oil (11.928 g, >100% yield (due to some solvent impurities)). The crude mesylate was also used in the next reaction without further purification.

Mesylate **98** (11.7 g, 46.6 mmol) and 1,8-diazabicyclo[5.4.0]undec-7-ene (13.2 mL, 88.3 mmol) were stirred together in a 50 mL round bottom flask equipped with stir bar and condenser. This mixture was heated to 80 °C for 2 h. After allowing the reaction mixture to cool to room temperature, diethyl ether (50 mL) and water (50 mL) were added. The organic and aqueous layers were separated, and the aqueous layer was extracted once more with diethyl ether (50 mL). The combined organic layers were washed with 1 M HCl aqueous solution (100 mL), dried over anhydrous magnesium sulfate, filtered, and the solvent removed *in vacuo* to give tetrahydropyridine **90** as a colourless oil (7.216 g, 100%). This material was deemed suitable for use in subsequent reactions without further purification, and the characterization data matched that previously reported.²⁶

Protection, oxidation, and dehydrogenation of 3-hydroxypiperidine to give enone **79**:



3-Hydroxypiperidine (0.9834 g, 9.72 mmol; purchased from Sigma-Aldrich) was dissolved in water (4.2 mL, 2.3 M) in a 25 mL round bottom flask equipped with a stir bar. The flask was placed in a 0 °C ice bath, and ethyl chloroformate (1.05 mL, 10.5 mmol) was added dropwise while rapidly stirring the reaction mixture. Potassium carbonate (1.780 g, 12.9 mmol) was then added portionwise to this mixture over 2 min, and the ice bath was removed. After 1.5

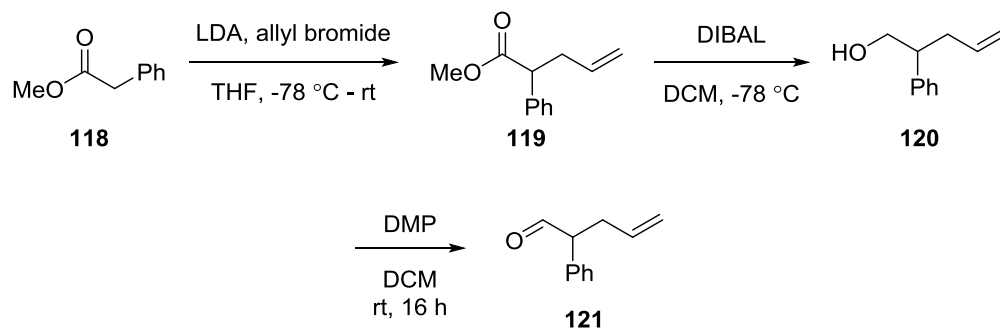
h, diethyl ether (10 mL) was added to the reaction mixture. The organic and aqueous layers were separated, and the aqueous layer was extracted twice more with ether (2 x 10 mL). The combined organic layers were then dried over anhydrous magnesium sulfate, filtered, and the solvent removed *in vacuo* to give alcohol **108** as a colourless oil (1.586 g, 94%); this was used in the next reaction without further purification.

Oxalyl chloride (0.95 mL, 11 mmol) was dissolved in dichloromethane (70 mL, 0.16 M) in a round bottom flask equipped with a stir bar, septum, and argon inlet. The flask was placed in a -78 °C dry ice/acetone bath, and dimethylsulfoxide (1.4 mL, 20 mmol) was added dropwise. This mixture was stirred for 5 min, and then alcohol **108** (1.586 g, 9.16 mmol) dissolved in dichloromethane (30 mL, 0.31 M) was transferred via cannula into the reaction mixture. The reaction mixture was stirred for 1 h, and then triethylamine (5.3 mL, 38 mmol) was added dropwise via syringe. The ice bath was removed and the reaction mixture allowed to warm up to room temperature over 3 h. Saturated aqueous ammonium chloride solution (100 mL) was added, and the organic and aqueous layers separated. The organic layer was washed once more with a mixture of saturated aqueous ammonium chloride and sodium chloride solutions (100 mL), dried over anhydrous magnesium sulfate, filtered, and the solvent evaporated *in vacuo* to give crude ketone **109**. The crude ketone was chromatographed using 20-30% ethyl acetate:hexanes ($R_f = 0.41$ in 50% ethyl acetate:hexanes) to give pure ketone **109** as a colourless oil (0.975 g, 62%). Characterization data matched that previously reported.⁴⁶

Ketone **109** (2.652 g, 15.5 mmol) was dissolved in a mixture of dimethylsulfoxide and toluene (1:2, 150 mL, 0.10 M) in a 500 mL round bottom flask equipped with a stir bar and condenser with a septum and argon inlet. Freshly-prepared⁴⁷ 2-Iodoxybenzoic acid (5.570 g, 20.0 mmol) was added, and the mixture was heated to 55 – 75 °C for 24 hours. After allowing the

reaction mixture to cool to room temperature, diethyl ether (100 mL) was added, and the organic layer was washed with saturated aqueous sodium bicarbonate solution (2 x 200 mL), water (200 mL), and saturated aqueous sodium chloride solution (200 mL). The organic layer was then dried over anhydrous magnesium sulfate, filtered, and the ether was evaporated *in vacuo*; due to the volatility of the product, toluene was evaporated by flushing the flask with air rather than rotary evaporation. The crude product was filtered through a silica gel plug, first with hexanes (5 mL) to remove toluene followed by 30% ethyl acetate in hexanes (100 mL) to recover the product. This method gave the still slightly impure enone **86** (0.459 g, 17%). The characterization data matched that previously reported.²⁶

Synthesis of aldehyde **121**:



Diisopropylamine (1.2 mL, 8.6 mmol) was dissolved in tetrahydrofuran (9 mL, 1 M) in a flame-dried 50 mL round bottom flask equipped with a stir bar, septum, and argon inlet. The flask was placed in a -78 °C dry ice/acetone bath, and *n*-butyllithium (3.4 mL, 2.5 M in di-*tert*-butyl ether, 8.5 mmol) was added dropwise. After 20 min, the reaction flask was transferred to a 0 °C ice bath. After 30 min, the flask was transferred back to the -78 °C dry ice/acetone bath. Methyl phenylacetate (1.0 mL, 7.1 mmol) dissolved in tetrahydrofuran (2.0 mL, 3.6 M) was transferred via cannula into the reaction mixture. After 30 min, the reaction mixture was

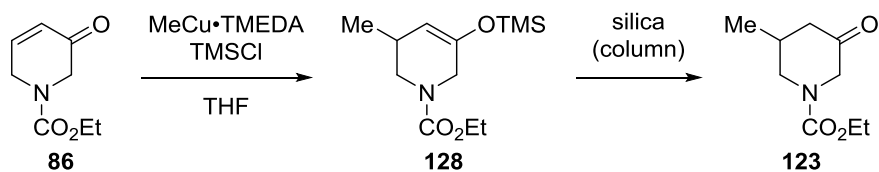
transferred to a 0 °C ice bath and stirred for an additional 30 min. Allyl bromide (0.70 mL, 8.1 mmol) was then added, and the reaction mixture was left to warm up to room temperature overnight while stirring. The reaction mixture was quenched with saturated aqueous ammonium chloride solution (20 mL) and extracted with ethyl acetate (2 x 20 mL). The organic layer was dried over anhydrous magnesium sulfate, filtered, and the solvent evaporated *in vacuo*. The crude residue was then dissolved in hexanes and filtered again through Celite to remove the remaining diisopropylammonium salts. The hexanes solution was evaporated *in vacuo* to give ester **119** as a colourless oil (1.527 g, >100% (with some solvent impurities)). Further purification was deemed unnecessary, and the characterization data matched that previously reported.⁴⁸

Ester **119** (7.1 mmol) was dissolved in dichloromethane (18 mL, 0.39 M) in a 50 mL round bottom flask equipped with a stir bar, septum, and argon inlet. This flask was placed in a -78 °C dry ice/acetone bath, and diisobutylaluminum hydride (8 mL, 1 M in DCM, 8 mmol) was added via syringe over about 12 minutes. After 1 h of stirring the reaction mixture at -78 °C, the reaction was quenched with acetone (2.0 mL, 27 mmol) and aqueous hydrochloric acid solution (1 M, 8 mL). After letting the reaction mixture warm up overnight, the organic layer was separated and the aqueous layer extracted twice more with dichloromethane (2 x 30 mL). The combined organic layers were washed with saturated aqueous sodium bicarbonate solution (100 mL), dried over anhydrous magnesium sulfate, filtered, and the solvent removed *in vacuo*. Column chromatography using 5% ethyl acetate:hexanes gave a mixture of aldehyde **121** and ester **119** (0.847 g; both compounds had the same R_f of 0.6 in 10% ethyl acetate:hexanes); flushing the column with 50% ethyl acetate:hexanes gave alcohol **120** (R_f ~0.1 in 10% ethyl

acetate:hexanes) as a colourless oil (0.301 g, 26%). Characterization data for alcohol **120** matched that previously reported.⁴⁹

Alcohol **120** (0.301 g, 1.86 mmol) was dissolved in dichloromethane (9 mL, 0.2 M) in a 25 mL round bottom flask equipped with a stir bar, septum, and argon inlet. Dess-Martin Periodinane (0.897 g, 2.11 mmol) was added, and the reaction mixture was stirred for 4.5 h. The solvent was then removed *in vacuo*, and diethyl ether was added (20 mL). The solid was filtered off, and the filtrate was washed with saturated sodium bicarbonate solution (2 x 20 mL). The organic layer was dried over anhydrous magnesium sulfate, filtered, and the solvent removed *in vacuo*. Column chromatography in 2.5% ethyl acetate:hexanes gave aldehyde **121** as a colourless oil (0.067 g, 22%). Characterization matched that previously reported.⁵⁰

Conjugate addition of methylcopper species into enone **86** to form ketone **123**:



Copper(I) iodide (0.315 g, 1.65 mmol, purified as per “Purification of Laboratory Chemicals”⁵¹ and dried under heat and vacuum) was added to a flame-dried 50 mL round bottom flask equipped with a stir bar, septum, and argon inlet. Anhydrous tetrahydrofuran (3.3 mL, 0.5 M) was added, and the mixture was stirred to form a slurry. *N,N,N',N'*-tetramethylethylenediamine (distilled over calcium hydride) (0.72 mL, 4.8 mmol) was added, and the mixture was cooled to -78 °C in an acetone/dry ice bath. Methyl lithium (1.3 mL, 1.3 M in diethyl ether, 1.7 mmol) was added dropwise, resulting in a colour change from dark green-brown to bright yellow with formation of a precipitate. After 30 min, chlorotrimethylsilane (0.50 mL, 3.9 mmol; distilled over calcium hydride) was added, followed by addition of enone **86**

(0.266 g, 1.57 mmol, 1.00 equiv.) in tetrahydrofuran (1.6 mL, 1.0 M) via cannula. After stirring for 1.5 h, the reaction mixture was quenched with saturated aqueous ammonium chloride solution (10 mL) and removed from the ice bath. Once warmed up to room temperature, the reaction mixture was extracted with diethyl ether (3 x 15 mL portions). The organic layers were combined and washed sequentially with saturated aqueous ammonium chloride solution (50 mL) and saturated aqueous sodium bicarbonate solution (50 mL), dried over anhydrous magnesium sulfate, filtered, and evaporated *in vacuo*. The crude TMS-enol ether **128** was re-dissolved in dichloromethane (5 mL) and stirred with p-toluenesulfonic acid monohydrate (~5 mg; recrystallized from ethanol/water) for 1.5 hours. The reaction was quenched with saturated aqueous sodium bicarbonate solution (5 mL). The organic layer was separated, and the aqueous layer was extracted with dichloromethane (2 x 5 mL portions). The organic layers were combined, dried over anhydrous magnesium sulfate, and filtered, followed by evaporation of the solvent under reduced pressure. Column chromatography using 25% ethyl acetate:hexanes with ~1% triethylamine (R_f of 0.46 in 50% ethyl acetate:hexanes) gave 0.140 g (48% yield) of ketone **123** as a colourless oil.

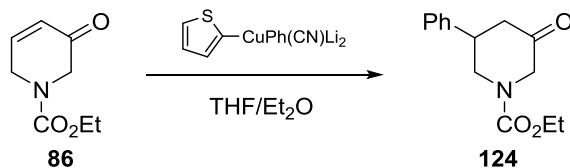
^1H NMR (400 MHz, CDCl_3): δ 4.11-4.04 (m, 3H), 3.89-3.78 (m, 2H), 3.00-2.95 (m, 1H), 2.50 (br d, $J = 12$ Hz, 1H), 2.15-2.02 (m, 2H), 1.20 (t, $J = 8$ Hz, 3H), 0.98 (d, $J = 7$ Hz, 3H).

^{13}C NMR (125 MHz, CDCl_3): δ 205.1, 155.3, 61.8, 53.6, 49.0, 46.7, 29.5, 18.7, 14.6.

IR(cast film, CDCl_3): 2926, 2933, 1704, 1460, 1428, 1273, 1224, 1207, 1121, 1015 cm^{-1} .

High Resolution EI-MS calculated for $\text{C}_9\text{H}_{15}\text{NO}_3$ (M^+) m/z : 185.1052; found m/z : 185.1050.

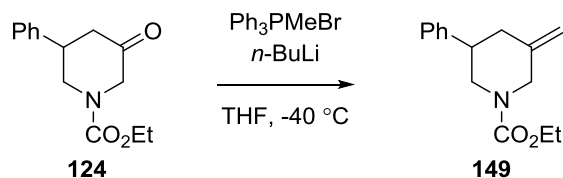
Conjugate addition of phenylthienylcyanocuprate into enone **86** to form ketone **124**:



Thiophene (0.13 mL, 1.6 mmol, freshly distilled from calcium hydride) was added to a 25 mL flame-dried round bottom flask equipped with stir bar, septum, and argon inlet. Tetrahydrofuran was added (1.0 mL, 1.6 M), and the flask was placed in a -78 °C dry ice/acetone bath. *n*-Butyllithium (0.80 mL, 1.9 M in hexanes, 1.5 mmol) was added dropwise, and the reaction flask was moved to an ice/brine bath (~ -10 °C). Copper(I) cyanide (0.146 g, 1.63 mmol, purified as per “Purification of Laboratory Chemicals”⁵¹ and dried under heat and vacuum) was added to a 50 mL flame-dried round bottom flask equipped with stir bar, septum, and argon inlet. Diethyl ether (1.5 mL, 1.1 M) was added, and vigorous stirring formed a slurry. This flask was placed in a -78 °C ice bath, and the lithium thiophene mixture was transferred over via cannula. The flask was switched back to the ice/brine bath and stirred for 30 min before phenyllithium (0.85 mL, 1.9 M in di-*tert*-butyl ether, 1.6 mmol) was added dropwise. The flask was switched to a -40 °C dry ice/acetonitrile bath and was allowed to stir for 30 min before enone **79** (0.229 g, 1.35 mmol) in tetrahydrofuran (1.5 mL, 0.90 M) was cannulated into the reaction mixture. Aluminum foil was placed over the reaction mixture, and it was stirred for another 2 h. The reaction mixture was then quenched with a mixture of concentrated ammonium hydroxide solution and saturated ammonium chloride aqueous solution (1 mL:9 mL). The organic and aqueous layers were separated, and the aqueous layer extracted with diethyl ether (5 mL). The combined organic layers were washed with saturated aqueous ammonium chloride solution (10 mL) and saturated aqueous sodium chloride solution (10 mL), dried over anhydrous magnesium sulfate, filtered, and the solvent removed *in vacuo*. The crude product was chromatographed

using 20-25% ethyl acetate:hexanes ($R_f = 0.28$ in 30% ethyl acetate:hexanes) to give ketone **115** as a colourless oil (0.053 g, 16%); the compound could not be purified sufficiently for full characterization, so it was subjected directly to the Wittig reaction.

Wittig reaction on ketone **124** to form alkene **149**:



Methyltriphenylphosphonium bromide (0.335 g, 0.938 mmol; purchased from Sigma-Aldrich) was dissolved in tetrahydrofuran (1.3 mL, 0.72 M) in a 25 mL round bottom flask equipped with stir bar, septum, and argon inlet. The flask was placed in a 0 °C ice bath, and *n*-butyllithium (0.35 mL, 2.5 M, 0.88 mmol) was added dropwise, forming a bright red solution. This mixture was stirred for 5 min, and then ketone **124** (0.115 g, 0.465 mmol) in tetrahydrofuran (2.2 mL, 0.21 M) was transferred via cannula into the reaction mixture. This reaction was stirred overnight, followed by the addition of diethyl ether (5 mL) and filtration of this mixture through Celite. The filtrate was washed with water (10 mL), and the aqueous layer was extracted with diethyl ether (10 mL). The combined organic layers were dried over anhydrous magnesium sulfate, filtered, and the solvent removed *in vacuo*. The crude product was chromatographed using 5% ethyl acetate:hexanes ($R_f = 0.28$ in 10% ethyl acetate:hexanes) to give alkene **149** as a colourless oil (0.036 g, 32%).

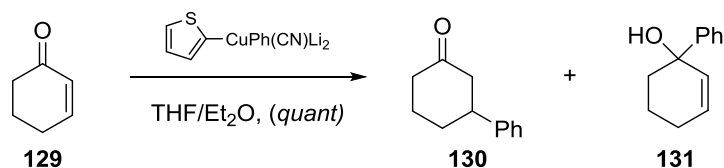
$^1\text{H NMR}$ (500 MHz, CDCl_3): δ 7.34-7.31 (m, 2H), 7.26-7.23 (m, 3H), 4.95 (br s, 1H), 4.85 (br s, 1H), 4.60-4.50 (m, 1H), 4.32-4.01 (m, 3H), 3.49 (br d, $J = 14$ Hz, 1H), 2.99-2.90 (m, 1H), 2.84-2.79 (m, 1H), 2.63 (br d, $J = 14$ Hz, 1H), 2.41 (app t, $J = 13$ Hz, 1H), 1.20 (br s, 3H).

^{13}C NMR (125 MHz, CDCl_3): δ 155.4, 142.4, 141.8, 128.6, 127.0, 126.9, 110.9, 61.4, 50.0, 43.5, 40.0, 29.7, 14.8.

IR(cast film, CDCl_3): 3074, 2982, 2930, 2851, 1700.9, 1657, 1468, 1427, 1385, 1230, 1207, 1115, 1013, 900, 758, 700 cm^{-1} .

High Resolution ESI-MS calculated for $\text{C}_{15}\text{H}_{21}\text{NO}_2$ ($[\text{M}+\text{H}]^+$) m/z : 246.1489; found m/z : 246.1489.

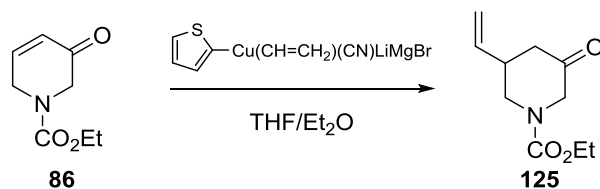
Conjugate addition of phenylthienylcyanocuprate into cyclohexenone to form ketone **130**:



Thiophene (0.10 mL, 1.2 mmol, freshly distilled from calcium hydride) was added to a flame-dried 25 mL round bottom flask equipped with stir bar, septum, and argon inlet. Tetrahydrofuran was added (0.80 mL, 1.5 M), and the flask was placed in a $-78\text{ }^\circ\text{C}$ dry ice/acetone bath. *n*-Butyllithium (0.85 mL, 1.4 M in hexanes, 1.2 mmol) was added dropwise, and the reaction flask was moved to an ice/brine bath ($\sim -10\text{ }^\circ\text{C}$). Copper(I) cyanide (0.111 g, 1.24 mmol, purified as per “Purification of Laboratory Chemicals”⁵¹ and dried under heat and vacuum) was added to a 50 mL flame-dried round bottom flask equipped with stir bar, septum, and argon inlet. Diethyl ether (1.1 mL, 1.1 M) was added, and vigorous stirring formed a slurry. This flask was placed in a $-78\text{ }^\circ\text{C}$ dry ice/acetone bath, and the lithium thiophene mixture was transferred over via cannula. The flask was switched back to the ice/brine bath and stirred for 30 min before phenyllithium (0.70 mL, 1.9 M in di-*tert*-butyl ether, 1.3 mmol) was added dropwise. The flask was switched to a $-40\text{ }^\circ\text{C}$ dry ice/acetonitrile bath and was stirred for 30 min before cyclohexenone **129** (0.10 mL, 1.0 mmol) in tetrahydrofuran (1.0 mL, 1.0 M) was added into the

reaction mixture via cannula. Aluminum foil was placed over the reaction mixture, and it was stirred for another 2 h. The reaction mixture was then quenched with a mixture of concentrated ammonium hydroxide solution and saturated ammonium chloride aqueous solution (1 mL:9 mL). The organic and aqueous layers were separated, and the aqueous layer extracted with diethyl ether (5 mL). The combined organic layers were washed with saturated aqueous ammonium chloride solution (10 mL) and saturated aqueous sodium chloride solution (10 mL), dried over anhydrous magnesium sulfate, filtered, and the solvent removed *in vacuo*. The crude oil was chromatographed using 20% ethyl acetate:hexanes ($R_f = 0.24$ in 20% ethyl acetate:hexanes) to give ketone **130** as a colourless oil (0.248 g, >100% including solvent impurities and a small amount of allylic alcohol **131**). Characterization data matched that previously reported.⁵²

Conjugate addition of vinylthienylcyanocuprate into enone **86** to form ketone **125**:



The experimental procedure is identical to that reported above except for the use of vinylmagnesium bromide (1 M in THF) in place of the phenyllithium solution and enone **86** in place of cyclohexenone **129**. The crude product was chromatographed using 20% ethyl acetate:hexanes ($R_f = 0.33$ in 30% ethyl acetate:hexanes) to give impure ketone **125** as a colourless oil (0.045 g, 8%).

¹H NMR (500 MHz, CDCl₃): δ 5.79 (ddd, $J = 17$ Hz, $J = 11$ Hz, $J = 7$ Hz, 1H), 5.17 (dt, $J = 11$ Hz, $J = 1$ Hz, 1H), 5.15 (dt, $J = 17$ Hz, $J = 1$ Hz, 1H), 4.20-4.15 (m, 3H), 4.05-3.90 (m, 2H), 3.28

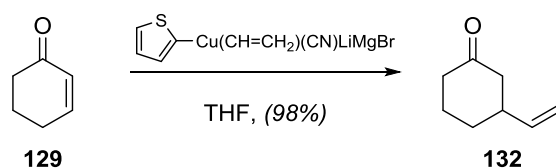
(app t, $J = 10$ Hz, 1H), 2.80-2.76 (m, 1H), 2.67-2.62 (m, 1H), 2.40 (dd, $J = 16$ Hz, $J = 10$ Hz, 1H), 1.29 (t, $J = 7$ Hz, 3H).

^{13}C NMR (125 MHz, CDCl_3): δ 204.4, 155.3, 137.3, 116.4, 61.9, 53.9, 47.0, 43.8, 37.9, 14.6.

IR (cast film, CDCl_3): 3083, 2982, 2932, 1703, 1643, 1469, 1429, 1267, 1222, 1119, 1007, 923, 769 cm^{-1} .

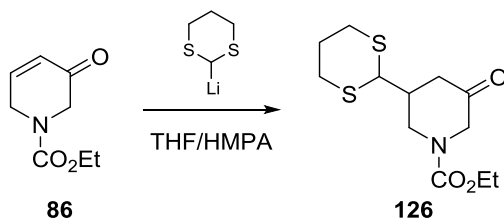
High Resolution EI-MS calculated for $\text{C}_{10}\text{H}_{15}\text{NO}_3$ (M^+) m/z : 197.1052; found m/z : 197.1052.

Conjugate addition of vinylthienylcyanocuprate into cyclohexenone to form ketone **132**:



The experimental procedure is identical to that reported for formation of ketone **130** except for the use of vinylmagnesium bromide (1 M in THF) in place of the phenyllithium solution. The crude product was chromatographed using 10% ether:hexanes ($R_f = 0.32$ in 20% ether:hexanes) to give ketone **132** as a colourless oil (0.137 g, 98%). Characterization data matched that previously reported.⁵³

Conjugate addition of lithium dithiane into enone **86** to form ketone **126**:

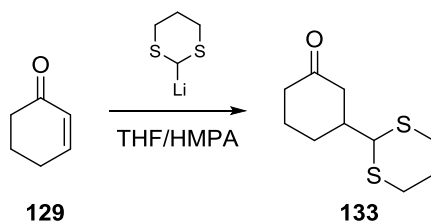


1,3-Dithiane (0.165 g, 1.37 mmol) was added to a flame-dried 25 mL round bottom flask fitted with a magnetic stir bar and septum. The flask was evacuated and filled with an argon

atmosphere. Tetrahydrofuran (2.4 mL, 0.57 M) was added, the mixture stirred to dissolve the dithiane and then cooled down to $-78\text{ }^{\circ}\text{C}$ in a dry ice/acetone bath. *n*-Butyllithium (1.05 mL, 1.3 M in hexanes, 1.3 mmol) was added dropwise to the dithiane solution. The reaction flask was transferred to an ice-brine bath for 15 min and then cooled back down to $-78\text{ }^{\circ}\text{C}$. Hexamethylphosphoramide (0.48 mL, 2.8 mmol, dried over 5 \AA molecular sieves) was added, and then enone **86** (0.242 g, 1.43 mmol) in tetrahydrofuran (1.0 mL, 1.4 M) was added to the reaction mixture via cannula. The flask was allowed to warm up to room temperature over 1 h. Diethyl ether (5 mL) and water (5 mL) were added. The organic layer was removed, and the aqueous layer was extracted twice more with diethyl ether (2 x 5 mL). The combined organic layers were dried over anhydrous magnesium sulfate, filtered, and evaporated under reduced pressure. Column chromatography using 30% ethyl acetate:hexanes ($R_f = 0.64$ in 50% ethyl acetate:hexanes) afforded ketone **126** (0.020 g, 5%). The product could not be purified sufficiently for full characterization, though ^1H NMR data for the partially-purified product is available.

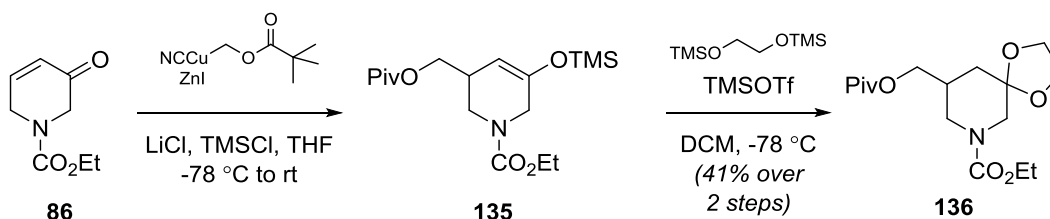
^1H NMR (300 MHz, CDCl_3): δ 4.23-4.08 (m, 5H), 3.85 (d, $J = 18\text{ Hz}$, 1H), 3.39 (dd, $J = 13\text{ Hz}$, $J = 10\text{ Hz}$, 1H), 2.93-2.81 (m, 3H), 2.75 (dd, $J = 16\text{ Hz}$, $J = 5\text{ Hz}$, 1H), 2.62-2.45 (m, 2H), 2.16-2.11 (m, 1H), 1.96-1.86 (m, 1H), 1.30-1.21 (m, 4H).

Conjugate addition of lithium dithiane into cyclohexenone to form ketone **133**:



The experimental procedure is identical to that reported for formation of ketone **126** except for the use of cyclohexenone **129** in place of enone **86**. Column chromatography using 20% ethyl acetate:hexanes ($R_f = 0.65$ in 30% ethyl acetate:hexanes) afforded ketone **133** (0.107 g, 57%). Characterization data matched that previously reported.⁵⁴

Conjugate addition of Knochel's organocopper/zinc reagent into enone **86** to form acetal **136**:



Zinc dust (3.25 g, 49.7 mmol, purified as per “Purification of Laboratory Chemicals”⁵¹) was added to a flame-dried 25 mL round bottom flask equipped with a stir bar, septum, and argon inlet. 1,2-Dibromoethane (1.3 mL, 15 mmol) and chlorotrimethylsilane (1.9 mL, 15 mmol, distilled over calcium hydride) were added via syringe and the mixture stirred. The flask was put in a cold water bath (~10 °C). Iodomethyl pivalate (6.20 g, 25.6 mmol, synthesized from chloromethyl pivalate³⁴) in tetrahydrofuran (16 mL, 1.6 M) was added into the zinc mixture via cannula. This reaction mixture was stirred for 30 min. Copper(I) cyanide (0.900 g, 10.0 mmol, purified as per “Purification of Laboratory Chemicals”⁵¹ and dried under heat and vacuum) and lithium chloride (0.890 g, 21.0 mmol, dried under heat and vacuum) were added to a flame-dried 50 mL round bottom flask equipped with a stir bar, septum, and argon inlet. Tetrahydrofuran (9.9 mL, 1.0 M) was added, the mixture stirred to form a slurry, and the flask placed in a -78 °C dry ice/acetone bath. The zinc mixture was transferred into the copper mixture via cannula, and this new reaction mixture was stirred for 30 min. Chlorotrimethylsilane (1.1 mL, 8.7 mmol) was added followed by addition of enone **86** (1.334 g, 7.886 mmol) in tetrahydrofuran (7.9 mL, 1.0

M). Aluminum foil was put over the reaction, and the reaction was allowed to warm up to room temperature overnight slowly via eventual warming of the ice bath. Saturated aqueous ammonium chloride solution (40 mL) was added to the reaction mixture. The reaction mixture was extracted with diethyl ether (3 x 40 mL). The combined organic layers were washed with saturated aqueous ammonium chloride solution (120 mL) followed by saturated aqueous sodium chloride solution (120 mL). The organic layer was dried over anhydrous magnesium sulfate, filtered, and the solvent evaporated *in vacuo* to give silyl enol ether **135** as a colourless oil. This crude product was placed in a 50 mL round bottom flask equipped with stir bar, septum, and argon inlet, and it was dissolved in dichloromethane (10 mL, 0.79 M). 1,2-Bis(trimethylsiloxy)ethane (2.5 mL, 10 mmol, synthesized from ethylene glycol⁵⁵) was added and the reaction flask placed in a -40 °C dry ice/acetonitrile bath. Trimethylsilyl triflate (1.9 mL, 10 mmol) was added dropwise and the reaction mixture stirred for 2.5 h. This mixture was then quenched with saturated aqueous sodium bicarbonate (10 mL). The organic layer was removed, and the aqueous layer was extracted with dichloromethane (2 x 10 mL). The combined organic layers were washed with saturated aqueous sodium chloride (30 mL), dried over anhydrous magnesium sulfate, filtered, and the solvent removed *in vacuo*. Purification by column chromatography using 30% ethyl acetate:hexanes with ~1% triethylamine ($R_f = 0.47$ in 50% ethyl acetate:hexanes) gave acetal **136** as a colourless oil (1.068 g, 41%).

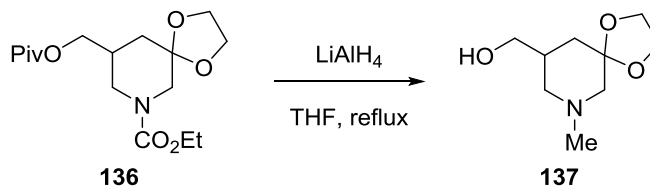
¹H NMR (500 MHz, CDCl₃): δ 4.17-4.08 (m, 3H), 4.00-3.86 (m, 7H), 2.81 (d, $J = 13$ Hz, 1H), 2.75-2.60 (m, 1H), 2.23-2.15 (m, 1H), 1.82 (dt, $J = 13$ Hz, $J = 2$ Hz, 1H), 1.53 (t, $J = 13$ Hz, 1H), 1.24 (t, $J = 7$ Hz, 3H), 1.20 (s, 9H).

¹³C NMR (125 MHz, CDCl₃): δ 178.1, 155.7, 105.3, 65.5, 64.9, 64.5, 61.5, 49.4, 46.0, 38.8, 36.8, 34.4, 27.2, 14.6.

IR(cast film, CDCl₃): 2976, 2906, 1729, 1701, 1537, 1465, 1429, 1368, 1284, 1226, 1158, 1094, 1010, 945, 902, 768 cm⁻¹.

High Resolution EI-MS calculated for C₁₆H₂₇NO₆ (M⁺) m/z: 329.1838; found m/z: 329.1830.

Reduction of acetal **136** to form piperidinol **137**:



Acetal **136** (1.068 g, 3.24 mmol) was dissolved in tetrahydrofuran (9 mL, 0.4 M) in a 25 mL round bottom flask equipped with stir bar, condenser, septum, and argon inlet. Lithium aluminum hydride (0.610 g, 95%, 15.3 mmol) was added portionwise over 10 min. The reaction mixture was heated at reflux for 6 h and then allowed to cool to room temperature. Sodium sulfate decahydrate was added until bubbling stopped, and this mixture was stirred overnight. The mixture was filtered through Celite using diethyl ether and the solvent evaporated *in vacuo* to give piperidinol **137** as a viscous, colourless oil (0.552 g, 91%).

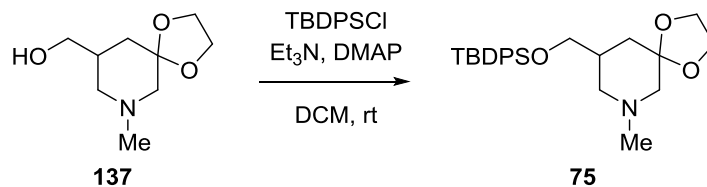
¹H NMR (500 MHz, CDCl₃): δ 4.01-3.94 (m, 4H), 3.56 (dd, *J* = 11 Hz, *J* = 6 Hz, 1H), 3.50 (dd, *J* = 11 Hz, *J* = 7 Hz, 1H), 2.90 (br dd, *J* = 11 Hz, *J* = 4 Hz, 1H), 2.66 (dt, *J* = 12 Hz, *J* = 2 Hz, 1H), 2.31 (s, 3H), 2.16-2.07 (m, 2H), 2.02 (d, *J* = 11 Hz, 1H), 1.80-1.75 (m, 2H), 1.26 (t, *J* = 13 Hz, 1H).

¹³C NMR (125 MHz, CDCl₃): δ 106.6, 65.6, 64.7, 62.0, 58.0, 46.3, 37.2, 36.0, 26.0.

IR(cast film, CDCl₃): 3177, 2951, 2888, 2851, 2777, 2737, 1463, 1380, 1281, 1127, 1096, 1040, 947, 863, 751 cm⁻¹.

High Resolution EI-MS calculated for C₉H₁₇NO₃ (M⁺) m/z: 187.1209; found m/z: 187.1209.

TBDPS protection of piperidinol **137** to form piperidine **75**:



Piperidinol **137** (0.263 g, 1.40 mmol) was dissolved in dichloromethane (3.0 mL, 0.47 M) in a round-bottom flask equipped with stir bar, septum, and argon inlet. Triethylamine (0.40 mL, 2.7 mmol) was added, followed by *tert*-butyldiphenylchlorosilane (0.45 mL, 1.7 mmol). 4-dimethylaminopyridine (0.018 g, 0.15 mmol) was added, and the reaction mixture was stirred overnight. The reaction mixture was filtered through Celite and the solvent removed *in vacuo*. Column chromatography using 80% ethyl acetate:hexanes with ~1% triethylamine ($R_f = 0.60$ in 10% methanol:dichloromethane) gave piperidine **75** as a colourless oil (0.534 g, 90%).

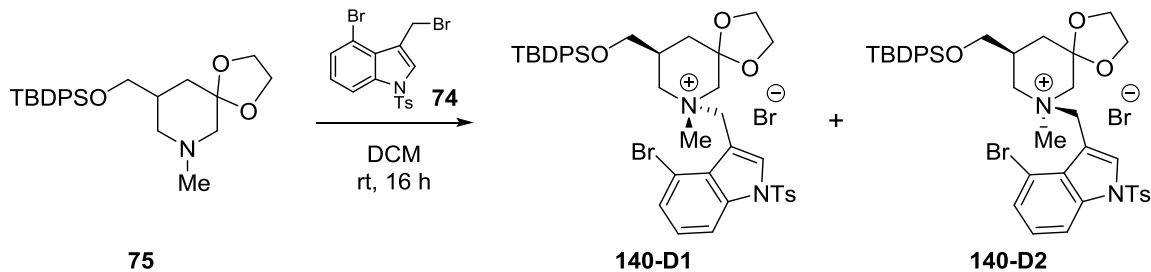
^1H NMR (500 MHz, CDCl_3): δ 7.68-7.66 (m, 4H), 7.47-7.39 (m, 6H), 4.03-3.96 (m, 4H), 3.60 (dd, $J = 10$ Hz, $J = 5$ Hz, 1H), 3.53 (dd, $J = 10$ Hz, $J = 7$ Hz, 1H), 2.98 (br dd, $J = 11$ Hz, $J = 4$ Hz, 1 H), 2.72 (dt, $J = 11$ Hz, $J = 2$ Hz, 1 H), 2.34 (s, 3 H), 2.25-2.18 (m, 1H), 1.99 (d, $J = 11$ Hz, 1H), 1.77 (t, $J = 11$ Hz, 1H), 1.77-1.73 (m, 1H), 1.32 (t, $J = 13$ Hz, 1H), 1.07 (s, 9H).

^{13}C NMR (125 MHz, CDCl_3): δ 135.6, 133.7, 129.6, 127.7, 106.8, 66.5, 64.64, 64.61, 62.0, 58.3, 46.4, 37.2, 35.9, 26.9, 19.3.

IR(cast film, CDCl_3): 3071, 3048, 2935, 2888, 2858, 2786, 1589, 1568, 1428, 1288, 1192, 1112, 1105, 824, 740, 703 cm^{-1} .

High Resolution ESI-MS calculated for $\text{C}_{25}\text{H}_{37}\text{NO}_3\text{Si}$ ($[\text{M}+\text{H}]^+$) m/z : 426.2459; found m/z : 426.2455.

Alkylation of piperidine **75** with indole derivative **74**:



Piperidine **75** (0.090 g, 0.21 mmol) was dissolved in dichloromethane (0.60 mL, 0.35 M) in a round-bottom flask equipped with stir bar, septum, and argon inlet. Indole derivative **74** (0.103 g, 0.23 mmol) was added and the reaction stirred overnight. The solvent was removed by rotary evaporation to give ammonium salt **140** as a beige solid; ^1H NMR of the product showed a 1:1 mixture of diastereomers via integration of the benzylic peaks. Unfortunately, conditions could not be found to crystallize the ammonium salt, so purification was not performed. Characterization data is nonetheless reported.

^1H NMR (400 MHz, CDCl_3): δ 8.08-7.18 (m, 36H), 5.64 (br s, 2H), 5.35 (d, $J = 14$ Hz, 1H), 5.18 (d, $J = 14$ Hz, 1H), 4.40-4.30 (m, 2H), 4.23-4.00 (m, 4H), 3.90 (q, $J = 7$ Hz, 1H), 3.74-3.70 (m, 3H), 3.62-3.43 (m, 4H), 3.56 (s, 3H), 3.34 (d, $J = 13$ Hz, 2H), 3.23 (s, 3H), 2.35 (s, 3H), 2.33-2.18 (m, 6H), 2.31 (s, 3H), 1.97 (t, $J = 13$ Hz, 1H), 1.88-1.84 (m, 1H), 1.74-1.63 (m, 2H), 1.02 (s, 9H), 0.81 (s, 9H).

^{13}C NMR (100 MHz, CDCl_3): δ 146.7, 146.3, 136.0, 135.9, 135.5, 135.4, 135.3, 134.8, 133.9, 133.8, 132.9, 132.7, 132.4, 132.2, 130.6, 130.4, 130.0, 129.5, 129.3, 128.0, 127.9, 127.6, 127.4, 127.1, 126.9, 126.8, 126.5, 113.6, 113.4, 113.2, 108.2, 107.2, 104.6, 104.3, 65.7, 65.6, 64.8, 64.7, 64.3, 64.0, 63.0, 62.3, 61.4, 61.0, 57.3, 54.7, 52.1, 48.0, 35.0, 33.9, 33.2, 32.4, 26.9, 26.6, 21.7, 21.6, 19.1, 18.9.

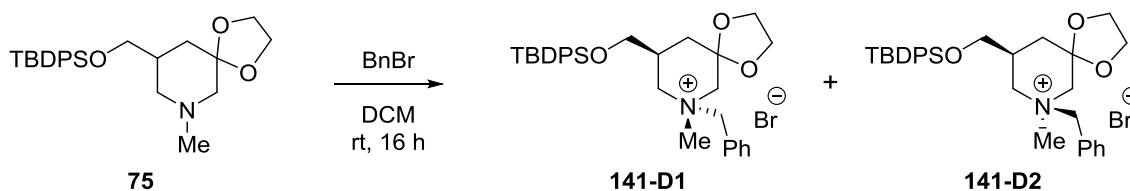
IR(cast film, CH₂Cl₂): 3070, 2957, 2930, 2892, 2857, 2187, 1596, 1550, 1471, 1379, 1176, 1112, 984, 733, 703, 674 cm⁻¹.

High Resolution ESI-MS calculated for C₄₁H₄₈N₂O₅SSi⁺ (M⁺) m/z: 787.2231; found m/z: 787.2221.

EA: Calculated: C, 56.68; H, 5.57; N, 3.22; S, 3.69. Found: C, 55.94; H, 5.71; N, 3.19; S, 3.68.

mp: 112-115 °C

Alkylation of piperidine **75** with benzyl bromide:



Piperidine **75** (0.116 g, 0.27 mmol) was dissolved in dichloromethane (0.60 mL, 0.45 M) in a round-bottom flask equipped with stir bar, septum, and argon inlet. Benzyl bromide (0.04 mL, 0.3 mmol) was added and the reaction stirred overnight. The solvent was removed by rotary evaporation to give ammonium salt **141** as a pale brown, viscous oil; ¹H NMR of the product showed a 1:1 mixture of diastereomers via integration of the benzylic peaks. Unfortunately, conditions could not be found to crystallize the ammonium salt, so purification was not performed. Characterization data is nonetheless reported, albeit with excess benzyl bromide present.

¹H NMR (400 MHz, CDCl₃): δ 7.71-7.25 (m, 30H), 5.32 (d, *J* = 13 Hz, 1H), 5.28 (d, *J* = 12 Hz, 1H), 5.21 (d, *J* = 13 Hz, 1H), 5.11 (d, *J* = 14 Hz, 1H), 4.71 (d, *J* = 13 Hz, 1H), 4.43-4.29 (m, 3H), 4.07-3.97 (m, 4H), 3.86-3.81 (m, 3H), 3.75-3.66 (m, 2H), 3.60-3.48 (m, 6H), 3.44 (s, 3H), 3.31

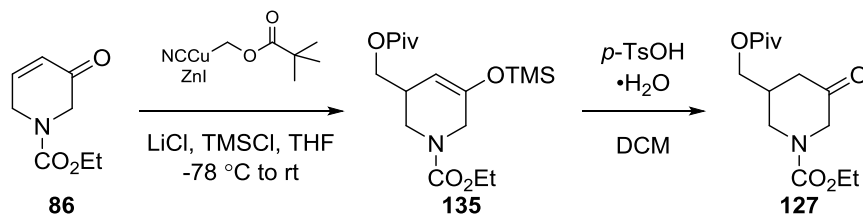
(s, 3H), 3.21 (t, $J = 12$ Hz, 1H), 2.78-2.67 (m, 1H), 2.33-2.23 (m, 1H), 1.87-1.67 (m, 4H), 1.06 (s, 9H), 0.95 (s, 9H).

^{13}C NMR (125 MHz, CDCl_3): δ 135.5, 135.4, 133.8, 133.1, 132.8, 132.6, 130.53, 130.47, 130.1, 130.0, 129.2, 128.0, 127.91, 127.87, 127.8, 126.9, 104.4, 104.2, 71.0, 65.44, 65.37, 65.3 (and one more peak; one of the cyclic acetal peaks is overlapping), 64.8, 64.7, 64.0, 62.3, 61.2, 60.3, 59.5, 52.4, 47.2, 34.9, 34.6, 33.4, 32.4, 26.9, 26.8, 19.2, 19.1.

IR(cast film, CDCl_3): 3070, 2959, 2931, 2893, 2858, 2186, 1589, 1472, 1428, 1113, 1065, 1028, 924, 908, 823, 732, 703 cm^{-1} .

High Resolution ESI-MS calculated for $\text{C}_{32}\text{H}_{42}\text{NO}_3\text{Si}^+$ (M^+) m/z : 516.2928; found m/z : 516.2925.

Conjugate addition of Knochel's organocopper/zinc reagent into enone **86** to form ketone **127**:



Zinc dust (0.625 g, 9.56 mmol, purified as per “Purification of Laboratory Chemicals”⁵¹ and dried under heat and vacuum) was added to flame-dried 25 mL round bottom flask equipped with a Teflon stir bar, septum, and argon inlet. 1,2-Dibromoethane (0.25 mL, 2.9 mmol) and chlorotrimethylsilane (0.35 mL, 2.8 mmol, distilled over calcium hydride) were added via syringe and the mixture stirred. The flask was put in a cold water bath. Iodomethyl pivalate (1.126 g, 4.65 mmol, synthesized from chloromethyl pivalate³⁴) in tetrahydrofuran (3.1 mL, 1.5 M) was transferred into the zinc mixture via cannula. This reaction mixture was stirred for 30 min. Copper(I) cyanide (0.179 g, 2.0 mmol, dried under vacuum and heating) and lithium

chloride (0.180 g, 4.25 mmol, dried under vacuum/heating) were added to a flame-dried 50 mL round bottom flask equipped with a Teflon stir bar, septum, and argon inlet. Tetrahydrofuran (1.8 mL, 1.1 M) was added, the mixture stirred to form a slurry, and the flask placed in a -78 °C dry ice/acetone bath. The zinc mixture was transferred via cannula into the copper mixture, and this new reaction mixture was stirred for 30 min. Chlorotrimethylsilane (0.21 mL, 1.7 mmol) was added via syringe followed by addition of enone **86** (0.249 g, 1.47 mmol) in tetrahydrofuran (1 mL, 1.5 M) via cannula. Aluminum foil was put over the reaction, and the reaction was allowed to warm up to room temperature overnight slowly via eventual warming of the ice bath. Saturated aqueous ammonium chloride solution (10 mL) was then added to the reaction mixture. The reaction mixture was extracted with diethyl ether (3 x 10 mL). The combined organic layers were washed with saturated aqueous ammonium chloride solution (25 mL) followed by saturated aqueous sodium chloride solution (25 mL). The organic layer was dried over anhydrous magnesium sulfate, filtered, and the solvent evaporated *in vacuo* to give silyl enol ether **135** as a colourless oil. This crude product was dissolved in dichloromethane (10 mL, 0.15 M), and *p*-toluenesulfonic acid monohydrate (0.010 g, 0.052 mmol) was added. This mixture was stirred for 2 h and then quenched with saturated aqueous sodium bicarbonate (10 mL). The organic layer was removed, and the aqueous layer was extracted with dichloromethane (2 x 10 mL). The combined organic layers were dried over anhydrous magnesium sulfate, filtered, and the solvent removed *in vacuo*. Purification by column chromatography using 25% ethyl acetate:hexanes ($R_f = 0.49$ in 50% ethyl acetate:hexanes) gave ketone **127** as a colourless oil (0.164 g, 39%). Although this compound could not be fully purified due to some decomposition occurring during chromatography, full characterization data is available.

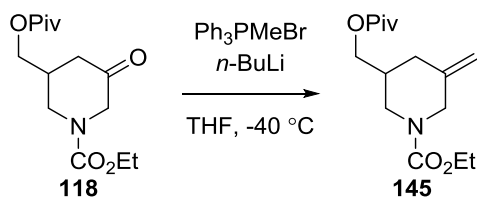
^1H NMR (500 MHz, CDCl_3): δ 4.11 (q, $J = 8$ Hz, 2H), 4.08 (d, $J = 20$ Hz, 1H), 4.02-3.85 (m, 4H), 3.29 (app t, $J = 10$ Hz, 1H), 2.56 (dd, $J = 16$ Hz, $J = 5$ Hz, 1H), 2.42 (m, 1H), 2.26 (dd, $J = 16$ Hz, $J = 10$ Hz, 1H), 1.22 (t, $J = 7$ Hz, 3H), 1.16 (s, 9H).

^{13}C NMR (125 MHz, CDCl_3): δ 204.0, 178.1, 155.2, 65.0, 61.9, 54.1, 44.5, 41.1, 38.8, 34.0, 27.2, 14.5.

IR (cast film, CDCl_3): 2977, 2874, 1730, 1704, 1433, 1283, 1225, 1157, 768 cm^{-1} .

High Resolution ESI-MS calculated for $\text{C}_{14}\text{H}_{23}\text{NNaO}_5$ ($[\text{M}+\text{Na}]^+$) m/z : 308.1468; found m/z : 308.1468.

Wittig reaction on ketone **127** to give alkene **145**:



Methyltriphenylphosphonium bromide (0.565 g, 1.58 mmol, purchased from Sigma-Aldrich) was dissolved in tetrahydrofuran (6.4 mL, 0.25 M) in a 50 mL round bottom flask equipped with stir bar, septum, and argon inlet. This flask was placed in a 0°C ice bath, and potassium *tert*-butoxide (0.167 g, 1.49 mmol) was added. The flask was removed from the ice bath and stirred for 30 min. The flask was placed back in the ice bath, and ketone **127** (0.175 g, 0.613 mmol) in tetrahydrofuran (15 mL, 0.041 M) was transferred via cannula into the reaction mixture. The ice bath was removed and the reaction mixture stirred for 45 min at room temperature. The reaction mixture was quenched with saturated aqueous ammonium chloride solution (20 mL) and extracted with ethyl acetate (3 x 20 mL). The combined organic layers were dried over anhydrous magnesium sulfate, filtered, and the solvent removed *in vacuo*. The

crude product was re-dissolved in diethyl ether (50 mL) and filtered through Celite to remove excess triphenylphosphine oxide. Column chromatography using 10% ethyl acetate:hexanes ($R_f = 0.34$ in 20% ethyl acetate:hexanes) gave alkene **145** as a colourless oil (0.075 g, 43%).

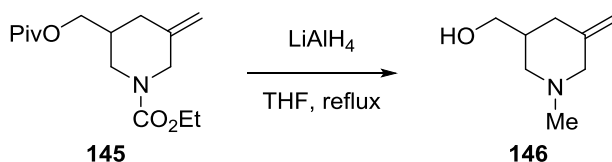
^1H NMR (500 MHz, CDCl_3): δ 4.89 (br s, 1H), 4.79 (s, 1H), 4.16-4.09 (m, 3H), 3.99-3.64 (m, 4H), 3.07 (br s, 1H), 2.38 (d, $J = 10$ Hz, 1H), 2.06-1.97 (m, 2H), 1.23 (t, $J = 7$ Hz, 3H), 1.20 (s, 9H).

^{13}C NMR (125 MHz, CDCl_3): δ 178.2, 155.4, 141.0, 111.4, 65.2, 61.4, 50.2, 45.9, 38.8, 36.2, 35.2, 27.2, 14.7.

IR (cast film, CDCl_3): 3077, 2978, 1731, 1702, 1657, 1481, 1467, 1429, 1284, 1226, 1158, 1120, 902, 769 cm^{-1} .

High Resolution ESI-MS calculated for $\text{C}_{15}\text{H}_{26}\text{NO}_4$ ($[\text{M}+\text{H}]^+$) m/z : 284.1856; found m/z : 284.1849.

Reduction of **145** to give piperidinol **146**:



Alkene **145** (0.419 g, 1.48 mmol) was dissolved in tetrahydrofuran (5.0 mL, 0.30 M) in a 25 mL round bottom flask equipped with stir bar, condenser, septum, and argon inlet. Lithium aluminum hydride (0.250 g, 95%, 6.26 mmol) was added portionwise over 10 min. The reaction mixture was heated at reflux for 2 h and then allowed to cool to room temperature. Sodium sulfate decahydrate was added until bubbling stopped, and this mixture was stirred overnight. The mixture was filtered through Celite using diethyl ether and the solvent evaporated *in vacuo*. Column chromatography using 5% methanol:dichloromethane with ~1% triethylamine ($R_f = 0.22$

in 10% methanol:dichloromethane) gave piperidinol **146** as a viscous, colourless oil (0.129 g, 61%).

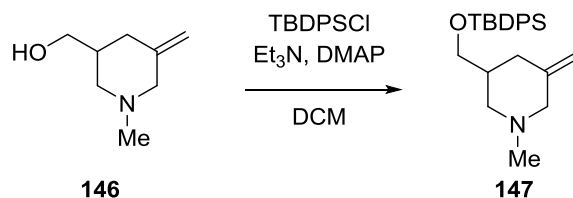
^1H NMR (400 MHz, CDCl_3): δ 4.82 (s, 1H), 4.80 (s, 1H), 3.89 (br s, 1H), 3.57 (dd, $J = 11$ Hz, $J = 5$ Hz, 1H), 3.48 (dd, $J = 11$ Hz, $J = 6$ Hz, 1H), 3.06 (d, $J = 12$ Hz, 1H), 2.83 (dd, $J = 11$ Hz, $J = 3$ Hz, 1H), 2.76 (d, $J = 12$ Hz, 1H), 2.31 (s, 3 H), 2.30 (dd, $J = 12$ Hz, $J = 4$ Hz, 1H), 2.18 (dd, $J = 11$ Hz, $J = 8$ Hz, 1H), 1.92-1.82 (m, 2H).

^{13}C NMR (100 MHz, CDCl_3): δ 142.3, 110.8, 65.5, 61.9, 58.2, 45.8, 38.5, 34.9.

IR (cast film, CDCl_3): 3370, 3074, 2936, 2842, 2775, 2674, 1657, 1461, 1143, 1073, 1036, 898 cm^{-1} .

High Resolution EI-MS calculated for $\text{C}_8\text{H}_{15}\text{NO}$ (M^+) m/z : 141.1154; found m/z : 141.1152.

TBDPS protection of piperidinol **146** to give piperidine **147**:



Piperidinol **146** (0.129 g, 0.913 mmol) was dissolved in dichloromethane (5.0 mL, 0.18 M) in a 25 mL round bottom flask equipped with stir bar, septum, and argon inlet. Triethylamine (0.30 mL, 2.2 mmol) was added, followed by *tert*-butyldiphenylchlorosilane (0.30 mL, 1.2 mmol). 4-dimethylaminopyridine (0.021 g, 0.17 mmol) was added, and the reaction mixture was stirred overnight. The reaction mixture was filtered through Celite and the solvent removed *in vacuo*. Column chromatography using 80% ethyl acetate:hexanes ($R_f = 0.43$ in 10% methanol:dichloromethane) gave piperidine **147** as a colourless oil (0.294 g, 85%).

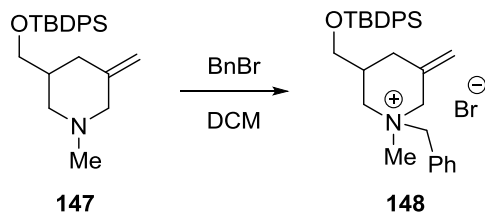
^1H NMR (400 MHz, CDCl_3): δ 7.71-7.68 (m, 4 H), 7.44-7.38 (m, 6 H), 4.85 (d, $J = 2$ Hz, 1H), 4.78 (d, $J = 2$ Hz, 1H), 3.61 (dd, $J = 10$ Hz, $J = 5$ Hz, 1 H), 3.57 (dd, $J = 10$ Hz, $J = 6$ Hz, 1H), 3.14 (d, $J = 12$ Hz, 1H), 2.92 (d, $J = 8$ Hz, 1H), 2.59 (d, $J = 12$ Hz, 1H), 2.32 (s, 3H), 2.30 (dd, $J = 12$ Hz, $J = 3$ Hz, 1H), 2.02-1.96 (m, 2H), 1.89-1.82 (m, 1H), 1.09 (s, 9H).

^{13}C NMR (100 MHz, CDCl_3): δ 143.7, 135.6, 133.8, 129.6, 127.7, 109.7, 66.6, 62.4, 58.7, 46.3, 39.7, 35.0, 26.9, 19.3.

IR(cast film, CDCl_3): 3071, 2932, 2857, 2774, 1658, 1589, 1472, 1428, 1112, 895, 824, 740, 702 cm^{-1} .

High Resolution ESI-MS calculated for $\text{C}_{24}\text{H}_{34}\text{NOSi}$ ($[\text{M}+\text{H}]^+$) m/z : 379.2331; found m/z : 379.2331.

Benylation of piperidine **147** to give quaternary piperidinium salt **148**:



Piperidine **147** (0.043 g, 0.11 mmol) was dissolved in dichloromethane (0.50 mL, 0.22 M) in a 10 mL round bottom flask equipped with stir bar, septum, and argon inlet. Benzyl bromide (0.016 mL, 0.13 mmol) was added and the reaction stirred overnight. The solvent was removed *in vacuo*; ^1H NMR of the crude product showed a 1:1 mixture of diastereomers via integration of the *N*-methyl peaks. The crude ammonium salt was purified by crystallization in a mixture of dichloromethane and diethyl ether to give ammonium salt **148** as a white solid (0.051 g, 84%); the diastereomeric ratio remained unchanged.

^1H NMR (400 MHz, CDCl_3): δ 7.72-7.30 (m, 30H), 5.36-5.28 (m, 3H), 5.24 (br s, 2H), 5.14 (s, 1H), 4.93 (d, $J = 14$ Hz, 1H), 4.71 (d, $J = 13$ Hz, 1H), 4.58 (d, $J = 13$ Hz, 1H), 4.52 (d, $J = 13$ Hz, 1H), 4.42 (d, $J = 13$ Hz, 1H), 4.36 (d, $J = 12$ Hz, 1H), 3.72-3.52 (m, 5H), 3.40 (t, 14 Hz, 1H), 3.32 (s, 3H), 3.08 (s, 3H), 2.59-2.48 (m, 1H), 2.42 (dd, $J = 14$ Hz, $J = 4$ Hz, 1H), 2.28 (dd, $J = 13$ Hz, $J = 3$ Hz, 1H), 2.24-1.97 (m, 5H), 1.03 (s, 9H), 0.94 (s, 9H).

^{13}C NMR (125 MHz, CDCl_3): δ 135.5, 135.4, 134.6, 134.4, 133.6, 132.84, 132.76, 132.7, 132.6, 130.7, 130.1, 130.0, 129.4, 129.1, 128.0, 127.9, 127.2, 127.0, 120.0, 119.9, 69.8, 67.2, 65.4, 65.3, 64.9, 61.1, 61.0, 60.6, 51.3, 45.2, 35.3, 34.7, 33.3, 33.0, 26.90, 26.84, 19.22, 19.17.

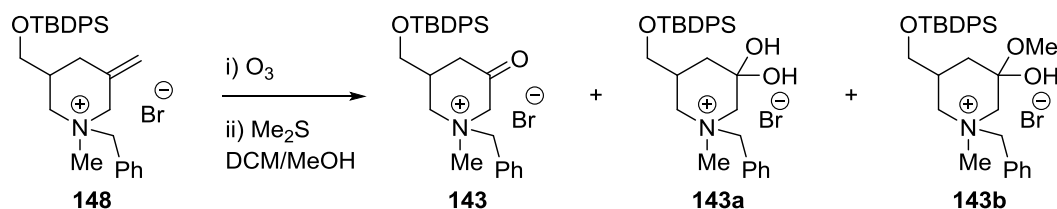
IR (cast film, CDCl_3): 3070, 2959, 2930, 2858, 2188, 1656, 1589, 1472, 1428, 1113, 924, 730, 703 cm^{-1} .

High Resolution ESI-MS calculated for $\text{C}_{31}\text{H}_{40}\text{NOSi}^+$ (M^+) m/z : 470.2874; found m/z : 470.2866.

EA: Calculated: C, 67.62; H, 7.32; N, 2.54. Found: C, 66.99; H, 7.25; N, 2.51.

mp: 182 $^\circ\text{C}$ (decomposition)

Ozonolysis on piperidinium salt **148** to give Stevens rearrangement precursor **143**:



Piperidinium salt **148** (0.110 g, 0.200 mmol) was dissolved in a 3:1 v/v mixture of dichloromethane and methanol (32 mL, 0.0063 M) in a 50 mL three-neck round bottom flask equipped with stir bar, septum, and thermometer adapter into which a glass pipette was placed (one neck left open). This reaction flask was placed in a -78 $^\circ\text{C}$ dry ice/acetone bath, and ozone was bubbled through via the glass pipette for 5 min followed by 30 min of purging with oxygen.

Dimethyl sulfide (0.26 mL, 3.5 mmol) was added, and the reaction mixture was allowed to warm up to room temperature overnight. The solvent was removed in vacuo, and column chromatography was performed on crude ketone **143** using 2% methanol:dichloromethane ($R_f = 0.40$ in 10% methanol:dichloromethane). This produced an inseparable mixture of ketone **143**, methanol hydrate **143a**, and hemi-acetal **143b** (0.083 g). Because of the inability to separate these products, full characterization data could not be obtained; however, the ^1H NMR spectrum is available, and the IR and MS data supporting the formation of this mixture of products is reported below.

IR(cast film, CH_2Cl_2): 3224, 3070, 2958, 2931, 2858, 1732, 1589, 1472, 1428, 1112, 823, 785, 738, 704 cm^{-1} .

High Resolution ESI-MS calculated for $\text{C}_{30}\text{H}_{38}\text{NO}_2\text{Si}^+$ (M^+) m/z : 472.2666; found m/z : 472.2663. Peaks were also observed for $\text{C}_{30}\text{H}_{40}\text{NO}_3\text{Si}^+$ ($[\text{M}+\text{H}_2\text{O}]^+$) m/z : 490.2774 and $\text{C}_{31}\text{H}_{42}\text{NO}_3\text{Si}^+$ ($[\text{M}+\text{CH}_3\text{OH}]^+$) m/z : 504.2927.

Chapter 3: Diastereoselective Alkylation of *N*-Substituted Piperidines

Section 3.1: Introduction

Quaternary ammonium salts are useful intermediates that can react via Stevens rearrangements (see Chapter 1, Section 1.4), Hofmann eliminations,⁵⁶ and Sommelet-Hauser rearrangements.¹¹ In particular, chiral quaternary ammonium salts that undergo Stevens rearrangements can transfer chirality from the quaternary nitrogen stereocentre to the adjacent carbon, making this transformation very valuable synthetically. In addition to being useful reactants, quaternary ammonium salts themselves have been used as ionic liquids,⁵⁷ structure-directing agents,⁵⁸ asymmetric organocatalysts,⁵⁹ chiral phase transfer catalysts,⁶⁰ and medicinal compounds (antibacterial, antifungal, and/or antitumour).⁶¹ In order to obtain chiral quaternary ammonium salts, we need to be able to alkylate tertiary amines in a diastereoselective fashion. However, despite its obvious importance, there seems to be very little research reported in this area in the last forty years. Additionally, McKenna expressed a desire for computational studies of diastereoselective alkylation of saturated nitrogen heterocycles in his 1970 review;⁶² however, this has still not been done, despite the advances in computational chemistry over the past four decades.

In this chapter, a brief overview of the state of knowledge in the field of diastereoselective *N*-quaternization of piperidines will be presented. Additionally, selected experimental results from three important papers in the field were subjected to computational analysis; the results from these three case studies will be presented.

Section 3.2: Literature Review and Analysis

Low nitrogen inversion barriers (around 5 – 9 kcal/mol for aliphatic amines)⁶³ cause cyclic amines to exist as a mixture of axial and equatorial conformers in rapid equilibrium. The equatorial conformer is typically the more stable conformer of *N*-substituted piperidines (for instance, equatorial *N*-methylpiperidine is 2.7 kcal/mol more stable than the axial conformer⁶⁴), although certain substitution patterns can reverse this conformational preference (the conformer of *cis*-2-ethyl-1,6-dimethylpiperidine with the *N*-methyl group axial is more stable by 0.14 kcal/mol⁶⁵).

Because of this equilibrium between conformers, the reaction of substituted *N*-alkylpiperidines follows the Curtin-Hammett Principle.⁶⁶ Reactions at nitrogen that occur much faster than interconversion between conformers, like protonation, create a product mixture that reflects the relative stabilities of the two reactant conformers (Figure 3); protonation is, in fact, a popular method for measuring the ratio of axial to equatorial reactant conformers.^{64,65} However, for reactions at nitrogen that are much slower than interconversion (e.g. alkylation and oxidation), the ratio of products then also depends upon the relative rates of reaction of the two conformers (Figure 4); the product ratio reflects the difference in transition state energies of the reaction of the two piperidine invertomers.

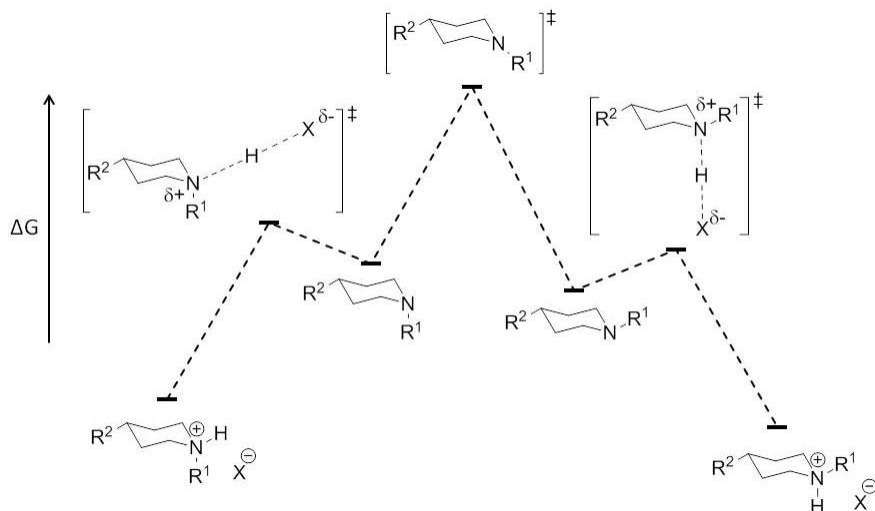


Figure 3. The first boundary condition of the Curtin-Hammett Principle illustrated by piperidine protonation.

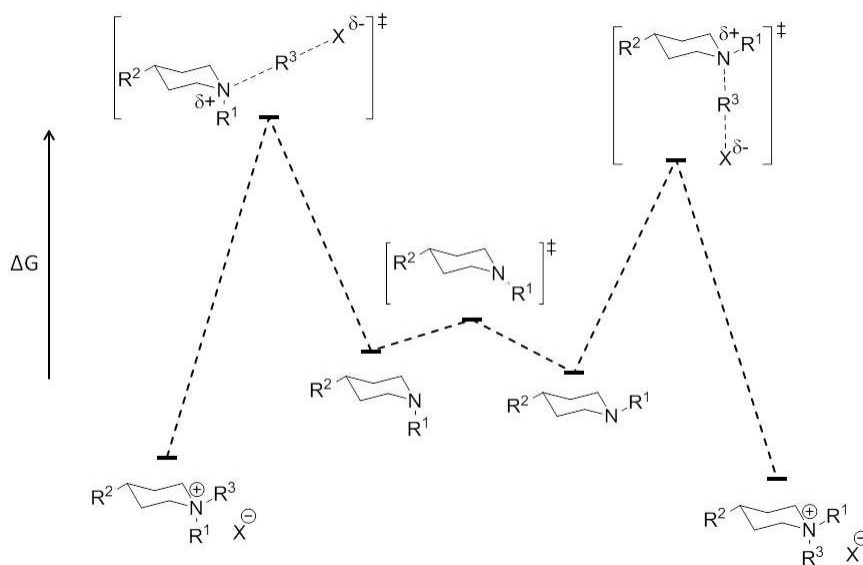


Figure 4. The second boundary condition of the Curtin-Hammett Principle illustrated by piperidine alkylation.

While Figure 3 and Figure 4 show nitrogen inversion as the only means of invertomer interconversion, it is possible for cyclic amines to transition between equatorial and axial

conformers via ring inversion, as well as processes that couple ring inversion and nitrogen inversion.⁶⁷

Because the *N*-alkylation of substituted *N*-alkylpiperidines to give diastereomeric products provides a very nice example of the reactivity of conformationally mobile systems, this reaction was studied extensively from the 1950s to the 1970s.^{62,68} Some general trends in the selectivity of this reaction were observed, though exceptions to these trends were also noted.

Section 3.2.1: Methylation of N-Alkylpiperidine Derivatives

It is generally accepted that *N*-methylation occurs primarily via axial attack, as determined via the comparison of diastereomeric ¹H NMR peaks. Typically, the integrations of the methyl group are used to determine the diastereomeric ratio, and the chemical shifts of these peaks are used to assign axial versus equatorial diastereomers; it is assumed (and has been confirmed in select cases)⁶⁹ that the deshielded methyl group is equatorial and the shielded methyl group is axial due to piperidine ring anisotropy.

Table 1. Literature examples of diastereoselective *N*-methylation of *N*-alkylpiperidines.^{70,71,72}

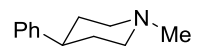
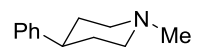
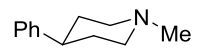
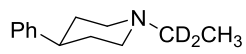
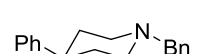
axial alkylation equatorial alkylation

Piperidine	Alkylating Agent	Solvent	% Axial Alkylation	% Equatorial Alkylation	Reference
	MeCl	1,2-dimethoxyethane	73	27	69
	Mel		82	18	
	MeOTs		83	17	
	MeOTs	acetone	80	20	
	MeOTs	acetone	85	15	70
	CD ₃ I	acetonitrile	68	32	71
		methanol	74	26	
	CD ₃ I	acetonitrile	79	21	71
		methanol	80	20	
	Mel	acetonitrile	73	27	71
		methanol	78	22	
	Mel	acetonitrile	79	21	71
		methanol	79	21	
	Mel	acetonitrile	>94	<6	71
	Mel	acetonitrile	76	24	71
		methanol	77	23	
	Mel	acetonitrile	>94	<6	71
	Mel	acetonitrile	89	11	71

Section 3.2.2: Ethylation of *N*-Alkylpiperidine Derivatives

N-Ethylation tends to occur preferentially via axial attack, but with lower selectivity than methylation, as can be seen in the examples in Table 2. A noted exception is the anomalous reactivity of triethyloxonium tetrafluoroborate, which gives a 1:1 mixture of diastereomers.⁷³

Table 2. Literature examples of diastereoselective *N*-ethylation of *N*-alkylpiperidine derivatives.^{70,71,73,74}

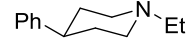
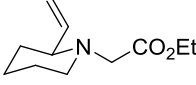
Piperidine	Alkylating Agent	Solvent	% Axial Alkylation	% Equatorial Alkylation	Reference
	EtOTs EtOTs	acetone	75 83	25 17	69, 70
	Et ₃ O ⁺ BF ₄ ⁻	dichloromethane	50	50	72
	Etl	acetone	60	40	72
	Etl	acetonitrile methanol	57 58	43 42	73
	Etl	acetonitrile methanol	57 60	43 40	73
	Etl	acetonitrile methanol	66 67	34 33	73
	Etl	acetonitrile methanol	78 81	22 19	73

Section 3.2.3: Benzylation of *N*-Alkylpiperidine Derivatives

N-Benzylation can give varying selectivities that are dependent on the alkylating agent and solvent (Table 3). For example, the benzylation of 4-*tert*-butyl-1-methylpiperidine with benzyl chloride occurs primarily via axial alkylation in methanol, but the selectivity reverses to

equatorial alkylation when the solvent is less polar (e.g. benzene).⁷⁵ Equatorial alkylation is most common.

Table 3. Literature examples of diastereoselective *N*-benzylation of *N*-alkylpiperidine derivatives.^{71,75,76,77}

Piperidine	Alkylating Agent	Solvent	% Axial Alkylation	% Equatorial Alkylation	Reference
	BnOTs	acetone	69	31	70
	BnCl	methanol	57	43	74
		acetonitrile	49	51	
		benzene	39	61	
	<i>p</i> -MeOBnCl	acetonitrile	48	52	75
	BnCl		33	67	
	<i>p</i> -NO ₂ BnCl		29	71	
	<i>p</i> -MeOBnCl	acetonitrile	43	57	75
	BnCl		34	66	
	<i>p</i> -NO ₂ BnCl		23	77	
	<i>p</i> -MeOBnCl	acetonitrile	40	60	75
	BnCl		31	69	
	<i>p</i> -MeOBnCl	acetone	53	47	76
	BnCl		66	34	
	BnBr	acetone	only product isolated		76

Section 3.2.4: Other Alkylating Agents in the Quaternization of *N*-Alkylpiperidine Derivatives

Typically, larger alkylating agents lead to preferential equatorial alkylation. However, as noted in Table 4, the structure of the substrate can lead to significant deviations from this trend.

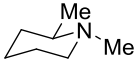
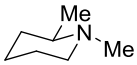
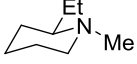
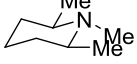
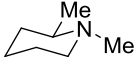
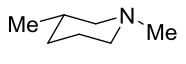
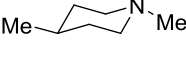
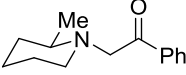
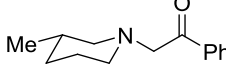
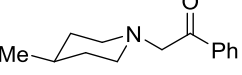
Table 4. Literature examples of diastereoselective *N*-alkylation of *N*-alkylpiperidine derivatives.^{71,77,78}

Piperidine	Alkylating Agent	Solvent	% Axial Alkylation	% Equatorial Alkylation	Reference
		acetone	50	50	70
		acetonitrile	only product isolated		76
			7	93	
		dichloromethane	6	94	77
			10	90	

Section 3.2.5: Alkylation of Conformationally Mobile Piperidine Systems

The vast majority of diastereoselective piperidine alkylations have been performed on 4-substituted piperidines in which the 4-substituent is sterically very bulky (*tert*-butyl, phenyl, cyclohexyl, etc.), greatly reducing the concentration of ring-inverted conformers in solution. While this simplifies the problem at hand, this does not represent all of the piperidine systems of interest to synthetic chemists. In the few examples of more conformationally mobile systems (e.g. when the substituent on the ring is small, like methyl), some of the trends noted previously, such as methylation and ethylation occurring preferentially via axial alkylation, are not necessarily followed (Table 5).

Table 5. Literature examples of diastereoselective *N*-alkylation of *N*-alkylpiperidine systems capable of ring inversion.^{73,65,79}

Piperidine	Alkylating Agent	Solvent	% Axial Alkylation	% Equatorial Alkylation	Reference
	Et ₃ O ⁺ BF ₄ ⁻ EtI	dichloromethane acetone	62 50	38 50	72
	CD ₃ I EtI	acetone	66 43	34 57	64
	CD ₃ I EtI	acetone	56 36	44 64	64
	CD ₃ I EtI	acetone	44 11	56 89	64
	CD ₃ I EtI	acetone	34 9	66 91	64
	PhCOCH ₂ Br PhCOCH ₂ Cl	acetonitrile	19 18	81 82	78
	PhCOCH ₂ Br PhCOCH ₂ Cl	acetonitrile	40 37	60 63	78
	PhCOCH ₂ Br PhCOCH ₂ Cl	acetonitrile	39 37	61 63	78
	Mel	acetonitrile	62	38	78
	Mel	acetonitrile	68	32	78
	Mel	acetonitrile	64	36	78

Section 3.2.6: Explanations Offered For Trends in N-Alkylation

The Hammond Postulate has been used often to explain the trend in selectivity of piperidine alkylations with different alkylating agents. In McKenna's⁷³ words, "The arguments employed have taken the general form: faster quaternisation : more reactant-like transition state: longer partial N – C (in attacking electrophile) bond : more axial quaternisation (and *vice versa* for slower quaternisation)." Though this rationalization works in most cases, this quote is from a paper in which ethylation with triethyloxonium tetrafluoroborate (more reactive yet less axial alkylation) versus ethyl iodide (less reactive yet more axial alkylation) is an apparent exception.

In terms of piperidine structure, Katritzky⁸⁰ offers this explanation: "as the steric hindrance to axial approach increases, more equatorial product is found". That is, larger alkylating agents favour equatorial alkylation over axial alkylation, which is what is observed in most cases: benzylation > ethylation > methylation in terms of amount of equatorial alkylation. As noted in Section 3.2.3, however, the alkylating agent (leaving group/counterion) and solvent used in the alkylation reactions have a large effect on selectivity; in some cases, the selectivity can be reversed from mostly equatorial to mostly axial by varying reaction conditions. In an example from Bottini and coworkers, the selectivity of the reaction of 4-*tert*-butyl-1-methylpiperidine with benzyl chloride changed from 1.35:1 axial:equatorial to 0.95:1 to 0.63:1 in methanol, acetonitrile, and benzene, respectively, favouring axial alkylation in methanol and equatorial alkylation in benzene.⁷⁵

In terms of solvent effects, the general trend observed in the alkylation of piperidines is that more polar solvents favour axial alkylation and less polar solvents favour equatorial alkylation. This agrees with the above arguments based on the Hammond Postulate; S_N2 reactions are known to occur more rapidly in polar solvents, as the charge separation in the

transition state is stabilized. The quaternization of amines is a special type of S_N2 reaction; the reactants are neutral, but the products are charged. Based on this property, this reaction also becomes more exergonic in more polar solvents, as the charged products are more stabilized than the neutral reagents. Because of this, the reaction is irreversible in polar solvents but may become reversible in nonpolar solvents; this idea is supported by recent computational studies of the reaction of ammonia with chloromethane.⁸¹ The fact that solvent may affect how reversible or irreversible this reaction is adds another layer of complexity to the question of diastereoselectivity in piperidine alkylation that has thus far not been sufficiently addressed.

Section 3.3: Case Studies

Although there was a lot of experimental work done on diastereoselective *N*-alkylpiperidine alkylation in the 1960s and early 1970s, many of the rationalizations postulated for the selectivity of this reaction with different piperidine derivatives, alkylating agents, and solvents have gone untested. Because computational methods are now widely available, these trends and hypotheses can be studied much more in depth. Three case studies were performed based on early experimental results in an effort to (a) see if the computational chemistry technology has come far enough to reproduce the overall trends and numbers seen in these early results and (b) provide clarity regarding the mechanistic details of these reactions.

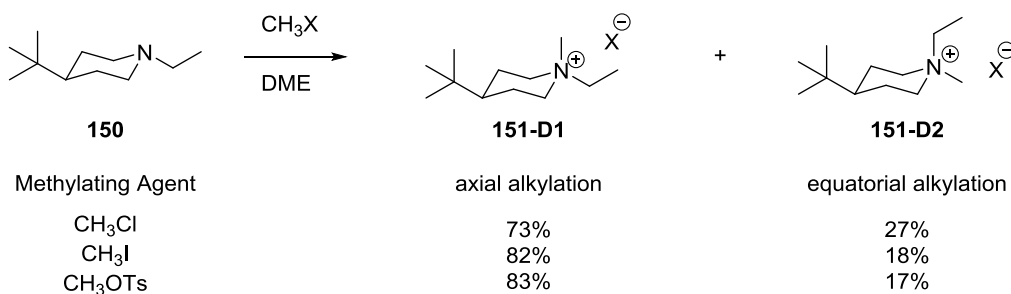
Section 3.3.1: Computational Details

DFT calculations were carried out using the B3LYP,⁸² M06-2x,⁸³ and mPW1PW (implemented using the keyword mPW1PW91)⁸⁴ functionals with the 6-31+G(d) and 6-311+G(d,p) basis sets in the Gaussian 09⁸⁵ suite of programs. Additionally, MP2⁸⁶ was used with

the 6-311+G(d,p) basis set for single point energy calculations. The SDB-cc-pVTZ⁸⁷ basis set, which combines the Stuttgart-Dresden-Bonn relativistic effective core potential (ECP)⁸⁸ along with the correlation consistent basis set cc-pVTZ⁸⁹ in order to take into account relativistic effects in larger atoms, was added onto iodine in the relevant systems. Frequency calculations were carried out to ensure that the intermediates had no negative frequencies and the transition states had only one imaginary frequency, as well as to calculate contributions to the Gibbs free energy (reported at 298.15 K and 1 atm). Intrinsic reaction coordinate (IRC)⁹⁰ calculations were carried out on the transition states to ensure that they connected the reactants with the products. Solvent was taken into account using the polarizable continuum model (PCM).⁹¹ Structures were optimized at the B3LYP/6-31+G(d) level in the appropriate solvent. Single-point energies were calculated at the M06-2x(mPW1PW, MP2)/6-311+G(d,p) level in the appropriate solvent. Notably, M06-2x and MP2 were explored due to their inclusion of dispersion effects, which B3LYP and mPW1PW lack. ΔG s were calculated using the results from single-point energy calculations along with contributions to the Gibbs free energy calculated at the B3LYP/6-31+G(d)/PCM level.

Section 3.3.2: House, 1972 – Methylation of 4-tert-butyl-1-ethylpiperidine

In their 1972 Journal of Organic Chemistry paper,⁷⁰ House and coworkers reported that more reactive methylating agents gave higher axial to equatorial product ratios in the alkylation of 4-*tert*-butyl-1-ethylpiperidine 150 (Scheme 44).



Scheme 44. Methylation of 4-*tert*-butyl-1-ethylpiperidine **150**.

Four transition states were calculated for each methylating agent – axial (**TS150-D1-ax**) and equatorial (**TS150-D2-eq**) alkylation to directly give **151-D1** and **151-D2**, as well as axial and equatorial alkylation on the piperidine chair conformers with the *tert*-butyl substituent axial (**TS150-D1-eq** and **TS150-D2-ax**; see Figure 5 for examples with methyl chloride as the alkylating agent). The difference in transition state energies was then used to calculate the theoretical product ratios according to the equation $[D1]/[D2] = e^{-\Delta G^\ddagger/RT}$, where **D1** and **D2** are the diastereomeric products, ΔG^\ddagger is the difference in transition state energies, R is the gas constant = 8.314 Jmol⁻¹K⁻¹, and T is the temperature = 298.15 K.⁶⁶

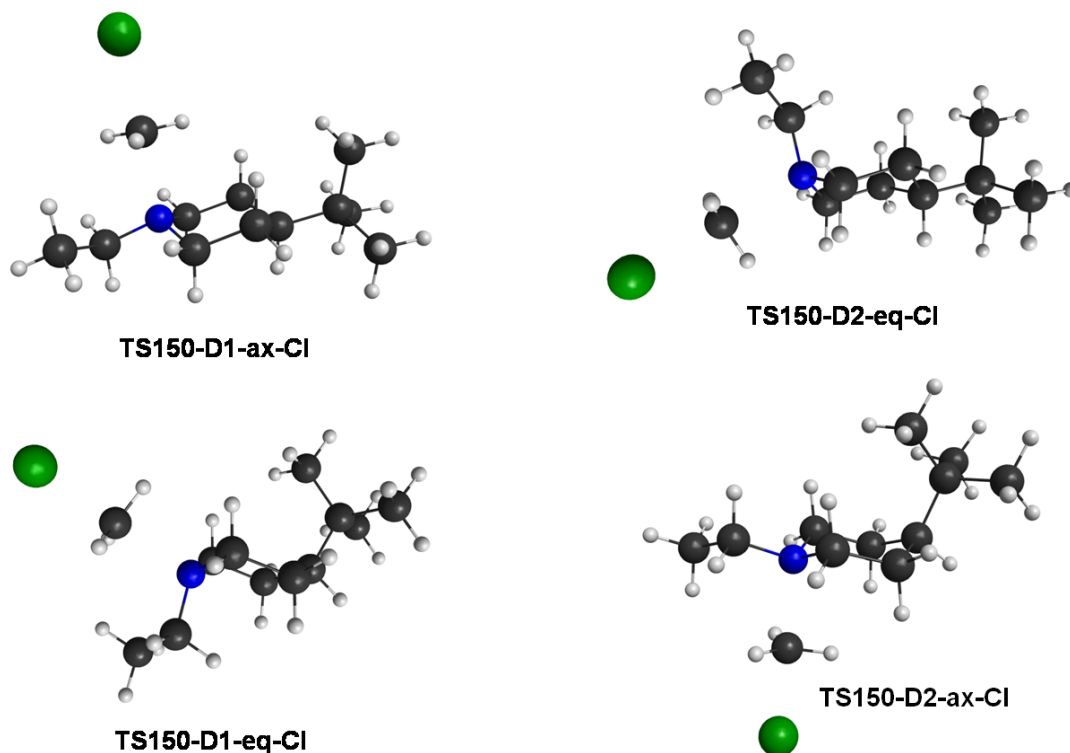


Figure 5. Transition structures in the reaction of 4-*tert*-butyl-1-ethylpiperidine **150** with methyl chloride; “TS” refers to transition structure, “150” refers to the reaction of **150**, “D1” refers to formation of the axial alkylation product **151-D1** vs. “2” forming the equatorial alkylation product **D2**, “ax” refers to axial alkylation vs. “eq” as equatorial alkylation, and “Cl” refers to the methylating agent used.

The results of these calculations are summarized in Table 6. Note that the only product ratios consistent with all of the reactions studied are obtained from the transition state energies calculated at the MP2/6-311+G(d,p)/PCM(DME) level. All of the DFT methods gave the opposite trend from the experimental data; this may be due to comparing results with different basis sets (SDB-cc-pVTZ on iodine in the methyl iodide reaction) and/or only taking into account one configuration/conformation of the *p*-toluenesulfonate anion in the methyl *p*-toluenesulfonate reaction. Additionally, only chair conformers were considered; though unlikely, it is possible that alkylation could occur on twist boat conformers.

Table 6. Transition state energies and the corresponding product ratios for each methylation reaction of 4-*tert*-butyl-1-ethylpiperidine **150** to form diastereomeric salts **151-D1** and **151-D2**.

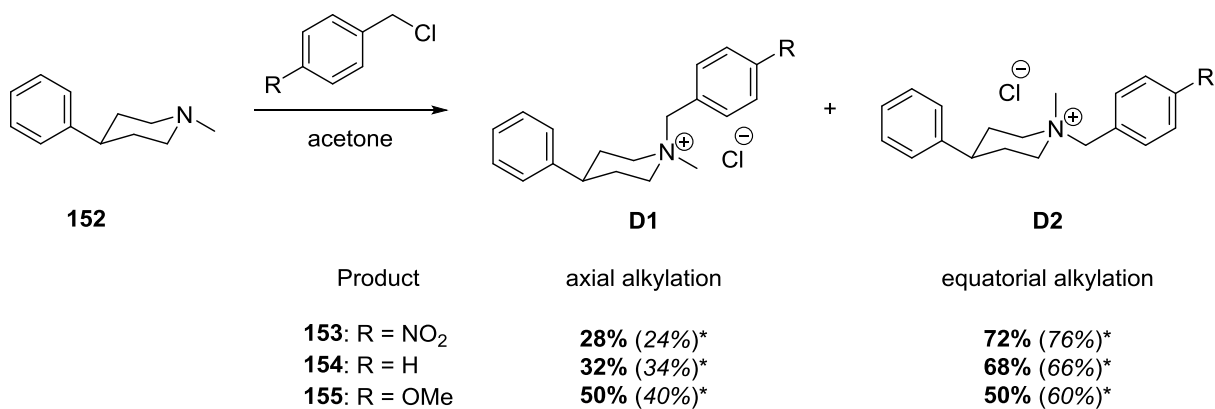
TS	Alkylating Agent	D1: D2	B3LYP	B3LYP	M06-2x	M06-2x	mPW1PW91	D1:D2	MP2	MP2
			ΔG^\ddagger	D1:D2	ΔG^\ddagger	D1:D2	ΔG^\ddagger		ΔG^\ddagger	D1:D2
TS150-D1-ax-Cl	MeCl	73	0.00	78	0.00	72	0.00	72	0.00	83
TS150-D2-eq-Cl	MeCl	27	0.76	22	0.55	28	0.57	28	0.93	17
TS150-D2-ax-Cl	MeCl	-	6.48	0	5.99	0	6.39	0	6.02	0
TS150-D1-eq-Cl	MeCl	-	7.10	0	6.55	0	6.81	0	6.85	0
TS150-D1-ax-I	MeI	82	0.00	73	0.00	68	0	70	0.00	83
TS150-D2-eq-I	MeI	18	0.59	27	0.46	32	0.50	30	0.95	17
TS150-D2-ax-I	MeI	-	6.08	0	5.70	0	6.03	0	5.88	0
TS150-D1-eq-I	MeI	-	6.61	0	6.17	0	6.41	0	6.52	0
TS150-D1-ax-OTs	MeOTs	83	0.00	73	0.00	65	0.00	70	0.00	85
TS150-D2-eq-OTs	MeOTs	17	0.58	27	0.36	35	0.50	30	1.03	15
TS150-D2-ax-OTs	MeOTs	-	4.72	0	5.79	0	6.47	0	6.05	0
TS150-D1-eq-OTs	MeOTs	-	7.10	0	6.44	0	6.91	0	6.94	0

The activation energies of axial alkylation are 21.8 kcal/mol for the reaction with MeCl, 20.7 kcal/mol for MeI, and 23.6 kcal/mol for MeOTs, meaning that the most active methylating agent is predicted to be methyl iodide and the least active is methyl *p*-toluenesulfonate. If this is true, this is not consistent with the hypothesis based on early experimental observations that the more active alkylating agent gives more axial alkylation product; experimentally, MeOTs gives the most axial alkylation, and, computationally, MeCl gives the most axial alkylation. While these inconsistencies could be due to computational limitations, there were inconsistencies noted in the experimental work, particularly in the methyl chloride reaction. The reaction was performed with twice the concentration of alkylating agent. The yield was 24.8% by

precipitation, raising the possibility that the product ratio reflects preferential crystallization of one diastereomer over the other rather than the inherent selectivity of the reaction. If we remove the methyl chloride results from consideration, all methods indicate very close, if not the same, diastereomeric product ratios for methyl iodide and methyl tosylate, which is consistent with experimental results. Additionally, it was confirmed that the transition states with the *t*-butyl substituent axial do not make a significant contribution to the product ratio.

Section 3.3.3: Katritzky, 1973 – Benzylation of 1-methyl-4-phenylpiperidine

Katritzky and coworkers' 1973 paper⁷⁶ studied the reaction of 1-methyl-4-phenylpiperidine **152** with various benzyl chloride derivatives – *p*-nitrobenzyl chloride, benzyl chloride, and *p*-methoxybenzyl chloride (Scheme 45). Interestingly, Katritzky reported different product ratios for this same reaction in his 1970 paper,⁸⁰ indicating a certain amount of error associated with the measurement of diastereomeric ratios. This further suggests that an exact match between the experimental numbers and computational numbers may not be realistic, and a focus on the qualitative trends may be the best approach to provide meaningful results and insights.



**values reported in Katritzky's 1970 paper*

Scheme 45. Benzylation of 1-methyl-4-phenylpiperidine **152**.

In benzylation, there are transition states that differ based solely on rotation of the benzyl group with respect to the piperidine (Figure 6). When the product ratio is calculated, all of these transition states must be taken into account.

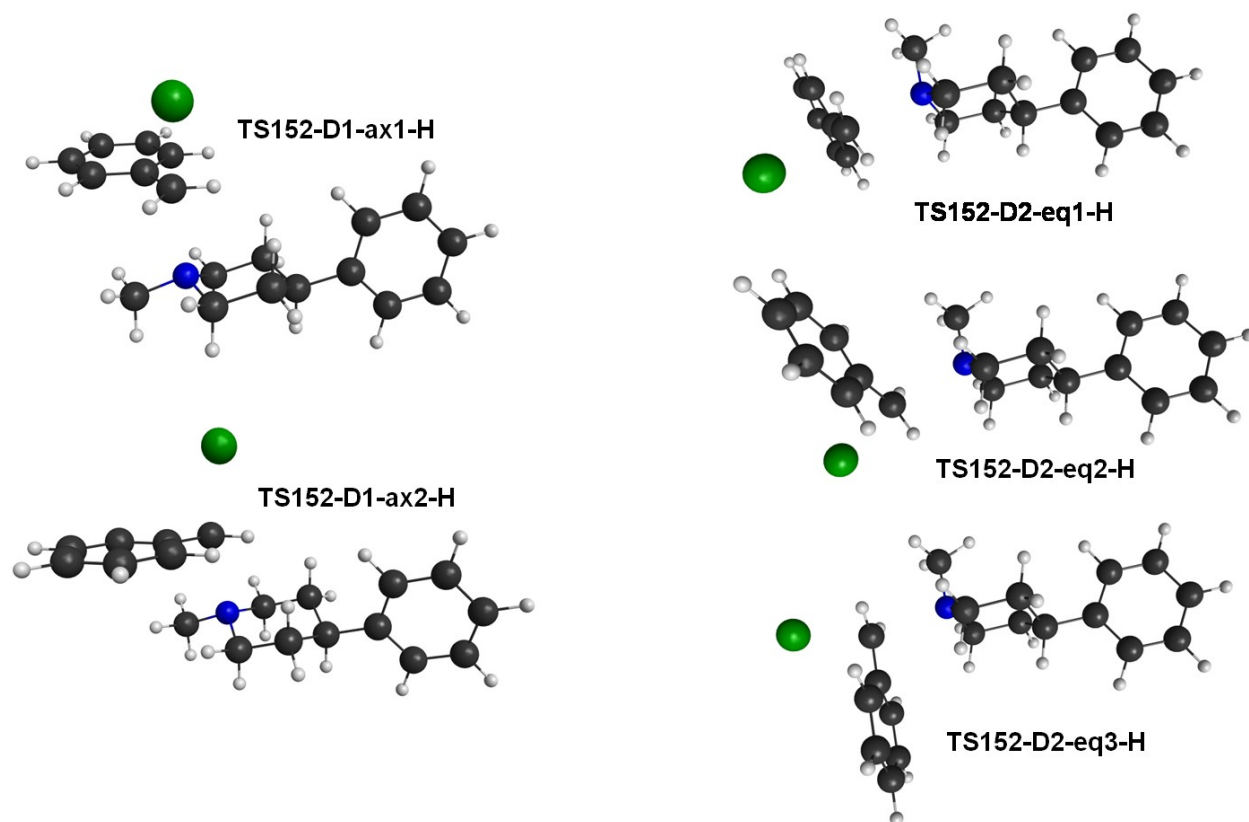


Figure 6. Transition structures in the reaction of 1-methyl-4-phenylpiperidine **152** with benzyl chloride to form diastereomeric salts **154-D1** and **154-D2**.

All computational methods employed provide the correct trend (Table 7; “**D1** total” refers to the total contribution of all transition states that lead to axial alkylation products **153-D1**, **154-D1**, or **155-D1**, and “**D2** total” refers to the total contribution of all transition states that lead to equatorial alkylation product **153-D2**, **154-D2**, or **155-D2**). Single point energy calculations with M06-2x provide numerical values very close to those reported in the 1973 paper. Note that transition states with the 4-phenyl substituent axial (akin to **TS150-D1-eq** and **TS150-D2-ax** in Figure 5) were also calculated, but they were found to be too high in energy to contribute significantly to the product distribution of the reaction; these results are included in the supporting information.

Table 7. Relative transition state Gibbs free energies (kcal/mol) and the corresponding product ratios (%) for each benzylation reaction; “152” refers to the reaction of 1-methyl-4-phenylpiperidine **152**, “D1” refers to the formation of axial alkylation product **153-D1**, **154-D1**, or **155-D1**, “ax1” refers to the first axial alkylation transition state, “O” refers to the use of *p*-methoxybenzyl chloride as the alkylating agent.

TS	Alkylating Agent	B3LYP	Product	M06-2x	Product	MP2	Product	Exptl
		ΔG^\ddagger	Ratio	ΔG^\ddagger	Ratio	ΔG^\ddagger	Ratio	Ratio
TS152-D1-ax1-O	<i>p</i> -MeOBnCl	0.39	26.3	0.32	18.4	0.12	28.3	
TS152-D1-ax2-O	<i>p</i> -MeOBnCl	0.00	51.1	0.00	31.4	0.00	34.8	
TS152-D2-eq1-O	<i>p</i> -MeOBnCl	1.34	5.3	0.44	14.9	0.76	9.6	
TS152-D2-eq2-O	<i>p</i> -MeOBnCl	1.11	7.9	0.32	18.2	0.59	12.9	
TS152-D2-eq3-O	<i>p</i> -MeOBnCl	1.00	9.4	0.36	17.2	0.53	14.2	
TS152-D1-ax1-H	BnCl	0.66	12.7	0.61	10.7	0.67	16.0	
TS152-D1-ax2-H	BnCl	0.00	38.5	0.00	30.0	0.00	49.5	
TS152-D2-eq1-H	BnCl	0.42	19.0	0.00	29.8	0.71	14.9	
TS152-D2-eq2-H	BnCl	0.75	10.9	0.49	13.0	1.11	7.6	
TS152-D2-eq3-H	BnCl	0.42	18.9	0.36	16.5	0.83	12.1	
TS152-D1-ax1-N	<i>p</i> -NO ₂ BnCl	0.14	11.5	0.21	12.1	0.25	23.4	
TS152-D1-ax2-N	<i>p</i> -NO ₂ BnCl	0.00	14.5	0.00	17.2	0.00	35.9	
TS152-D2-eq1-N	<i>p</i> -NO ₂ BnCl	-0.23	21.3	-0.26	26.6	0.68	11.3	
TS152-D2-eq2-N	<i>p</i> -NO ₂ BnCl	-0.13	18.0	-0.08	19.6	0.75	10.1	
TS152-D2-eq3-N	<i>p</i> -NO ₂ BnCl	-0.52	34.7	-0.21	24.4	0.37	19.2	
153-D1 total	<i>p</i> -MeOBnCl		77		50		63	50
153-D2 total	<i>p</i> -MeOBnCl		23		50		37	50
154-D1 total	BnCl		51		41		65	32
154-D2 total	BnCl		49		59		35	68
155-D1 total	<i>p</i> -NO ₂ BnCl		26		29		59	28
155-D2 total	<i>p</i> -NO ₂ BnCl		74		71		41	72

In order to provide rationalization for the selectivity trends seen in these reactions, the lowest energy axial transition states for each benzylating agent (**TS152-D1-ax2**, Figure 7) were examined. Here, the most “active” alkylating agent is *p*-methoxybenzyl chloride, having the earliest transition state and the lowest activation barrier based on the IRC plot of **TS152-D1-ax2** for each benzylating agent (Figure 8). The least active alkylating agent is *p*-nitrobenzyl chloride, having the latest transition state and the highest activation barrier. The early explanations of more active alkylating agent = earlier transition state = more axial alkylation indeed seem to hold true for this system. This is quite heartening, especially since benzylation in particular is the alkylation reaction most relevant to our studies towards lysergic acid (Chapter 2).

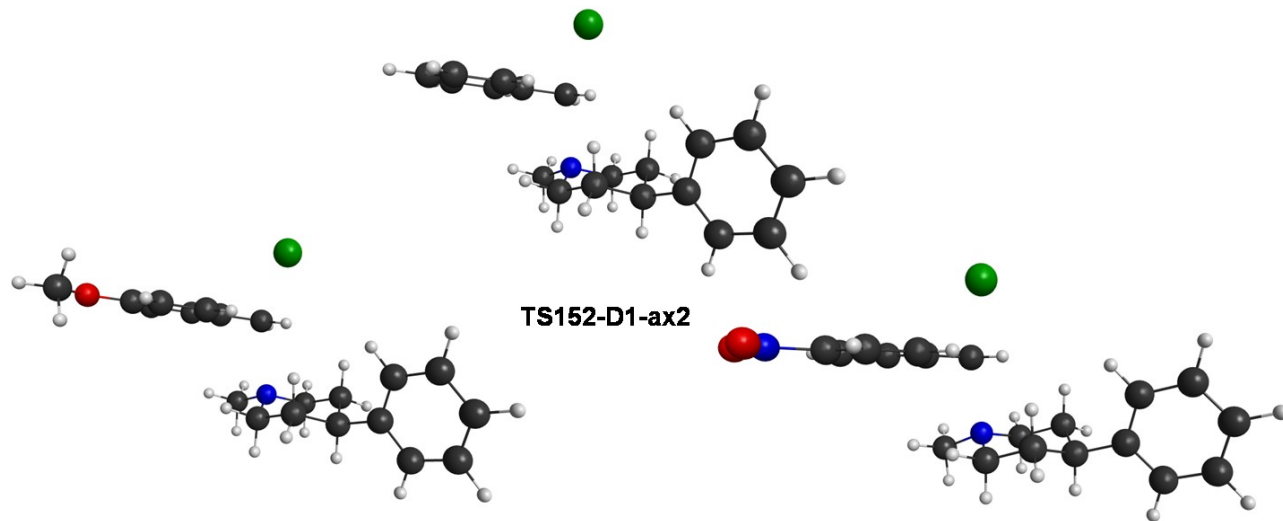


Figure 7. The lowest energy transition structures for the benzylation of 1-methyl-4-phenylpiperidine **152** with each alkylating agent.

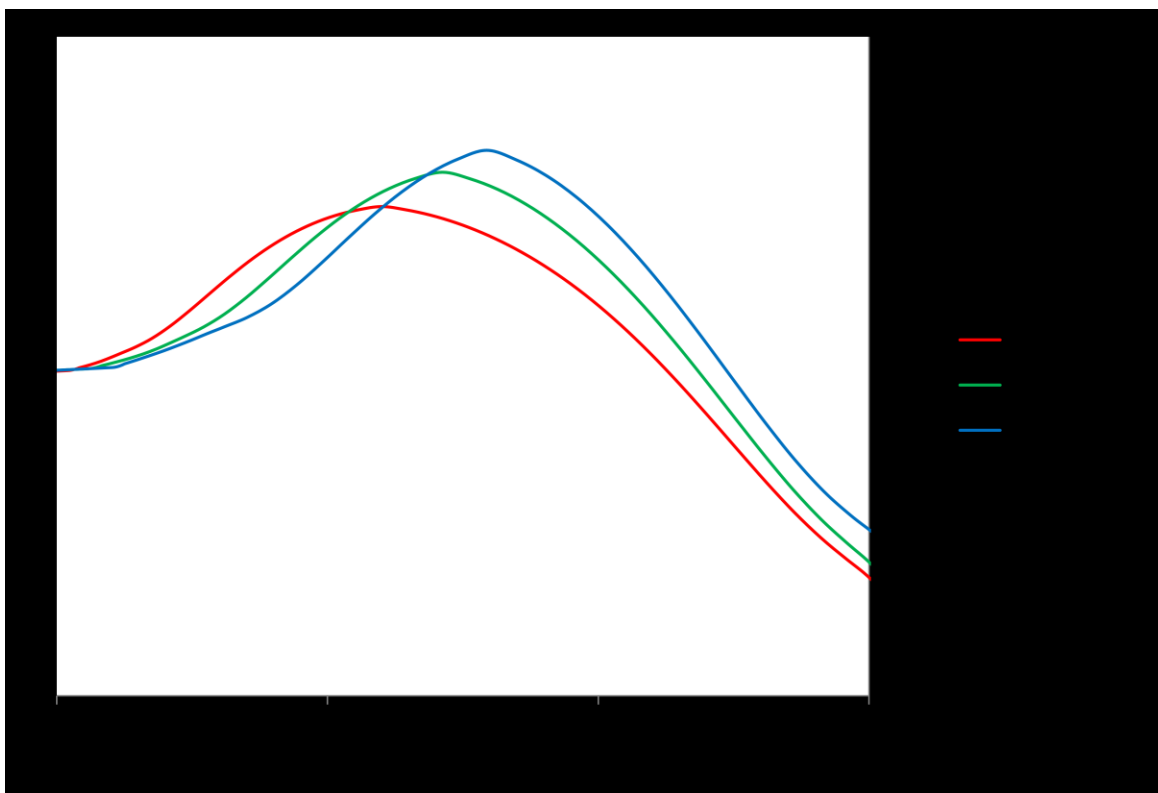
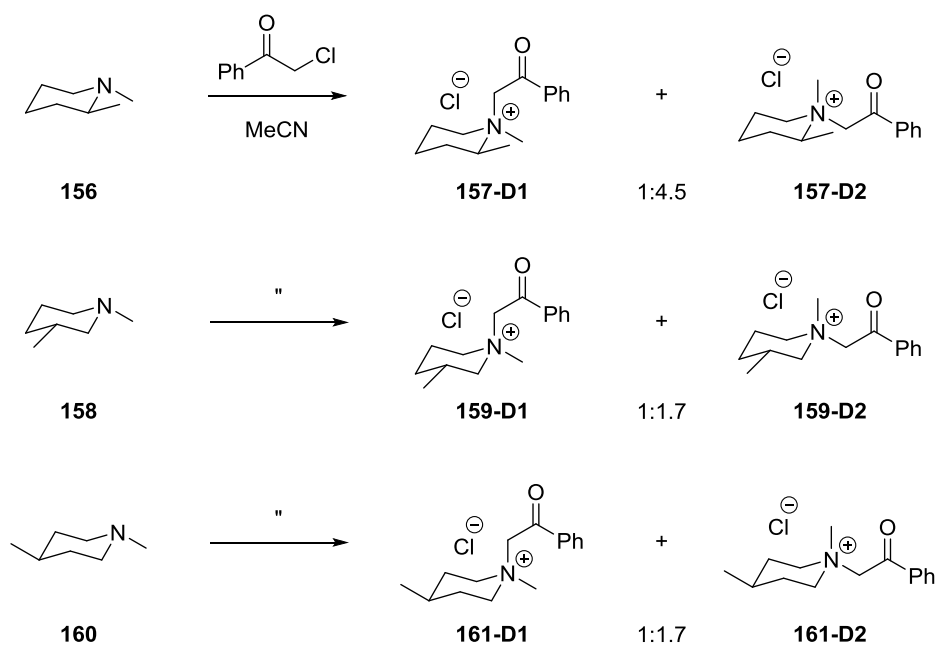


Figure 8. IRC plots of forming N-C bond distance (Å) versus ΔG (kcal/mol) for the benzylation of 1-methyl-4-phenylpiperidine **152** via transition states **TS152-D1-ax2**.

Section 3.3.4: Smith, 1973 – Reaction of 1,2-, 1,3-, and 1,4-dimethylpiperidine with 2-chloro-1-phenylethanone

In Smith and coworkers' 1973 paper,⁷⁹ alkylation of the conformationally mobile 1,2-, 1,3-, and 1,4-dimethylpiperidine systems (**156**, **158**, and **160**, respectively) were studied. All systems reacted to form predominantly equatorial alkylation product **D2**, though the reaction using 1,2-dimethylpiperidine **156** was much more selective (Scheme 46).



Scheme 46. Selectivity in the reactions of 1,2-, 1,3-, and 1,4-dimethylpiperidine with 2-chloro-1-phenylethanone.

Because of the conformational flexibility of the piperidine derivatives, four main conformers of starting material needed to be taken into account – the two invertomers at nitrogen with methyl equatorial and the two invertomers at nitrogen with methyl axial (Figure 9).

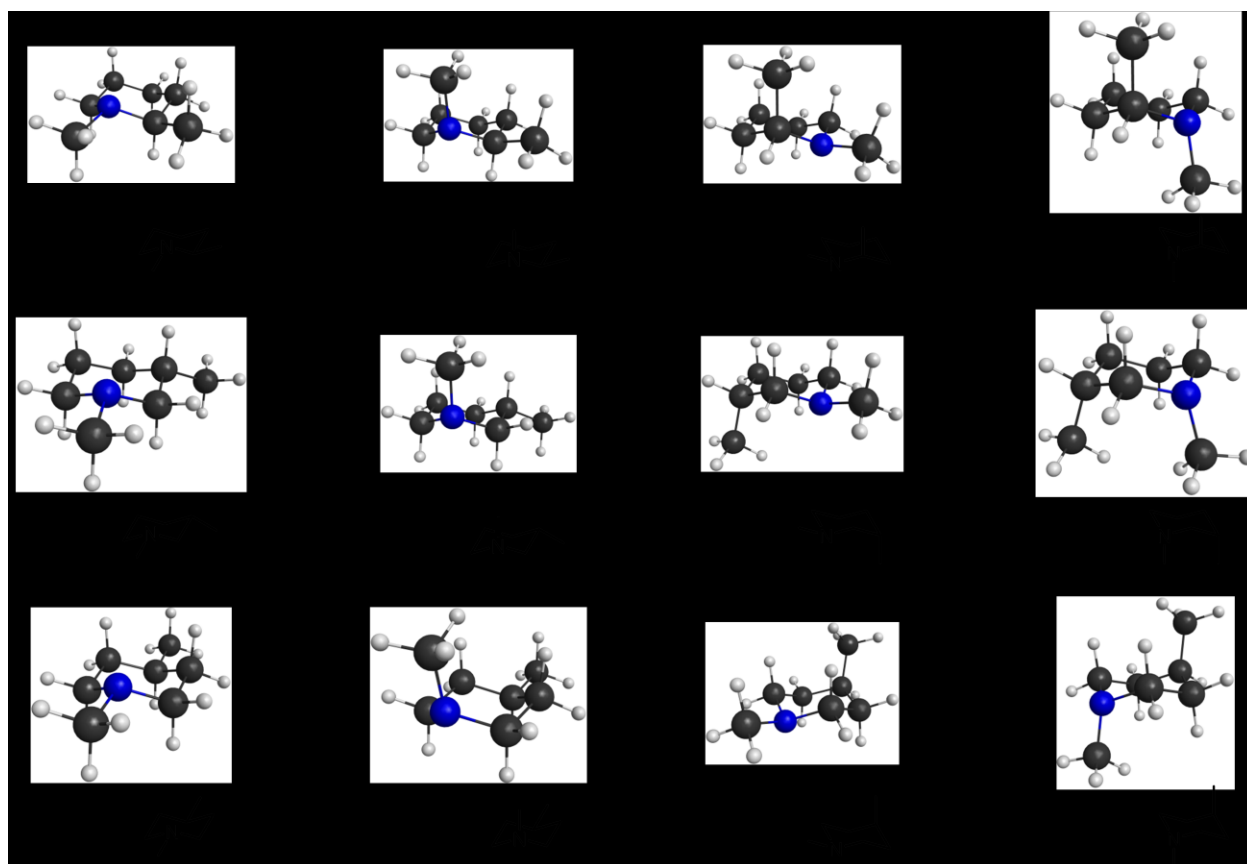


Figure 9. The main conformers of 1,2-, 1,3-, and 1,4-dimethylpiperidine with 3D structures and relative Gibbs free energies in kcal/mol calculated at B3LYP/6-31+G(d)/PCM(MeCN). Note that the 3D structures of **156-3**, **156-4**, **158-3**, and **158-4** are the enantiomers of the line drawing shown.

For each conformer, a total of six transition states was theoretically possible – threefold rotation of the alkylating agent in addition to a 180 degree “flip” of the phenacyl substituent – see Figure 10 for the example of all six the transition states in the alkylation of 1,3-dimethylpiperidine conformer **158-4**. Six is an upper limit; many transition states converged to the same transition state to avoid unfavourable steric interactions. In addition, due to the plane of symmetry in 1,4-dimethylpiperidine, only three unique transition states for each conformer could be found – see Figure 11 for the transition states of alkylation of conformer **160-1**.

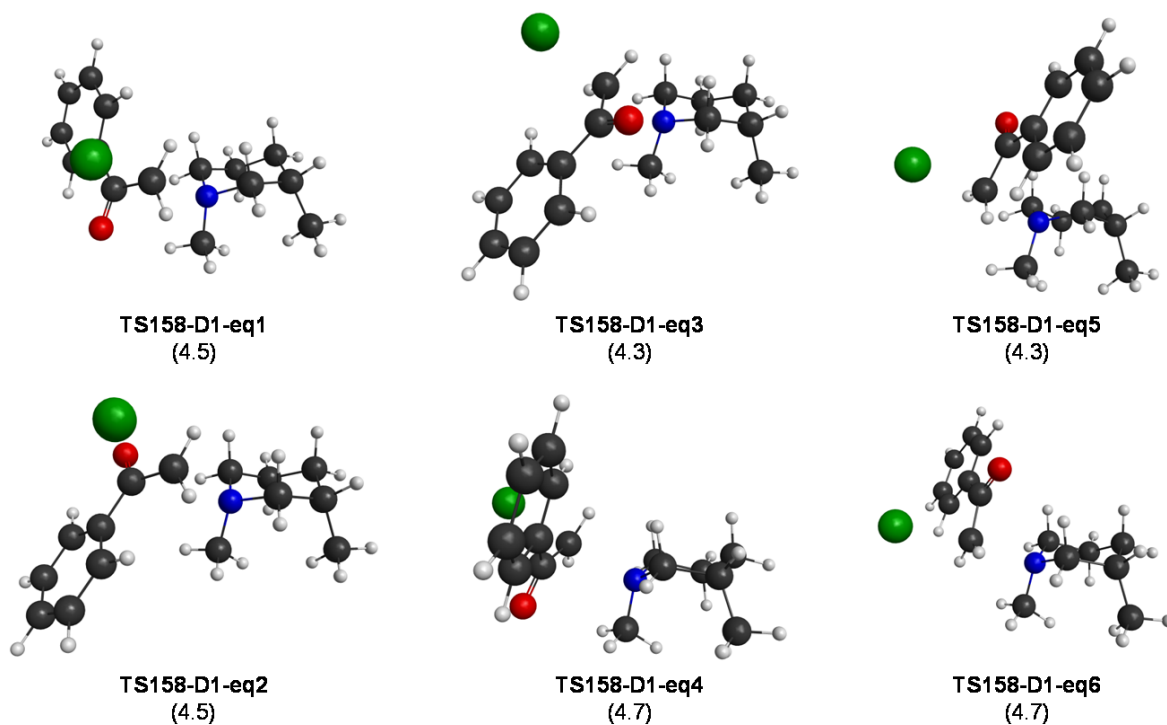


Figure 10. Transition states in the alkylation of 1,3-dimethylpiperidine conformer **158-4**. Gibbs free energies in kcal/mol at B3LYP/6-31+G(d)/PCM(MeCN) relative to the lowest energy transition state in this system (**TS158-D2-eq3**) are given in parentheses.

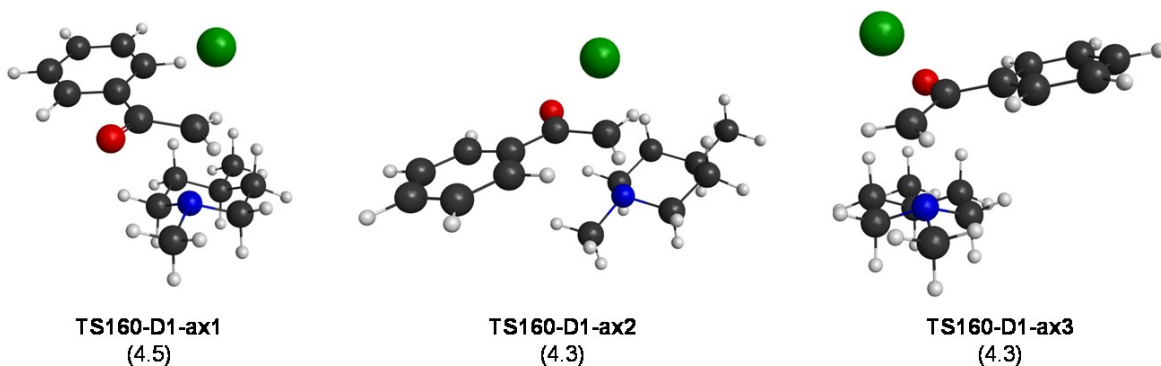


Figure 11. Transition states in the alkylation of 1,4-dimethylpiperidine conformer **160-1**. Gibbs free energies in kcal/mol at B3LYP/6-31+G(d)/PCM(MeCN) relative to the lowest energy transition state in this system (**TS160-D2-eq1**) are given in parentheses.

The computational results support the experimental observation of preferential equatorial alkylation in each system; the lowest energy transition state in each system is an equatorial

alkylation transition state (Figure 12). Additionally, formation of equatorial alkylation product **D2** is favoured in all three reactions with all of the DFT methods employed. The computational results using M06-2x seem to support the experimental numbers best, at least for the alkylation of 1,2- and 1,3-dimethylpiperidine (Table 8 and Table 9, respectively). All DFT methods give the correct trend for the alkylation of 1,2- and 1,3-dimethylpiperidine, with selectivity for equatorial alkylation being better for 1,2-dimethylpiperidine than for 1,3-dimethylpiperidine. MP2 gives ratios that differ significantly from the experimental observations, indicating no selectivity for the alkylation of 1,2-dimethylpiperidine and preferential axial alkylation for 1,3-dimethylpiperidine. The exception to these trends is the alkylation of 1,4-dimethylpiperidine (Table 10), where DFT methods give too high a selectivity for equatorial alkylation; for instance, B3LYP and mPW1PW91 indicate that it should be a more selective reaction than alkylation of 1,2-dimethylpiperidine. This does not agree with the experimental results, or the fact that the methyl substituent on the ring is furthest away, leading one to assume it will have a lower influence on the diastereoselectivity of the reaction. The only method that provides a reasonable diastereomeric ratio for the alkylation of 1,4-dimethylpiperidine is MP2, though it does not adequately describe the other two substrates.

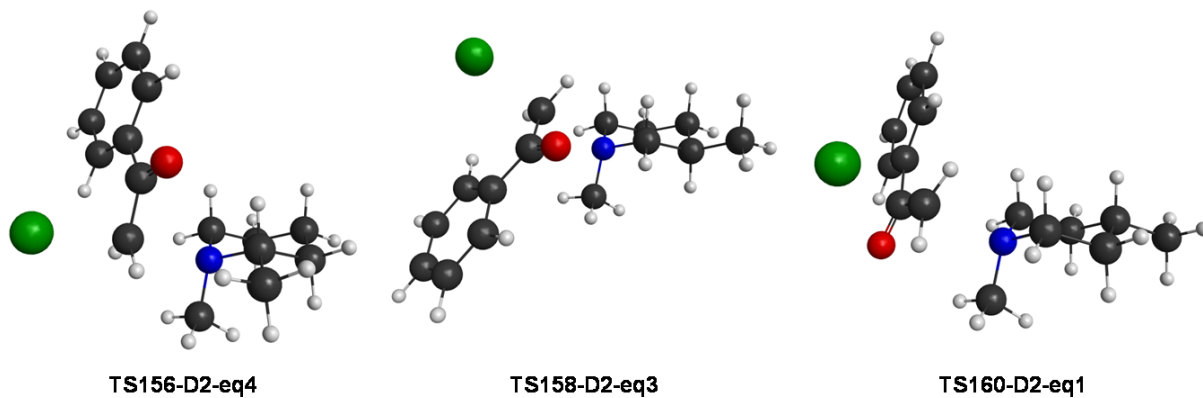


Figure 12. The lowest energy transition structures in the alkylation of 1,2-, 1,3-, and 1,4-dimethylpiperidine.

Table 8. Relative transition state Gibbs free energies (kcal/mol) and the corresponding product ratios (%) for the alkylation of 1,2-dimethylpiperidine **156**. Note that only transition states within 3 kcal/mol from the lowest energy transition state are included.

TS	B3LYP	Pdt	M06-2x	Pdt	MP2	Pdt	mPW1PW91	Pdt	Exptl
	ΔG^\ddagger	Ratio							
TS156-D1-ax1	0.57	10.9	0.69	9.0	0.60	12.4	0.64	10.3	
TS156-D1-ax2	0.81	7.2	0.40	14.8	0.00	33.9	0.78	8.2	
TS156-D1-ax3	1.25	3.5	1.52	2.2	1.60	2.3	1.37	3.0	
TS156-D1-eq1	2.86	0.2	2.54	0.4	3.23	0.1	2.70	0.3	
TS156-D1-eq2	2.85	0.2	2.55	0.4	3.01	0.2	2.79	0.3	
TS156-D1-eq3	2.37	0.5	1.56	2.1	2.35	0.6	2.05	1.0	
TS156-D2-ax1	2.25	0.6	1.75	1.5	1.62	2.2	2.16	0.8	
TS156-D2-ax2	2.01	1.0	1.77	1.5	2.23	0.8	1.95	1.1	
TS156-D2-ax3	2.30	0.6	1.75	1.5	1.57	2.4	2.29	0.6	
TS156-D2-ax4	1.72	1.6	1.31	3.2	1.74	1.8	1.64	1.9	
TS156-D2-eq1	0.30	17.2	0.69	9.1	1.15	4.9	0.43	14.7	
TS156-D2-eq2	0.37	15.3	0.57	11.1	1.23	4.3	0.42	15.0	
TS156-D2-eq3	0.48	12.7	0.41	14.5	0.61	12.1	0.53	12.5	
TS156-D2-eq4	0.00	28.5	0.00	28.9	0.25	22.1	0.00	30.4	
157-D1 total		22.5		28.9		49.6		23.0	<i>18.2</i>
157-D2 total		77.5		71.1		50.4		77.0	<i>81.8</i>

Table 9. Relative transition state Gibbs free energies (kcal/mol) and the corresponding product ratios (%) for the alkylation of 1,3-dimethylpiperidine **158**. Note that only transition states within 3 kcal/mol from the lowest energy transition state are included.

TS	B3LYP	Pdt	M06-2x	Pdt	MP2	Pdt	mPW1PW91	Pdt	Exptl
	ΔG^\ddagger	Ratio							
TS158-D1-ax1	0.86	5.9	0.37	10.6	0.09	25.0	0.85	5.9	
TS158-D1-ax2	0.80	6.4	0.53	8.1	0.84	7.1	0.84	6.0	
TS158-D1-ax3	0.58	9.4	0.25	12.8	0.52	12.2	0.61	8.9	
TS158-D1-ax4	1.09	4.0	0.40	9.9	0.00	29.2	1.14	3.6	
TS158-D2-eq1	0.24	16.6	0.22	13.6	0.86	6.8	0.20	17.7	
TS158-D2-eq2	0.45	11.6	0.38	10.4	1.30	3.3	0.46	11.4	
TS158-D2-eq3	0.00	24.8	0.00	19.7	0.89	6.5	0.00	24.9	
TS158-D2-eq4	0.52	10.2	0.51	8.3	0.95	5.9	0.48	11.1	
TS158-D2-eq5	0.48	11.0	0.65	6.6	1.17	4.1	0.51	10.4	
159-D1 total		25.7		41.4		73.5		24.4	<i>37.0</i>
159-D2 total		74.3		58.6		26.5		75.6	<i>63.0</i>

Table 10. Relative transition state Gibbs free energies (kcal/mol) and the corresponding product ratios (%) for the alkylation of 1,4-dimethylpiperidine **160**. Note that most transition states above 3 kcal/mol from the lowest energy transition state are excluded with some exceptions.

TS	B3LYP	Pdt	M06-2x	Pdt	MP2	Pdt	mPW1PW91	Pdt	Exptl
	ΔG^\ddagger	Ratio							
TS160-D1-ax1	1.35	4.2	0.98	6.8	0.39	16.8	1.41	3.8	
TS160-D1-ax2	0.66	13.3	0.33	20.4	0.39	16.8	0.70	12.4	
TS160-D1-eq1	3.16	0.2	2.49	0.5	2.76	0.3	2.13	1.1	
TS160-D1-eq3	3.05	0.2	2.26	0.8	2.97	0.2	2.19	1.0	
TS160-D1-eq3	3.08	0.2	2.46	0.6	2.44	0.5	2.26	0.9	
TS160-D2-ax1	3.30	0.2	2.40	0.6	2.59	0.4	2.08	1.2	
TS160-D2-ax2	3.33	0.1	2.32	0.7	1.93	1.2	2.49	0.6	
TS160-D2-eq1	0.00	40.5	0.00	35.3	0.00	32.3	0.00	40.8	
TS160-D2-eq2	0.43	19.4	0.35	19.7	0.35	18.0	0.46	18.6	
TS160-D2-eq3	0.37	21.7	0.52	14.6	0.52	13.4	0.43	19.6	
161-D1 total		18.1		29.0		34.6		19.2	<i>37.0</i>
161-D2 total		81.9		71.0		65.4		80.8	<i>63.0</i>

In the case studies based on work by House and Katritzky, the piperidine rings were locked into primarily one chair conformation by large substituents in the 4-position. In this case study, however, the piperidine rings are more conformationally mobile due to the ring substituent being the much smaller methyl group. The ammonium salt products are also likely more conformationally mobile. Assignment of the diastereomeric product chemical shifts in the ^1H NMR spectrum was done based on previous studies of less conformationally mobile salts; it was assumed that the deshielded signal was the equatorial substituent on the ring and the shielded signal was the axial substituent on the ring based on piperidine ring anisotropy. This may not be

true, depending on the substituents, and it might not be a reliable way to assign chemical shifts to a system that is very likely fluxional on the NMR time scale. A more in-depth experimental and computational analysis, including comparison of experimental and calculated chemical shifts, of this reaction is desired for these reasons.

Section 3.4: Summary and Future Plans

A systematic computational approach towards predicting diastereomeric product ratios in known piperidine alkylation reactions is useful, not just for potentially predicting product ratios in as yet untested reactions, but for helping us understand a reaction that has been shelved for several decades.

In our case study on Katritzky's 1973 benzylation reactions, data from DFT calculations correlated well with experimental values; the alkylation trend (qualitative data) and ratios (quantitative data) were both well matched. Examination of the IRC plots of the lowest energy axial transition state for each benzylating agent showed that the hypothesis from the old literature regarding more active alkylating agents resulting in earlier transition states and more axial alkylation held true, at least in this one case.

In our case study of House's 1972 methylation reactions, it is difficult to draw definitive conclusions about the reliability of the computational work due to inconsistencies in the alkylation procedures using different methyl sources; however, two of the three reactions are described very well by the computational data.

Smith's 1973 alkylation reactions on three different dimethyl-substituted piperidines made for a much more challenging case study, as the piperidine ring is no longer in mainly one chair conformation. In his analysis, Smith assumed that the chair form with the methyl group

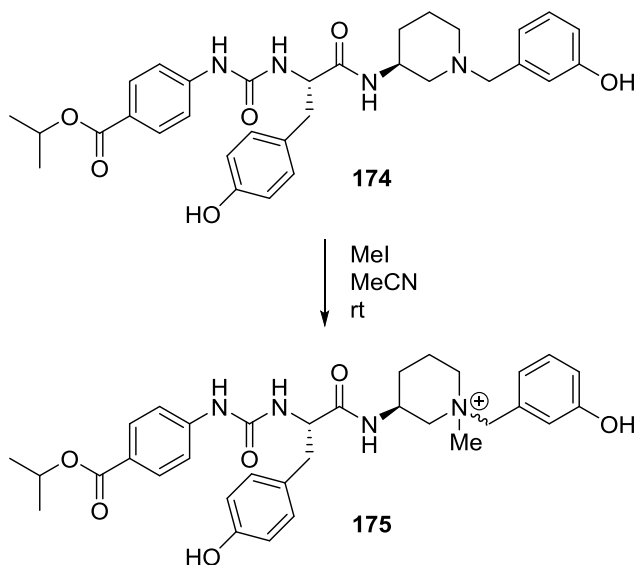
equatorial would dominate and, therefore, disregarded the potential for product formation via more than two transition states. Although data derived from DFT calculations support the experimental data for the alkylations of 1,2- and 1,3-dimethylpiperidine, the computationally-derived numbers for the 1,4-dimethylpiperidine predict much more equatorial alkylation than observed experimentally.

Although the results of these case studies are promising, more definitive conclusions could be drawn from computational work that is accompanied by new experimental studies that use more rigorous methods for the measurement of product ratios and assignment of product structures. Ideally, we would gather new data on these old reactions, conducting more than one trial of each reaction, obtaining higher quality NMR data, and obtaining crystal structures to confirm diastereomer assignment. Additionally, we could perform each of these reactions in different solvents and at different temperatures to find out more about how these factors contribute to the reaction rates and diastereomeric ratios.

With more time, more computational methods could be explored; while DFT is the obvious choice for the geometry optimization of these fairly large systems, we could look at more *ab initio* methods for single point energy calculations. Furthermore, only chair conformers were considered to undergo alkylation; in order to be rigorous, we should look at the entire potential energy surface for the piperidine starting materials and consider alkylation transition states on twist-boat conformers.

An additional drawback with the old experimental results is that the substituents on the piperidine ring are alkyl or aromatic groups, with most experimental reports based on conformationally-locked systems; we feel that systems with polar substituents on the piperidine ring and more conformationally mobile systems need to be explored. Chapter 4 of this thesis

describes alkylation of *N*-methyl and *N*-benzylpiperidines with an oxygen substituent in the 3-position (either OH or OTBDPS), as well as the use of computational chemistry to study the transition states in the reaction and predict chemical shifts of the products. A much larger substrate scope should ideally be explored, including smaller alkyl substituents and other polar substituents in the 2-, 3-, and 4-positions, as well as a larger variety of alkylating agents. Additionally, we should study some bioactive compounds; for example, compound **175** was found to be a promising asthma treatment, but the final piperidine alkylation step could not be performed in a diastereoselective fashion, so development of this drug was abandoned in favour of compounds without a stereocentre at the nitrogen of the piperidine ring.^{61e} This example underscores the need to study this seemingly simple reaction in a more detailed and rigorous fashion.



Scheme 47. Alkylation of piperidine derivative **174** to obtain drug candidate **175**.

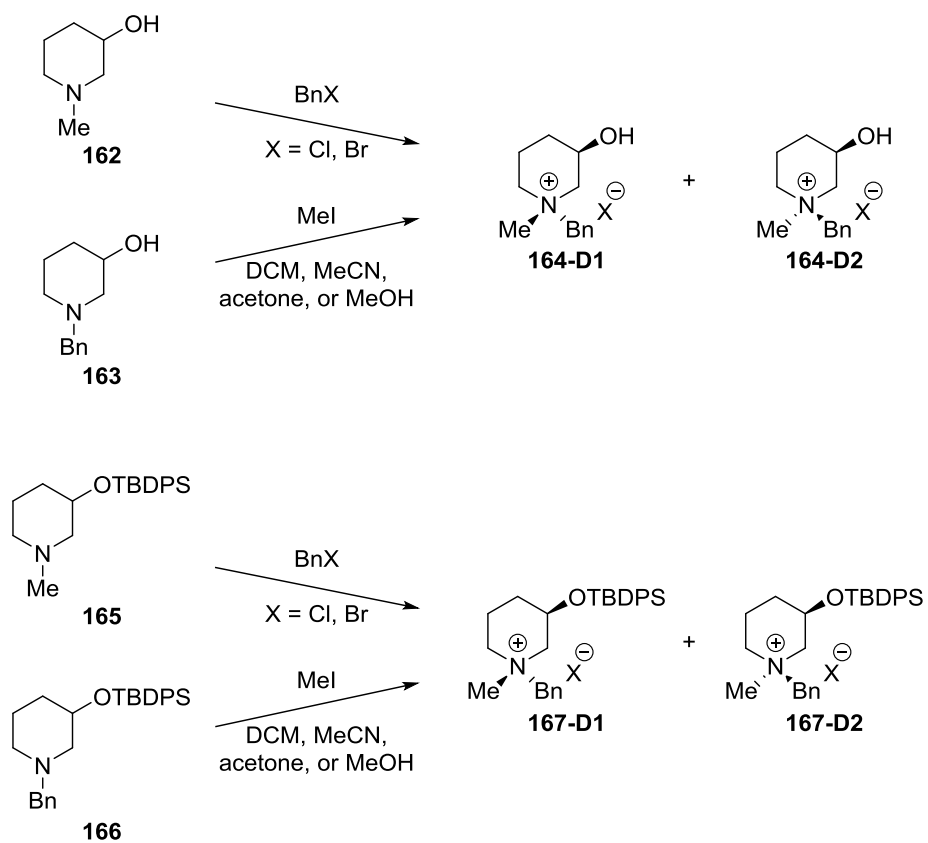
Chapter 4: New *N*-Alkylation Experiments and their Computational Analysis

Section 4.1: Introduction

Previous experimental work in diastereoselective piperidine alkylation has generally focused on conformationally locked piperidine rings and piperidine derivatives with alkyl substituents, usually in the 4-position. We hoped to expand the substrate scope of this reaction to systems with smaller, polar substituents on the 3-position of the piperidine ring, as well as obtain new experimental data to explore the predictive ability of computational work on this reaction.

*Section 4.2: Design and Execution of New *N*-Alkylation Experiments*

3-Hydroxy-1-methylpiperidine **162**, 1-benzyl-3-hydroxypiperidine **163**, and their TBDPS-protected derivatives, **165** and **166**, were chosen as small, easy to access, conformationally mobile piperidine derivatives on which to carry out alkylations with different alkylating agents in a variety of solvents (Scheme 48). *N*-methylpiperidines **162** and **165** were alkylated with benzyl bromide and benzyl chloride in dichloromethane, acetone, methanol, and acetonitrile (Table 11), and *N*-benzylpiperidines **163** and **166** were alkylated with methyl iodide in the same solvents (Table 12); each reaction was performed at least twice, more if the diastereomeric ratios differed significantly in the two trials.⁹² The typical differences in *dr* were 1-2 %. Note that the solvents are listed in order of polarity based on dielectric constant.⁹³



Scheme 48. Alkylation of piperidine derivatives **162**, **163**, **165**, and **166**.

Table 11. Benzylation of *N*-methylpiperidines **162** and **165**. Reactions were performed at room temperature, and the diastereomeric ratio was determined via integration of the appropriate ¹H NMR signals (see text for further information).

X	Solvent	3-hydroxy-1-methylpiperidine (162)			3-(<i>tert</i> -butyldiphenylsiloxy)-1- methylpiperidine (165)		
		Reaction Time (h)	164-D1 (%)	164-D2 (%)	Reaction Time (h)	167-D1 (%)	167-D2 (%)
Br	DCM	<1	36	64	< 1	49	51
Br	Acetone	1	41	59	< 1	47	53
Br	MeOH	2	43	57	< 1	52	48
Br	MeCN	1	39	61	< 1	46	54
Cl	DCM	< 1	36	64	24	49	51
Cl	Acetone	24	41	59	48	45	55
Cl	MeOH	48	41	59	21	53	47
Cl	MeCN	1	38	62	24	43	57

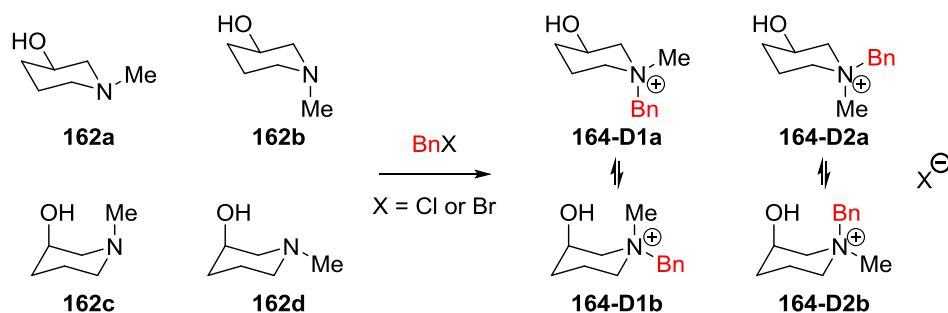
Table 12. Methylation of *N*-benzylpiperidine derivatives **163** and **166**. Reactions were performed at room temperature, and the diastereomeric ratio was determined via integration of the appropriate ¹H NMR signals (see text for further information).

X	Solvent	1-benzyl-3-hydroxypiperidine (163)			3-(<i>tert</i> -butyldiphenylsiloxy)-1- methylpiperidine (166)		
		Reaction Time (h)	164-D1 (%)	164-D2 (%)	Reaction Time (h)	167-D1 (%)	167-D2 (%)
I	DCM	0.5	46	54	3	31	69
I	Acetone	0.5	45	55	2	34	66
I	MeOH	0.5	40	60	19	31	68
I	MeCN	0.5	46	54	1	37	63

The preferred formation of the axial alkylation product for the methylation of *N*-benzylpiperidines **163** and **166** (%D2 > %D1) and preferred formation of the equatorial

alkylation product for the benzylation of *N*-methylpiperidines **162** and **165** (%**D2** >%**D1**) is in line with trends seen previously for piperidine *N*-alkylation (Chapter 3). Previous literature data also detail the increase in the amount of axial alkylation product observed in more polar solvents; however, we could see no obvious dependence of the product ratio on solvent polarity. This may have to do with the presence of the alcohol substituent or the fact that we have used a different solvent polarity scale than previous researchers.⁷⁵ Another well-documented trend in the literature is the increase in reaction rate with increase in solvent polarity (especially protic solvents), an effect that has been supported computationally;⁸¹ however, we noted that the use of protic solvent methanol had the opposite effect, slowing the reaction down. It is possible that this is due to the alcohol substituent, which likely has a greater solvation sphere in protic solvents, creating a barrier to alkylation and reducing the nucleophilicity of the adjacent nitrogen.⁹⁴

The experimental diastereomeric ratios were determined via integration of the appropriate ¹H NMR signals. In the case of the 3-hydroxypiperidinium salt **163**, the proton at the 3-position of the piperidine ring was used to measure the diastereomeric ratio (*dr*), as this was quite often the best-resolved signal; for the TBDPS-protected piperidinium salt **166**, the benzylic proton signals were used. Although the *dr* was easy to determine, the assignment of diastereomers was more complicated. In this reaction, there is the potential to form two diastereomers, each with two possible chair conformers; Scheme 49 demonstrates this idea using the example of the benzylation of 3-hydroxy-1-methylpiperidine **162**, though this applies to all systems studied in this chapter. Due to this complicated assignment of diastereomers, ¹H NMR chemical shifts were simulated by DFT calculations (in the absence of crystal structures to unequivocally assign diastereomer identities).



Scheme 49. Benzylation of the four main conformers of 3-hydroxy-1-methylpiperidine **162** to form two diastereomeric products **164-D1** and **164-D2**.

Section 4.3: Diastereomer Assignment Using Simulated NMR Chemical Shifts

The identity of each diastereomer was assigned based on the comparison of computationally-derived ¹H NMR chemical shifts with experimental chemical shifts.

Section 4.3.1: Computational Details

Calculations were performed with Gaussian 09.⁸⁵ Computed chemical shifts were determined using the GIAO method⁹⁵ in Gaussian 09 at the mPW1PW91/6-311+G(2d,p)/SMD(CHCl₃)//B3LYP/6-31+G(d,p) level of theory,^{82,84} and are empirically scaled. Empirical scaling was performed using the equation $\delta = - (b - \sigma) / m$, where δ is the computed chemical shift, σ is the computed isotropic shielding constant, m is the slope, and b is the intercept. For the ¹H NMR shifts, the values of $m = -1.0936$ and $b = 31.8018$ were used as recommended by Tantillo *et al.* on cheshirenmr.info.⁹⁶ SMD refers to inclusion of solvent effects using the SMD implicit solvent model.⁹⁷ For diastereomer **164-D1**, eight conformers were located, with three predicted to be significant contributors (greater than 1% of the conformer population) based on computed free energies at the B3LYP/6-31+G(d,p) level of theory. For diastereomer **164-D2**, nine conformers were located, with six of them predicted to be significant

contributors. For diastereomer **170-D1**, six conformers were located, with four of them predicted to be significant contributors; for diastereomer **170-D2**, six conformers were located, with five of them predicted to be significant contributors. The computed shifts for compounds **164-D1**, **164-D2**, **170-D1**, and **170-D2** reflect a Boltzmann-weighted average. Unique conformers were located by systematic examination of the various degrees of freedom of the compounds (ring inversion, rotation of the benzyl group, and rotation of the O-H bond) followed by geometry optimization.

Section 4.3.2: Hydroxyl-substituted Piperidinium Salt 164

In the case of piperidinium salt **164**, the chemical shift of the methyl group on the nitrogen was chosen as the most easily differentiated NMR signal (Figure 13). This is due to the structure of the lowest energy conformers (**164-D1** has the methyl group axial, and **164-D2** has the methyl group equatorial), as well as the fact that it was easy to determine which methyl group had the higher integration in the ^1H NMR spectrum.

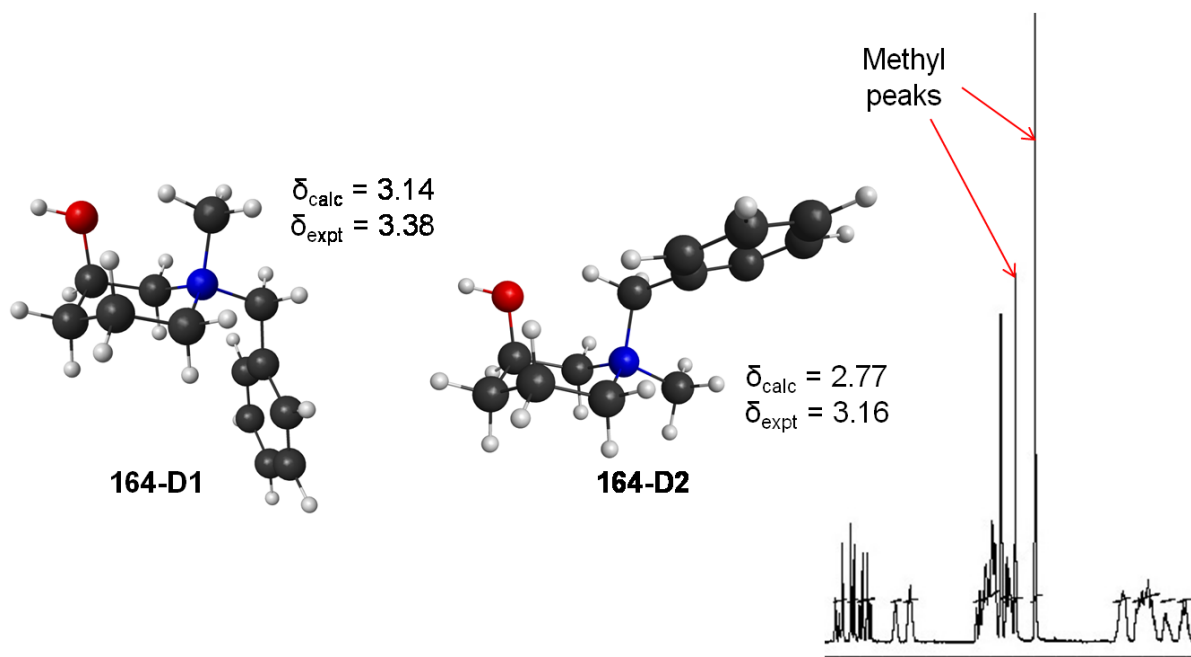


Figure 13. Identifying ^1H NMR chemical shifts of **164-D1** and **164-D2**. Structures optimized at B3LYP/6-31+G(d,p), NMR calculations at mPW1PW91/6-311+G(2d,p)/SMD(CHCl_3). Calculated chemical shifts reflect a weighted average of contributions of all conformers with a >1% contribution to the population, though only the lowest energy conformer of each diastereomer is shown. Experimental chemical shifts are reported in CDCl_3 .

Interestingly, the axial methyl group of **164-D1** was found to be deshielded with respect to the equatorial methyl group. This may be due to deshielding effects of the phenyl ring based on the position of the methyl and benzyl groups relative to one another in the lowest energy conformer of **164-D1**; this is contrasted with the relative positions of the equatorial methyl and axial benzyl groups in **164-D2**, in which the methyl group is in the shielding region of the phenyl ring. An additional explanation for the deshielding of the axial methyl group has to do with its proximity to the alcohol oxygen; it is possible that there is an O-CH interaction that is lengthening the CH bonds on the methyl group, resulting in deshielded methyl protons. O-CH interactions involving ammonium salts have been well-documented in the literature.⁹⁸ The reason these results are so interesting is that, typically, in previous reports of diastereoselective

piperidine alkylation, it was assumed that the axial methyl was shielded and the equatorial methyl deshielded due to anisotropy of the piperidine ring; most literature data relies on this assumption for the assignment of diastereomers.^{62,68} It is possible, based on our computational results, that some diastereomers may have been misassigned in the old literature.

It is also notable that the lowest energy conformer of each diastereomer of piperidinium salt **164** has the hydroxyl group axial, which is counterintuitive in terms of steric effects; the A-value of OH is 0.33 – 0.96 kcal/mol, depending on solvent.⁹⁹ However, it may be favourable to have a heteroatom axial in a piperidinium salt because it allows for non-classical hydrogen bonding between the methyl or benzylic hydrogens (Figure 14), which also supports our explanation for the deshielded axial groups in the NMR calculations.⁹⁸ The stabilizing effect of an axial alcohol substituent in protonated piperidine systems can also be observed via the reduction in acidity of the piperidinium salt.¹⁰⁰

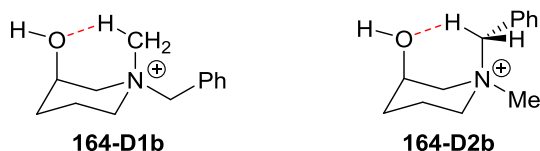


Figure 14. Hydrogen bonding of the alcohol oxygen with a proton on the axial methyl or benzyl group of diastereomeric piperidinium salts **164**.

Section 4.3.3: *tert*-Butyldiphenylsiloxy-substituted Piperidinium Salt **167**

In the case of piperidinium salt **167**, it was determined that including the entire TBDPS group in the computed structures would be quite difficult due to the large number of atoms and electrons, as well as the added degrees of freedom due to rotation of the phenyl groups. Thus,

this group was replaced with a simpler TMS group for both NMR calculations and reaction mechanism calculations.

The findings for the TMS-protected piperidinium salt **170** echoed those found for the simple hydroxyl system; both low energy conformers have the heteroatom in the axial position despite the greater steric demand of this substituent now that the proton has been replaced with a silyl group (Figure 15). Although the conformer structures are similar to **164**, the methyl signals in the ^1H NMR spectrum often overlapped with other signals, making it difficult to obtain a reliable ratio measurement; thus, the benzylic proton signals were chosen to make our assignment, in addition to providing us with the diastereomeric ratio. It was most notable in the ^1H NMR spectrum of **167** that one diastereomer (the major diastereomer) had very distinct signals for each benzylic proton, whereas, for the other diastereomer, the signals converged to appear as an apparent singlet. Based on the computed NMR data, diastereomer **170-D2** is expected to have benzylic protons with very different chemical shifts (>1 ppm difference), whereas **170-D1** is expected to have benzylic protons with very similar chemical shifts (<0.05 ppm difference). This provides the basis for our diastereomeric assignment of piperidinium salt **167**.

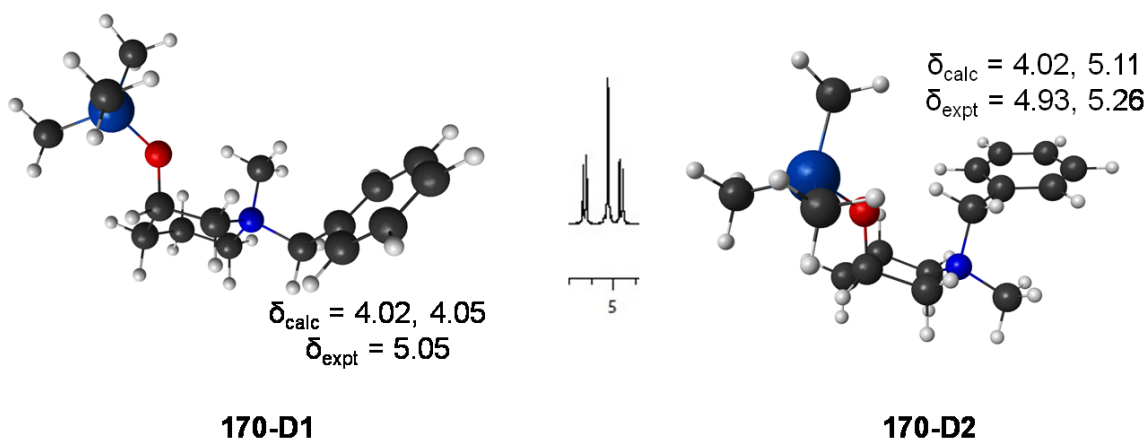


Figure 15. Identifying ^1H NMR chemical shifts of **170-D1** and **170-D2**. Structures optimized at B3LYP/6-31+G(d,p), NMR calculations at mPW1PW91/6-311+G(2d,p)/SMD(CHCl_3). Calculated chemical shifts reflect a weighted average of contributions of all conformers with a >1% contribution to the population, though only the lowest energy conformer of each diastereomer is shown. Experimental chemical shifts are reported in CDCl_3 .

It can be noted that the calculated chemical shift values are lower than those obtained experimentally. This may be due to the fact that neither solvent nor a counterion were included in the geometry optimization step; inclusion of these factors could change the electron density around the ammonium ion. However, we wanted to use a proven method for calculating the chemical shifts, hence the optimization in the gas phase. As for the counterion, we would have to sample many structures in which the anion is in different places with respect to the ammonium ion to account for its effects rigorously, and this was going to be too expensive both in terms of computational resources and time.

Section 4.4: Computational Analysis of New Alkylation Experiments

DFT calculations were employed to investigate the mechanism of the two sets of alkylation reactions. Because piperidine conformational changes occur much faster than alkylation,⁶³ these reactions are assumed to follow the second boundary condition of the Curtin-

Hammett Principle;⁶⁶ that is, product ratios are based on differences in transition state energies. With that in mind, all conformeric transition states for each reaction were found systematically, and the Gibbs free energy was used to predict the contribution of each transition state to the product ratio.

Section 4.4.1: Computational Details

DFT calculations were carried out using the B3LYP⁸² and M06-2x⁸³ functionals with the 6-31+G(d) and 6-311+G(d,p) basis sets in the Gaussian 09⁸⁵ suite of programs. The SDB-cc-pVTZ⁸⁷ basis set, which combines the Stuttgart-Dresden-Bonn relativistic effective core potential (ECP)⁸⁸ along with the correlation consistent basis set cc-pVTZ⁸⁹ in order to take into account relativistic effects in larger atoms, was added onto iodine in the reaction of 1-benzyl-3-hydroxypiperidine with methyl iodide. Frequency calculations were carried out to ensure that the intermediates had no negative frequencies and the transition states only had one imaginary frequency, as well as to calculate contributions to the Gibbs free energy (reported at 298.15 K and 1 atm). Intrinsic reaction coordinate (IRC)⁹⁰ calculations were carried out on the transition states to ensure that they connected the two associated intermediates. Solvent was taken into account using the polarizable continuum model (PCM).⁹¹ Structures were optimized at the B3LYP/6-31+G(d) level in the appropriate solvent. Single-point energies were calculated at the M06-2x/6-311+G(d,p) level in the appropriate solvent. Notably, M06-2x was utilized due to its inclusion of dispersion effects, which B3LYP lacks. ΔG s were calculated using the results from single-point energy calculations along with contributions to the Gibbs free energy calculated at the B3LYP/6-31+G(d)/PCM level. Product ratios were obtained via comparison of the differences in transition state energies of all transition states using the equation $\mathbf{D1/D2} = e^{-\Delta G^\ddagger/RT}$

where R is the gas constant = 8.3145 J/(mol*K) and T is the temperature = 298.15 K. Note that solving a set of N equations with N variables was required to account for all N transition state contributions.

Section 4.4.2: Alkylation Reactions to form Piperidinium Salt 164

The total contribution of all conformeric transition states to **164-D1** versus **164-D2** for benzylation of 3-hydroxy-1-methylpiperidine **162** with benzyl chloride in dichloromethane is shown in Table 13 and methylation of 1-benzyl-3-hydroxypiperidine **163** with methyl iodide in dichloromethane is shown in Table 14. Gratifyingly, calculations predicted the correct identity of the major diastereomer, as well as diastereomeric ratios in good agreement with experimental values, including the fact that benzylation is more selective than methylation.

Table 13. Experimental and calculated product ratios in the reaction of 3-hydroxy-1-methylpiperidine **162** with benzyl chloride in DCM.

Transition State	ΔG^\ddagger (kcal/mol)	Product Ratio (%)	Exptl D1:D2 (%)
TS162-D1-ax1	1.05	4.4	
TS162-D1-ax2	1.44	2.3	
TS162-D1-ax3	1.68	1.5	
TS162-D1-ax4	0.66	8.6	
TS162-D1-ax5	1.34	2.7	
TS162-D1-ax6	1.35	2.7	
TS162-D1-eq1	0.99	4.9	
TS162-D1-eq2	1.82	1.2	
TS162-D1-eq3	3.48	0	
TS162-D1-eq4	1.06	4.3	
TS162-D1-eq5	0.92	5.5	
TS162-D1-eq6	1.59	1.8	
TS162-D1-eq7	1.89	1.1	
Total D1		41.0	36
TS162-D2-ax1	0.83	6.5	
TS162-D2-ax2	0.95	5.2	
TS162-D2-ax3	0.00	26.1	
TS162-D2-ax4	1.90	1.0	
TS162-D2-eq1	1.45	2.3	
TS162-D2-eq2	1.97	0.9	
TS162-D2-eq3	1.73	1.4	
TS162-D2-eq4	1.35	2.7	
TS162-D2-eq5	1.40	2.4	
TS162-D2-eq6	1.61	1.7	
TS162-D2-eq7	1.51	2.0	
TS162-D2-eq8	1.16	3.7	
TS162-D2-eq9	1.29	3.0	
Total D2		59.0	64

Table 14. Experimental and calculated product ratios in the reaction of 1-benzyl-3-hydroxypiperidine **163** with methyl iodide in DCM.

Transition State	ΔG^\ddagger (kcal/mol)	Product Ratio (%)	Exptl D1:D2 (%)
TS163-D1-ax1	0.42	5.5	
TS163-D1-ax2	0.72	3.3	
TS163-D1-ax3	0.64	3.8	
TS163-D1-ax4	0.83	2.7	
TS163-D1-ax5	0.00	11.2	
TS163-D1-ax6	0.22	7.7	
TS163-D1-eq1	1.13	1.7	
TS163-D1-eq2	1.11	1.7	
TS163-D1-eq3	1.16	1.6	
TS163-D1-eq4	0.94	2.3	
TS163-D1-eq5	1.16	1.6	
TS163-D1-eq6	1.17	1.6	
TS163-D1-eq7	1.47	0.9	
TS163-D1-eq8	1.56	0.8	
TS163-D1-eq9	2.11	0.3	
Total D1		46.7	46
TS163-D2-ax1	1.04	1.9	
TS163-D2-ax2	0.14	8.9	
TS163-D2-ax3	0.51	4.7	
TS163-D2-ax4	0.96	2.2	
TS163-D2-ax5	0.41	5.6	
TS163-D2-ax6	0.64	3.8	
TS163-D2-ax7	0.60	4.1	
TS163-D2-ax8	0.34	6.3	
TS163-D2-ax9	0.34	6.3	
TS163-D2-eq1	1.70	0.6	
TS163-D2-eq2	0.55	4.5	
TS163-D2-eq3	0.80	2.9	
TS163-D2-eq4	1.19	1.5	
TS163-D2-eq5	4.33	0	
Total D2		53.3	54

A trend noted in the old literature is preferential axial alkylation for small alkylating agents (methyl, ethyl) and preferred equatorial alkylation for larger alkylating agents (benzyl, 2-chlorophenylethanone).¹⁰¹ In our reactions, we see preferential formation of **164-D2**, which, based on assumptions from previous literature, should be from equatorial benzylation of **162b** to form **164-D2a** (Scheme 49) and axial alkylation of the all-equatorial conformer of **163** with methyl iodide to form **164-D2a**. Based on the lowest energy benzylation transition states (Figure 16), however, we see that axial benzylation of **162d** is the most favourable way of forming **164-D2**. Based on the preference for this sterically more encumbered transition state, we postulate that the OH group is helping direct the alkylation. It is also interesting to note that the second lowest energy transition state is also axial alkylation, this time forming diastereomer **164-D1**. A similar effect can be seen in the methylation transition states (Figure 17). Note that, although the lowest energy methylation transition state forms diastereomer **164-D1**, **164-D2** is still favoured as the major diastereomer when all conformeric transition states are taken into account.

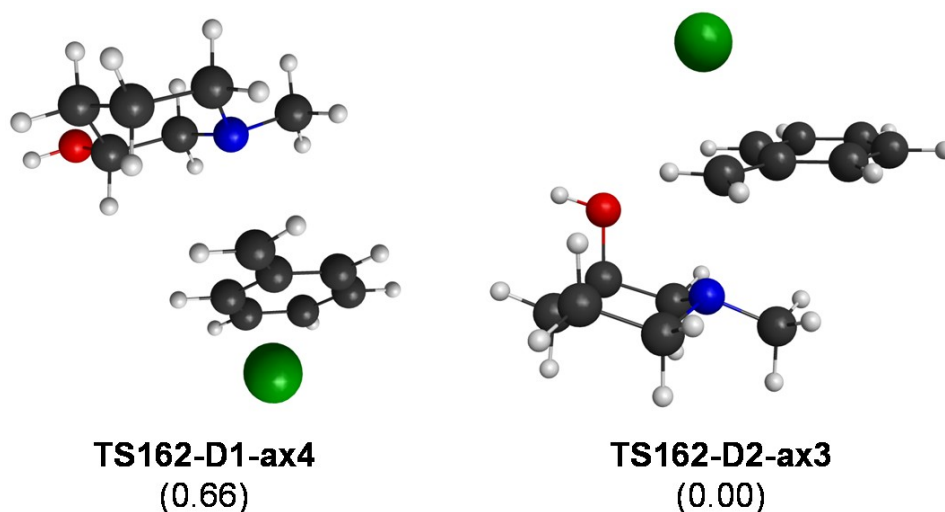


Figure 16. Lowest energy transition states in the reaction of 3-hydroxy-1-methylpiperidine **162** with benzyl chloride in DCM. Structures optimized at B3LYP/6-31+G(d)/PCM(DCM) with single point energies at M06-2x/6-311+G(d,p)/PCM(DCM) (relative Gibbs free energies in kcal/mol shown in parentheses).

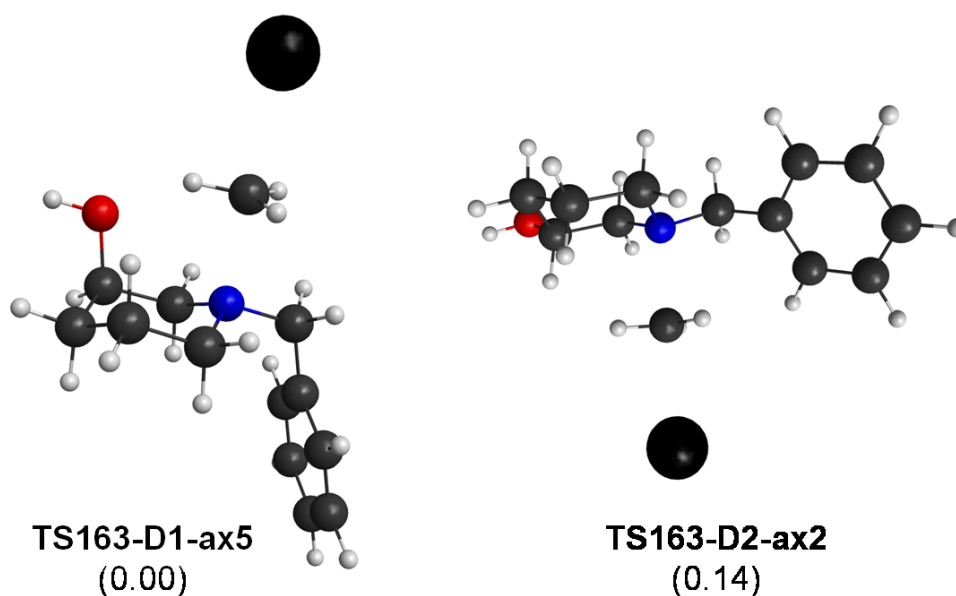
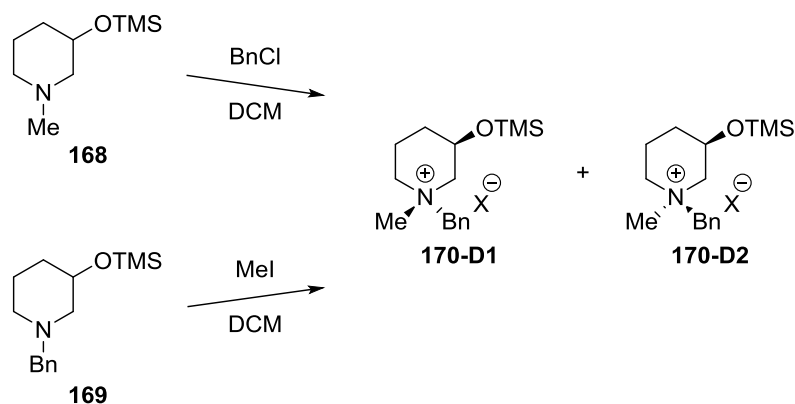


Figure 17. Lowest energy transition states in the reaction of 1-benzyl-3-hydroxypiperidine **163** with methyl iodide in DCM. Structures optimized at B3LYP/6-31+G(d)/PCM(DCM) with single point energies at M06-2x/6-311+G(d,p)/PCM(DCM) (relative Gibbs free energies in kcal/mol shown in parentheses).

Section 4.4.3: Alkylation Reactions to form Piperidinium Salt 167

The experimental results in the alkylation of TBDPS-protected piperidine systems **165** and **166** are more in line with those previously seen; methylation is more selective than benzylation. The computational results for the model TMS-protected systems **168** and **169** (Scheme 49), however, do not seem to predict the results for the TBDPS-protected systems very well. Benzylation is predicted to be somewhat selective for formation of diastereomer **170-D2**, but the experimental results show no preference for **167-D1** or **167-D2** (Table 15). Methylation is predicted to be somewhat selective for formation of diastereomer **170-D1**, but the experimental data shows preference for **170-D2** (Table 16). This is possibly where the use of a TMS group in place of TBDPS makes a large difference and our model breaks down.



Scheme 50. Alkylation of the model TMS-protected piperidines **168** and **169**.

Table 15. Calculated product ratios in the reaction of 1-methyl-3-(trimethylsilyloxy)piperidine **168** with benzyl chloride in DCM compared with the experimental ratio for the benzylation of 3-(*tert*-butyldiphenylsilyloxy)-1-methylpiperidine **165**.

Transition State	ΔG^\ddagger (kcal/mol)	Product Ratio (%)	170-D1:170-D2 (%)	167-D1:167-D2 (%)
TS168-D1-ax1	0.65	12.7		
TS168-D1-ax2	3.52	0		
TS168-D1-ax3	1.78	1.9		
TS168-D1-ax4	3.21	0		
TS168-D1-eq1	1.15	5.5		
TS168-D1-eq2	1.56	2.8		
TS168-D1-eq3	1.81	1.8	24.7	49
TS168-D2-ax1	0.33	22.0		
TS168-D2-ax2	0.00	38.4		
TS168-D2-eq1	1.47	3.2		
TS168-D2-eq2	3.43	0		
TS168-D2-eq3	0.79	10.1		
TS168-D2-eq4	2.98	0		
TS168-D2-eq5	1.91	1.5		
TS168-D2-eq6	4.19	0	75.3	51

Table 16. Calculated product ratios in the reaction of 1-benzyl-3-(trimethylsiloxy)piperidine **169** with methyl iodide in DCM compared with the experimental ratio for the methylation of 1-benzyl-3-(*tert*-butyldiphenylsiloxy)piperidine **166**.

Transition State	ΔG^\ddagger (kcal/mol)	Product Ratio (%)	170-D1:170-D2 (%)	167-D1:167-D2 (%)
TS169-D1-ax1	1.10	6.7		
TS169-D1-ax2	1.40	4.0		
TS169-D1-ax3	0.00	42.9		
TS169-D1-eq1	1.71	2.4		
TS169-D1-eq3	2.27	0.9		
TS169-D1-eq4	2.62	0.5	57.4	31
TS169-D2-ax2	1.43	3.9		
TS169-D2-ax4	0.54	17.4		
TS169-D2-ax5	2.34	0.8		
TS169-D2-ax6	0.75	12.0		
TS169-D2-eq1	1.18	5.9		
TS169-D2-eq2	1.66	2.6	42.6	69

Interestingly, the lowest energy transition states leading to each diastereomer in each reaction are still both axial alkylation transition states (Figure 18 and Figure 19). In particular, in both the benzylation and methylation reactions, axial alkylation of the conformer in which the OTMS group is axial is the most favourable reaction pathway despite the added steric bulk of the TMS group; it is possible that this transition state would not be as favourable with a larger group such as TBDPS on the oxygen, bringing the computed product ratios closer to the experimental ratios.

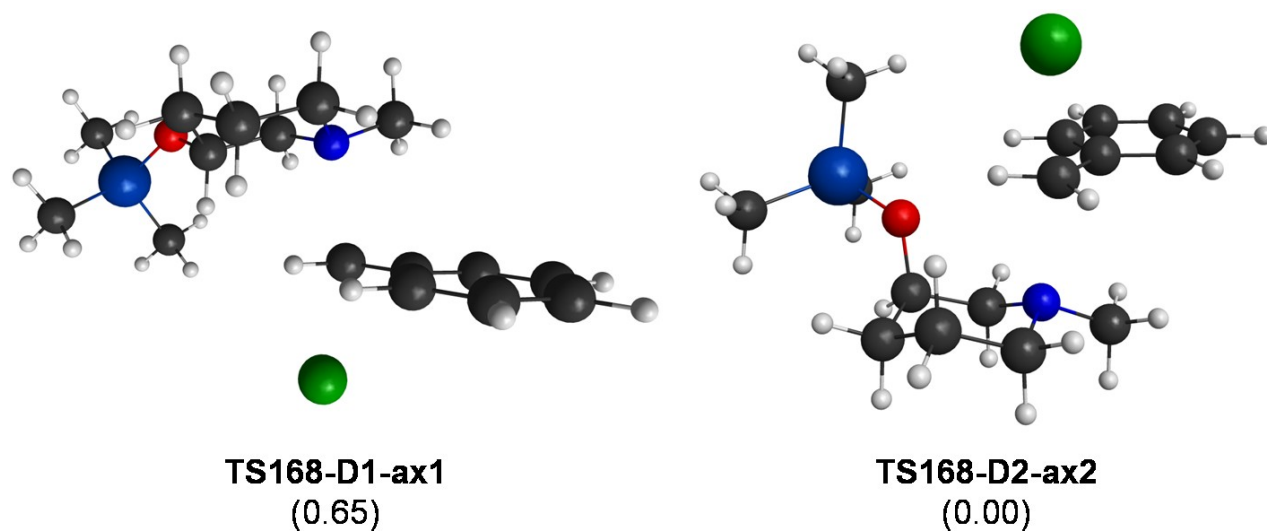


Figure 18. Lowest energy transition states in the reaction of 1-methyl-3-trimethylsilylpiperidine **168** with benzyl chloride in DCM. Structures optimized at B3LYP/6-31+G(d)/PCM(DCM) with single point energies at M06-2x/6-311+G(d,p)/PCM(DCM) (relative Gibbs free energies in kcal/mol shown in parentheses).

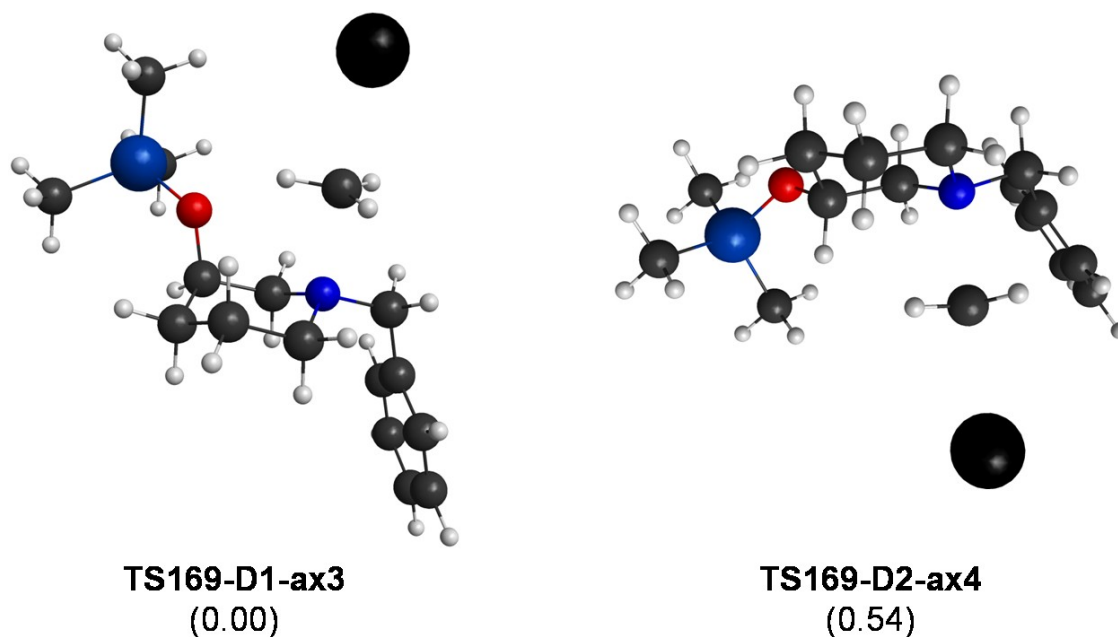
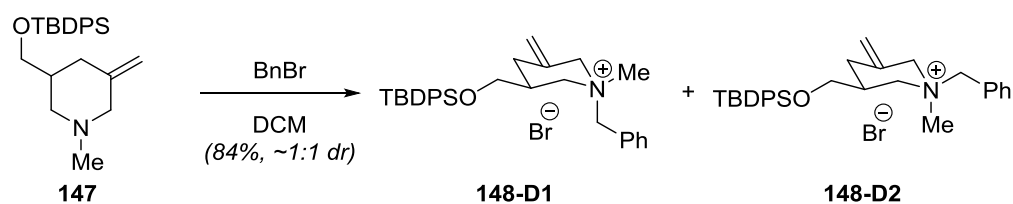


Figure 19. Lowest energy transition states in the reaction of 1-benzyl-3-trimethylsilylpiperidine **169** with methyl iodide in DCM. Structures optimized at B3LYP/6-31+G(d)/PCM(DCM) with single point energies at M06-2x/6-311+G(d,p)/PCM(DCM) (relative Gibbs free energies in kcal/mol shown in parentheses).

Section 4.5: Further Study of the Alkylation of Lysergic Acid Synthesis Intermediate **147**

In Chapter 2, it was noted that alkylation of piperidine derivative **147** with benzyl bromide in dichloromethane led to a 1:1 diastereomeric ratio of piperidinium salt **148** (Scheme 51). This was unfortunate, as we would have liked to form only the axial alkylation product **148-D1** for our lysergic acid synthesis, which we assumed we would get based on the results of Vedejs' alkylation work.⁷⁷



Scheme 51. Benzylation of piperidine **147**.

Section 4.5.1: New Alkylation Experiments on Piperidine **147**

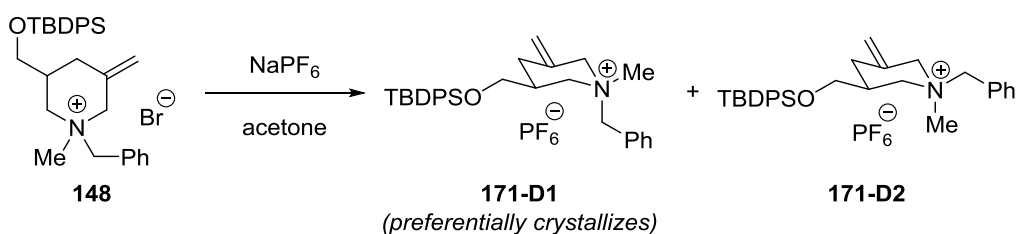
The benzylation of piperidine **147** with benzyl bromide was repeated in dichloromethane, acetone, and methanol; only one trial was performed for each solvent due to the small amount of material on hand. It was interesting to note that acetone gave the lowest amount of the “axial alkylation product” **148-D1** and methanol gave the highest amount, results agreeing with those reported previously in the literature (ignoring spurious results from DCM).⁶⁸

Table 17. Benzylation of *N*-methylpiperidine derivative **147**.

Solvent	Reaction Time (h)	148-D1 (%)	148-D2 (%)
DCM	0.5	43	57
Acetone	0.5	37	63
MeOH	0.5	48	52

Section 4.5.2: Assignment of Diastereomeric Piperidinium Salts **148-D1** and **148-D2**

In order to confirm unequivocally which diastereomer corresponded to which in the ^1H NMR spectrum of piperidinium salt **148**, an X-ray crystallographic structure was desired. Bromide salt **148** was transformed into hexafluorophosphate salt **171** using salt metathesis (Scheme 52); diastereomer **171-D1** was preferentially crystallized from a mixture of benzene and toluene, providing an X-ray quality crystal for characterization (Figure 20).



Scheme 52. Salt metathesis on piperidinium salt **148**.

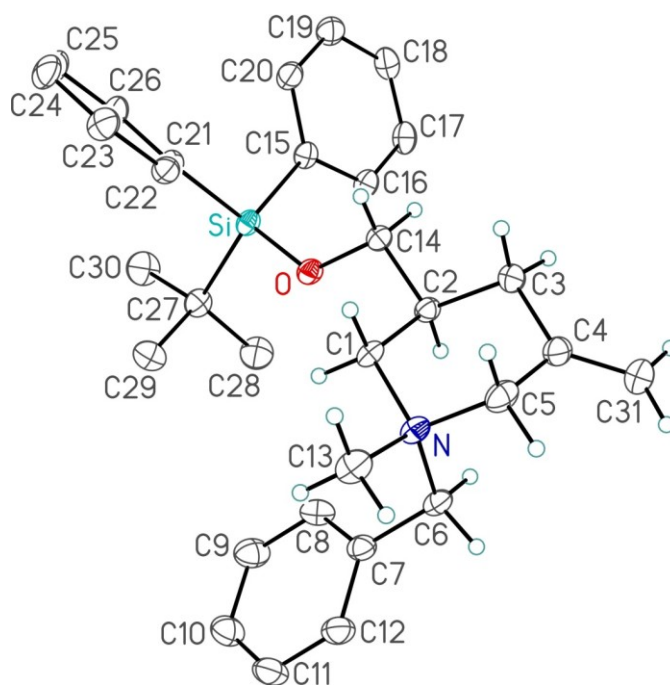


Figure 20. ORTEP diagram of piperidinium salt **171-D1**.¹⁰²

Because we wanted to see if our computational NMR analysis of the previously-studied diastereomeric piperidinium salts **164** and **167** was accurate, we applied this technique to piperidinium salt **173** (Figure 21), the TMS-substituted analogue of **148**.¹⁰³ This time, there were two obvious signals to use based on the ¹H NMR spectra – the alkene protons and the benzylic protons. In the ¹H NMR spectrum of the diastereomer characterized by X-ray crystallography, **171-D1**, we observed that the alkene protons were shifted downfield compared to those of **171-D2**, and the benzylic protons of **171-D1** were shifted upfield with a large chemical shift difference compared to the downfield apparent singlet belonging to the benzylic protons of **171-D2**. Both of these shifts correspond to the calculated ¹H NMR chemical shifts of **173**. This gives us confidence that our previous diastereomer assignments in Section 4.3 for **164** and **167** are correct.

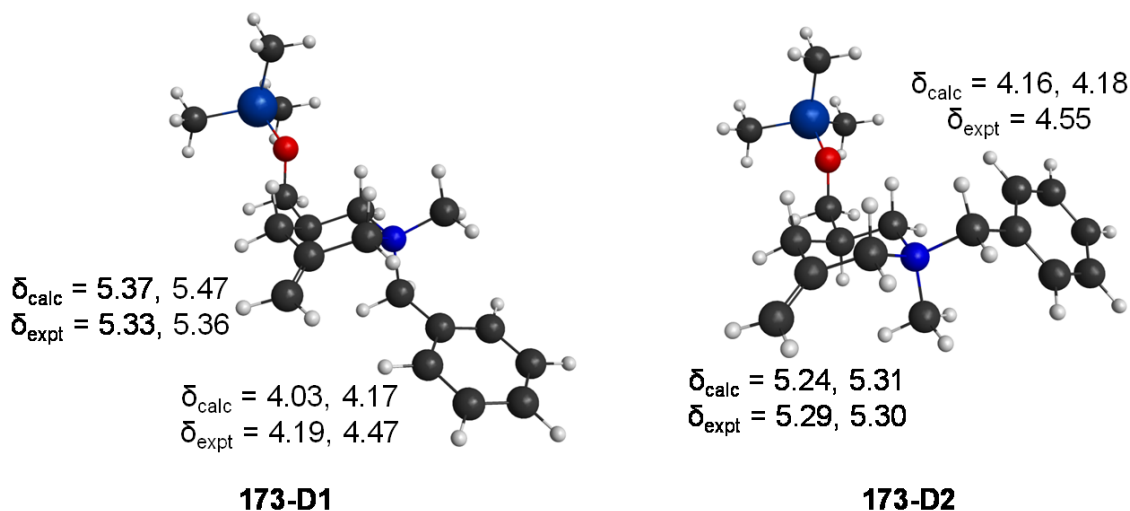
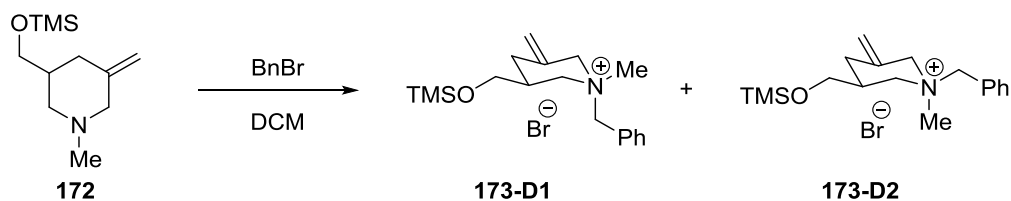


Figure 21. Identifying ¹H NMR chemical shifts of **173-D1** and **173-D2**. Structures optimized at B3LYP/6-31+G(d,p), NMR calculations at mPW1PW91/6-311+G(2d,p)/SMD(CHCl₃). Calculated chemical shifts reflect a weighted average of contributions of all conformers with a >1% contribution to the population, though only the lowest energy conformer of each diastereomer is shown. Experimental chemical shifts are reported in CDCl₃.

Section 4.5.3: Computational Analysis of the Alkylation of Piperidine **147**¹⁰⁴

As was done with *tert*-butyldiphenylsiloxy-substituted piperidines **165** and **166**, the TBDPS group on **147** was replaced with a TMS group for computational work (Scheme 53). The computational results point to a very slight preference for diastereomer **173-D1**, which is opposite to what the experimental results show (Table 18). This is likely due to the replacement of the TBDPS group with TMS. We also cannot rule out a breakdown of the Curtin-Hammett Principle; for completeness, the entire potential energy surface of this reaction, including transition states between reactant and product conformers, should be explored.



Scheme 53. The computationally-studied benzylation of piperidine **172** with benzyl bromide.

Table 18. Calculated product ratios in the reaction of piperidine **172** with benzyl bromide in DCM compared with the experimental ratio for the benzylation of piperidine **147**. Only transition states within 3 kcal/mol of the lowest energy transitions state are included.

Transition State	ΔG^\ddagger (kcal/mol)	Product Ratio (%)	173-D1:173-D2 (%)	148-D1:148-D2 (%)
TS172-D1-ax1	1.08	3.3		
TS172-D1-ax2	0.13	16.6		
TS172-D1-ax3	0.55	8.2		
TS172-D1-ax4	1.38	2.0		
TS172-D1-ax5	0.60	7.5		
TS172-D1-ax6	0.00	20.6		
TS172-D1-eq5	2.63	0.2	58.5	43
TS172-D2-ax2	2.91	0.2		
TS172-D2-ax5	2.61	0.3		
TS172-D2-eq1	1.68	1.2		
TS172-D2-eq2	1.50	1.6		
TS172-D2-eq3	0.59	7.6		
TS172-D2-eq4	1.93	0.8		
TS172-D2-eq5	0.87	4.7		
TS172-D2-eq6	1.13	3.0		
TS172-D2-eq7	1.57	1.5		
TS172-D2-eq8	1.08	3.3		
TS172-D2-eq9	0.10	17.3	41.5	57

The lowest energy transition states for this reaction point to a more conventional reaction pathway; that is, the “axial alkylation product” **173-D1** is formed preferentially via axial alkylation, and the “equatorial alkylation product” **173-D2** is formed preferentially via equatorial alkylation (with the substituent on the ring in the equatorial position) (Figure 22). This is possibly due to the fact that the oxygen on the substituent is one carbon removed from the ring, making it much less likely to electronically influence the relative stability of the conformeric transition states.

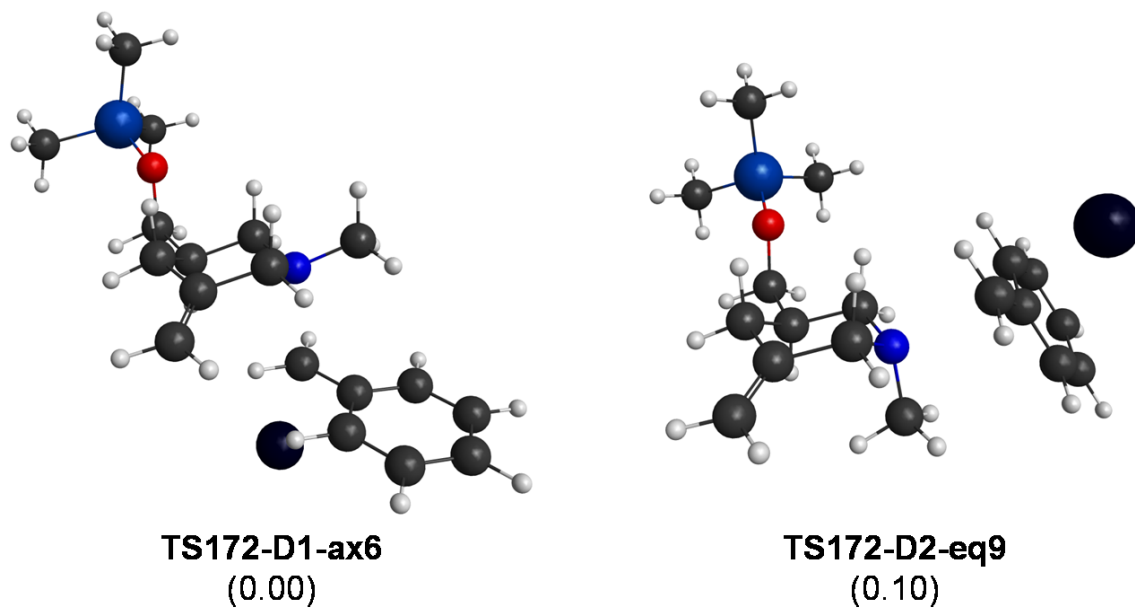


Figure 22. Lowest energy transition states in the reaction of **172** with benzyl bromide in DCM. Structures optimized at B3LYP/6-31+G(d)/PCM(DCM) with single point energies at M06-2x/6-311+G(d,p)/PCM(DCM) (relative Gibbs free energies in kcal/mol shown in parentheses).

Section 4.6: Summary and Future Plans

In our new alkylation studies, 3-hydroxy-1-methylpiperidine **162** and 3-(*tert*-butyldiphenylsiloxy)-1-methylpiperidine **165** were benzylated, and 1-benzyl-3-hydroxypiperidine **163** and 1-benzyl-3-(*tert*-butyldiphenylsiloxy)piperidine **166** were methylated in four different solvents. Reaction of **162** and **162** formed differing amounts of diastereomeric piperidinium salts **164-D1** and **164-D2**, and **165** and **166** formed differing amounts of **167-D1** and **167-D2** (Section 4.2, Scheme 48). The mechanistic details of these reactions were studied using DFT calculations; this served to compare and contrast the selectivity of these reactions, as well as to determine whether or not computational chemistry has evolved far enough to accurately predict the outcome of this type of reaction.

In contrast to trends noted in the early literature, benzylation of **162** was more stereoselective than methylation of **163**, and the use of a protic solvent slowed the reaction rather

than speeding it up. Additionally, according to the computational data, which reproduced the experimental data quite well, axial alkylation was determined to be the major path for formation of both diastereomers for both reactions; this challenges the long-held assumption that one diastereomer is formed via axial alkylation and the other via equatorial alkylation. Equally intriguing was the finding that the lowest energy conformers of both **164-D1** and **164-D2** had the hydroxyl group axial, contrary to what one would assume based on steric arguments. Finally, it was discovered that, in the case of piperidinium salt **164**, the axial methyl group was deshielded compared to the equatorial methyl group, which also challenges previously-held assumptions that, due to piperidine ring anisotropy, the axial methyl group of a piperidinium salt should be shielded.

The results of alkylation reactions on TBDPS-substituted piperidines **165** and **166** were less clear-cut, with no clear trend for product diastereomeric ratio or reaction time as a function of solvent polarity. Observations were made, however, that methylation was more selective and that the use of methanol as a solvent switched the identity of the major diastereomer, which are both in line with observations noted previously in the literature. The computational results were much less accurate in this reaction; this may be at least partially due to the fact that the TBDPS group was switched out for a TMS group to make the calculations feasible. Like the alkylation of piperidines **162** and **163**, axial alkylation was found to be the most favourable reaction pathway to form both diastereomers of TMS-substituted piperidinium salt **170**. Additionally, the lowest energy conformers of both **170-D1** and **170-D2** were also found to be those with the OTMS group axial; this echoes the results of computational work on piperidinium salt **164** and indicates a strong electronic effect on the conformation that outweighs the steric strain present in the axial conformers.

One of the biggest challenges in previous experimental work in this field was identification of diastereomeric products; we demonstrated that comparison of experimental ^1H NMR chemical shifts with theoretically derived values is an effective tool in determining diastereomer identities in the absence of crystallographic data. In particular, with the availability of crystallographic data for the assignment of piperidinium salt **148**, we were able to show that the computational NMR data leads to the correct assignment of diastereomers **148-D1** and **148-D2**, even with the TBDPS group replaced with the smaller TMS group. This leads us to believe that (1) we correctly assigned the diastereomers of piperidinium salts **164** and **167**, and (2) this is an invaluable tool in the study of reactions that form diastereomeric mixtures.

Lysergic acid precursor **147** was subjected to similar experimental and computational studies as the other piperidine derivatives in this chapter; the computational study could not reproduce the experimental numbers or trends, likely due to the replacement of the TBDPS group with TMS for computational simplicity. Nevertheless, with some fine-tuning, these methods of analysis could be quite useful in the study of synthetically-relevant systems.

The intriguing results detailed in this chapter indicate the need to study this reaction further, both for its potential ability to form useful diastereoenriched piperidinium salts, as well as for its demonstration that even seemingly simple reactions can be complex in the microscopic state. As mentioned at the end of Chapter 3, many more piperidine substrates should be studied, including alkyl groups and substituents with heteroatoms at the 2-, 3-, and 4-positions. Solvent, temperature, and leaving group effects should be included in these studies.

In these studies, we have assumed that the Curtin-Hammett Principle holds. However, to be rigorous, computational studies that look more closely at the potential energy surfaces of the piperidine substrates should be undertaken, including transition states between

conformers/invertomers, in order to make sure that conformer interconversion happens much faster than alkylation. Additionally, we have looked at the alkylation of chair conformers of the piperidine substrates only; it is possible that twist-boat conformers could undergo alkylation via transition states that may be competitive with the chair conformer transition states. We also need to look at the potential energy surface of the product piperidinium salts to ensure that alkylation is an irreversible reaction in all cases.

Section 4.6: Experimental

Section 4.6.1: General Methods

All chemicals were purchased from Sigma-Aldrich, Fluka, Caledon, or Alfa Aesar and used as such unless stated otherwise. For flash chromatography, technical grade solvents were used without further purification. For reactions, acetonitrile, acetone, and methanol were dried over 4 Å molecular sieves overnight. Tetrahydrofuran was distilled from sodium/benzophenone under an atmosphere of argon and dichloromethane was distilled from calcium hydride under an atmosphere of argon.

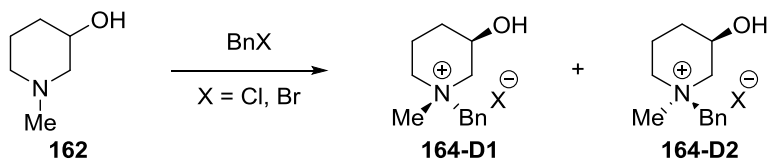
Reactions were magnetically stirred and monitored by TLC unless otherwise stated. Chromatographic purification was performed as flash chromatography (Silicycle SiliFlash® F60 silica gel) using the solvents indicated as eluent with 0.3-0.5 bar pressure. Thin layer chromatography (TLC) was performed on Merck silica gel 60 F254 TLC glass plates and visualized with UV light and potassium permanganate stain. The yields given refer to spectroscopically pure compounds unless otherwise stated.

¹H and ¹³C NMR spectra were recorded on Agilent/Varian DD2 MR (400 MHz), Agilent/Varian Inova (400 MHz or 500 MHz), Agilent/Varian Mercury (400 MHz), or

Agilent/Varian VNMRS (500 MHz) spectrometers in the solvents indicated. All signals are reported in ppm with the internal chloroform signal at 7.26 ppm or 77.0 ppm or the internal methanol signal at 3.31 ppm or 49.0 ppm as standard. The data is being reported as (s=singlet, d=doublet, t=triplet, q=quadruplet, m=multiplet or unresolved, br=broad signal, app=apparent, coupling constant(s) in Hz, integration). Infrared spectra were recorded on a Matteson Galaxy Series FT-IR 300 spectrophotometer as thin films. Absorptions are given in wavenumbers (cm^{-1}). Mass spectrometric measurements were performed as high resolution ESI measurements on an Agilent Technologies 6220 oaTOF high-resolution mass spectrometer.

Section 4.6.2: Experimental Procedures

N-Benzylation of 3-hydroxy-1-methylpiperidine **162**:



To a solution of 3-hydroxy-1-methylpiperidine **162** (0.100 g, 0.87 mmol) in dichloromethane, acetonitrile, acetone, or methanol (1.75 mL, 0.5 M), benzyl bromide (0.163 g, 0.96 mmol) or benzyl chloride (0.121 g, 0.96 mmol) was added. The reaction mixture was stirred until the starting material was consumed as seen by TLC (3-hydroxy-1-methylpiperidine **162** has an $R_f = 0.30$ in 10% methanol:dichloromethane while piperidinium salt **164** has an $R_f = 0.10$) (4 h to 48 h). The solvent was evaporated under reduced pressure, and piperidinium salt **164** was obtained as a white solid (quantitative yield, mixture of diastereomers).

^1H NMR (400 MHz, CD_3OD): δ 7.64-7.51 (m, 10H), 4.83-4.66 (m, 2H), 4.56 (AB q, 2H, $J = 13$ Hz), 4.27 (m, 1H), 4.14 (m, 1H), 3.52-3.35 (m, 6H), 3.25-3.20 (m, 2H), 3.17 (s, 3H), 2.99 (s, 3H), 2.22-2.13 (m, 2H), 2.03-1.87 (m, 4H), 1.80-1.73 (m, 1H), 1.65-1.56 (m, 1H).

^{13}C NMR (100 MHz, CD_3OD): δ 133.1, 132.9, 130.5, 130.4, 128.9, 128.8, 127.3, 127.1, 68.9 (two diastereomeric peaks overlapping by HSQC), 63.6, 63.3, 62.5, 62.1, 60.4, 60.2, 48.7 (second diastereomeric peak under the solvent signal by HSQC), 29.9, 28.7, 17.3, 16.3.

IR(cast film, MeOH): 3285, 2953, 1626, 1476, 1457, 1216, 1077, 1023, 915, 878, 765, 706 cm^{-1} .

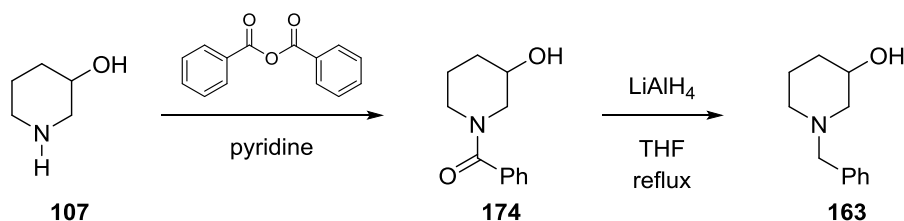
High Resolution ESI-MS calculated for $\text{C}_{13}\text{H}_{20}\text{NO}^+$ (M^+) m/z : 206.1539; found m/z : 206.1539.

mp(Cl salt) = 193 $^\circ\text{C}$ (decomposition); mp(Br salt) = 153 $^\circ\text{C}$ (decomposition).

EA(Cl salt): Calculated: C, 64.59; H, 8.34; N, 5.79. Found: C, 64.60; H, 8.32; N, 5.77.

EA(Br salt): Calculated: C, 54.55; H, 7.04; N, 4.89. Found: C, 54.44; H, 7.01; N, 4.89.

Preparation of 1-benzyl-3-hydroxypiperidine **163**:

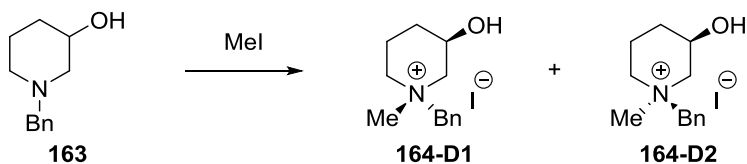


3-Hydroxypiperidine **107** (0.499 g, 4.93 mmol) was dissolved in dichloromethane (5.5 mL, 0.90 M) in a 25 mL round bottom flask fitted with a magnetic stir bar and septum with argon inlet. Pyridine (0.42 mL, 5.21 mmol) was added, and the reaction mixture was cooled to 0 $^\circ\text{C}$ while being magnetically stirred. Benzoic anhydride (1.236 g, 5.46 mmol) was added slowly at 0 $^\circ\text{C}$, and then the ice bath was removed. The reaction mixture was stirred at room temperature for 24 h under argon, and then aqueous sodium hydroxide solution (10 mL, 1 M) was added. The organic layer was separated, and the aqueous layer was extracted with ethyl acetate (2 x 10 mL). The combined organic layers were dried over anhydrous magnesium sulfate and filtered. The solvent was evaporated under reduced pressure to obtain crude *N*-benzoyl-3-hydroxypiperidine as a waxy orange solid. This solid was chromatographed on silica gel starting at 60% ethyl

acetate:hexanes and increasing to 100% ethyl acetate. Pure *N*-benzoyl-3-hydroxypiperidine **174** was obtained as a white solid (0.786 g, 78%). Characterization data matched that previously reported.¹⁰⁵

N-Benzoyl-3-hydroxypiperidine **174** (0.71 g, 3.2 mmol) was added to a 25 mL round bottom flask fitted with a magnetic stir bar, condenser, and septum with argon inlet. Tetrahydrofuran (6 mL, 0.5 M) was added, and the solution was cooled to 0 °C in an ice bath. Lithium aluminum hydride (95%, 0.24 g, 6.0 mmol) was added slowly while the reaction mixture was being stirred. The reaction mixture was then refluxed for 2 h. The reaction mixture was then allowed to cool to room temperature. Sodium sulfate decahydrate was added to the reaction mixture at 0 °C until bubbling ceased, and then this mixture was stirred overnight at room temperature. The reaction mixture was dried over anhydrous magnesium sulfate followed by filtration through a pad of Celite. The solvent was removed under reduced pressure to give 1-benzyl-3-hydroxypiperidine as a yellow oil. This oil was purified by column chromatography using 2% methanol:dichloromethane ($R_f = 0.37$ in 10% methanol:dichloromethane), providing piperidinol **163** as a pale yellow oil (0.40 g, 60%). Characterization data matched that previously reported.¹⁰⁵

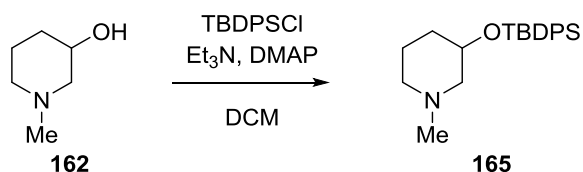
N-Methylation of 1-benzyl-3-hydroxypiperidine **163**:



To a solution of 1-benzyl-3-hydroxypiperidine (0.050 g, 0.24 mmol) in dichloromethane, acetonitrile, acetone, or methanol (0.6 mL, 0.4 M) in a 25 mL round bottom flask was added methyl iodide (0.035 g, 0.25 mmol). The reaction mixture was stirred for 30 min. The reaction

could not be monitored by TLC, as the R_f of piperidine **163** was the same as piperidinium salt **164** ($R_f = 0.37$ in 10% methanol:dichloromethane). The solvent was then evaporated under reduced pressure to give the piperidinium salt as a pale yellow oil (100% yield). The spectroscopic data is the same as for the Br and Cl salts.

TBDPS protection on 3-hydroxy-1-methylpiperidine **162**:



3-Hydroxy-1-methylpiperidine **162** (1.0 mL, 8.7 mmol) was dissolved in dichloromethane (18 mL, 0.48 M) in a round-bottom flask fitted with a stir bar, septum, and argon inlet. Triethylamine (2.5 mL, 18 mmol), *tert*-butyldiphenylchlorosilane (2.7 mL, 10 mmol), and 4-dimethylaminopyridine (0.120 g, 0.982 mmol) were added sequentially, and this reaction mixture was stirred overnight. The reaction mixture was then filtered through Celite and evaporated to give the crude product as a yellow oil. Column chromatography using 80% ethyl acetate:hexanes ($R_f = 0.47$ in 10% methanol:dichloromethane) gave piperidine **165** as a pale yellow oil (1.064 g, 35%).

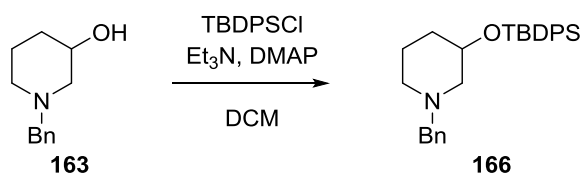
¹H NMR (400 MHz, CDCl₃): δ 7.69-7.66 (m, 4H), 7.44-7.34 (m, 6H), 3.80-3.73 (m, 1H), 2.80 (br dd, $J = 11$ Hz, $J = 4$ Hz, 1H), 2.60 (br d, $J = 11$ Hz, 1H), 2.20 (s, 3H), 1.91-1.77 (m, 3H), 1.63-1.58 (m, 1H), 1.41-1.20 (m, 2H), 1.06 (s, 9H).

¹³C NMR (100 MHz, CDCl₃): δ 135.8, 134.5, 129.6, 127.6, 69.2, 63.4, 55.3, 46.2, 33.4, 27.0, 23.7, 19.2.

IR (cast film, CDCl₃): 3071, 3049, 2938, 2892, 2857, 2780, 1590, 1465, 1428, 1369, 1262, 1170, 1138, 1112, 1025, 987, 824, 739, 702 cm⁻¹.

High Resolution ESI-MS calculated for $C_{22}H_{32}NOSi$ ($[M+H]^+$) m/z : 354.2248; found m/z : 354.2249.

TBDPS protection on 1-benzyl-3-hydroxypiperidine **163**:



1-Benzyl-3-hydroxypiperidine **163** (0.896 g, 4.68 mmol) was dissolved in dichloromethane (10 mL, 0.47 M) in a round-bottom flask fitted with a stir bar, septum, and argon inlet. Triethylamine (1.4 mL, 10 mmol), *tert*-butyldiphenylchlorosilane (1.5 mL, 5.8 mmol), and 4-dimethylaminopyridine (0.089 g, 0.728 mmol) were added sequentially, and this reaction mixture was stirred overnight. The reaction mixture was then filtered through Celite and evaporated to give the crude product as a yellow oil. Column chromatography using 10% ethyl acetate:hexanes ($R_f = 0.35$ in 10% ethyl acetate:hexanes) gave piperidine **166** as a pale yellow oil (0.225 g, 11%).

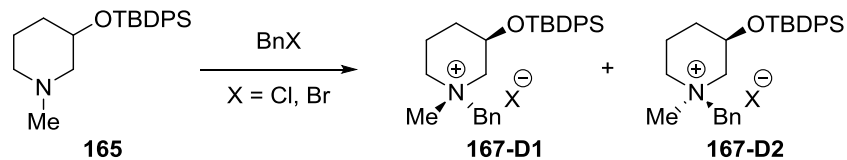
1H NMR (400 MHz, $CDCl_3$): δ 7.77-7.66 (m, 4H), 7.47-7.26 (m, 11H), 3.86-3.79 (m, 1H), 3.48 (s, 2H), 2.85 (br dd, $J = 10$ Hz, $J = 4$ Hz, 1H), 2.64 (br d, $J = 11$ Hz, 1H), 2.05-1.95 (m, 2H), 1.85-1.79 (m, 1H), 1.69-1.64 (m, 1H), 1.46-1.30 (m, 2H), 1.09 (s, 9H).

^{13}C NMR (100 MHz, $CDCl_3$): δ 138.4, 135.8, 134.5, 129.5, 129.1, 128.1, 127.5, 126.9, 69.2, 63.0, 61.2, 53.2, 33.8, 27.0, 23.5, 19.2.

IR (cast film, $CDCl_3$): 3070, 3048, 3028, 2936, 2857, 2798, 1589, 1472, 1428, 1158, 1111, 1085, 823, 739, 701 cm^{-1} .

High Resolution ESI-MS calculated for $C_{28}H_{36}NOSi$ ($[M+H]^+$) m/z : 430.2561; found m/z : 430.2560.

Benzylation of **165**:



To a solution of 3-(*tert*-butyldiphenylsiloxy)-1-methylpiperidine **165** (0.100 g, 0.283 mmol) in dichloromethane, acetonitrile, acetone, or methanol (0.60 mL, 0.47 M), benzyl bromide (0.04 mL, 0.3 mmol) or benzyl chloride (0.04, 0.3 mmol) was added. The reaction mixture was stirred until the starting material was consumed as seen by TLC (piperidine **165** stains yellow in potassium permanganate stain while the product piperidinium salt **167** stains a purple/pink colour; both had the same $R_f = 0.43$ in 10% methanol:dichloromethane). The solvent was evaporated under reduced pressure, and piperidinium salt **167** was obtained as a white solid (quantitative yield, mixture of diastereomers).

^1H NMR (400 MHz, CDCl_3): δ 7.55-7.22 (m, 30H), 5.26 (d, $J = 13$ Hz, 1H), 5.05 (s, 2H), 4.93 (d, $J = 13$ Hz, 1H), 4.20-4.11 (m, 3H), 3.88-3.85 (m, 2H), 3.71-3.59 (m, 2H), 3.42-3.37 (m, 1H), 3.28 (br s, 4H), 2.82-2.80 (m, 4H), 2.24-2.20 (m, 1H), 2.17-1.89 (m, 3H), 1.78-1.65 (m, 4H), 1.00 (s, 9H), 0.97 (s, 9H).

^{13}C NMR (100 MHz, CDCl_3): δ 135.5, 135.4, 133.4, 133.3, 132.4, 132.34, 132.27, 131.9, 130.6, 130.3, 129.0, 128.9, 128.1, 128.0, 126.9, 126.8, 70.3, 68.2, 65.6, 64.9, 63.3, 62.4, 60.6, 59.3 (two diastereomeric peaks overlapping by HSQC), 47.8, 47.1, 30.0, 28.5, 26.9 (two diastereomeric peaks overlapping by HSQC), 18.9, 17.9, 16.1.

IR (cast film, CDCl_3): 3070, 3049, 2960, 2894, 2859, 2190, 1589, 1472, 1428, 1112, 1042, 924, 730, 703 cm^{-1} .

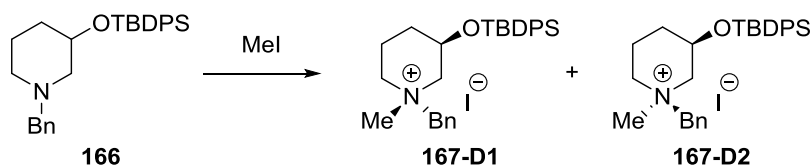
High Resolution ESI-MS calculated for $\text{C}_{29}\text{H}_{38}\text{NOSi}^+$ (M^+) m/z : 444.2717; found m/z : 444.2716.

mp(Cl salt) = 172 °C (decomposition); mp(Br salt) = 180 °C (decomposition).

EA(Cl salt): Calculated: C, 72.54; H, 7.98; N, 2.92. Found: C, 70.42; H, 7.79; N, 2.78.

EA(Br salt): Calculated: C, 66.39; H, 7.30; N, 2.67. Found: C, 66.32; H, 7.31; N, 2.73.

Methylation of **166**:



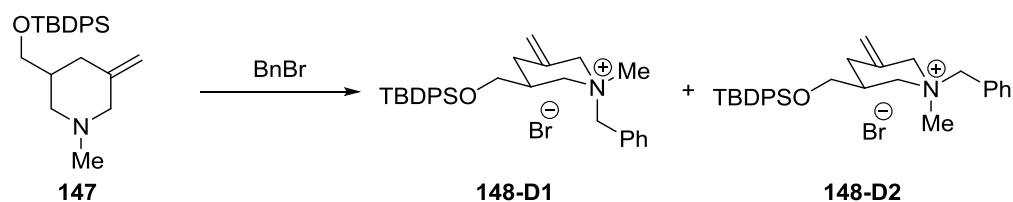
To a solution of 1-benzyl-3-(*tert*-butyldiphenylsiloxy)piperidine **166** (0.050 g, 0.12 mmol) in dichloromethane, acetonitrile, acetone, or methanol (0.30 mL, 0.40 M) in a 25 mL round bottom flask under argon atmosphere was added methyl iodide (0.01 mL, 0.2 mmol). The reaction mixture was stirred until the starting material was consumed (<0.5 h) by TLC (piperidine **166** stains yellow in potassium permanganate stain while the product piperidinium salt **167** stains a purple/pink colour; product $R_f = 0.43$ in 10% methanol:dichloromethane). The solvent was then evaporated under reduced pressure to give the piperidinium salt as a pale yellow solid (100% yield).

The spectroscopic data is the same as for the Br and Cl salts.

mp = 90 °C (decomposition).

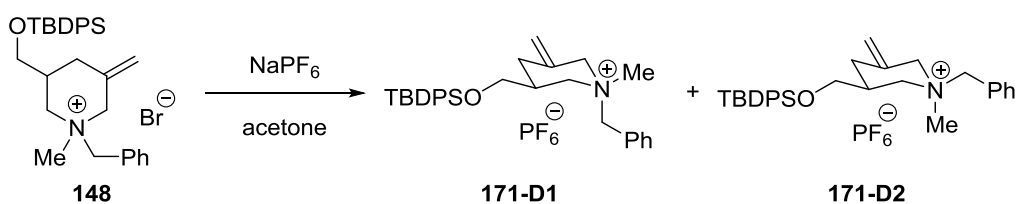
EA: Calculated: C, 60.94; H, 6.70; N, 2.45. Found: C, 60.99; H, 6.71; N, 2.30.

Benylation of **147**:



To a solution of piperidine **147** (0.060 g, 0.16 mmol) in dichloromethane, acetone, or methanol (0.95 mL, 0.17 M), benzyl bromide (0.02 mL, 0.2 mmol) was added. The reaction mixture was stirred until the starting material was consumed as seen by TLC. The solvent was evaporated under reduced pressure, and the piperidinium salt was obtained as a white solid (quantitative yield, mixture of diastereomers). Characterization data is reported in Appendix A.

Salt metathesis on **148**:



Piperidinium salt **148** (0.225 g, 0.409 mmol) was dissolved in acetone (4.0 mL, 0.10 M) in a round-bottom flask equipped with a stir bar, septum, and argon inlet. Sodium hexafluorophosphate (0.115 g, 0.685 mmol) was added, and the reaction mixture was stirred overnight. The reaction mixture was then filtered through Celite and the solvent evaporated *in vacuo*. The product was crystallized from a mixture of dichloromethane and diethyl ether to give piperidinium salt **171** as a mixture of diastereomers (0.153 g, 61%).

^1H NMR (400 MHz, CDCl_3): δ 7.64-7.34 (m, 30H), 5.32 (s, 1H), 5.29 (s, 1H), 5.24 (s, 1H), 5.20 (s, 1H), 4.57 (s, 2H), 4.47 (d, $J = 14$ Hz, 1H), 4.16 (d, $J = 13$ Hz, 1H), 4.10 (d, $J = 14$ Hz, 1H), 3.93 (d, $J = 13$ Hz, 1H), 3.89 (d, $J = 13$ Hz, 1H), 3.84 (d, $J = 13$ Hz, 1H), 3.74 (dd, $J = 11$ Hz, $J = 5$ Hz, 1H), 3.67 (dd, $J = 11$ Hz, $J = 4$ Hz, 1H), 3.60-3.50 (m, 3H), 3.45-3.41 (m, 1H), 3.31-3.25 (m, 1H), 2.96 (t, $J = 12$ Hz, 1H), 2.92 (s, 3H), 2.87 (s, 3H), 2.59-2.50 (m, 1H), 2.54 (dd, $J = 8$ Hz, $J = 4$ Hz, 1H), 2.30 (app q, $J = 13$ Hz, 1H), 2.10-2.05 (m, 3H), 1.05 (s, 9H), 0.96 (s, 9H).

^{13}C NMR (125 MHz, CDCl_3): δ 135.5, 135.4, 134.0, 133.7, 133.2, 132.7, 132.6, 132.5, 130.9, 130.14, 130.11, 130.0, 129.6, 129.4, 128.01, 127.95, 126.6, 126.2, 120.43, 120.39, 71.2, 67.8, 65.6, 65.2, 64.7, 61.7, 61.3, 60.7, 51.5, 45.2, 35.2, 34.5, 32.8, 32.5, 26.9, 26.8, 19.22, 19.16.

IR (cast film, CDCl_3): 3071, 3051, 2955, 2932, 2900, 2858, 1663, 1589, 1474, 1428, 1388, 1115, 842, 801, 739, 703 cm^{-1} .

High Resolution ESI-MS calculated for $\text{C}_{31}\text{H}_{40}\text{NOSi}^+$ (M^+) m/z : 470.2874; found m/z : 470.2865.

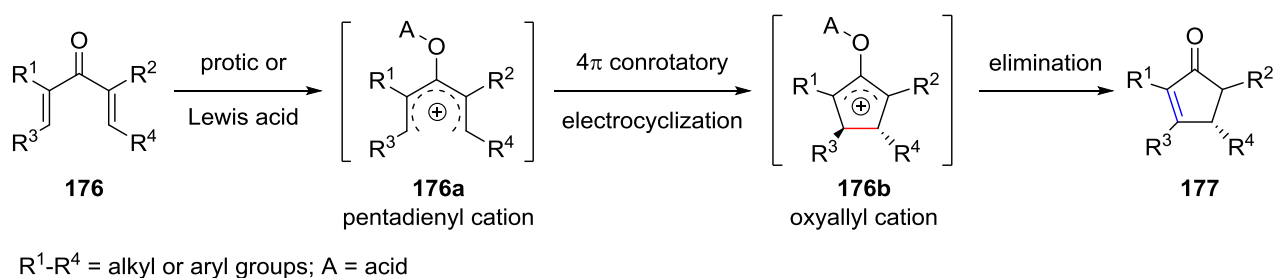
mp = 167 $^\circ\text{C}$ (decomposition).

EA: Calculated: C, 60.47; H, 6.55; N, 2.27. Found: C, 60.42; H, 6.56; N, 2.35.

Chapter 5: The Computational Mechanistic Study of an Interrupted Nazarov Reaction

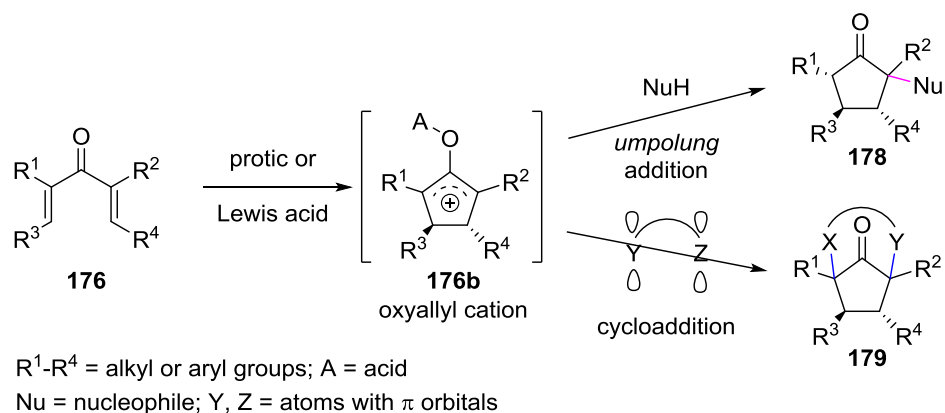
Section 5.1: The Nazarov and Interrupted Nazarov Reactions

The Nazarov reaction is the 4π conrotatory electrocyclization of a Brønsted or Lewis acid-activated divinyl ketone to give an oxyallyl cation followed by elimination to give a cyclopentenone (Scheme 54).¹⁰⁶



Scheme 54. The Nazarov reaction.

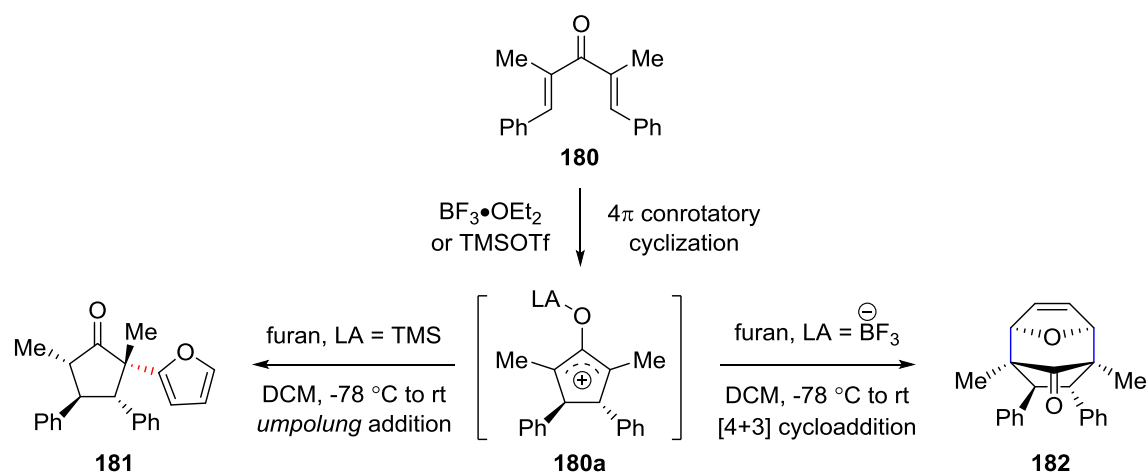
The interrupted Nazarov reaction involves nucleophilic trapping of the intermediate oxyallyl cation **176b** to form more complex structures; it also allows for retention of both stereocentres formed in the electrocyclization, as well as the introduction of synthetically-valuable functional groups, depending on the identity of the nucleophile (Scheme 55).¹⁰⁷



Scheme 55. The interrupted Nazarov reaction.

Section 5.2: Experimental Findings in the Interrupted Nazarov Reaction with Furan

In the course of his PhD studies,¹⁰⁸ Dr. Yen-Ku Wu discovered an interesting divergence in the course of the Nazarov reaction of divinyl ketone **180** interrupted by furan; depending on whether boron trifluoride etherate or trimethylsilyl triflate was used as the Lewis acid, [4+3] cycloadduct **182** or Friedel-Crafts product **181** was formed, respectively (Scheme 56). The divergent reactivity was unexpected and intriguing. Additionally, the stereochemistry of Friedel-Crafts product **181** was unanticipated; it implies that furan attacked the oxyallyl cation *syn* to the adjacent phenyl group, which is the more sterically-demanding approach.



Scheme 56. Divergent reactivity in the Nazarov reaction of divinyl ketone **180** interrupted by furan.

X-ray crystal structures of the two different products were obtained (Figure 23). This confirmed the unanticipated stereochemistry of Friedel-Crafts product **181**; additionally, it was noted that the C1-C2 bond of cycloadduct **182**, corresponding to the one bond formed in the case of **181**, is shorter than the C5-C6 bond (1.56 Å vs. 1.58 Å). This led to the idea that the [4+3] cycloadduct may be an intermediate in the formation of Friedel-Crafts product **181** via breaking of the longer, weaker C5-C6 bond.

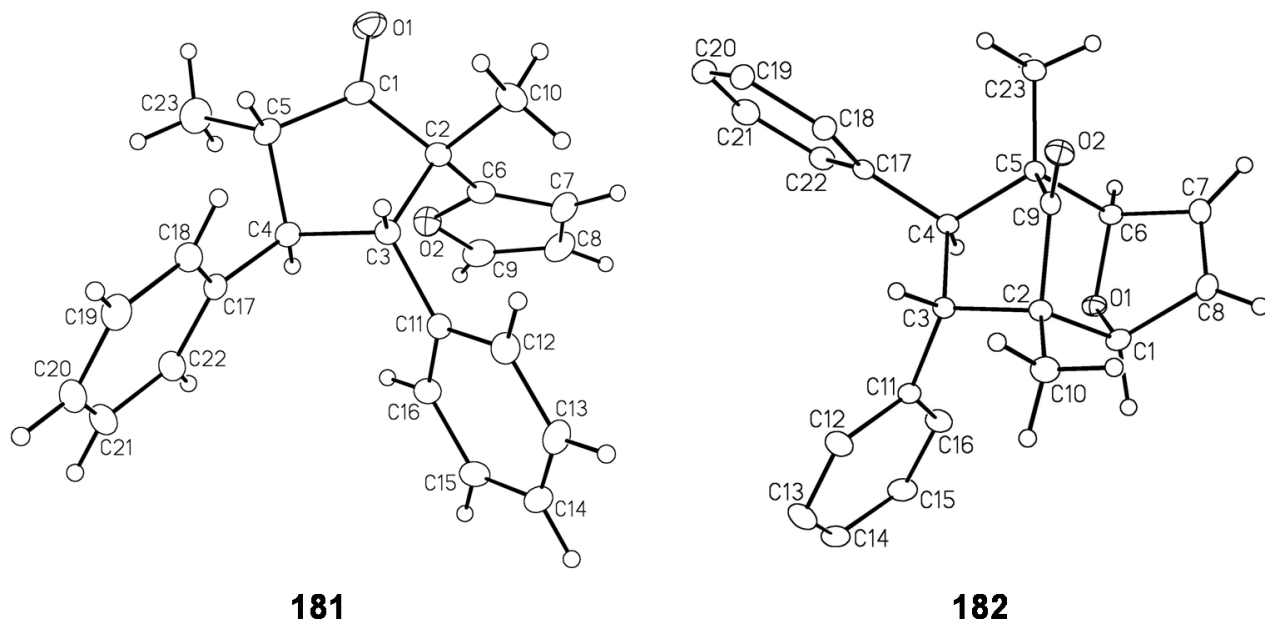
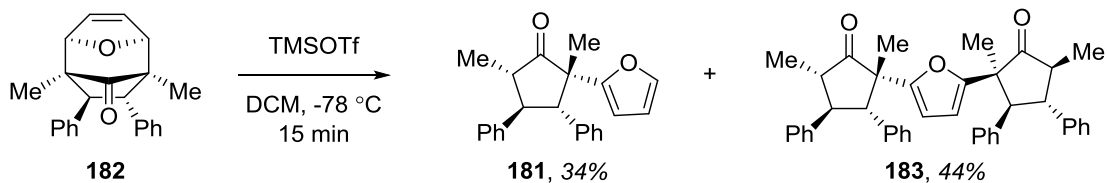


Figure 23. ORTEP diagrams of interrupted Nazarov products **181** and **182**.¹⁰²

Subjecting cycloadduct **182** to the trimethylsilyl triflate conditions resulted in bond cleavage to give the singly-bonded product **181**, as well as an unusual 2:1 adduct **183** (Scheme 57), the structure of which was confirmed by X-ray diffraction analysis (Figure 24); this result was seen as further evidence that cycloadduct **182** could be an intermediate in the formation of Friedel-Crafts product **181**.



Scheme 57. Reaction of cycloadduct **182** with trimethylsilyl triflate.

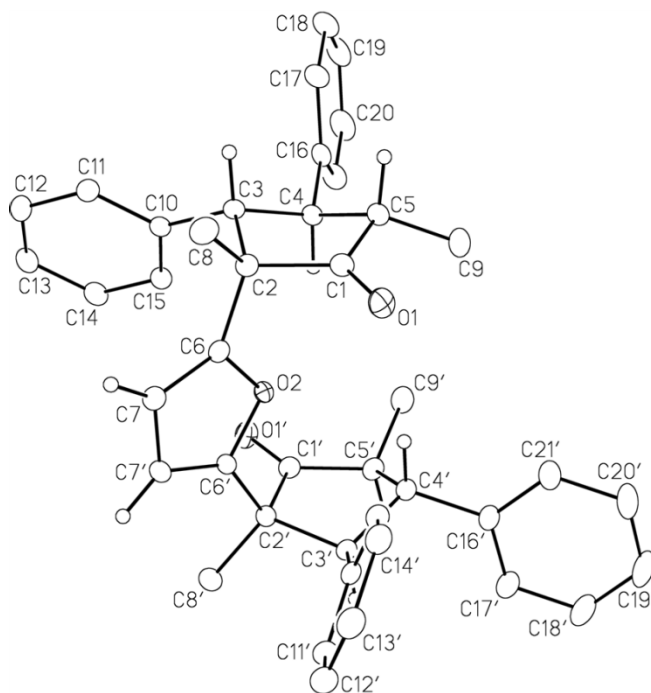


Figure 24. ORTEP diagram of adduct **183**.¹⁰²

With these experimental results in hand, we wanted to understand (1) why furan approaches oxyallyl cation **180a** from the more sterically-encumbered side (*syn* to the adjacent phenyl), and (2) why the Lewis acid used dictates the product formed.

Section 5.3: Computational Findings in the Interrupted Nazarov Reaction with Furan

Reaction pathways starting from both the TMS- and BF₃-activated oxyallyl cation **180a** (Scheme 56) were studied using DFT calculations.

Section 5.3.1: Computational Details

DFT calculations were carried out using the B3LYP⁸² and M06-2x⁸³ functionals with the 6-311+G(d,p) basis set in the Gaussian 09⁸⁵ suite of programs. Frequency calculations were carried out to ensure that the intermediates had no negative frequencies and the transition states

had only one imaginary frequency, as well as to calculate the contribution to the Gibbs free energy (reported at 195.15 K and 1 atm). Intrinsic reaction coordinate (IRC)⁹⁰ calculations were carried out on the transition states to ensure that they connected the two associated intermediates. Dichloromethane as the solvent was taken into account using the polarizable continuum model (PCM).⁹¹ For intermediates and transition states activated by TMS, the gas phase geometries calculated at B3LYP/6-311+G(d,p) were used; however, for the intermediates and transition states activated by BF₃, some gas phase geometries were found to be inaccurate, so the geometries used were calculated at the same level in dichloromethane. For all species, ΔGs were calculated using the results from single-point energy calculations at the M06-2x/6-311+G(d,p)/PCM(DCM) level using the thermal contributions to the Gibbs free energy calculated at the same level as the geometry optimization.

Section 5.3.2: Regarding the Stereochemistry of 181

Eight possible transition states were identified for formation of the first bond between oxyallyl cation **180a** and furan; these transition states were located for both the TMS-complexed oxyallyl cation (Figure 25) and the BF₃-complexed oxyallyl cation (Figure 26). Compact transition states (**TS-TMS-3,7** and **TS-BF₃-3,7**, in which the π orbitals on the furan that are not participating in bond formation are in the position to interact with the carbonyl) were found to be favored over the extended transition states (**TS-TMS-1,5** and **TS-BF₃-1,5**) by 3.6–5.0 kcal/mol, presumably due to enhanced electrostatic interactions (commonly referred to as secondary orbital interactions) in the compact transition states.¹⁰⁹ In this reaction, the extended transition state is further disfavoured by a steric component due to the adjacent phenyl ring. Between the two possible compact transition structures, addition *syn* to the adjacent phenyl (**TS-TMS-3**) is

favoured over *anti* addition (**TS-TMS-7**) by at least 3.9 kcal/mol in the TMS-activated system and 4.4 kcal/mol in the BF₃-activated system (**TS-BF₃-3** versus **TS-BF₃-7**). These computational results support the observed stereochemistry of Friedel-Crafts product **181**.

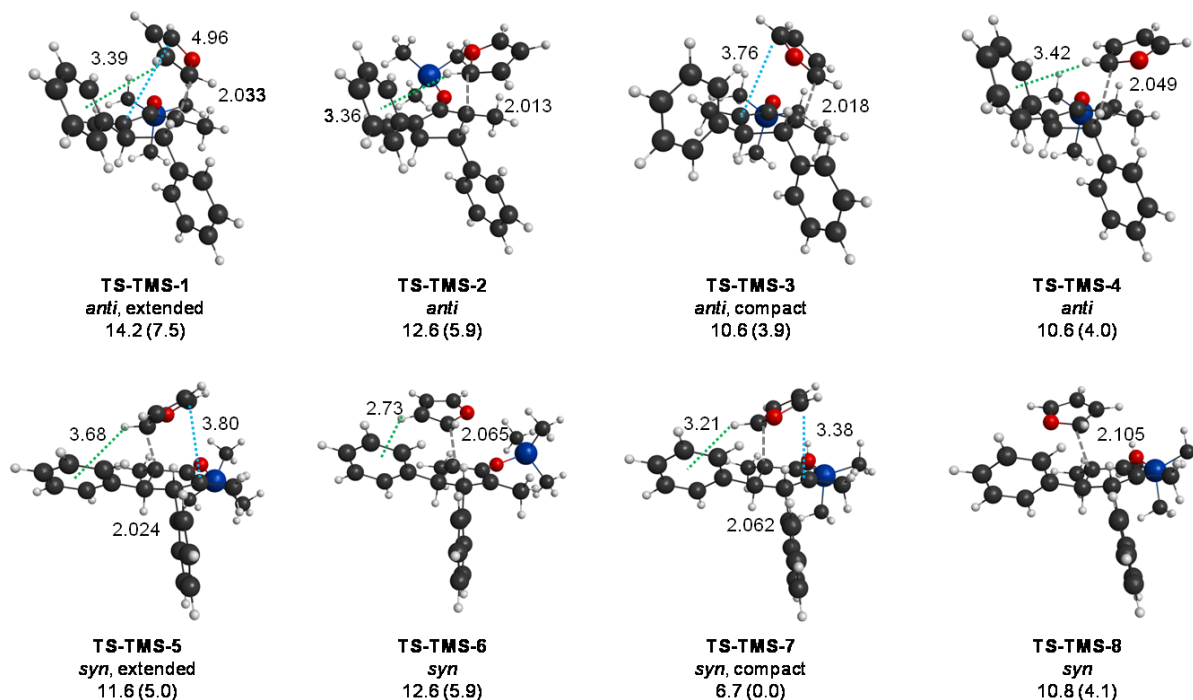


Figure 25. B3LYP/6-311+G(d,p) gas phase geometries of the eight isomeric transition states of furan capture of the oxyallyl cation activated by TMS. Values in parentheses are relative energies in kcal/mol obtained from single point energies in M06-2x/6-311+G(d,p)/PCM(DCM) with thermal contributions to the Gibbs free energy from the gas phase B3LYP/6-311+G(d,p) calculations. Indicated distances are in Angstroms. The gray lines indicate the forming bond distance, the green lines indicate CH- π interaction distances, and the blue lines indicate p-orbital interaction (non-bond forming) distances.

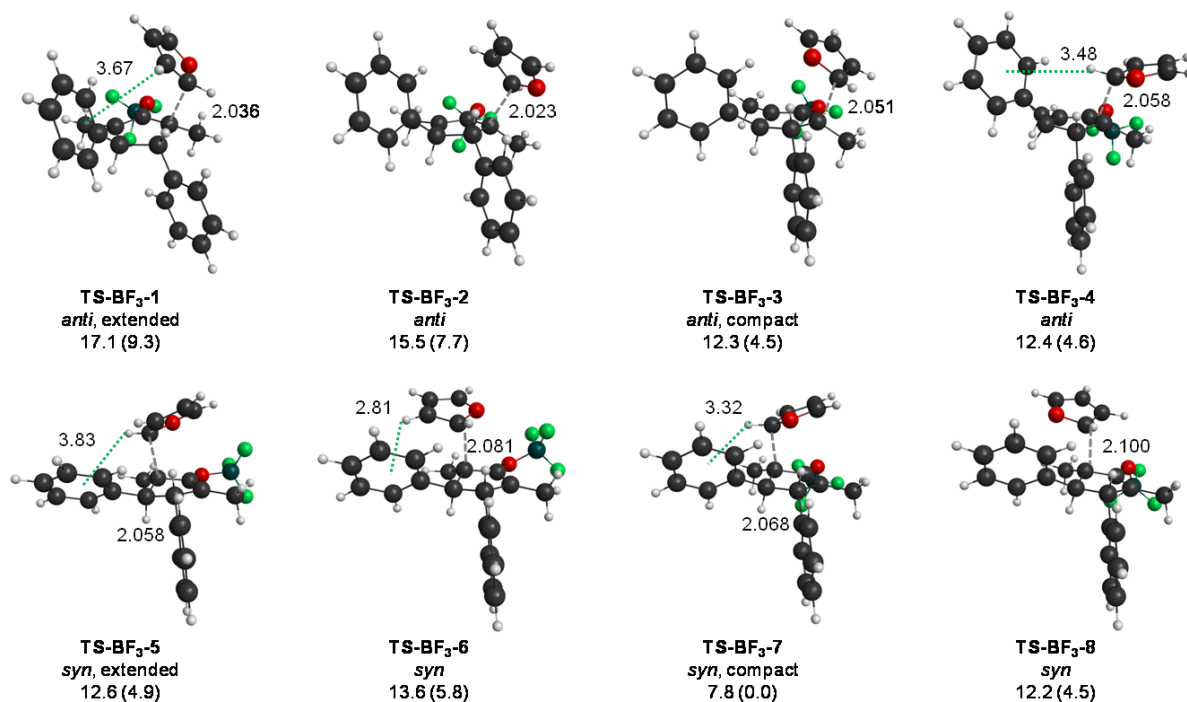


Figure 26. B3LYP/6-311+G(d,p)/PCM(DCM) geometries of the eight isomeric transition states of furan capture of the oxyallyl cation activated by BF₃. Values in parentheses are relative energies in kcal/mol obtained from single point energies in M06-2x/6-311+G(d,p)/PCM(DCM) with thermal contributions to the Gibbs free energy from the B3LYP/6-311+G(d,p)/PCM(DCM) calculations. Indicated distances are in Angstroms. The gray lines indicate the forming bond distance, the green lines indicate CH- π interaction distances, and the blue lines indicate p-orbital interaction (non-bond forming) distances.

These results may be ascribed to favourable CH- π interactions between the hydrogen on the 2-position of furan and the π system of the neighbouring phenyl ring.¹¹⁰ In TS-TMS-7, the hydrogen attached to the carbon on the furan that is undergoing bond formation is 3.21 Å from the center of the adjacent phenyl ring. This distance is longer than the typical sp² CH- π interaction, reported by Nishio to be 2.73 Å \pm 0.13;¹¹¹ however, Houk has reported examples as long as 3.2 Å.¹¹² Additionally, it was observed that this transition state is only favored by 2.0 kcal/mol at the B3LYP/6-311+G(d,p)/PCM(DCM) level. Because M06-2x models dispersion effects, like CH- π interactions, more accurately,¹¹³ it is likely this is at least one of the reasons for the extra 1.9 kcal/mol stability of the *syn* transition state using this functional for single point

energy calculations. Additionally, Houk has reported CH- π interactions in comparable reactions between furan and an acyclic oxyallyl cation.¹¹⁴

In addition to the absence of a CH- π interaction, the *anti* transition structure (**TS-TMS-3**) may be disfavoured due to torsional interactions between the adjacent phenyl and methyl groups as the furan approaches (Figure 27). **TS-TMS-3** exhibits substantial eclipsing strain, whereas the *syn* addition of furan leads to a considerably more staggered transition structure (**TS-TMS-7**). The occurrence of torsional steering has been well-documented in the literature.¹¹⁵

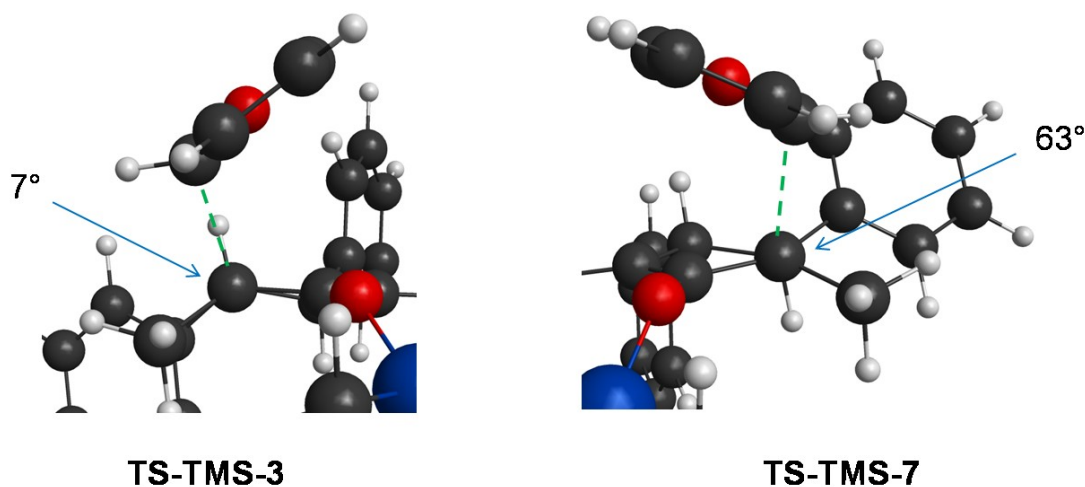


Figure 27. Torsional steering in the reaction of furan with TMS-activated oxyallyl cation **180a**. Only the relevant sections of **TS-TMS-7** and **TS-TMS-3** are presented for clarity. The values indicated are the dihedral angles between the adjacent methyl and phenyl groups.

Section 5.3.3: Regarding the Formation of **181** versus **182**

The single bond-forming transition states in Section 5.3.2 provide the entry into the mechanism of formation of both Friedel-Crafts product **181** and cycloadduct **182**; no concerted [4+3] transition states could be found. Previous work by Cramer indicates that more electrophilic oxyallyl cations are more likely to go through stepwise [3+2] and [4+3] cycloadditions.¹¹⁶

Additionally, Pérez has shown that 5-membered heterocycles like furan and *N*-methylpyrrole are more apt to undergo stepwise Diels-Alder reactions, whereas cyclopentadiene preferentially undergoes concerted Diels-Alder reactions.¹¹⁷ In fact, Pérez shows competing mechanisms between cycloaddition and electrophilic aromatic substitution (monoaddition) for furan and *N*-methylpyrrole, which echoes what we see in our interrupted Nazarov chemistry. Fernández and Cossío have also reported a stepwise mechanism for an intramolecular [4+3] cycloaddition of an oxyallyl cation with an attached furan.¹¹⁸

The reaction paths from each single bond-forming transition state were followed to cyclization (Figure 28-Figure 43). Note that some reaction paths do not show cyclization of the intermediate, as rotation to one of the other intermediates would be required before cyclization (e.g. **IN-TMS-2** would have to undergo bond rotation to become **IN-TMS-3** before cyclization could occur). For the lowest energy transition states for each Lewis acid (**TS-TMS-7** and **TS-BF₃-7**), the structure and energy of the Friedel-Crafts product-Lewis acid adduct was also found (Figure 34 and Figure 42).

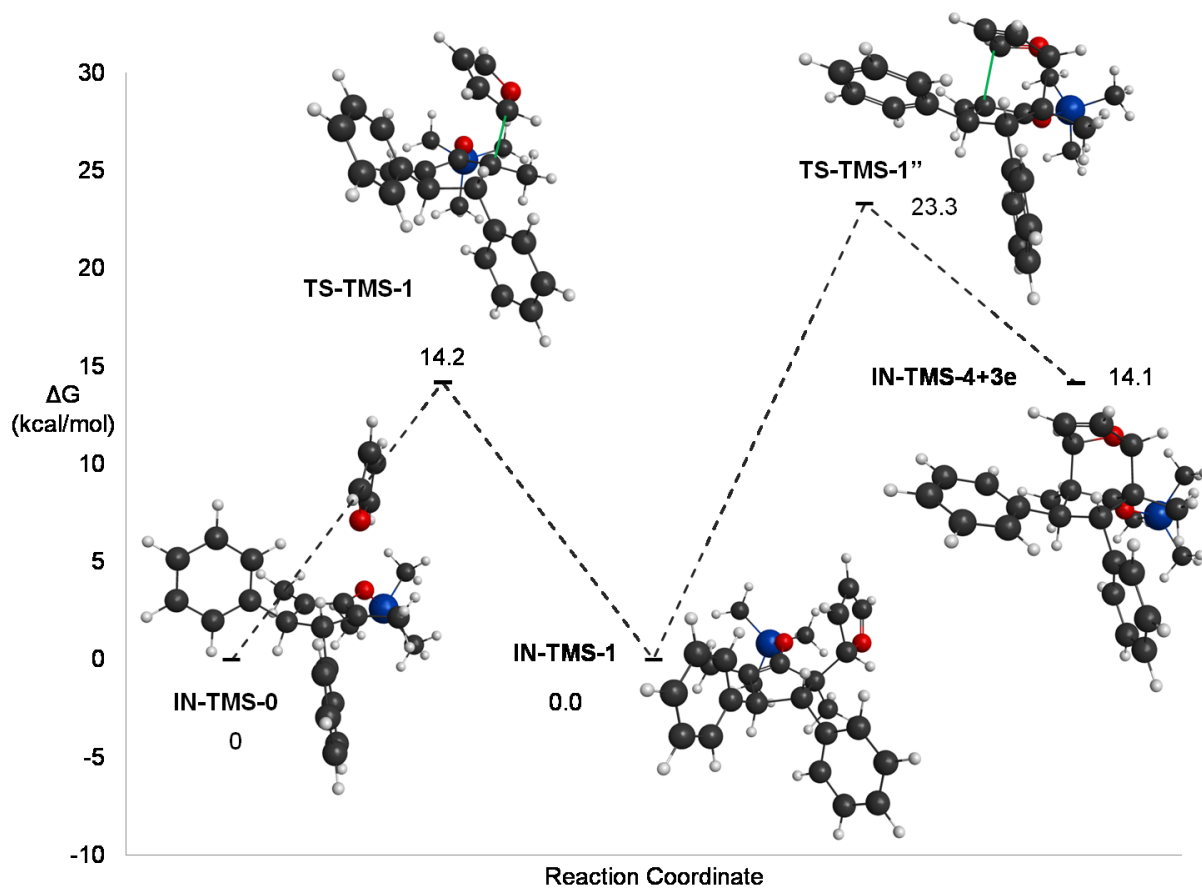


Figure 28. Stationary points in the reaction of TMS-activated oxyallyl cation **180a** with furan via **TS-TMS-1**. Values in parentheses are relative energies in kcal/mol obtained from single point energies in M06-2x/6-311+G(d,p)/PCM(DCM) with thermal contributions to the Gibbs free energy from the B3LYP/6-311+G(d,p) calculations.

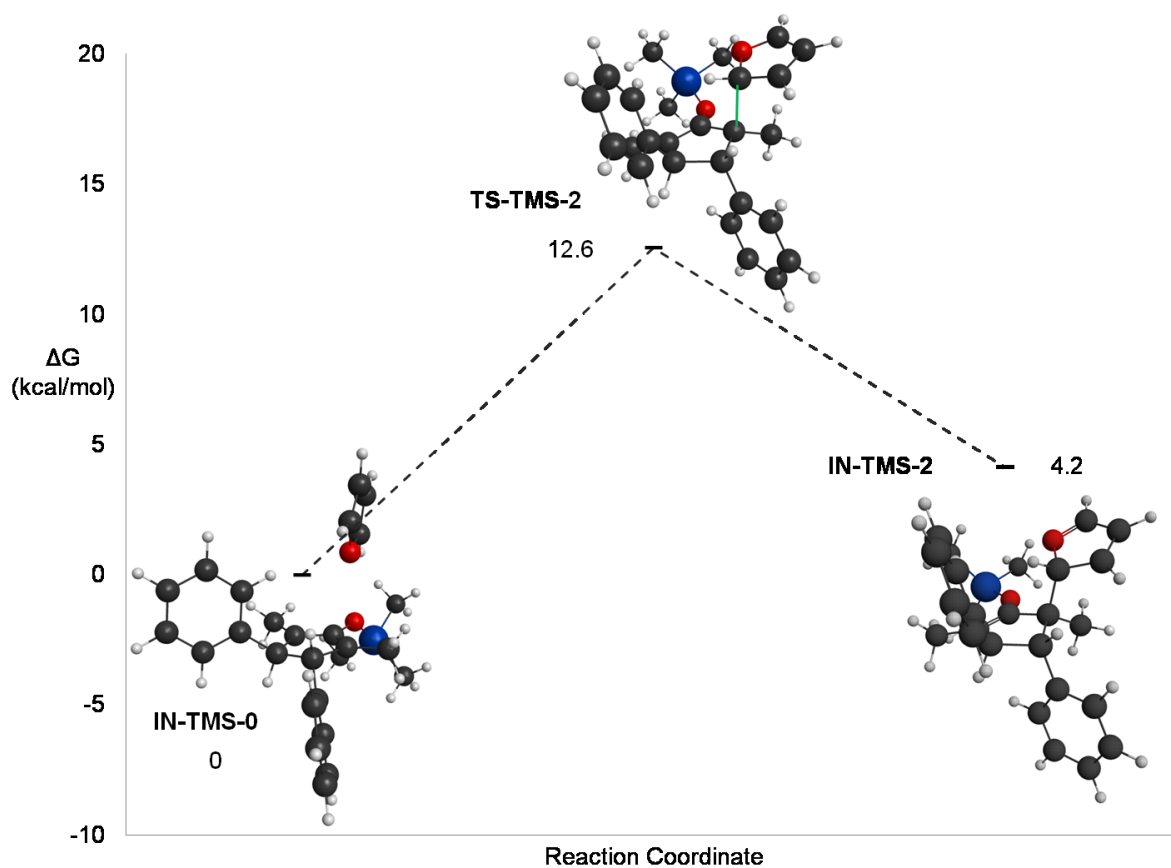


Figure 29. Stationary points in the reaction of TMS-activated oxyallyl cation **180a** with furan via **TS-TMS-2**. Values in parentheses are relative energies in kcal/mol obtained from single point energies in M06-2x/6-311+G(d,p)/PCM(DCM) with thermal contributions to the Gibbs free energy from the B3LYP/6-311+G(d,p) calculations.

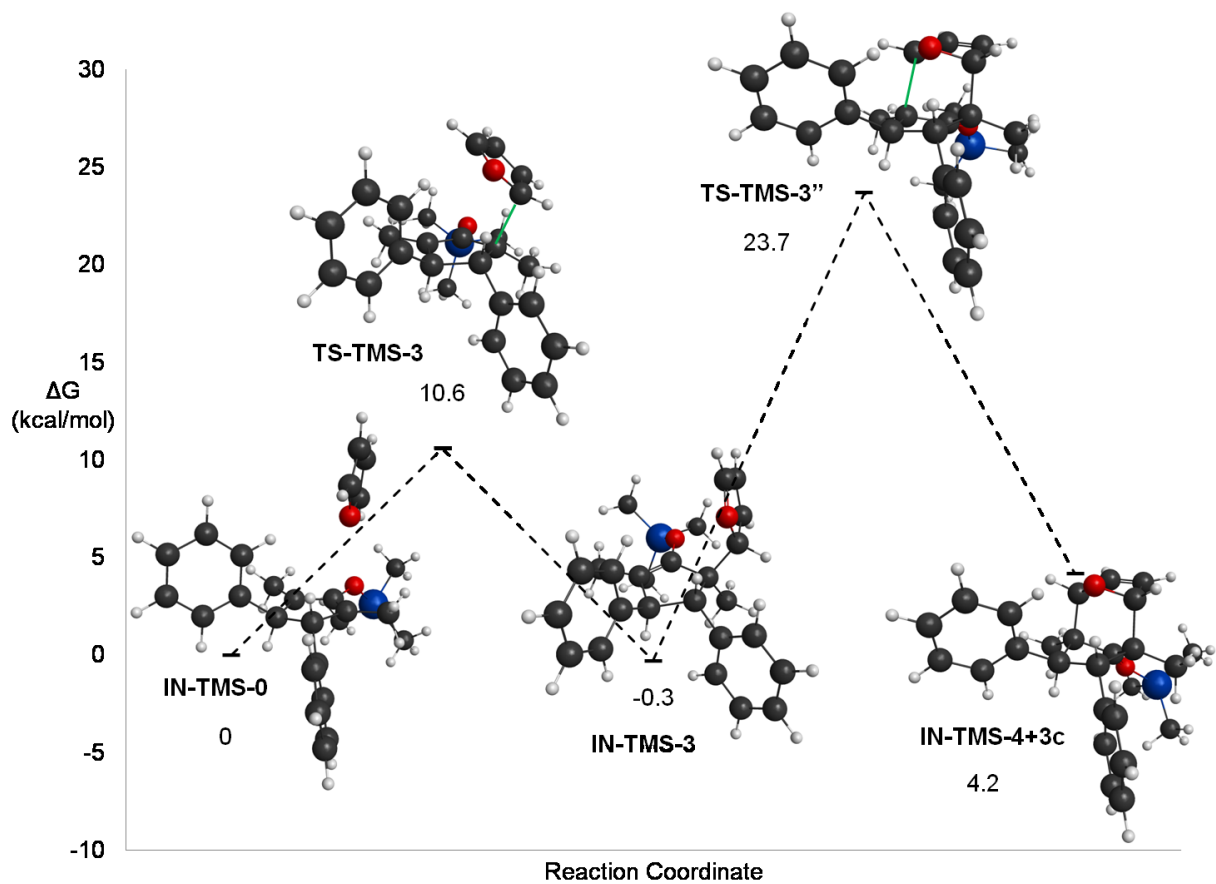


Figure 30. Stationary points in the reaction of TMS-activated oxyallyl cation **180a** with furan via **TS-TMS-3**. Values in parentheses are relative energies in kcal/mol obtained from single point energies in M06-2x/6-311+G(d,p)/PCM(DCM) with thermal contributions to the Gibbs free energy from the B3LYP/6-311+G(d,p) calculations.

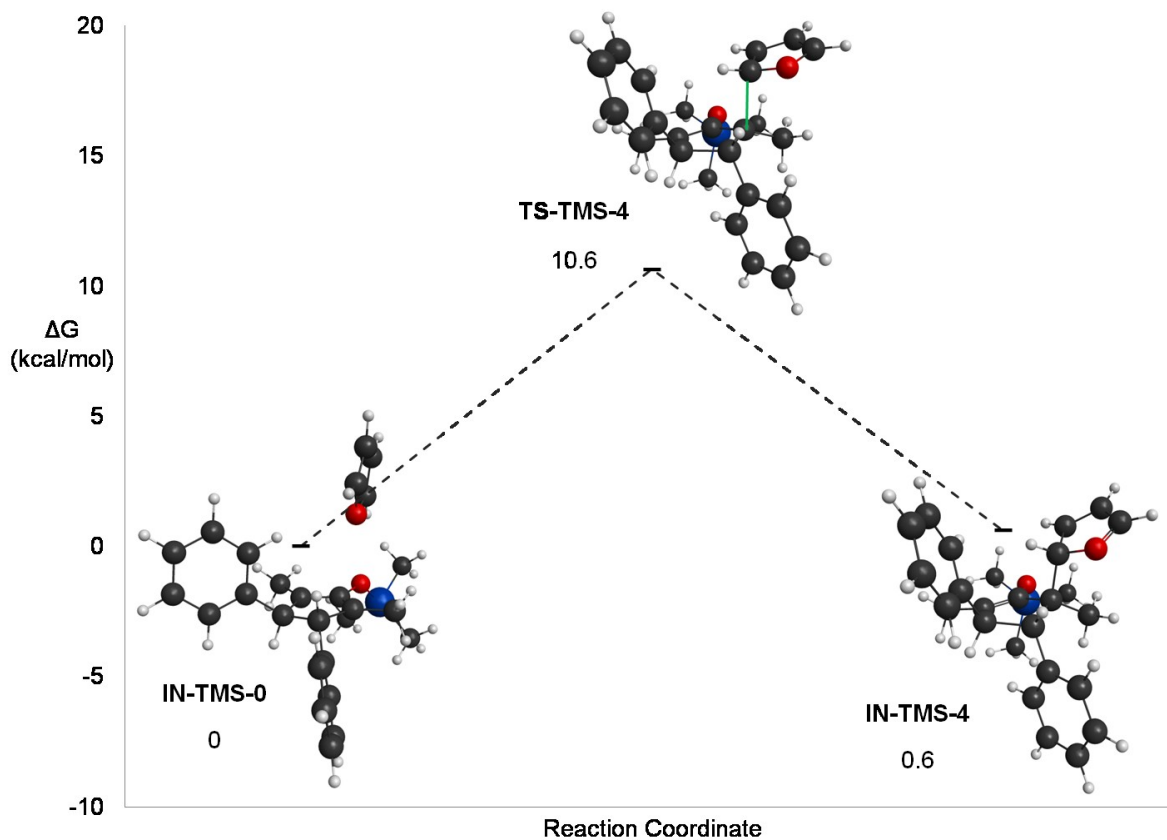


Figure 31. Stationary points in the reaction of TMS-activated oxyallyl cation **180a** with furan via **TS-TMS-4**. Values in parentheses are relative energies in kcal/mol obtained from single point energies in M06-2x/6-311+G(d,p)/PCM(DCM) with thermal contributions to the Gibbs free energy from the B3LYP/6-311+G(d,p) calculations.

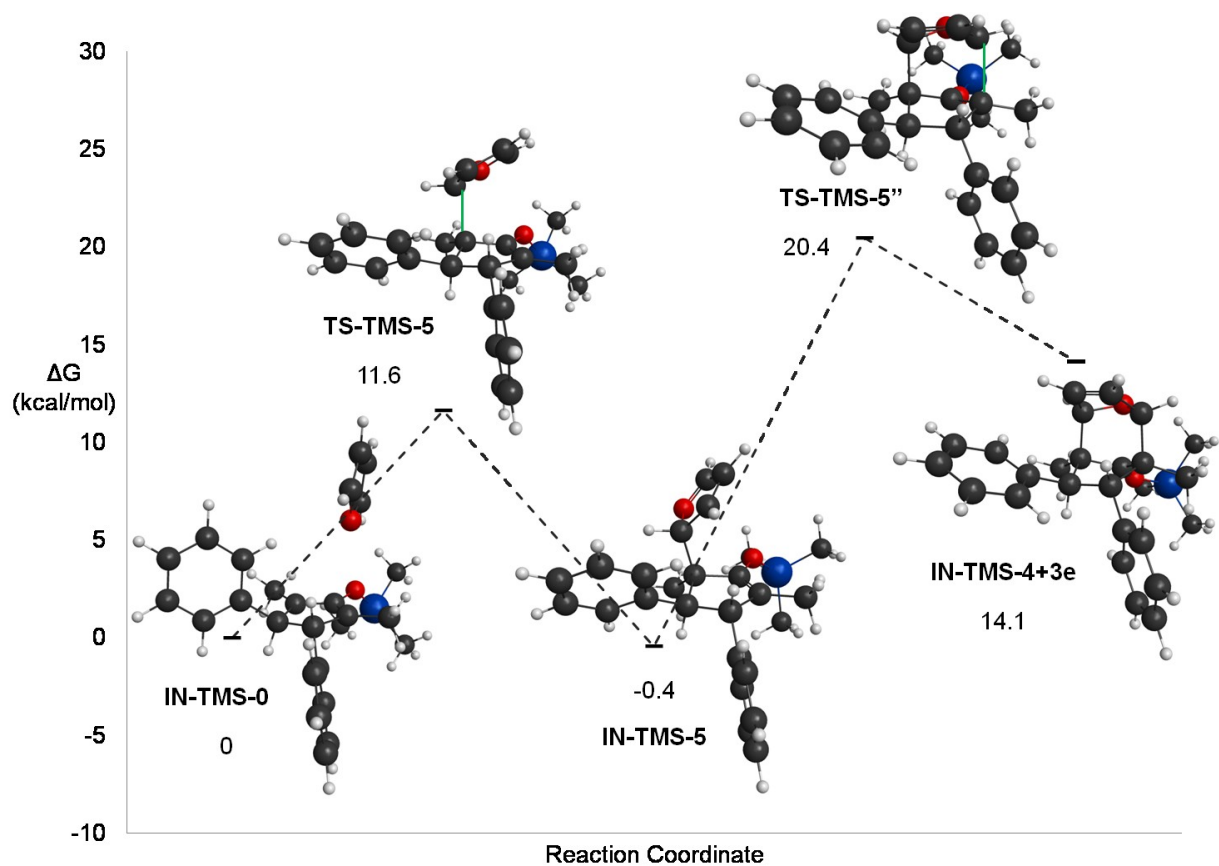


Figure 32. Stationary points in the reaction of TMS-activated oxyallyl cation **180a** with furan via **TS-TMS-5**. Values in parentheses are relative energies in kcal/mol obtained from single point energies in M06-2x/6-311+G(d,p)/PCM(DCM) with thermal contributions to the Gibbs free energy from the B3LYP/6-311+G(d,p) calculations.

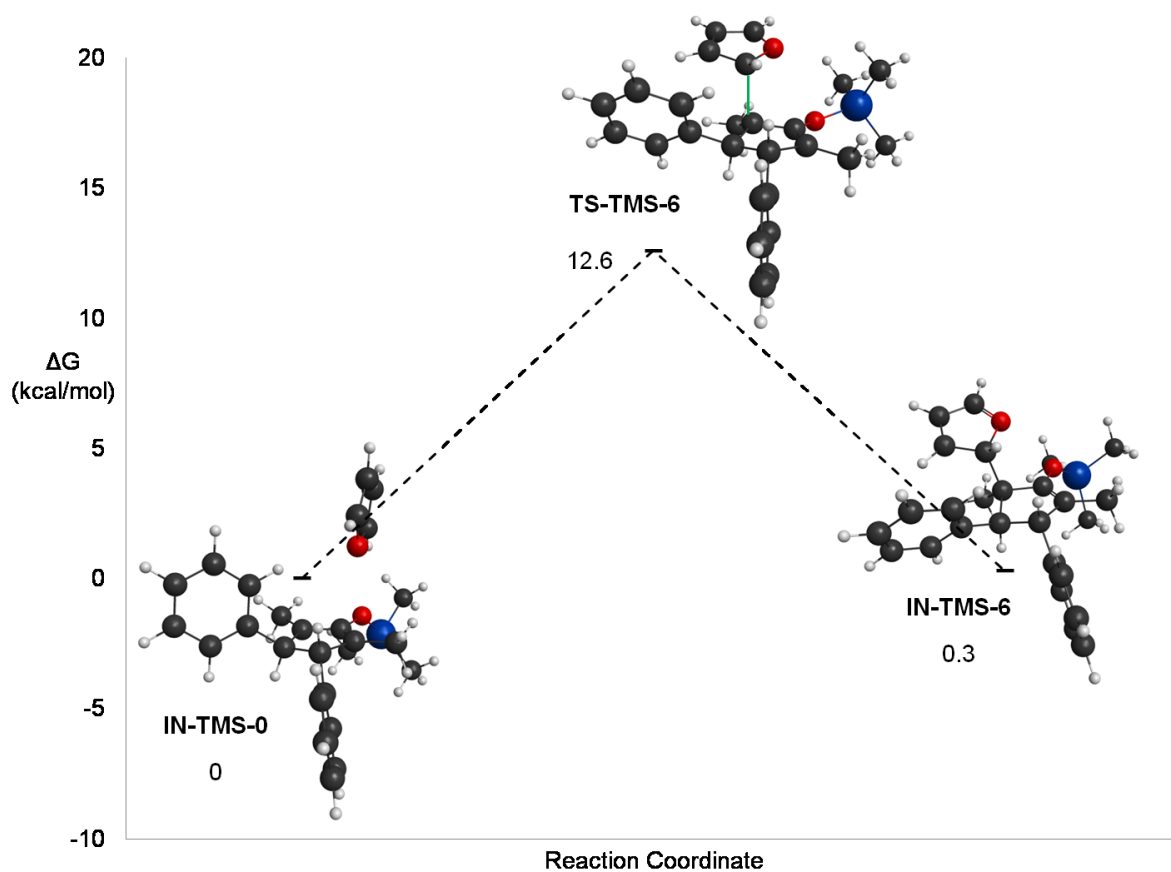


Figure 33. Stationary points in the reaction of TMS-activated oxyallyl cation **180a** with furan via **TS-TMS-6**. Values in parentheses are relative energies in kcal/mol obtained from single point energies in M06-2x/6-311+G(d,p)/PCM(DCM) with thermal contributions to the Gibbs free energy from the B3LYP/6-311+G(d,p) calculations.

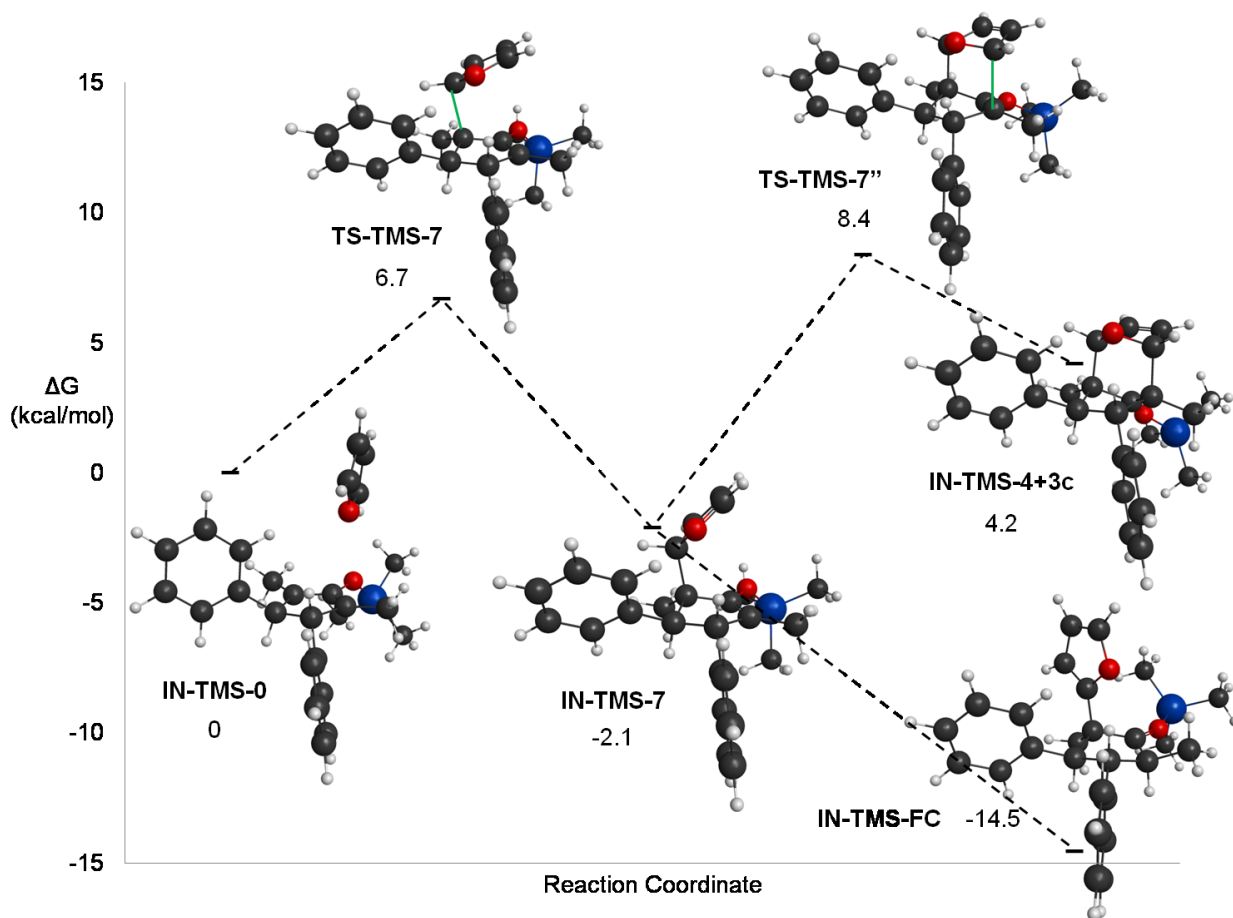


Figure 34. Stationary points in the reaction of TMS-activated oxyallyl cation **180a** with furan via **TS-TMS-7**. Values in parentheses are relative energies in kcal/mol obtained from single point energies in M06-2x/6-311+G(d,p)/PCM(DCM) with thermal contributions to the Gibbs free energy from the B3LYP/6-311+G(d,p) calculations.

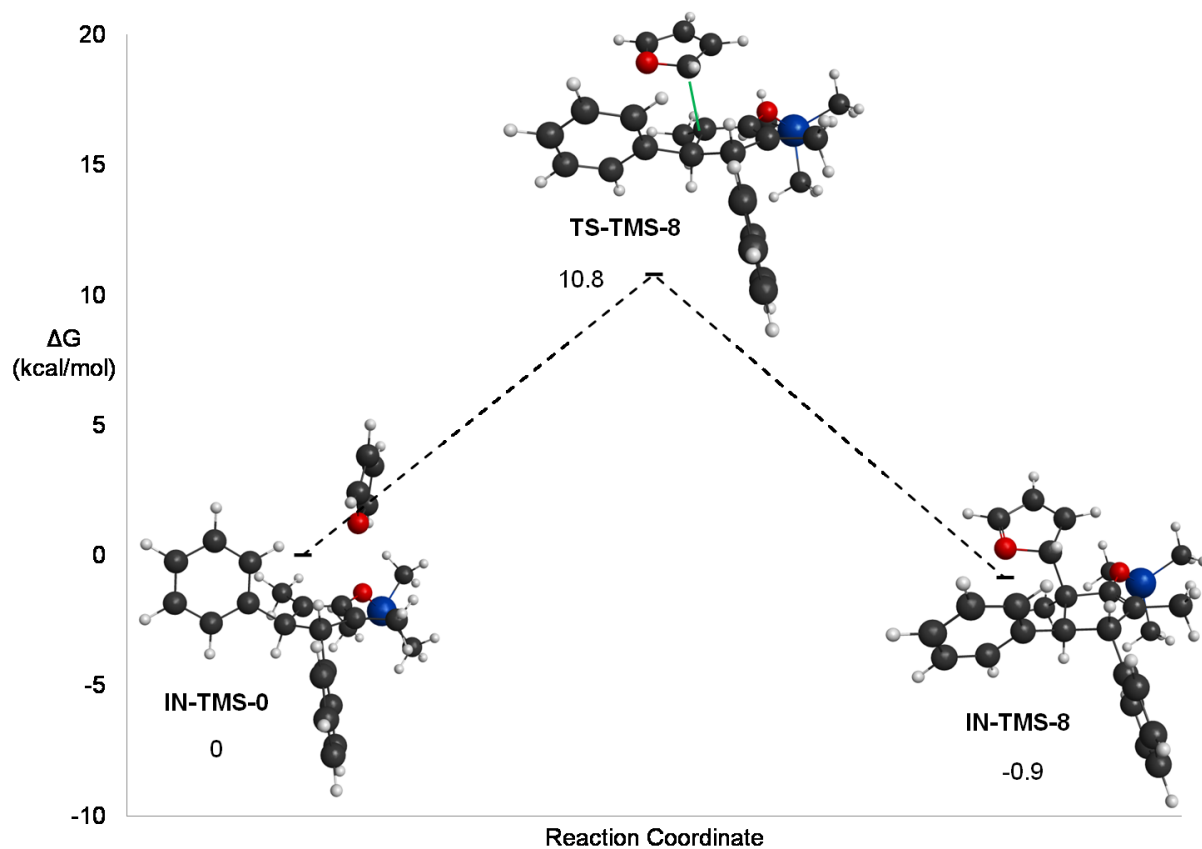


Figure 35. Stationary points in the reaction of TMS-activated oxyallyl cation **180a** with furan via **TS-TMS-8**. Values in parentheses are relative energies in kcal/mol obtained from single point energies in M06-2x/6-311+G(d,p)/PCM(DCM) with thermal contributions to the Gibbs free energy from the B3LYP/6-311+G(d,p) calculations.

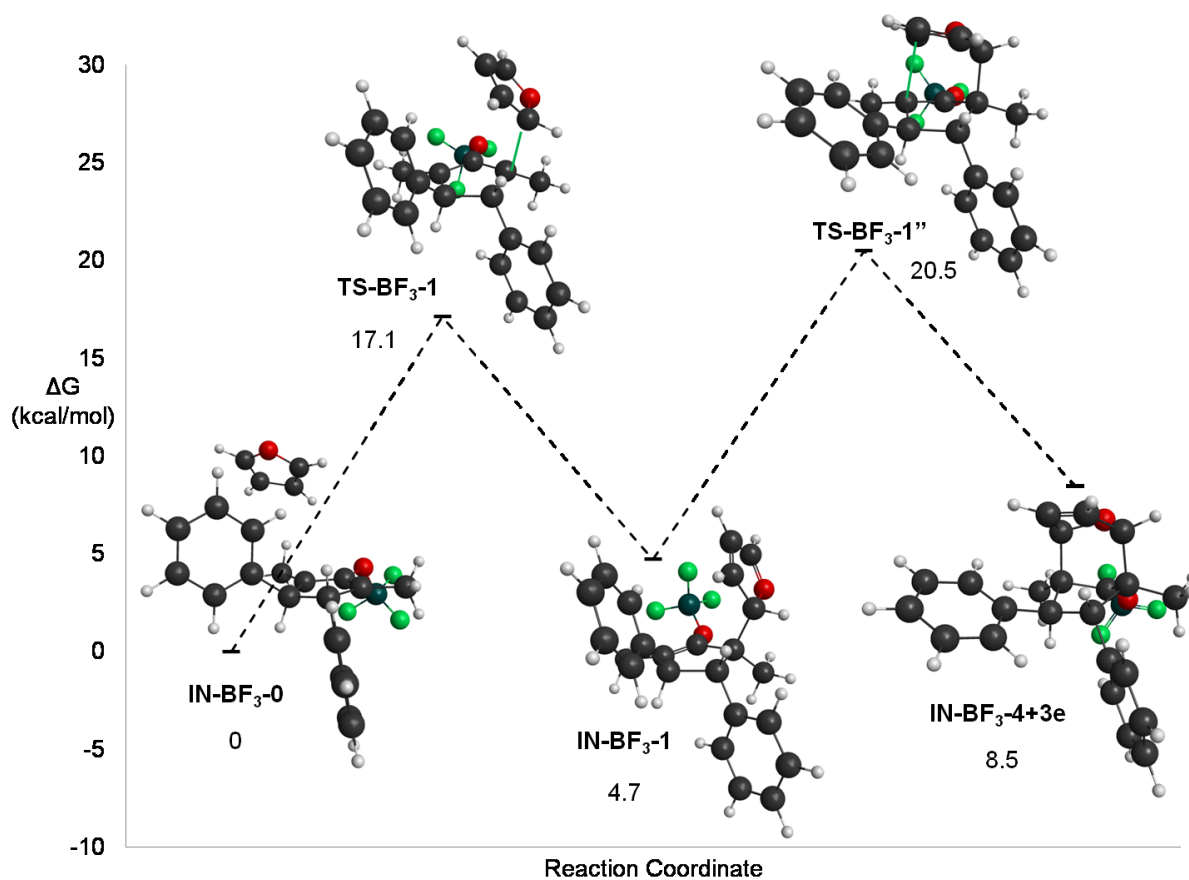


Figure 36. Stationary points in the reaction of BF₃-activated oxyallyl cation **180a** with furan via **TS-BF₃-1**. Values in parentheses are relative energies in kcal/mol obtained from single point energies in M06-2x/6-311+G(d,p)/PCM(DCM) with thermal contributions to the Gibbs free energy from the B3LYP/6-311+G(d,p)/PCM(DCM) calculations.

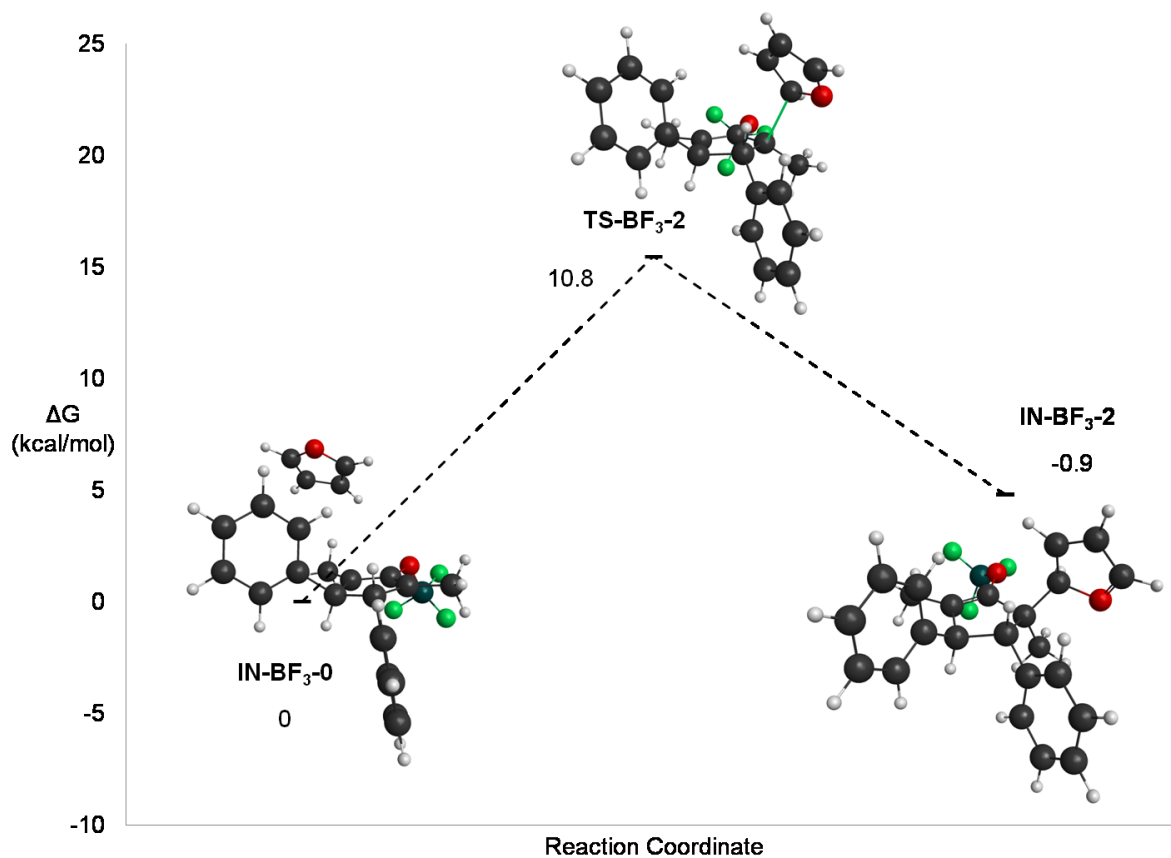


Figure 37. Stationary points in the reaction of BF₃-activated oxyallyl cation **180a** with furan via **TS-BF₃-2**. Values in parentheses are relative energies in kcal/mol obtained from single point energies in M06-2x/6-311+G(d,p)/PCM(DCM) with thermal contributions to the Gibbs free energy from the B3LYP/6-311+G(d,p)/PCM(DCM) calculations.

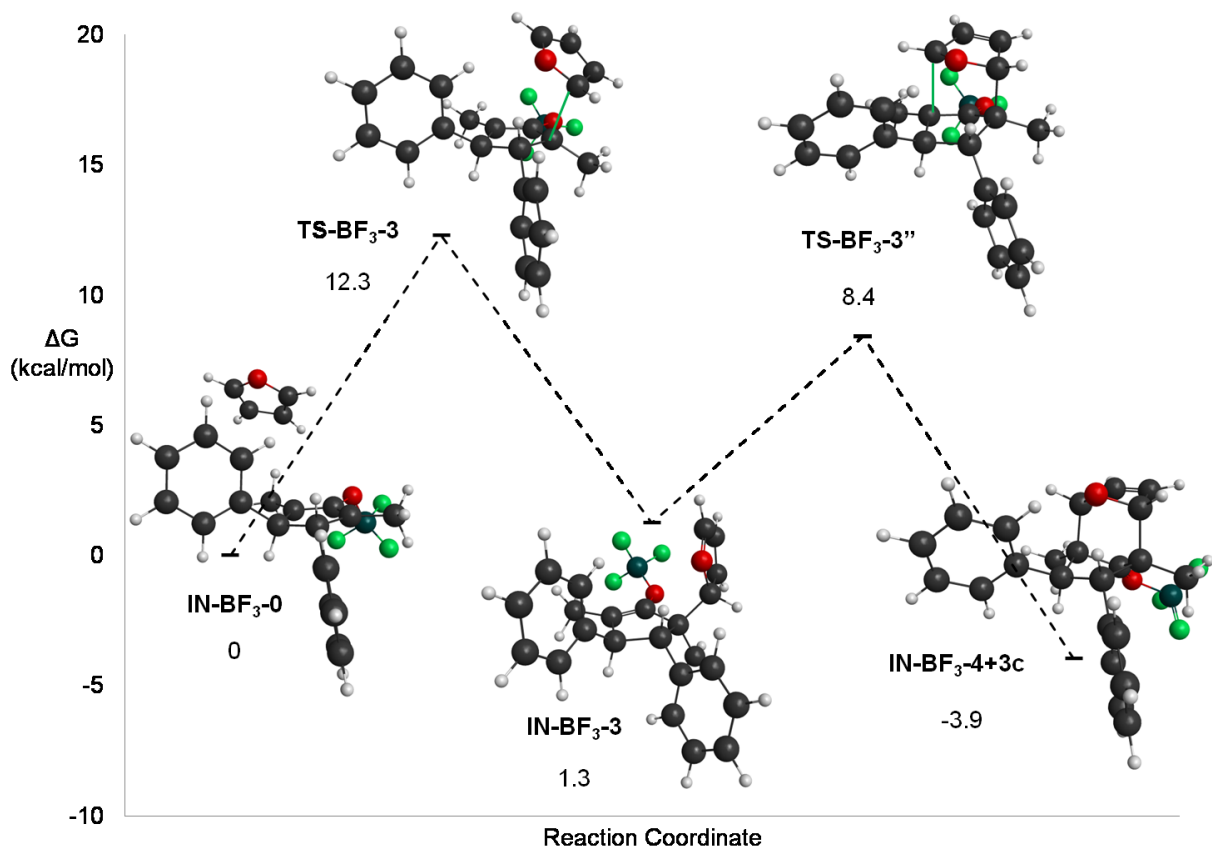


Figure 38. Stationary points in the reaction of BF₃-activated oxyallyl cation **180a** with furan via **TS-BF₃-3**. Values in parentheses are relative energies in kcal/mol obtained from single point energies in M06-2x/6-311+G(d,p)/PCM(DCM) with thermal contributions to the Gibbs free energy from the B3LYP/6-311+G(d,p)/PCM(DCM) calculations.

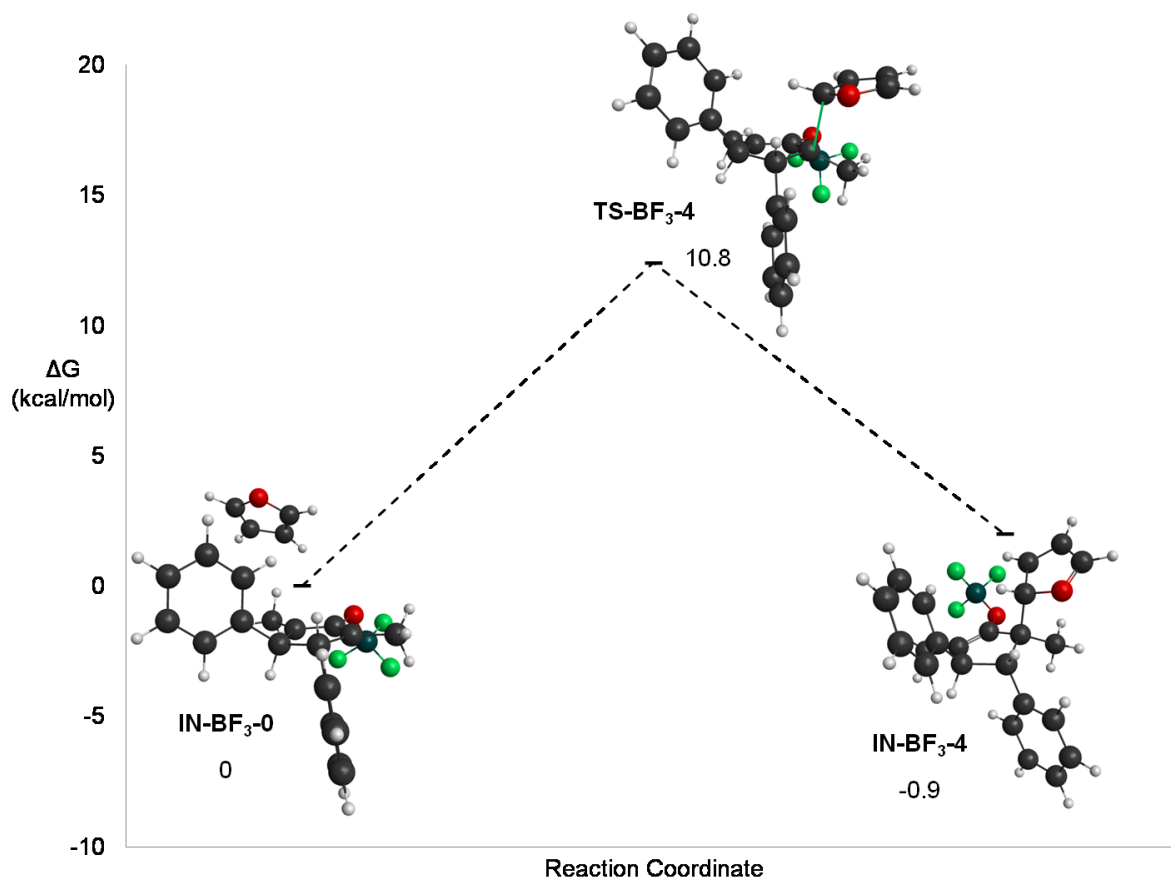


Figure 39. Stationary points in the reaction of BF₃-activated oxyallyl cation **180a** with furan via **TS-BF₃-4**. Values in parentheses are relative energies in kcal/mol obtained from single point energies in M06-2x/6-311+G(d,p)/PCM(DCM) with thermal contributions to the Gibbs free energy from the B3LYP/6-311+G(d,p)/PCM(DCM) calculations.

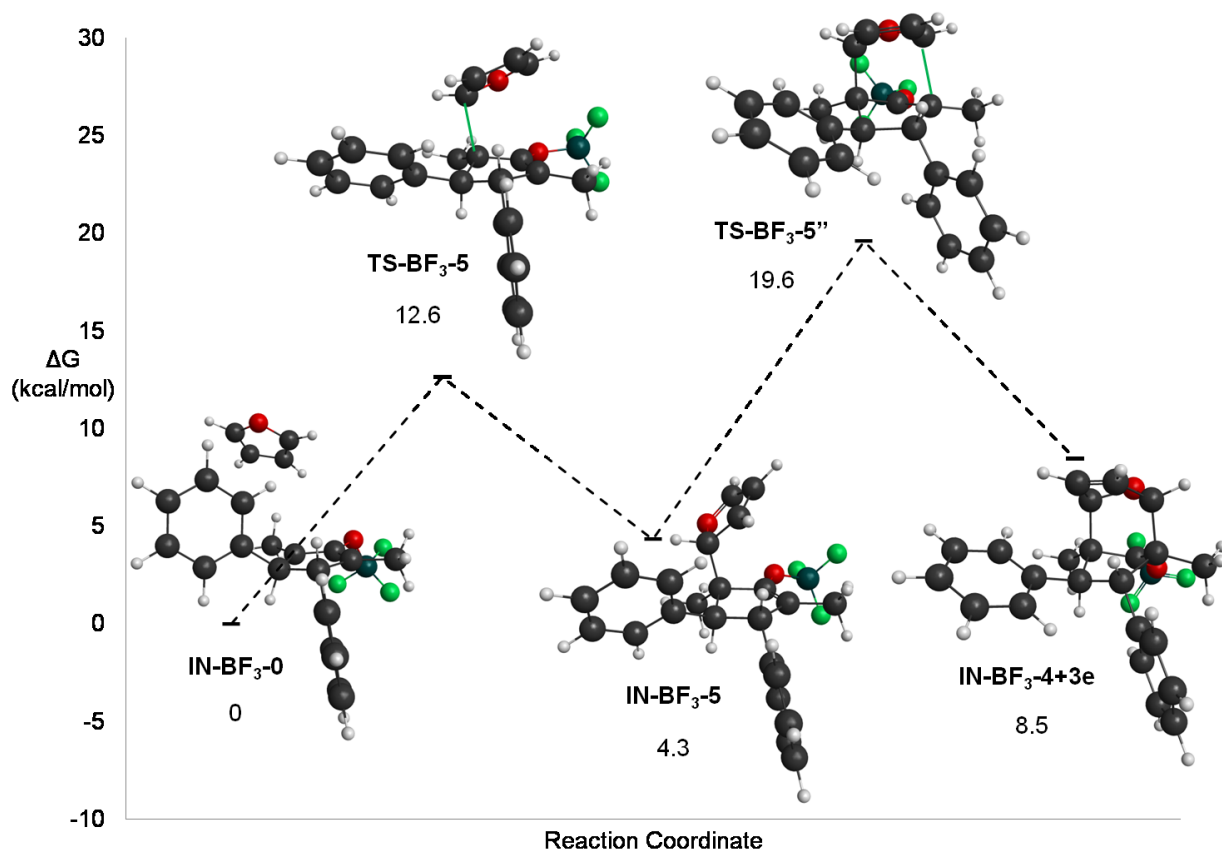


Figure 40. Stationary points in the reaction of BF_3 -activated oxyallyl cation **180a** with furan via TS-BF_3-5 . Values in parentheses are relative energies in kcal/mol obtained from single point energies in M06-2x/6-311+G(d,p)/PCM(DCM) with thermal contributions to the Gibbs free energy from the B3LYP/6-311+G(d,p)/PCM(DCM) calculations.

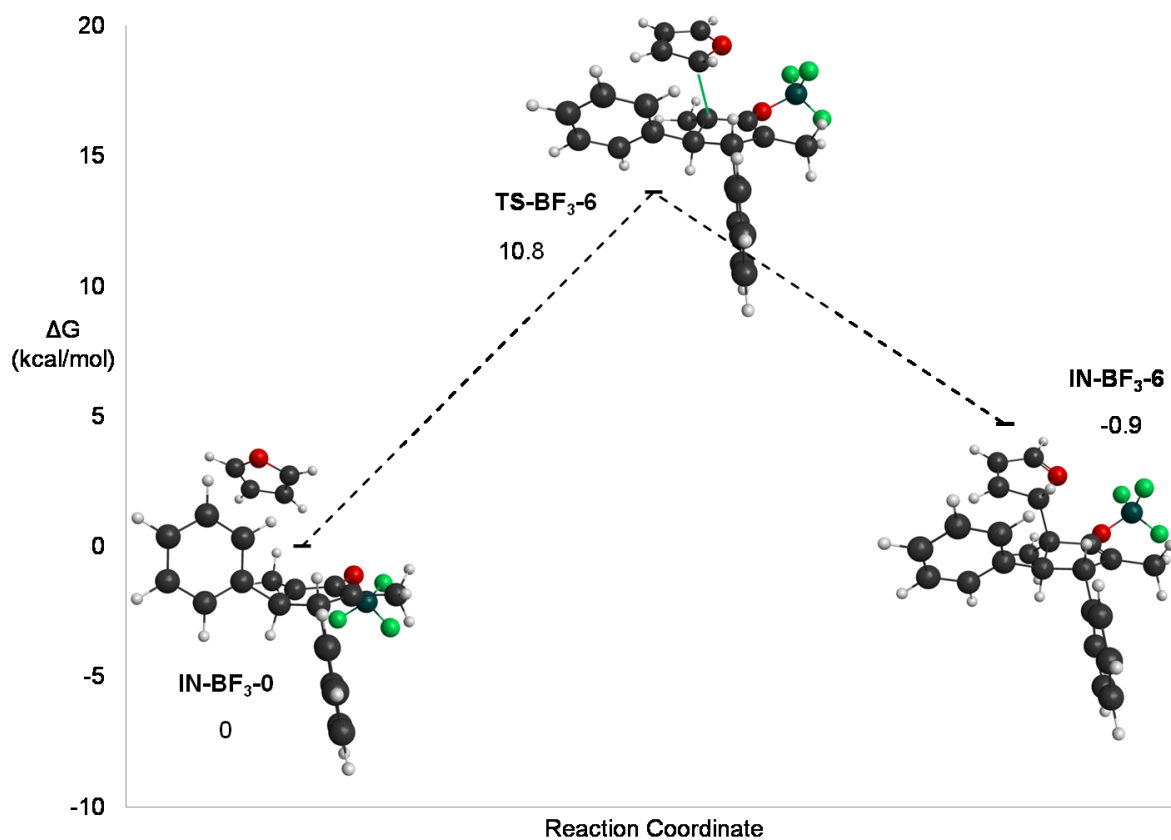


Figure 41. Stationary points in the reaction of BF₃-activated oxyallyl cation **180a** with furan via **TS-BF₃-6**. Values in parentheses are relative energies in kcal/mol obtained from single point energies in M06-2x/6-311+G(d,p)/PCM(DCM) with thermal contributions to the Gibbs free energy from the B3LYP/6-311+G(d,p)/PCM(DCM) calculations.

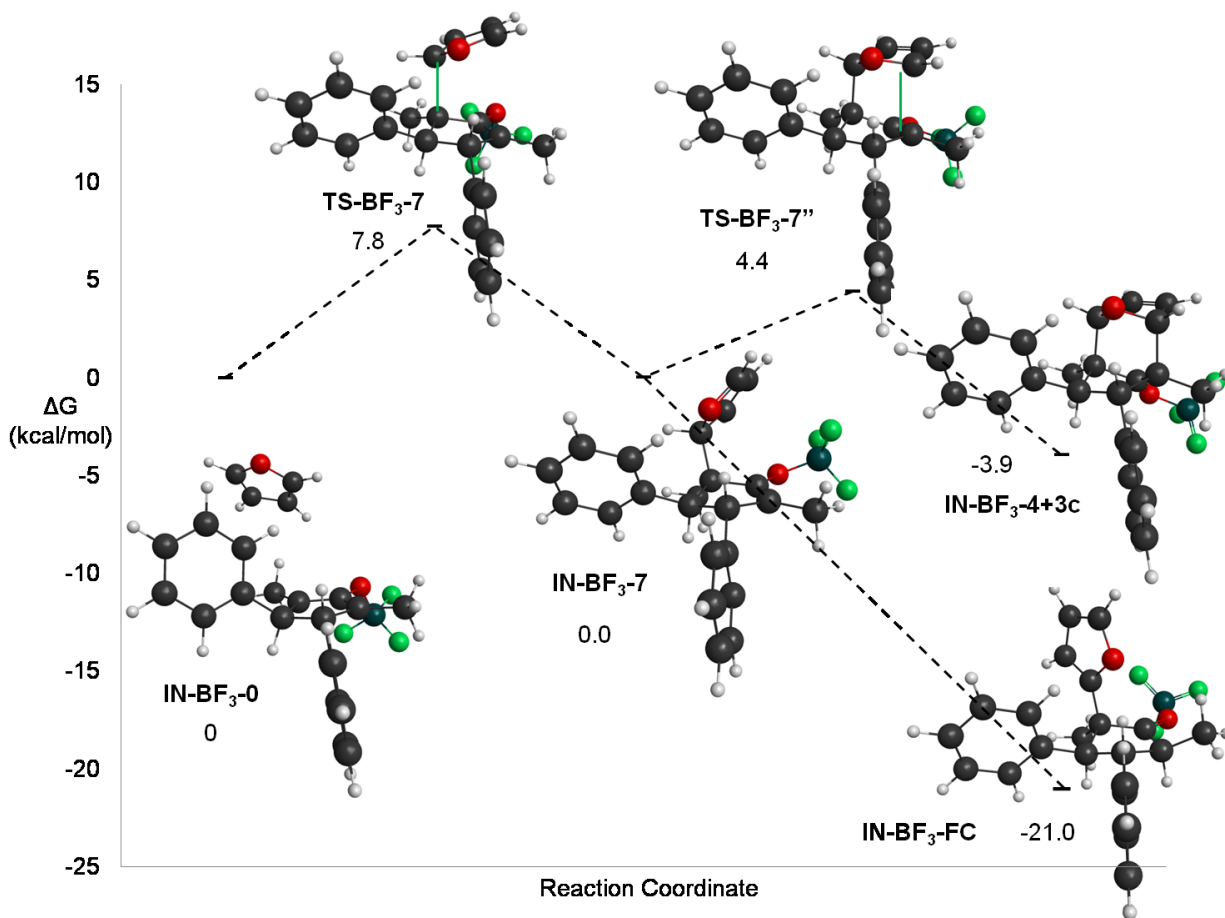


Figure 42. Stationary points in the reaction of BF_3 -activated oxyallyl cation **180a** with furan via **TS-BF₃-7**. Values in parentheses are relative energies in kcal/mol obtained from single point energies in M06-2x/6-311+G(d,p)/PCM(DCM) with thermal contributions to the Gibbs free energy from the B3LYP/6-311+G(d,p)/PCM(DCM) calculations.

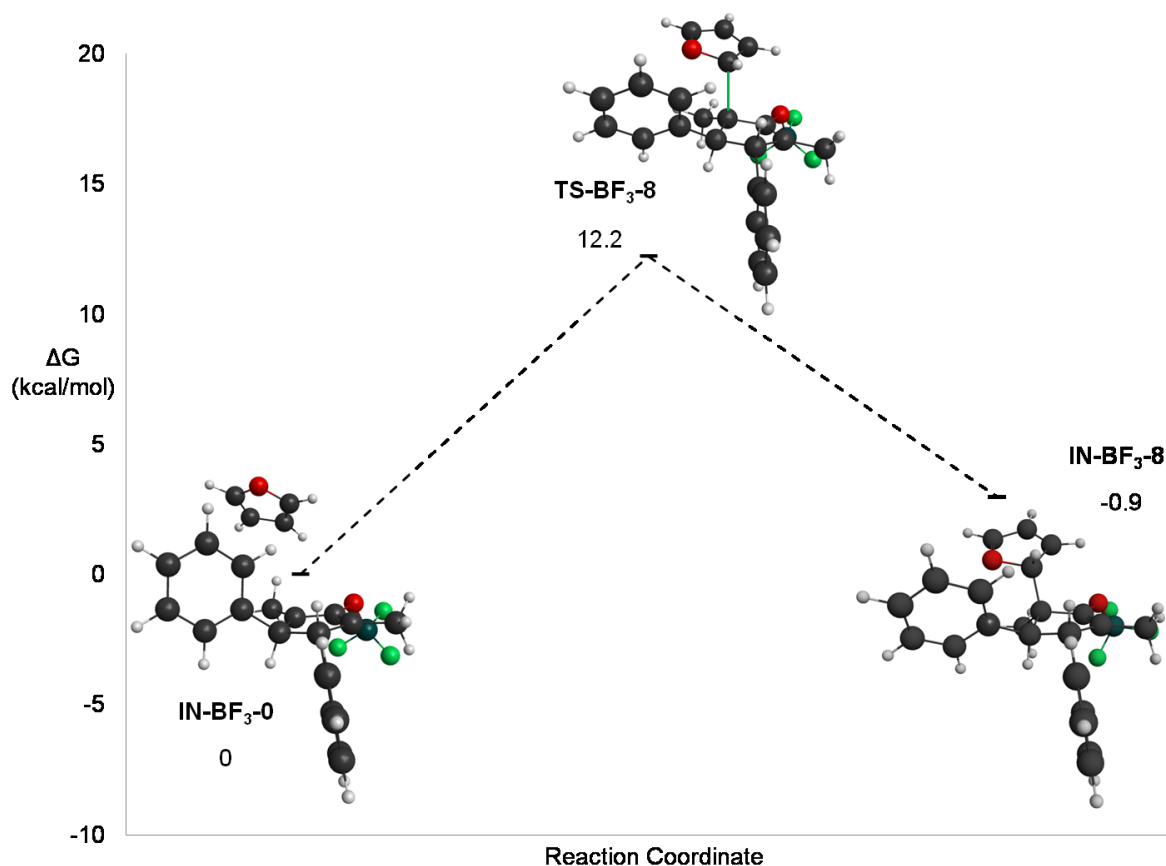


Figure 43. Stationary points in the reaction of BF_3 -activated oxyallyl cation **180a** with furan via **TS-BF₃-8**. Values in parentheses are relative energies in kcal/mol obtained from single point energies in M06-2x/6-311+G(d,p)/PCM(DCM) with thermal contributions to the Gibbs free energy from the B3LYP/6-311+G(d,p)/PCM(DCM) calculations.

Looking closer at the most likely reaction paths to Friedel-Crafts product **181** and [4+3] cycloadduct **182** (via the lowest energy transition states **TS-TMS-7** and **TS-BF₃-7**, Figure 34 and Figure 42, respectively), it was apparent that the reaction course diverged after the first bond-forming event between oxyallyl cation **180a** and furan. The reaction with $\text{BF}_3\cdot\text{OEt}_2$ favours cycloaddition; the formation of the second bond to produce the cycloadduct is exergonic and has a lower activation barrier than the first bond formation. Although the BF_3 -complexed Friedel-Crafts product **IN-BF₃-FC** is lower in energy than the complexed cycloadduct **IN-BF₃-4+3c**, this product is not seen in the reaction, presumably because this reaction is kinetically controlled;

because we are unsure of the species that promotes the proton transfer to provide the Friedel-Crafts product, we cannot present a transition structure for this process. This is in contrast to the TMSOTf-mediated reaction, in which cycloadduct formation is an unfavorable process, being endergonic and kinetically inaccessible. In fact, this supports the experimentally-observed “reversal” of the cycloadduct to the Friedel-Crafts product when exposed to TMSOTf.

As it was still unclear to us as to why such similar transition states (**TS- BF₃-7**” and **TS-TMS-7**”) had such different activation barriers, we visualized the frontier molecular orbitals (FMOs) of both transition states (Figure 44 and Figure 45).¹¹⁹ The highest occupied molecular orbital (HOMO) of **TS-BF₃-7**” has a significant amount of electron density between the two carbons where the bond formation is occurring; however, the HOMO of **TS-TMS-7**” has virtually no electron density between these two carbons. While we are unsure of the cause of this difference, it is apparent that bond formation is quite favourable in the BF₃ case, but not in the TMS case. It is possible that the much larger TMS group is sterically hindering bond formation/cycloadduct formation.

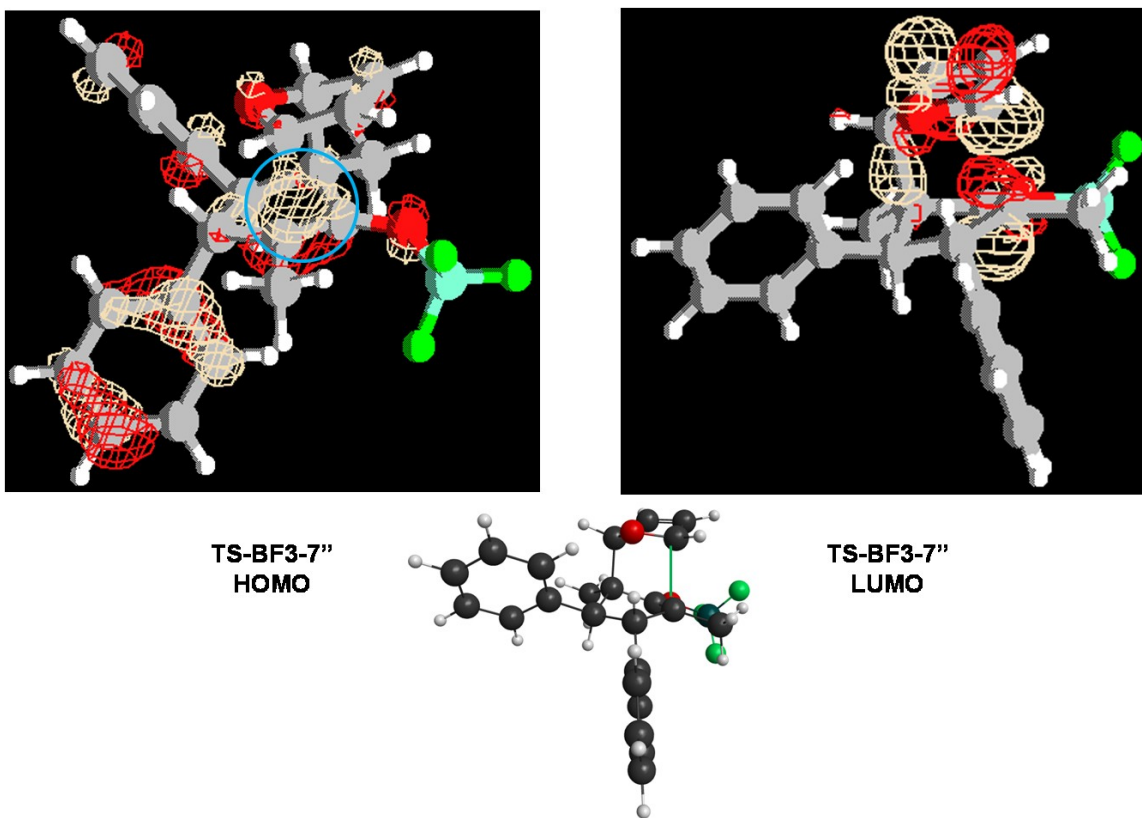


Figure 44. The frontier molecular orbitals of **TS-BF₃-7''**. The blue circle highlights the area of high electron density between the carbons undergoing bond formation.

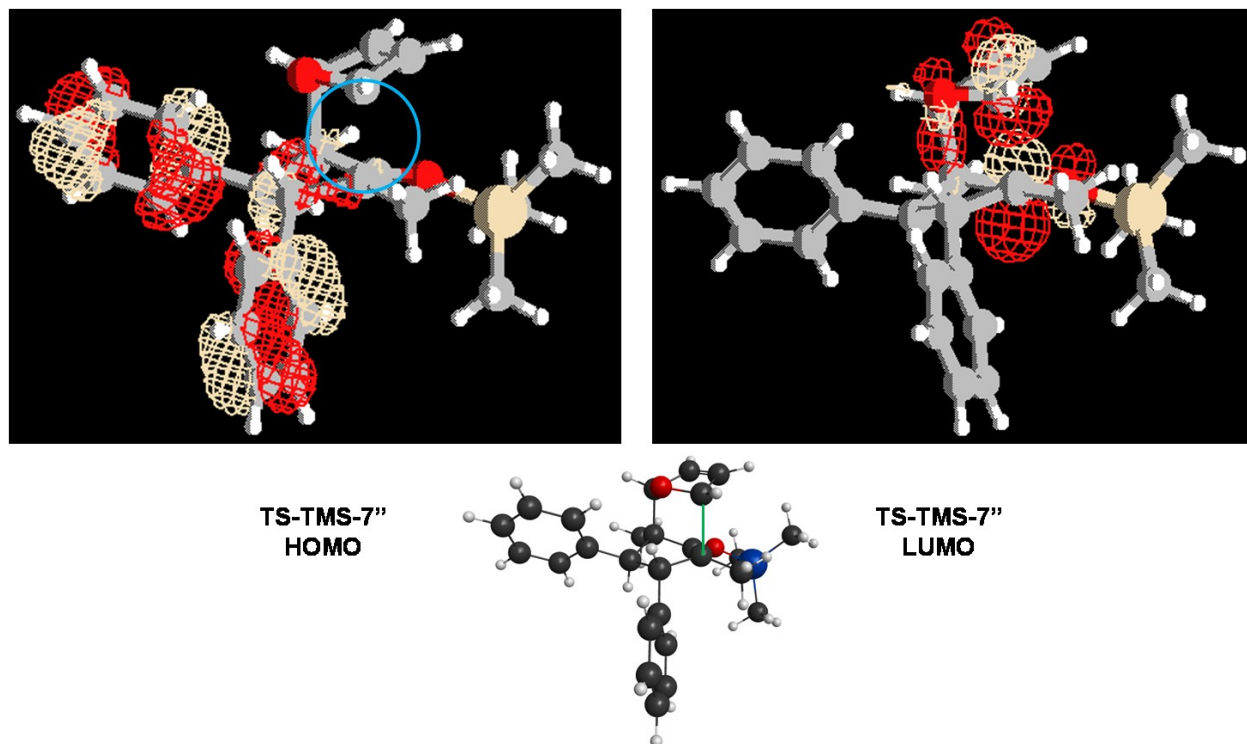


Figure 45. The frontier molecular orbitals of **TS-TMS-7''**. The blue circle highlights the lack of electron density between the carbons undergoing bond formation.

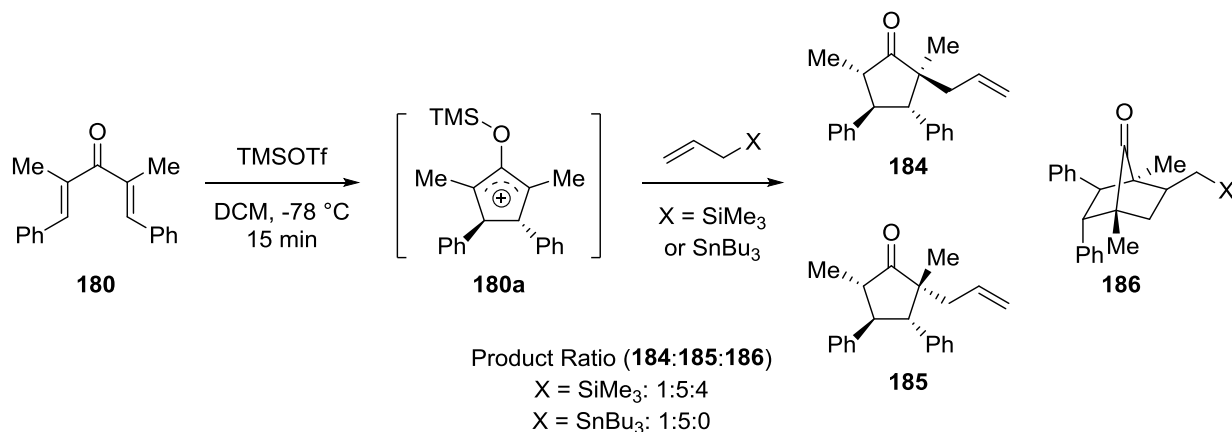
Section 5.4: Summary and Future Plans

Unexpected outcomes in the case of the interrupted Nazarov reaction of divinyl ketone **180** with furan (Section 5.2, Scheme 56) were investigated using DFT computations. An explanation was found for the unusual diastereoselectivity of the reaction of TMS-activated oxyallyl cation **180a** with furan to give Friedel-Crafts product **181**. The lowest activation barriers were observed for when furan approached the Nazarov oxyallyl cation in a compact fashion *syn* to the adjacent phenyl group. More significantly, we showed that both torsional steering and CH- π interactions likely play crucial roles in directing furan *syn* to the adjacent phenyl substituent.

Computational data support the divergence in reactivity of oxyallyl cations based on the identity of the Lewis acid activator; the formation of the second bond to furnish cycloadduct **182** is kinetically favoured in the BF_3 -mediated reaction but disfavoured in the TMS-mediated

reaction. This also provides insight as to why [4+3] adduct **182** was stereoselectively converted to Friedel-Crafts product **181** and 2,5-disubstituted furan **183** upon treatment with TMSOTf.

The success of this computational study in explaining unusual experimental findings and providing valuable insight into the reactivity of synthetically-relevant systems is heartening. In terms of the interrupted Nazarov reaction, there are many more interesting experimental results that would benefit from computational study; for instance, it would be interesting to investigate the mechanism of the allylation of the oxyallylcation intermediate, also performed by Dr. Yen-Ku Wu (Scheme 58).¹⁰⁸ In particular, it would be interesting to see if some of the same factors (such as torsional steering and CH- π interactions) are responsible for the diastereoselectivity, as well as to investigate how the allylating agent used results in the different product ratios seen.



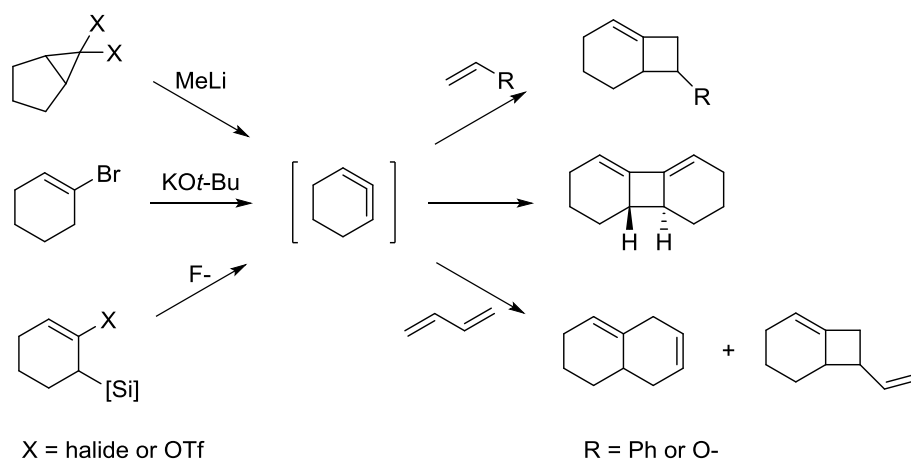
Scheme 58. The Nazarov cyclization of divinyl ketone **180** followed by trapping of the oxyallylcation with allyl silanes and allyl stannanes.

The computational study of other unanticipated experimental outcomes observed in the West group is currently underway. For example, Chapter 6 describes a study on cycloallene chemistry. We believe other projects involving the West group's diazoazide and Stevens rearrangement chemistry would also gain advantage from computational investigation.

Chapter 6: Computational Mechanistic Studies of Cycloadditions between 1,2-Cyclohexadiene and Various Dipolar Compounds

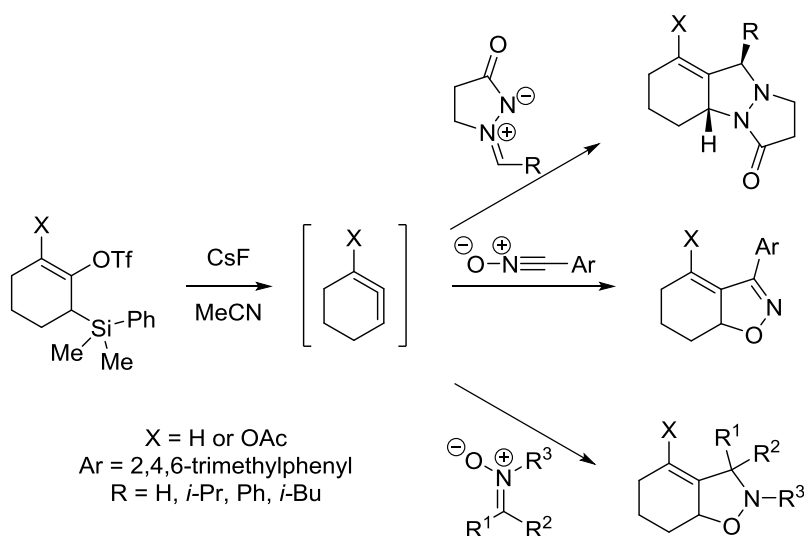
Section 6.1: Introduction

Cyclic allenes are reactive intermediates that exhibit the potential to be useful synthetic building blocks; however, much of the literature concerning cyclic allenes, especially 1,2-cyclohexadienes, is limited to their preparation, existence, and reactivity with simple traps (Scheme 59). There remains a scarcity of strategies tapping into their synthetic utility.¹²⁰



Scheme 59. Examples of the preparation and reactivity of 1,2-cyclohexadiene.

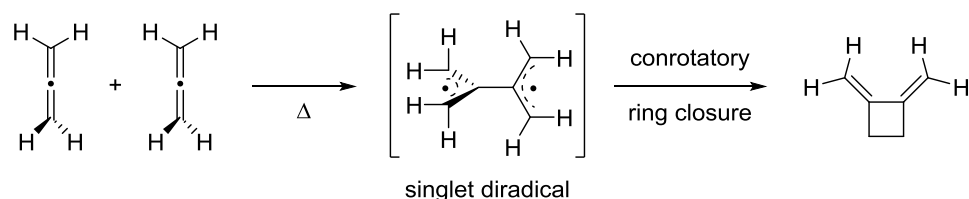
Using the desilylative method of cycloallene generation, Verner Lofstrand has been exploring the reactivity of 1,2-cyclohexadiene and 1-acetoxy-1,2-cyclohexadiene with various 1,3-dipoles to form interesting polycyclic scaffolds (Scheme 60).¹²¹ We wished to study these reactions computationally to understand their selectivity and mechanistic details.



Scheme 60. Examples of cycloadditions between 1,2-cyclohexadienes and 1,3-dipoles.

Section 6.2: Computational Study of 1,2-Cyclohexadiene Dimerization

The dimerization of acyclic allenes was recently studied computationally by Johnson and coworkers (Scheme 61).¹²² It was determined that allene dimerizes via a singlet diradical mechanism in the gas phase.

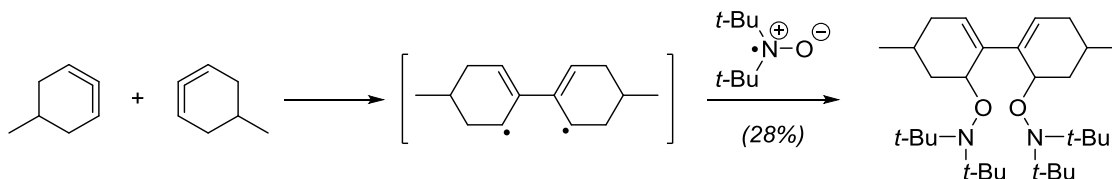


Scheme 61. The dimerization of allene as reported by Johnson.

1,2-Cyclohexadiene is assumed to go through a similar mechanism to form the corresponding [2+2] cycloadduct, though no computational studies have been reported (Scheme 62).^{120f} An experimental mechanistic study performed in 1977 by Bottini and coworkers seems to support the idea of a stepwise, diradical mechanism based on the observed trapping of the intermediate diradical with di-*tert*-butylnitroxide (Scheme 60).¹²³



Scheme 62. The dimerization of 1,2-cyclohexadiene.



Scheme 63. Trapping of the diradical intermediate in the dimerization of 1,2-cyclohexadienes.

To date, there have been no other experimental or computational reports regarding the mechanism of 1,2-cyclohexadiene dimerization; thus, we opted to perform a computational mechanistic study of this reaction, both in the gas phase (as reported before for allene) and in solution, as the inclusion of solvent effects may prove more experimentally relevant.

Section 6.2.1: Computational Details

DFT calculations were carried out using the B3LYP⁸² functional with the 6-31+G(d) basis set in the Gaussian 09⁸⁵ suite of programs. UB3LYP and the keyword “guess=mix” were used for diradical structures. Frequency calculations were carried out to ensure that the intermediates had no negative frequencies and the transition states only had one imaginary frequency, as well as to calculate contributions to the Gibbs free energy (reported at 298.15 K and 1 atm). Intrinsic reaction coordinate (IRC)⁹⁰ calculations were carried out on the transition states to ensure that they connected the two associated intermediates. In some cases, IRC calculations failed due to the small imaginary frequency obtained (typically, this happened for

singlet diradical transition states); in this case, the imaginary frequency was visualized, structures at maximum displacement from the transition state saved, and these structures subjected to geometry optimization. Solvent was taken into account using the polarizable continuum model (PCM).⁹¹ Structures were optimized at the B3LYP/6-31+G(d) level in the gas phase or in acetonitrile, as noted. ΔG s were calculated at the B3LYP/6-31+G(d) level.

Section 6.2.2: Computational Results

Three initial cycloallene dimerization transition states were calculated in the gas phase – singlet diradical, triplet diradical, and dipolar (Figure 46). Surprisingly, contrary to allene dimerization, formation of a singlet cycloallene diradical intermediate had the highest energy transition state. Similarly, the triplet diradical mechanism was considered highly unfavourable due to the energetic cost of forming a triplet diradical cycloallene to initiate this reaction pathway. These results suggest that cycloallene dimerization proceeds via a dipolar mechanism, forming an intermediate that contains an allyl anion and an allyl cation.

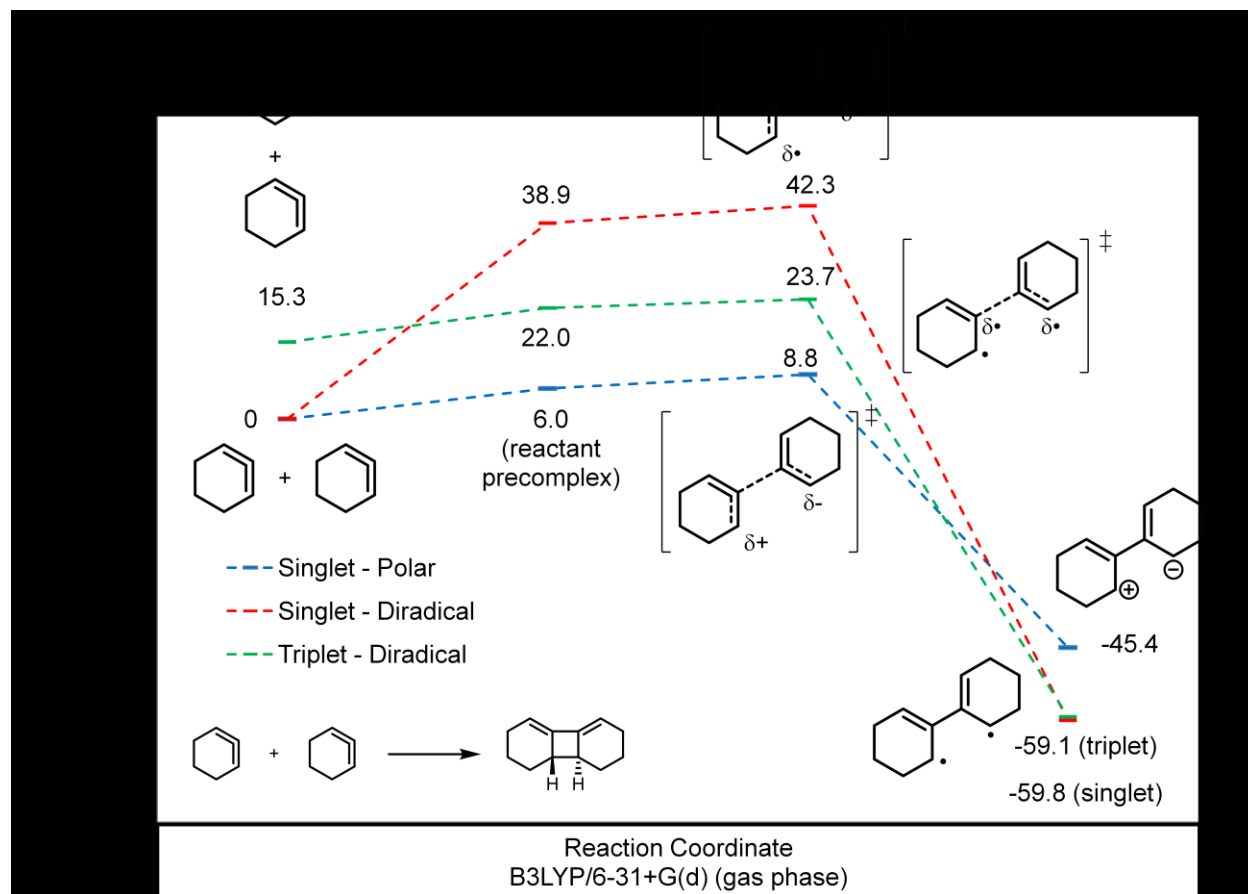


Figure 46. Gas phase mechanisms of 1,2-cyclohexadiene dimerization.

When solvent effects were taken into account using PCM to model the reaction in acetonitrile, the singlet diradical transition state could no longer be found; based on the gas phase results, it is likely much higher in energy than either the dipolar or triplet diradical transition states. Comparing the dipolar and triplet diradical mechanisms (Figure 32), a similar conclusion could be drawn as from the gas phase results – the dipolar transition state is much lower in energy than the triplet starting material, so it is likely that the dimerization mechanism is also dipolar in acetonitrile. Although quite preliminary, these results are interesting, as they raise questions regarding the assumption that cycloallenes react preferentially via radical mechanisms.

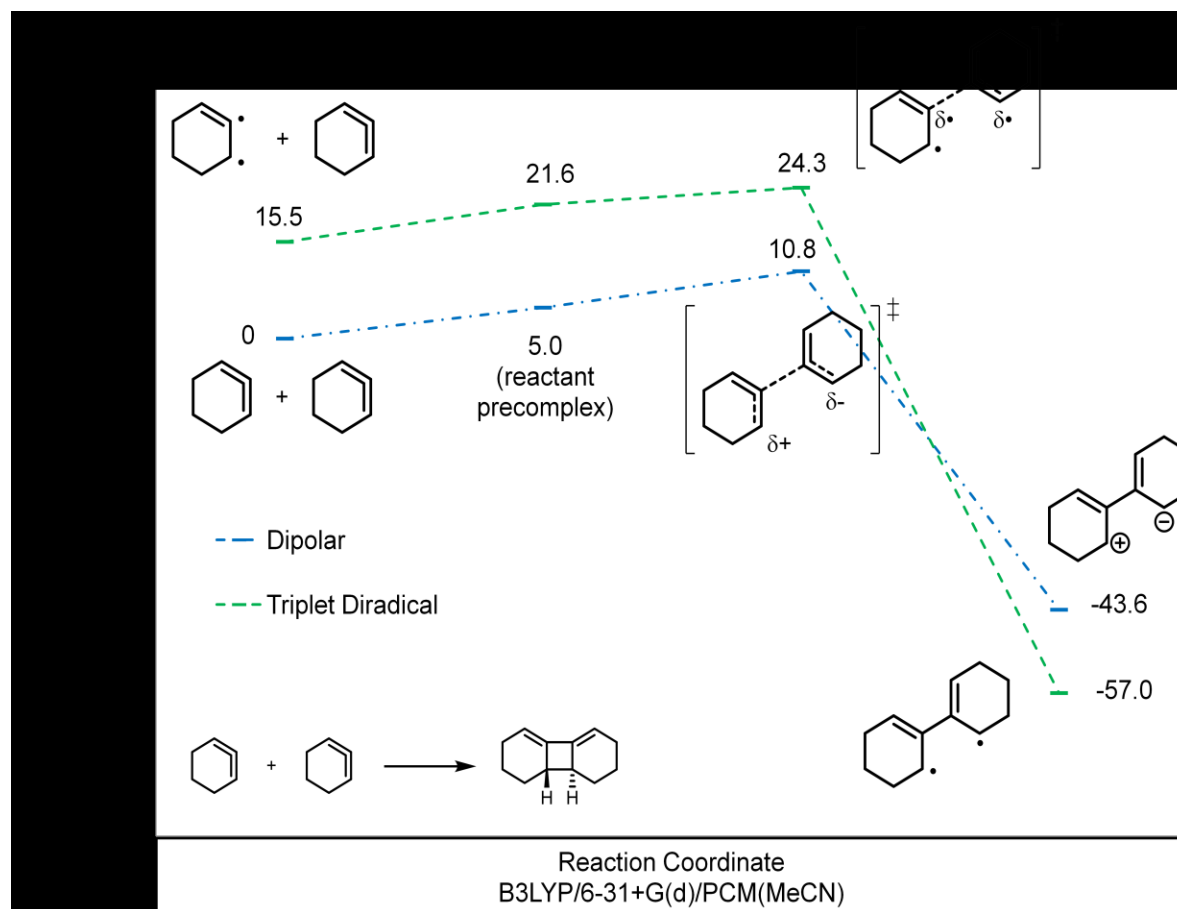
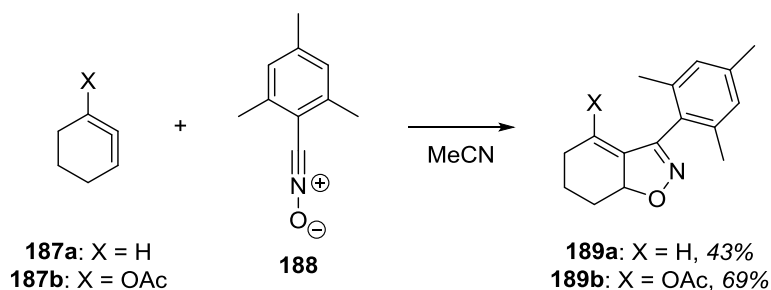


Figure 47. Dimerization mechanisms of 1,2-cyclohexadiene in acetonitrile.

Section 6.3: Reactions of Cycloallenes with Nitrile Oxides

Experimentally, acetoxy-substituted 1,2-cyclohexadiene **187b** reacts faster than unsubstituted 1,2-cyclohexadiene **187a** with nitrile oxide **188** (Scheme 64).¹²¹ DFT calculations were performed to discern whether the cycloaddition reaction proceeds through a concerted or stepwise mechanism, as well as to obtain some insight into the difference in reaction rate between the two cycloallenes.



Scheme 64. Reaction of 1,2-cyclohexadienes with nitrile oxide **188**.

Section 6.3.1: Computational Details

DFT calculations were carried out using the B3LYP⁸² and M06-2x⁸³ functionals with the 6-31+G(d) and 6-311+G(d,p) basis sets in the Gaussian 09⁸⁵ suite of programs. UB3LYP or UM06-2x and the keyword “guess=mix” were used for diradical structures. Frequency calculations were carried out to ensure that the intermediates had no negative frequencies and the transition states only had one imaginary frequency, as well as to calculate contributions to the Gibbs free energy (reported at 298.15 K and 1 atm). Intrinsic reaction coordinate (IRC)⁹⁰ calculations were carried out on the transition states to ensure that they connected the two associated intermediates. In some cases, IRC calculations failed due to the small imaginary frequency obtained (typically, this happened for singlet diradical transition states); in this case, the imaginary frequency was visualized, structures at maximum displacement from the transition state saved, and these structures subjected to geometry optimization. Solvent was taken into account using the polarizable continuum model (PCM).⁹¹ Structures were optimized at the B3LYP/6-31+G(d) level in acetonitrile. Single-point energies were calculated at the M06-2x/6-311+G(d,p) level in acetonitrile. Notably, M06-2x was utilized due to its inclusion of dispersion effects, which B3LYP lacks. ΔG s were calculated using the results from single-point energy

calculations along with contributions to the Gibbs free energy calculated at the B3LYP/6-31+G(d)/PCM level.

Section 6.3.2: Computational Results

An asynchronous, concerted cycloaddition mechanism and a triplet diradical stepwise mechanism were found for both cycloallenes (Figure 48 and Figure 49). Comparing the two mechanisms, it is apparent that triplet 1,2-cyclohexadienes are too high in energy to compete with a concerted reaction pathway. Additionally, the activation barrier for cycloallene **187b** is lower than that for **187a**, supporting the experimentally observed higher reaction rate of **187b**.

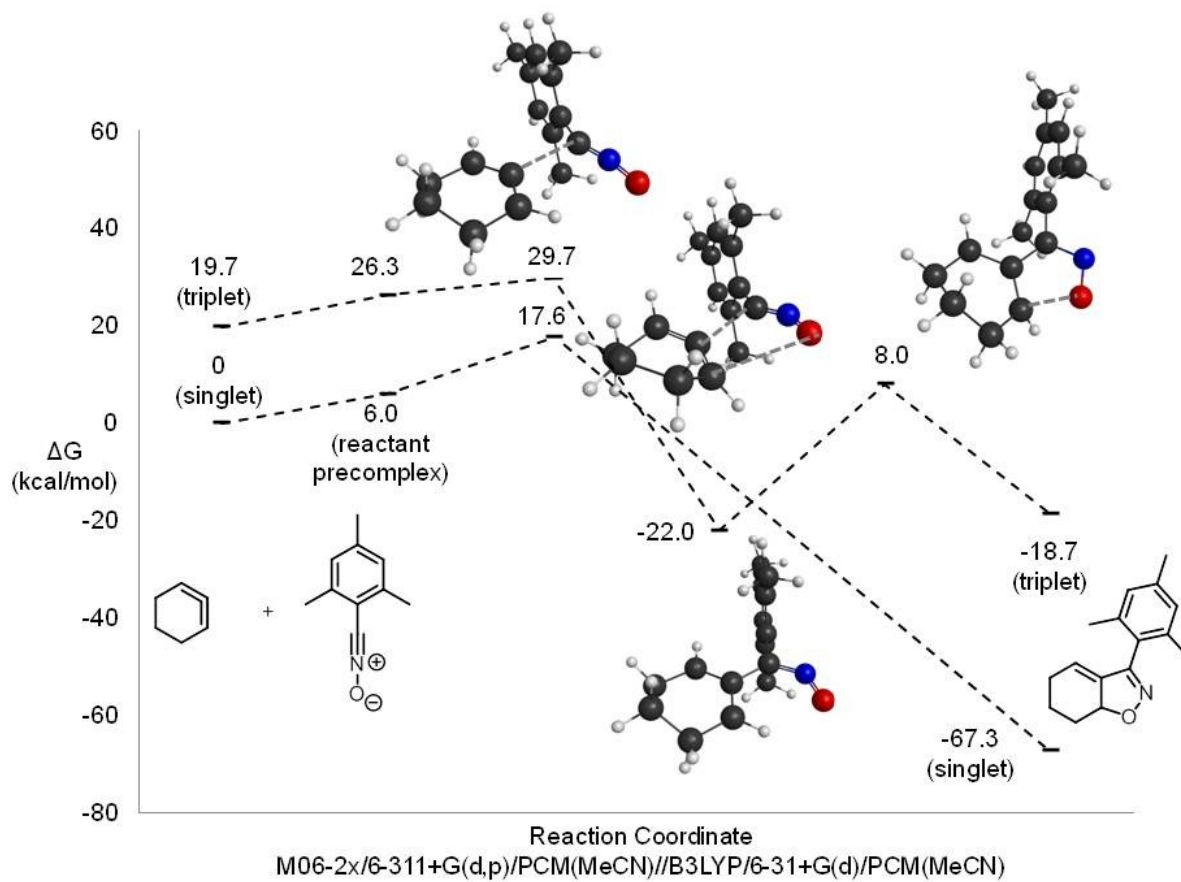


Figure 48. Calculated mechanisms of cycloaddition between 1,2-cyclohexadiene **187a** and nitrile oxide **188**.

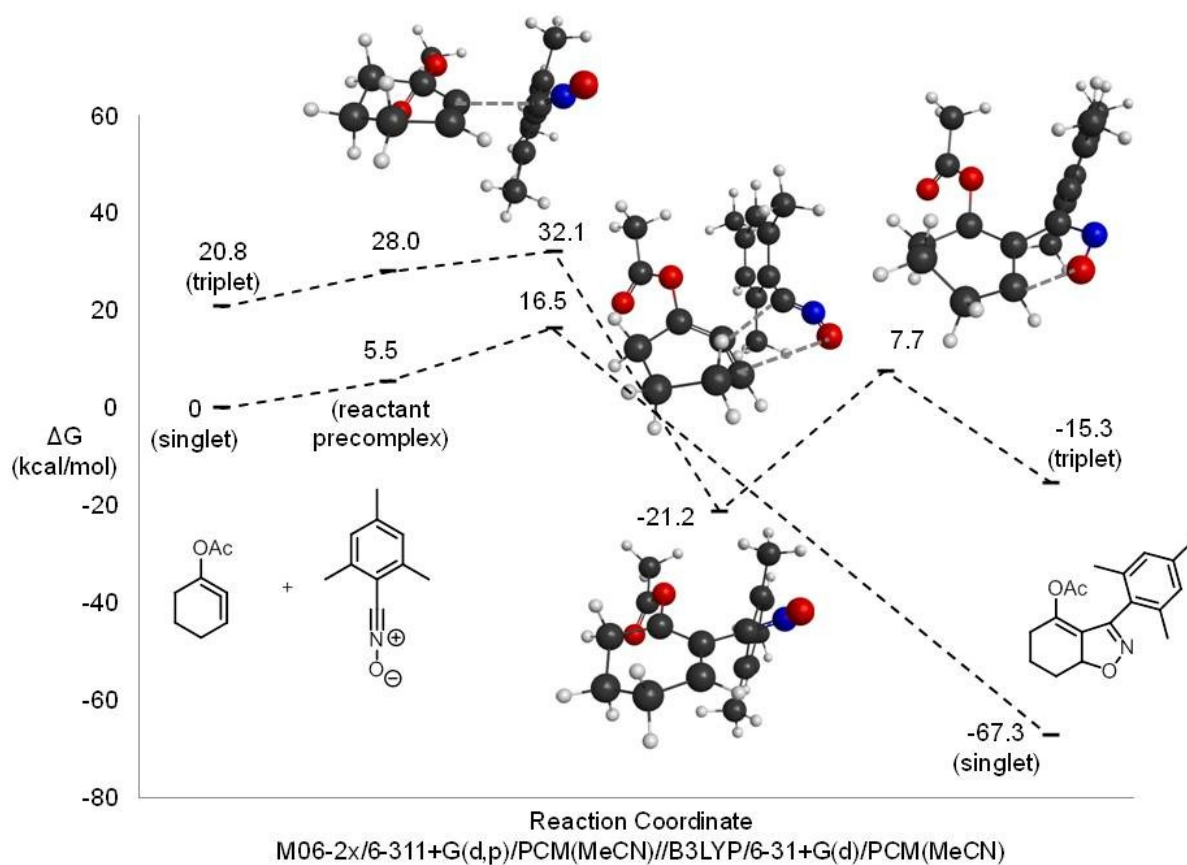


Figure 49. Calculated mechanisms of cycloaddition between 1,2-cyclohexadiene **187b** and nitrile oxide **188**.

Similarly to earlier computational observations (Section 6.2), a singlet diradical transition state for the cycloaddition of 1,2-cyclohexadiene **187a** could only be found in the gas phase with a very high activation barrier at the B3LYP/6-31+G(d) level (Figure 50); thus, a singlet diradical mechanism is unlikely to compete with the very favourable concerted cycloaddition mechanism.

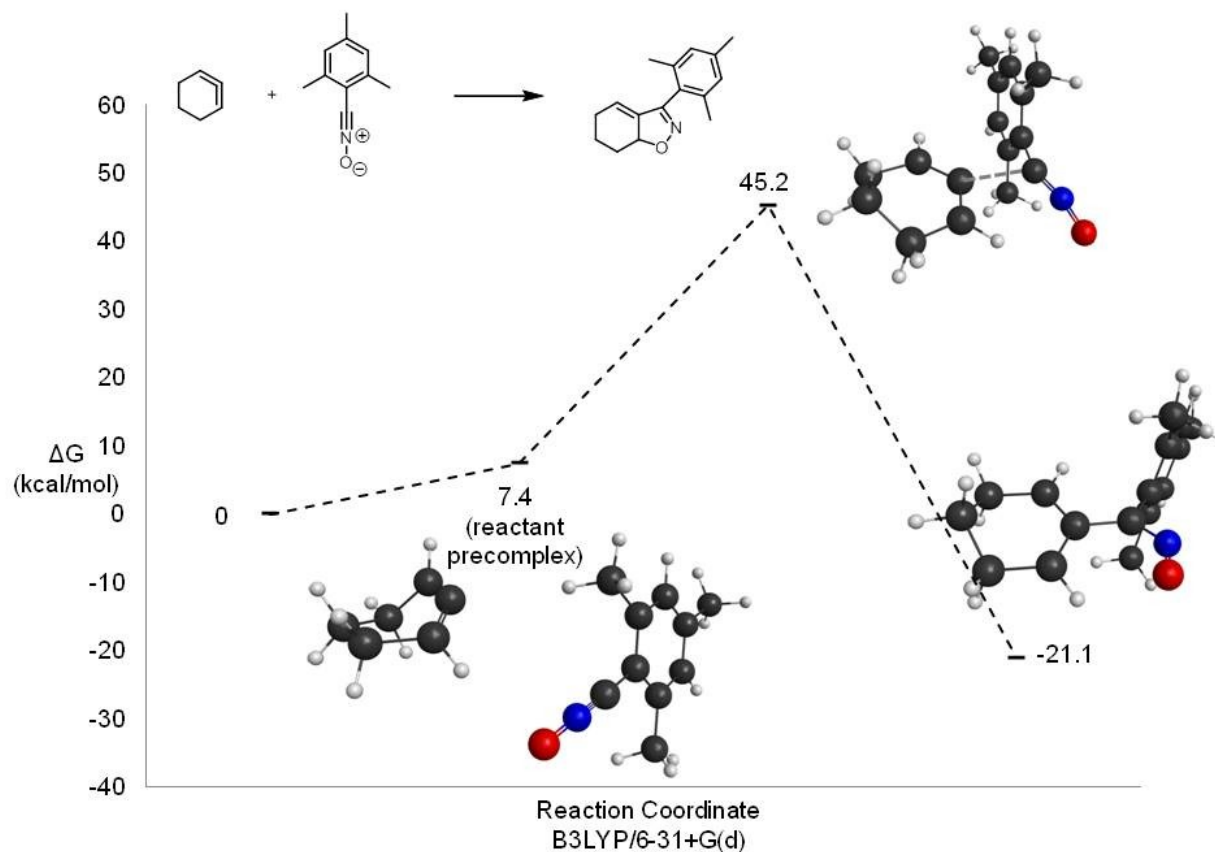
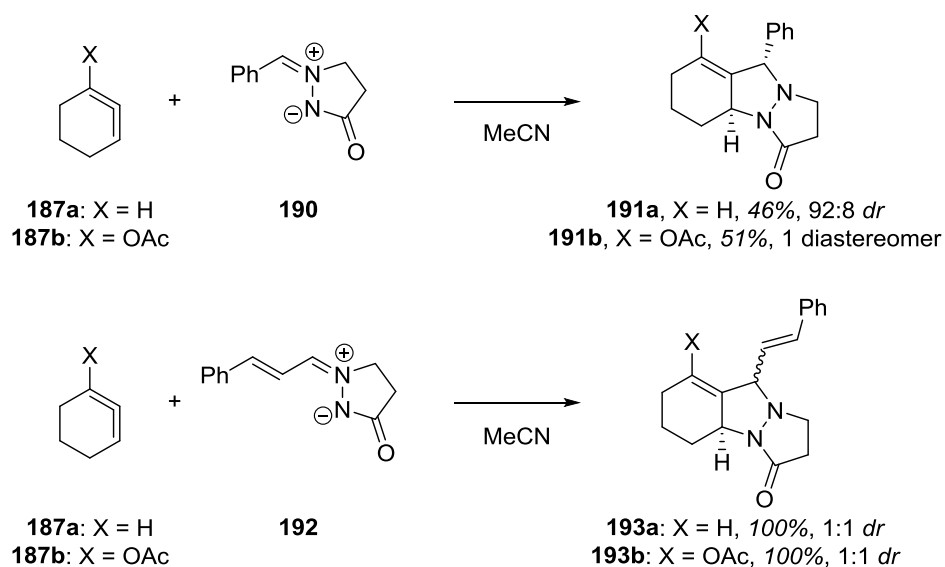


Figure 50. Singlet diradical mechanism for cycloaddition in the gas phase.

Section 6.4: Reactions of Cycloallenes with Azomethine Imines

Cycloadditions between cycloallenes **187a** and **187b** and azomethine imines **190** and **192** were also studied (Scheme 65).^{121,124} It was observed that, with simple phenyl substitution on the azomethine imine, both cycloallenes gave cycloadducts **191** in good diastereoselectivity; however, with styryl substitution on the azomethine imine, cycloadducts **193** were formed in a 1:1 diastereomeric mixture. DFT calculations were performed to discern whether the cycloaddition proceeds in a concerted or stepwise fashion, as well as to understand the difference in selectivity between the cycloadditions with azomethine imines **190** and **192**.



Scheme 65. Cycloadditions between 1,2-cyclohexadienes and azomethine imines.

Section 6.4.1: Computational Details

DFT calculations were carried out using the B3LYP⁸² functional with the 6-31+G(d) basis set in the Gaussian 09⁸⁵ suite of programs. UB3LYP and the keyword “guess=mix” were used for diradical structures. Grimme’s dispersion correction GD3¹²⁵ was added onto the B3LYP calculations, as some transition states did not converge with B3LYP alone. Frequency calculations were carried out to ensure that the intermediates had no negative frequencies and the transition states only had one imaginary frequency, as well as to calculate contributions to the Gibbs free energy (reported at 298.15 K and 1 atm). Intrinsic reaction coordinate (IRC)⁹⁰ calculations were carried out on the transition states to ensure that they connected the two associated intermediates. In some cases, IRC calculations failed due to the small imaginary frequency obtained (typically, this happened for singlet diradical transition states); in this case, the imaginary frequency was visualized, structures at maximum displacement from the transition state saved, and these structures subjected to geometry optimization. Solvent was taken into

account using the polarizable continuum model (PCM).⁹¹ Structures were optimized at the B3LYP-D3/6-31+G(d) level in acetonitrile. Single-point energies were calculated at the MP2/6-311+G(d,p) level in acetonitrile (UMP2 for diradical structures).⁸⁶ ΔG s were calculated using the results from single-point energy calculations along with contributions to the Gibbs free energy calculated at the B3LYP-D3/6-31+G(d)/PCM level. Product ratios were obtained via comparison of the differences in transition state energies of all transition states using the equation $P1/P2 = e^{-\Delta G_{\ddagger}/RT}$ where R is the gas constant = 8.3145 J/(mol*K) and T is the temperature = 298.15 K.

Section 6.4.2: Computational Results

The difference in selectivity between cyclohexadiene **187a** and **187b** in the cycloaddition with phenyl-substituted azomethine imine **190** was reproduced well using MP2 to calculate single point energies (Figure 51 and Figure 52). Once again, it was observed that the triplet starting materials were too high in energy to compete with the concerted mechanism. Though we have thus far been unable to locate singlet diradical transition states in this reaction, we cannot rule out a competitive singlet diradical mechanism.

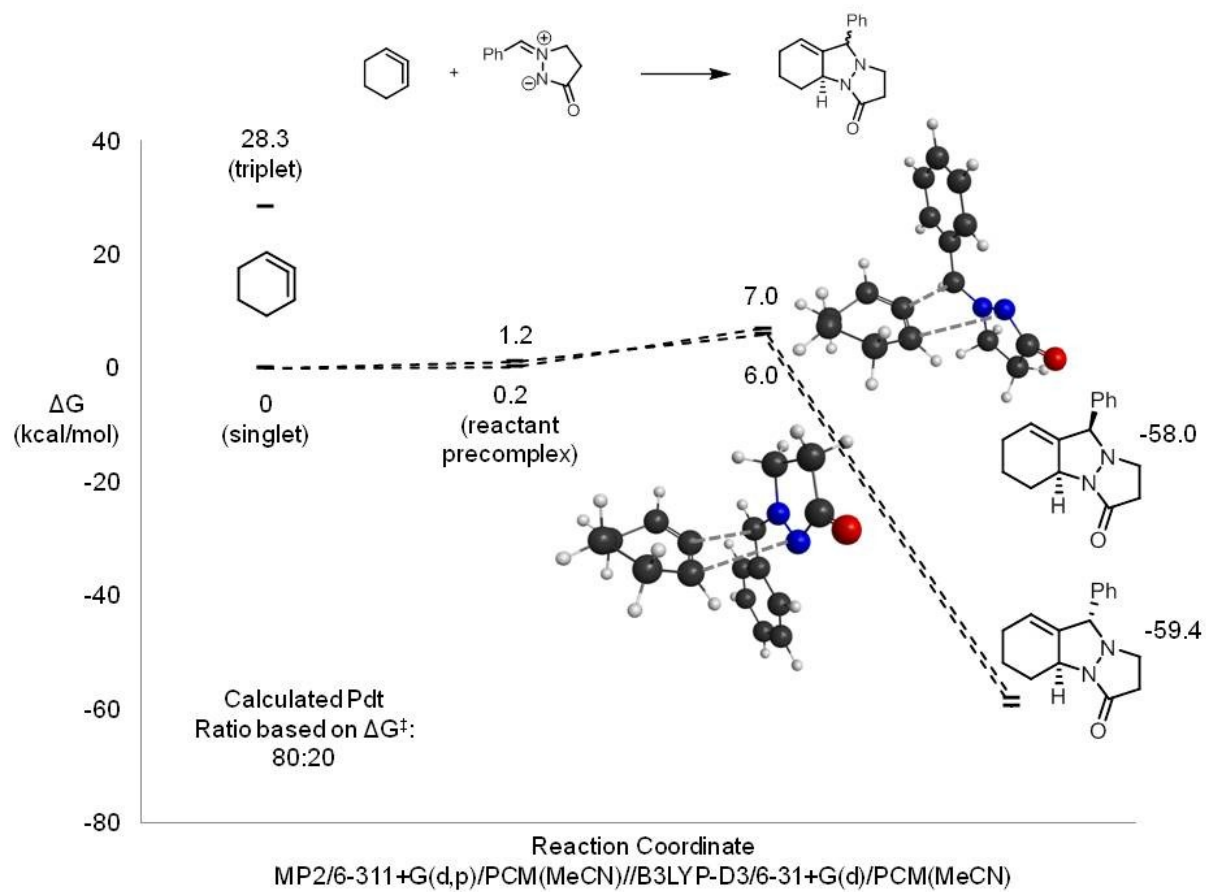


Figure 51. The mechanism of cycloaddition of 1,2-cyclohexadiene **187a** and azomethine imine **190**.

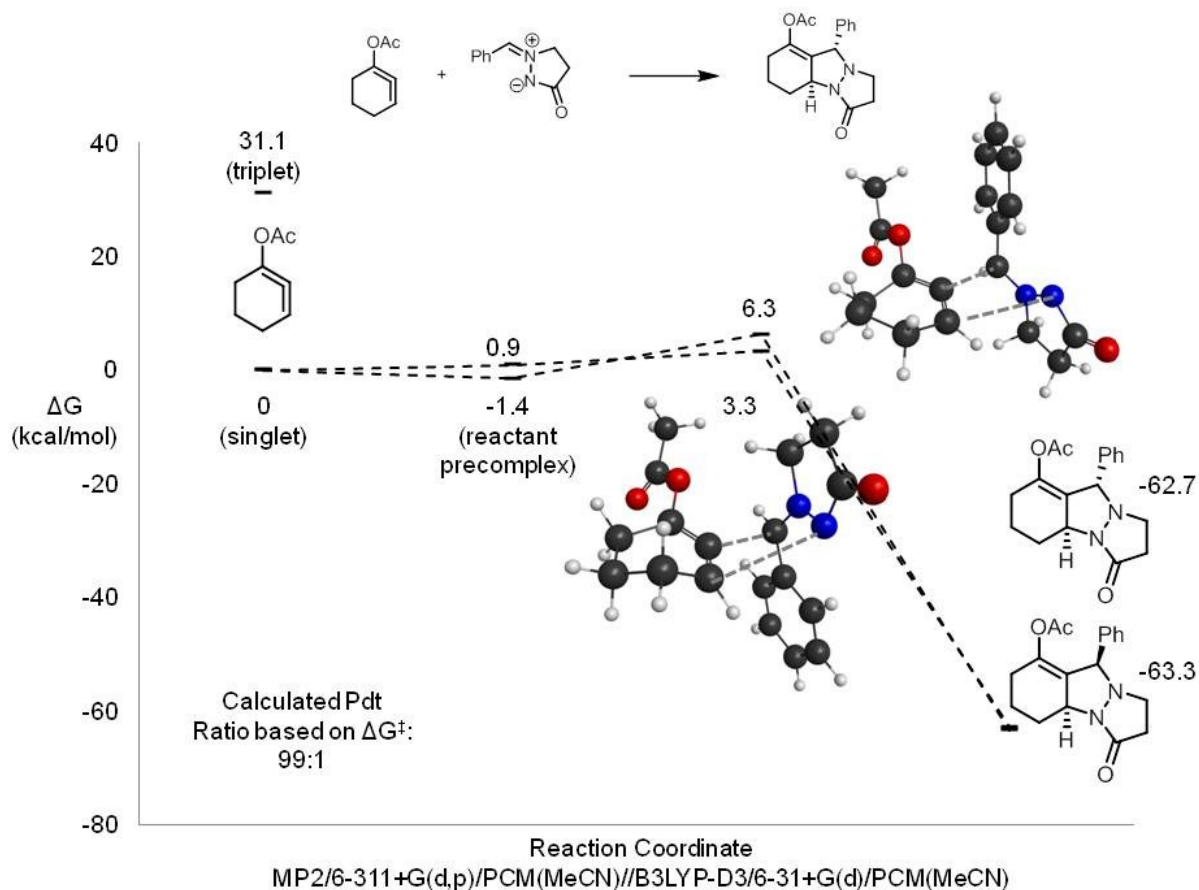


Figure 52. The mechanism of cycloaddition of 1,2-cyclohexadiene **187b** and azomethine imine **190**.

The computational results using MP2 failed to describe the reaction between 1,2-cyclohexadiene **187a** and styryl-substituted azomethine imine **192**, with a predicted *dr* of 94:6 versus an experimental *dr* of 1:1 (Figure 53). In this case, it is very likely that a competing singlet diradical pathway is responsible for the lack of diastereoselectivity. Some preliminary results at the B3LYP/6-31+G(d)/PCM(MeCN) level support this idea (Table 19); two singlet diradical transition states were located, both of which are slightly lower in energy than the concerted transition states. However, more stationary points in the singlet diradical mechanism and higher level calculations need to be performed in order to come to a definite conclusion

regarding this mechanism. Another notable observation regarding the singlet diradical mechanism is the similarity in the concerted and singlet diradical transition structures (Figure 54); this underscores the challenge inherent in finding singlet diradical transition states.

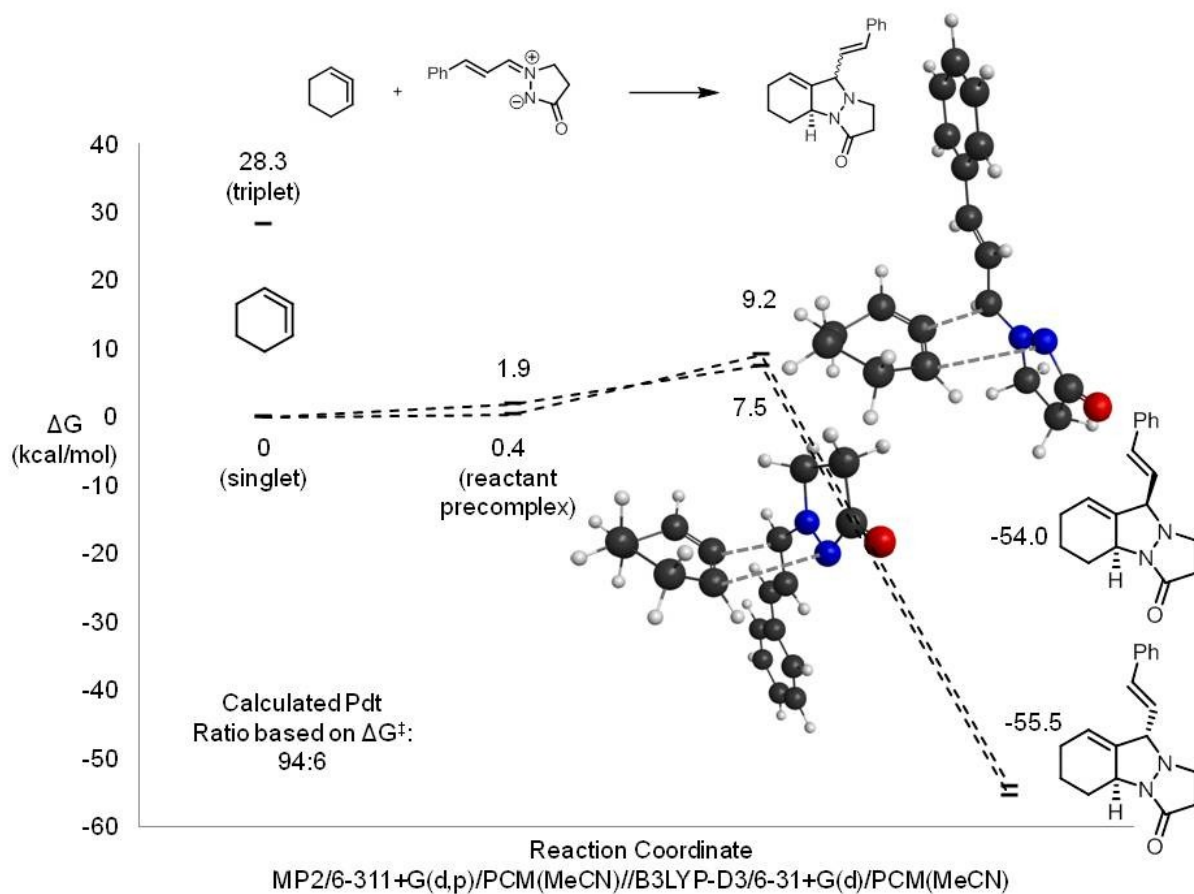


Figure 53. The mechanism of cycloaddition of cycloallene **187a** and azomethine imine **192**.

Table 19. Relative ΔG s (kcal/mol) of singlet intermediates and transition states in the cycloaddition of cycloallene **187a** and azomethine imine **192** at the B3LYP/6-31+G(d)/PCM(MeCN) level. “Path 1” refers to the reaction pathway that forms (an intermediate on the way to) the “*endo*” product (where the hydrogens on the two stereocentres are *cis* to one another), and “Path 2” refers to the eventual formation of the “*exo*” product.

Structure	Concerted Pathway		Diradical Pathway	
	Path 1	Path 2	Path 1	Path 2
Separate Reactants	0.0	0.0	0.0	0.0
Reactant Pre-complex	6.5	6.3	6.4	6.1
Transition State	20.7	20.7	20.2	20.6
Diradical Intermediate			4.0	-8.6
Cycloadduct	-36.1	-34.8		

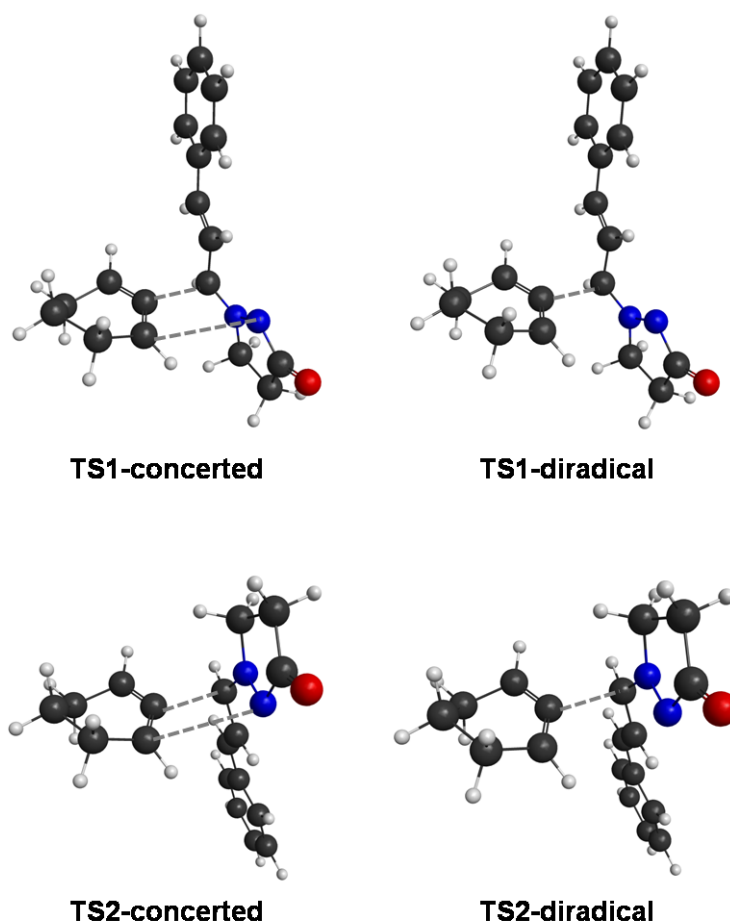
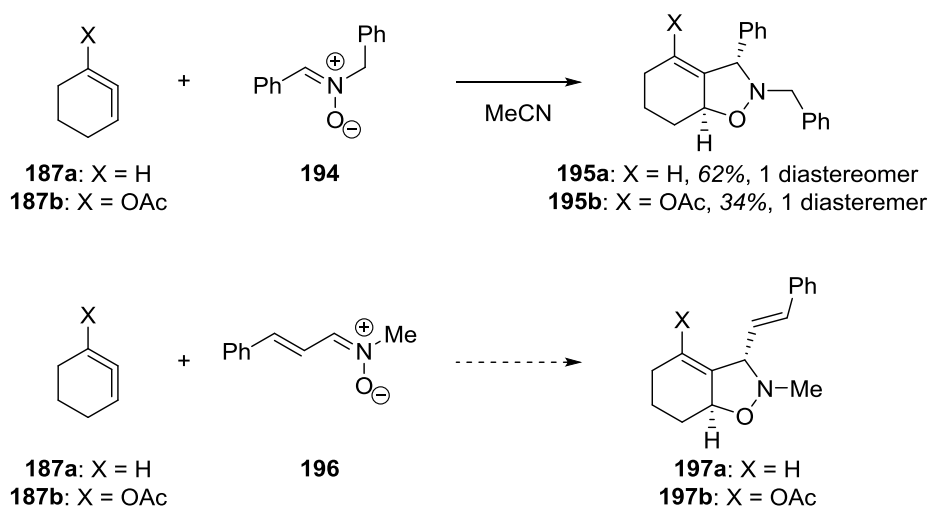


Figure 54. Diastereomeric concerted and singlet diradical transition structures in the reaction of cycloallene **187a** with azomethine imine **192** at the B3LYP/6-31+G(d)/PCM(MeCN) level. “TS1” refers to the transition state in the reaction pathway that forms (an intermediate on the way to) the “*endo*” product (where the hydrogens on the two stereocentres are *cis* to one another), and “TS2” refers to the eventual formation of the “*exo*” product.

Section 6.5: Reactions of Cycloallenes with Nitrones

The cycloaddition between 1,2-cyclohexadienes **187a** and **187b** and phenyl-substituted nitronone **194** was investigated experimentally and found to give excellent diastereoselectivity.¹²¹ We were interested to see whether or not the same selectivity trend found for azomethine imines would exist for nitrones. DFT calculations were carried out to determine if the cycloaddition between 1,2-cyclohexadienes **187a** and **187b** and styryl-substituted nitronone **196** (preliminary experimental studies showed very low yields in this reaction, preventing any solid conclusions regarding selectivity from being made) would give similarly low diastereoselectivity as that seen with styryl-substituted azomethine imine **192** (Scheme 66).



Scheme 66. Cycloadditions between 1,2-cyclohexadienes and nitrones.

Section 6.5.1: Computational Details

The computational details for this section are the same as those outlined in Section 6.4.1.

Section 6.5.2: Computational Results

As with the azomethine imines, experimental selectivities in the cycloadditions of cycloallenes **187a** and **187b** with nitrene **194** were reproduced well by the computational results (Figure 55 and Figure 56). Once again, the triplet state of the cycloallene was found to be much too high in energy for a triplet diradical mechanism to compete with the concerted cycloaddition mechanism. However, we cannot rule out competition from a singlet diradical mechanism based on the data we have so far. Note that one of the reactant precomplexes in the concerted cycloaddition of acetoxy-substituted 1,2-cyclohexadiene **187b** and nitrene **194** did not converge; this is likely due to the very small energy difference between the reactants and the transition state, making the potential energy surface fairly flat in this region.

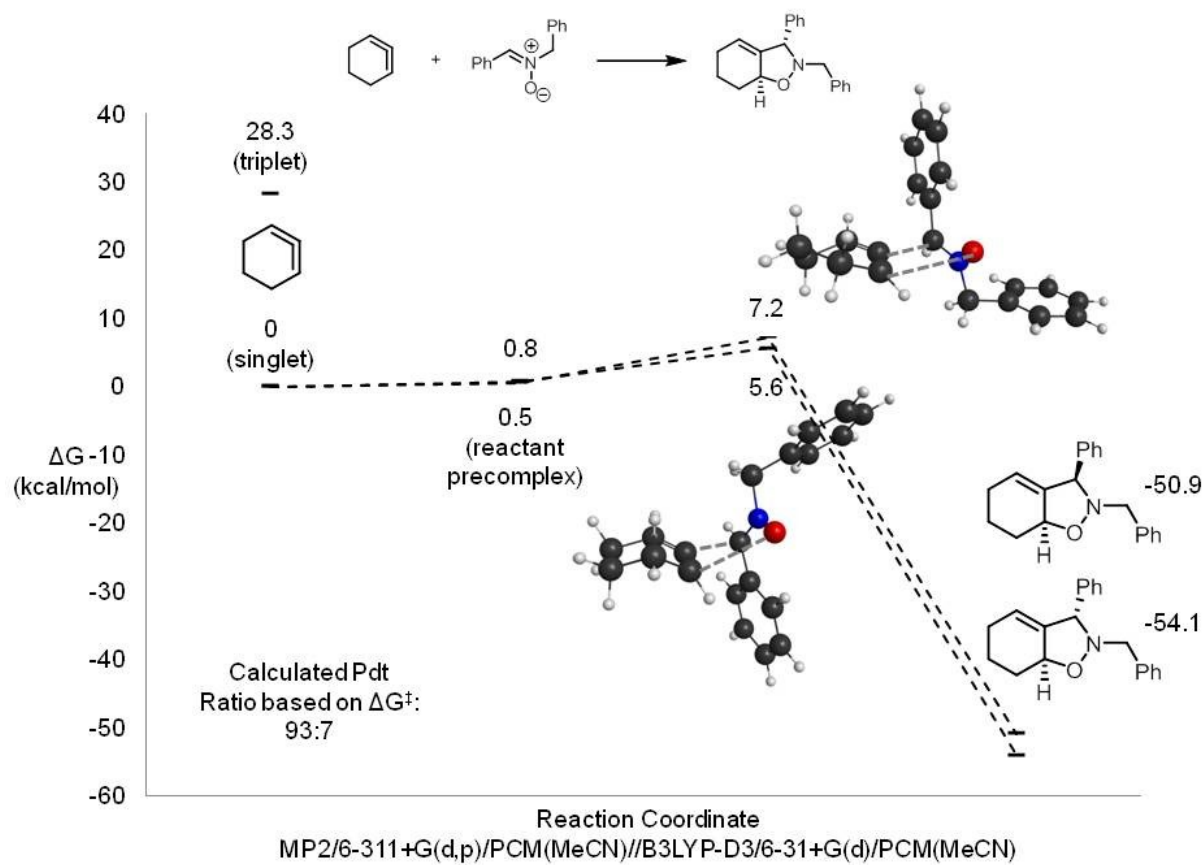


Figure 55. Mechanisms of cycloaddition of cycloallene **187a** with nitron **194**.

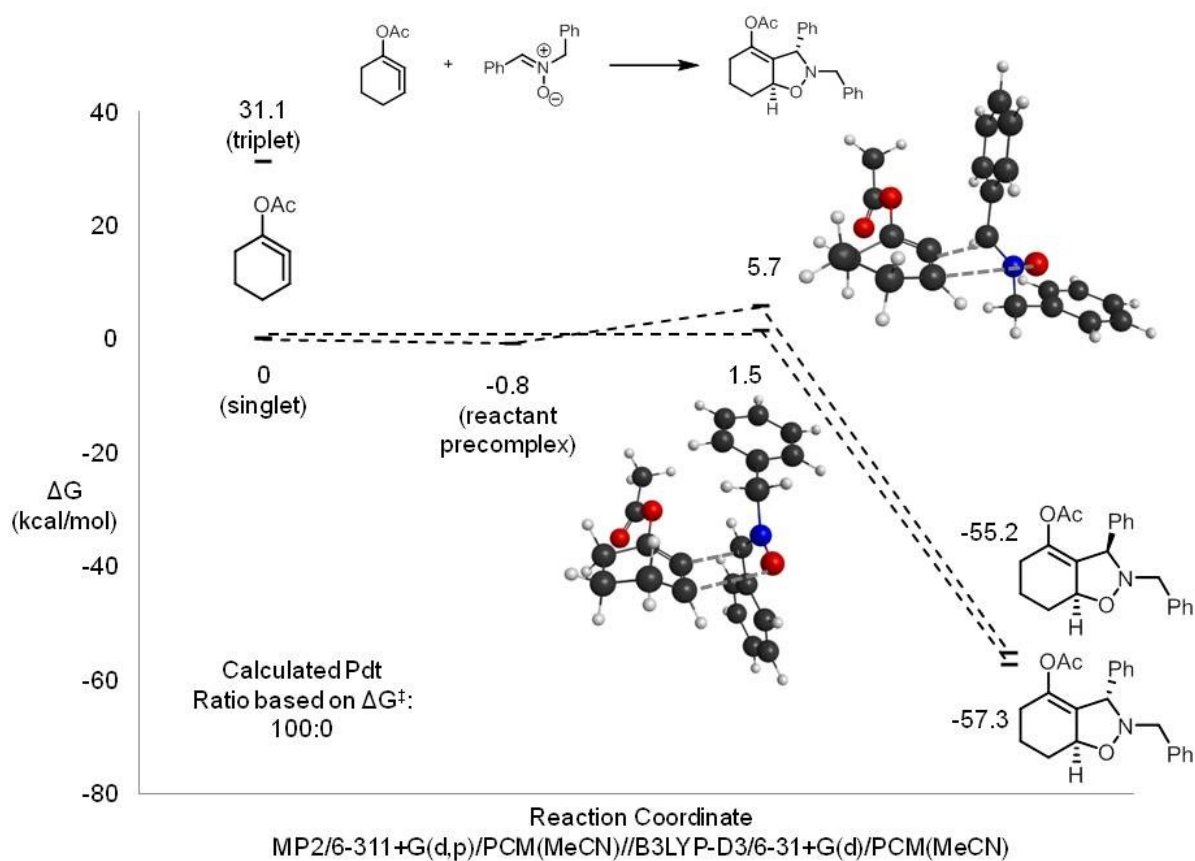


Figure 56. Mechanisms of cycloaddition of cycloallene **187b** with nitron **194**.

The computational results for the cycloaddition of cycloallene **187a** and styryl-substituted nitron **196** are similar to those for styryl-substituted azomethine imine **192** (Figure 57); while the computational results predict high diastereoselectivity for this reaction, it is quite likely that a singlet diradical mechanism will erode the diastereoselectivity based on the experimental and computational results in the azomethine imine case. The search for such a singlet diradical mechanism is ongoing.

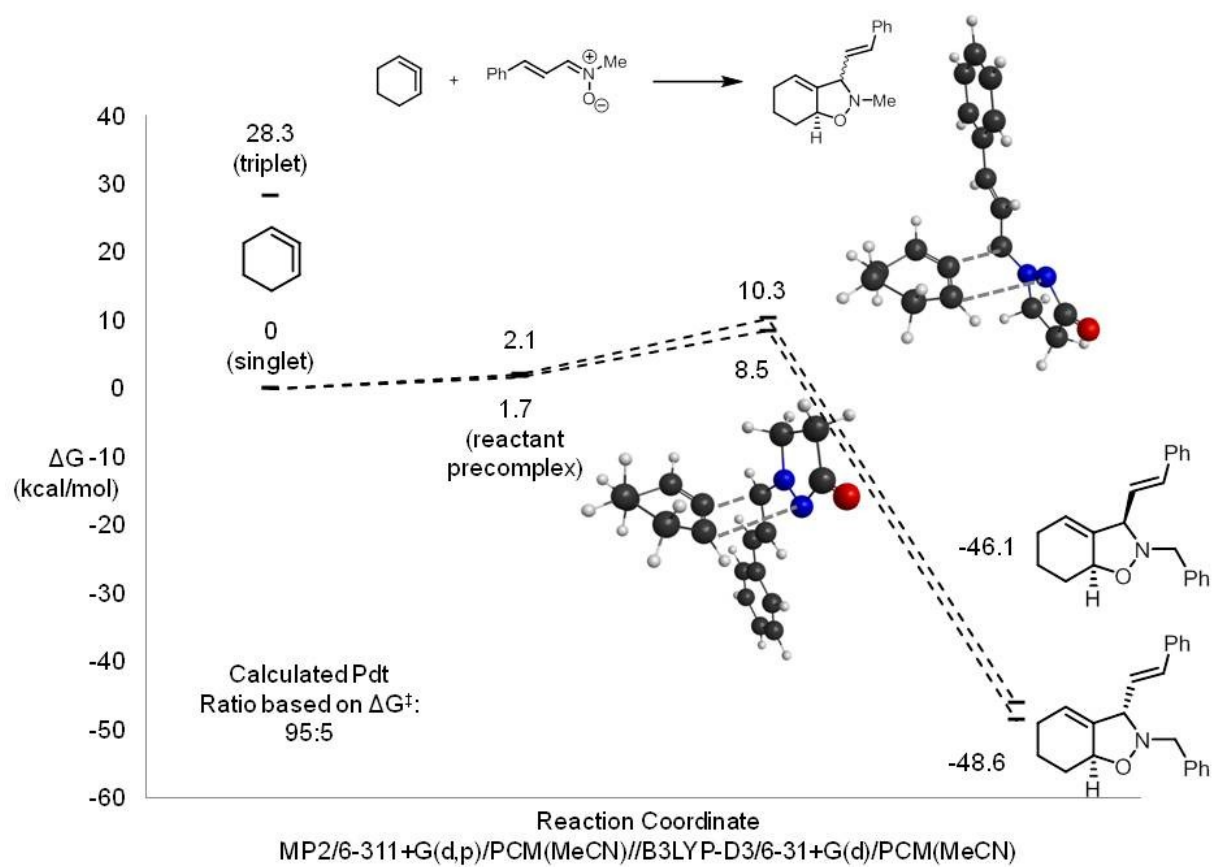
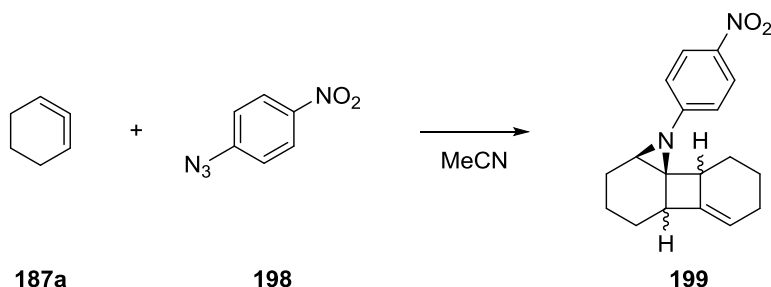


Figure 57. Mechanisms of cycloaddition of cycloallene **187a** with nitronium **196**.

Section 6.6: Identification of an Unusual Cycloallene Cycloaddition Product via Simulated ^1H NMR Chemical Shifts

The reaction of 1,2-cyclohexadiene **187a** with 4-nitrophenylazide **198** gave unexpected cycloaddition product **199** (Scheme 67).¹²¹



Scheme 67. Reaction of 1,2-cyclohexadiene **187a** with azide **198** to form 2:1 adduct **199**.

In order to ascertain the relative configuration of the four stereocentres formed in the reaction, 2D NMR and nOe experiments were carried out; unfortunately, these experiments were unable to discern between the four possible diastereomers (Figure 58). In order to identify which diastereomer was produced in this reaction, computational work was undertaken to provide simulated ^1H NMR chemical shifts with which the experimental chemical shifts could be compared.

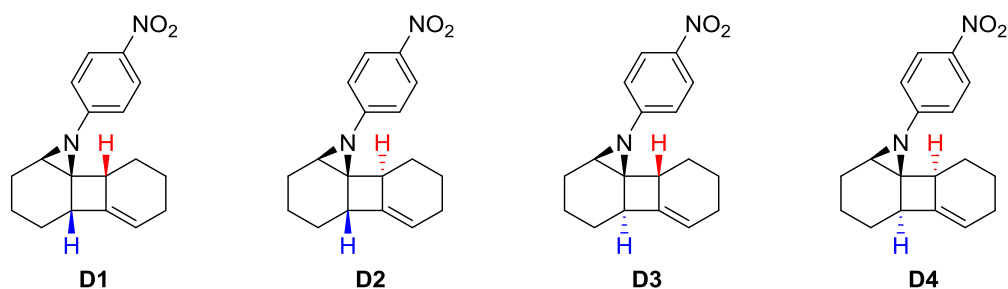


Figure 58. The four possible diastereomers of 2:1 adduct **199**.

Section 6.6.1: Computational Details

Calculations were performed with Gaussian 09.⁸⁵ Computed chemical shifts were determined using the GIAO method⁹⁵ in Gaussian 09 at the mPW1PW91/6-311+G(2d,p)/SMD(CHCl₃)/B3LYP/6-31+G(d,p) level of theory,^{82,84} and are empirically scaled. Empirical scaling was performed using the equation $\delta = - (b - \sigma) / m$, where δ is the computed chemical shift, σ is the computed isotropic shielding constant, m is the slope, and b is the intercept. For the ¹H NMR shifts, the values of $m = -1.0936$ and $b = 31.8018$ were used as recommended by Tantillo et al. on cheshirenmr.info.⁹⁶ SMD refers to inclusion of solvent effects using the SMD implicit solvent model.⁹⁷ For all four diastereomeric structures of **199**, a conformational search using MMFF94¹²⁶ was performed with Marvin Sketch 5.12.0.¹²⁷ For diastereomer **D1**, seven conformers were located, with two predicted to be significant contributors (greater than 1% of the conformer population) based on computed free energies at the B3LYP/6-31+G(d,p) level of theory. For diastereomer **D2**, four conformers were located, with two of them predicted to be significant contributors. For diastereomer **D3**, two conformers were located, with only one predicted to be a significant contributor. For diastereomer **D4**, five conformers were located, with two of them predicted to be significant contributors. The computed shifts for diastereomers **D1**, **D2**, and **D4** reflect a Boltzmann-weighted average.

Section 6.6.2: Computational Results

Resolved peaks in the ¹H NMR spectrum of **199** were assigned to the proton(s) with the closest computed chemical shift for each diastereomer (Figure 59); the corrected mean absolute deviation (CMAD) and the largest absolute deviation were identified (Table 20). Based on the CMAD values, diastereomer **D1** is the correct structure of cycloadduct **199**, though the largest

absolute deviation slightly favours diastereomer **D2**; we believe that the CMAD, which takes into account all deviations, is the better predictor for structure.

Table 20. Comparison of the experimental ^1H NMR chemical shifts for **199** and the computed chemical shifts for diastereomers **D1-D4**.

Nucleus	Exptl	Scaled	Exptl	Scaled	Exptl	Scaled	Exptl	Scaled
	D1	D1	D2	D2	D3	D3	D4	D4
14H	3.45	3.47	3.21	3.09	2.57	3.14	3.21	3.33
15H	3.21	3.37	3.45	3.21	3.45	3.54	3.45	3.38
25H	2.57	2.62	2.57	2.58	3.21	3.15	2.57	2.99
26H	1.81	1.60	1.81	1.76	1.81	1.82	1.81	1.88
27H	2.01	2.04	2.01	1.90	2.01	1.95	2.01	2.04
28H		1.39		1.22		1.45		1.35
29H		1.29	0.91	0.78		1.59	0.91	1.11
30H	1.81	1.85	1.81	1.71	1.81	1.87		1.39
31H		1.21		1.26	1.70	1.77	1.70	1.65
32H		1.16		1.38	0.91	1.25	1.70	1.66
33H	0.91	0.95	1.70	1.53		1.36		1.28
34H	5.47	5.49	5.47	5.60	5.47	5.59	5.47	5.46
35H	2.14	2.14	2.01	2.15	2.14	2.37	2.14	2.15
36H	2.01	2.04	2.14	2.25	2.01	2.12	2.01	2.13
37H	1.70	1.43		1.50		1.34	1.81	1.76
38H	1.70	1.60	1.70	1.59	1.70	1.69		1.41
avg(39H,42H)	8.14	8.09	8.14	8.08	8.14	8.10	8.14	7.99
avg(40H,41H)	7.01	6.86	7.01	6.79	7.01	6.78	7.01	6.76
CMAD		0.08		0.12		0.14		0.11
Largest $\Delta\delta$		0.27		0.24		0.57		0.42

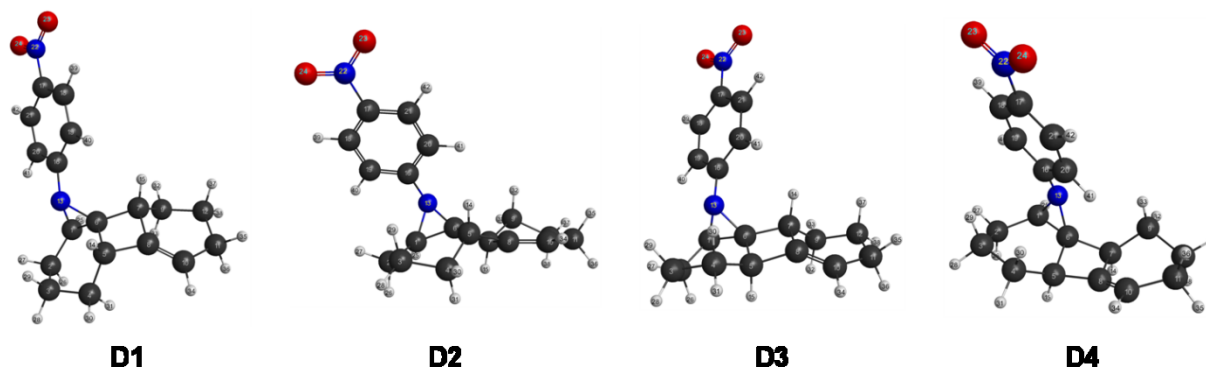


Figure 59. The lowest energy conformer of each diastereomer of **199** at the B3LYP/6-31+G(d,p) level.

Section 6.7: Summary and Future Plans

The interesting reactivity of 1,2-cyclohexadienes in cycloadditions with 1,3-dipoles such as nitrile oxides, azomethine imines, and nitrones has been studied experimentally by Verner Lofstrand. These experiments were subjected to computational analysis in order to understand the mechanism and selectivity of these reactions. Although these computational results are quite preliminary, they have proved to be quite insightful already.

The assumption of preferred diradical mechanisms for the reaction of 1,2-cyclohexadienes in [2+2] cycloadditions has been challenged by our computational results; our findings indicate that the dimerization of 1,2-cyclohexadiene likely occurs via a dipolar mechanism. These results are very preliminary, coming from low level B3LYP/6-31+G(d) calculations; in order to form more solid conclusions, these calculations should be repeated with a more rigorous method, such as CCSD, and with a larger basis set.

Computational work on the nitrile oxide reactions supports a concerted cycloaddition mechanism; both triplet and singlet diradical mechanisms proceed via much higher activation barriers. Additionally, the computational results predict a lower activation barrier for the reaction with 1-acetoxy-1,2-cyclohexadiene **187b**, which explains why this cycloallene is observed to

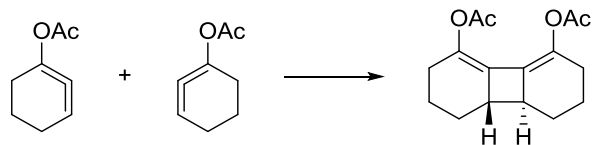
react faster experimentally. The possibility that these reactions occur via stepwise dipolar mechanisms still needs to be investigated.

The selectivity observed experimentally in the cycloadditions with phenyl-substituted azomethine imine **190** are reproduced very well at the MP2/6-311+G(d,p)/PCM(MeCN)//B3LYP-D3/6-31+G(d)/PCM(MeCN) level. However, reactions with the styryl-substituted azomethine imine **192** are predicted to be much more selective than observed experimentally; based on preliminary findings, this is likely due to competitive singlet diradical mechanisms that lower the selectivity of the reactions. Investigation into higher level computational methods that accurately describe both closed shell structures and structures with radical character equally is planned to better predict experimental outcomes.

The computational study of nitronc cycloadditions produced similar findings to those in the azomethine imine reactions; prediction of the selectivity of the cycloadditions between the cycloallenes and phenyl-substituted nitronc **194** was accurate, but we are skeptical of the results with styryl-substituted nitronc **196**. We believe that a singlet diradical mechanism is also competitive with the concerted mechanism, and we are in the process of finding singlet diradical transition states to support this theory.

The computational study of cycloallene reactions is far from complete; in particular, the challenge of finding singlet diradical transition states demands a great deal of time and effort. Thus, the search for singlet diradical stationary points in each of the cycloaddition reactions studied is ongoing. Additionally, we would like to undertake computational work to study the mechanism of the reaction of 1,2-cyclohexadiene with azide **198** to produce unexpected cycloadduct **199** (Scheme 67). It would also be interesting to subject the dimerization of acetoxy-

substituted 1,2-cyclohexadiene **187b** to computational work to see how the structures and energies of the stationary points change.



Scheme 68. Dimerization of 1-acetoxy-1,2-cyclohexadiene.

Despite the fact that this study is a work in progress, we feel that the computational work completed so far is very promising and could lead to a whole new understanding of the reactivity of cycloallenes.

References

-
- ¹ Jacobs, W. A.; Craig, L. C. *J. Biol. Chem.* **1934**, *104*, 547-551.
- ² Haarmann, T.; Rolke, Y.; Giesbert, S.; Tudzynski, P. *Mol. Plant Pathol.* **2009**, *10*, 563-577.
- ³ *The Merck Index*, 14th ed.; Merck and Co. Inc., Whitehouse Station, NJ, 2006; pp 231, 261, 977, 1047, 1057, 1236.
- ⁴ Total syntheses of lysergic acid: (a) Kornfeld, E. C.; Fornefeld, E. J.; Kline, G. B.; Mann, M. J.; Morrison, D. E.; Jones, R. G.; Woodward, R. B. *J. Am. Chem. Soc.* **1956**, *78*, 3087-3114, (b) Oppolzer, W.; Francotte, E.; Bättig, K. *Helv. Chim. Acta* **1981**, *64*, 478-481, (c) Hendrickson, J. B.; Wang, J. *Org. Lett.* **2004**, *6*, 3-5, (d) Moldvai, I.; Temesvári-Major, E.; Incze, M.; Szentirmay, É.; Gács-Baitz, E.; Szántay, C. *J. Org. Chem.* **2004**, *69*, 5993-6000, (e) Inuki, S.; Oishi, S.; Fujii, N.; Ohno, H. *Org. Lett.* **2008**, *10*, 5239-5242, (f) Inuki, S.; Iwata, A.; Oishi, S.; Fujii, N.; Ohno, H. *J. Org. Chem.* **2011**, *76*, 2072-2083, (g) Liu, Q.; Jia, Y. *Org. Lett.* **2011**, *13*, 4810-4813, (h) Umezaki, S.; Yokoshima, S.; Fukuyama, T. *Org. Lett.* **2013**, *15*, 4230-4233.
- ⁵ Formal syntheses of lysergic acid: (a) Julia, M.; Le Goffic, F.; Igolen, J.; Baillarge, M. *Tetrahedron Lett.* **1969**, *20*, 1569-1571, (b) Ramage, R.; Armstrong, V. W.; Coulton, S. *Tetrahedron* **1981**, *37*, 157-164, (c) Kiguchi, T.; Hashimoto, C.; Naito, T.; Ninomiya, I. *Heterocycles* **1982**, *19*, 2279-2282, (d) Rebek, J. Jr.; Tai, D. F. *Tetrahedron Lett.* **1983**, *24*, 859-860, (e) Kurihara, T.; Terada, T.; Yoneda, R. *Chem. Pharm. Bull.* **1986**, *34*, 442-443, (f) Cacchi, S.; Ciattini, P. G.; Morera, E.; Ortar, G. *Tetrahedron Lett.* **1988**, *29*, 3117-3120, (g) Saá, C.; Crotts, D. D.; Hsu, G.; Vollhardt, K. P. C. *Synlett* **1994**, 487-489, (h) Kurokawa, T.; Isomura, M.; Tokuyama, H.; Fukuyama, T. *Synlett.* **2009**, 775-778.

-
- ⁶ Synthesis of lysergic acid intermediates: (a) Uhle's Ketone: Teranishi, K.; Hayashi, S.; Nakatsuka, S.; Goto, T. *Tetrahedron Lett.* **1994**, *35*, 8173-8176, (b) Kornefeld's Ketone and analogues: Bur, S. K.; Padwa, A. *Org. Lett.* **2002**, *4*, 4135-4137.
- ⁷ Stoll, A.; Hofmann, A. d-Lysergic Acid Diethylamide. US 2438259, March 23, 1948.
- ⁸ Myers, A. G. Zheng, B. *J. Am. Chem. Soc.* **1996**, *118*, 4492-4493.
- ⁹ Xu, Z.; Hu, W.; Liu, Q.; Zhang, L.; Jia, Y. *J. Org. Chem.* **2010**, *75*, 7626-7635.
- ¹⁰ Stevens, T. S.; Creighton, E. M.; Gordon, A. B.; MacNicol, M. *J. Chem. Soc.* **1928**, 3193-3197.
- ¹¹ Sweeney, J. B. *Chem. Soc. Rev.* **2009**, *38*, 1027-1038.
- ¹² West, F. G.; Naidu, B. N. *J. Am. Chem. Soc.* **1993**, *115*, 1177-1178.
- ¹³ Stevens, T. S. *J. Chem. Soc.* **1930**, 2107-2119. For Stevens' further mechanistic explorations, see (b) Thomson, T.; Stevens, T. S. *J. Chem. Soc.* **1932**, 55-69. (c) Dunn, J. L.; Stevens, T. S. *J. Chem. Soc.* **1932**, 1926-1931. (d) Johnstone, R. A. W.; Stevens, T. S. *J. Chem. Soc.* **1955**, 4487-4488. (e) Millard, B. J.; Stevens, T. S. *J. Chem. Soc.* **1963**, 3397-3403.
- ¹⁴ (a) Schöllkopf, U.; Ludwig, U.; Ostermann, G.; Patsch, M. *Tetrahedron Lett.* **1969**, *39*, 3415-3418, (b) Lepley, A. R. *J. Am. Chem. Soc.* **1969**, *91*, 1237-1239, (c) Ollis, W. D.; Rey, M.; Sutherland, I. O.; Closs, G. L. *J. Chem. Soc., Chem. Comm.* **1975**, 543 - 545, (d) Dolling, U. H.; Closs, G. L.; Cohen, A. H.; Ollis, W. D. *J. Chem. Soc., Chem. Comm.* **1975**, 545-547, (e) Ollis, W. D.; Rey, M.; Sutherland, I. O. *J. Chem. Soc., Perkin Trans. I* **1983**, 1009-1027.
- ¹⁵ (a) Campbell, A.; Houston, A. H. J.; Kenyon, J. *J. Chem. Soc.* **1947**, 93-95, (b) Brewster, J. H.; Kline, M. W. *J. Am. Chem. Soc.* **1952**, *74*, 5179-5182, (c) Dewar, M. J. S. *Ann. Reports* **1951**, *48*, 127.
- ¹⁶ Dewar, M. J. S.; Ramsden, C. A. *J. Chem. Soc., Perkin Trans. I* **1974**, 1839-1844.

-
- ¹⁷ (a) Heard, G. L.; Frankcombe, K. E.; Yates, B. F. *Aust. J. Chem.* **1993**, *46*, 1375–1388, (b) Heard, G. L.; Yates, B. F. *Aust. J. Chem.* **1994**, *47*, 1685–1694, (c) Heard, G. L.; Yates, B. F. *Aust. J. Chem.* **1995**, *48*, 1413–1423, (d) Heard, G. L.; Yates, B. F. *J. Comp. Chem.* **1996**, *17*, 1444–1452, (e) Heard, G. L.; Yates, B. F. *J. Org. Chem.* **1996**, *61*, 7276–7284.
- ¹⁸ Dai, Q.; Zhou, Z.; Zhang, D. *Science in China* **2000**, *43*, 576–586.
- ¹⁹ Ghigo, G.; Cagnina, S.; Maranzana, A.; Tonachini, G. *J. Org. Chem.* **2010**, *75*, 3608–3617.
- ²⁰ Biswas, B.; Collins, S. C.; Singleton, D. A. *J. Am. Chem. Soc.* **2014**, *136*, 3740–3743. Note that this study mistakenly names the reaction studied the Sommelet-Hauser rearrangement, which is a similar, though different, reaction.
- ²¹ (a) Vanecko, J. A.; Wan, H.; West, F. G.; *Tetrahedron* **2006**, *62*, 1043–1062, (b) Smith, M. B.; March, J. *March's Advanced Organic Chemistry*, 6th Ed.; John Wiley & Sons, Inc.: New Jersey, 2007; Chapter 18–21, pp 1621–1624.
- ²² (a) West, F. G.; Naidu, B. N. *J. Am. Chem. Soc.* **1994**, *116*, 8420–8421, (b) Vanecko, J. A.; West, F. G. *Org. Lett.* **2005**, *7*, 2949–2952.
- ²³ Rosset, I. G.; Dias, R. M. P.; Pinho, V. D.; Burtoloso, A. C. B. *J. Org. Chem.* **2014**, *79*, 6748–6753.
- ²⁴ Glaeske, K. W.; West, F. G. *Org. Lett.* **1999**, *1*, 31–33.
- ²⁵ For recent reviews, see: (a) Müller, D.; Alexakis, A. *Chem. Commun.* **2012**, *48*, 12037–12049, (b) Hawner, C.; Alexakis, A. *Chem. Commun.* **2010**, *46*, 7295–7306, (c) Jerphagnon, T.; Pizzuti, M. G.; Minaard, A. J.; Feringa, B. L. *Chem. Soc. Rev.* **2009**, *38*, 1039–1075.
- ²⁶ Imanishi, T.; Shin, H.; Hanaoka, M.; Momose, T.; Imanishi, I. *Chem. Pharm. Bull.* **1982**, *30*, 3617–3623.
- ²⁷ Salmond, W. G.; Barta, M. A.; Havens, J. L. *J. Org. Chem.* **1978**, *43*, 2057–2059.

-
- ²⁸ Westerlund, A.; Carlson, R. *Synth. Commun.* **1999**, *29*, 4035-4042.
- ²⁹ (a) Nicolaou, K. C.; Zhong, Y.-L.; Baran, P. S. *J. Am. Chem. Soc.* **2000**, *122*, 7596-7597, (b) Nicolaou, K. C.; Montagnon, T.; Baran, P. S. *Angew. Chem. Int. Ed.* **2002**, *41*, 993-996.
- ³⁰ Sakagami, H.; Kamikubo, T.; Ogasawara, K. *Chem. Commun.* **1996**, 1433-1434.
- ³¹ D'hooghe, M.; Baele, J.; Contreras, J.; Boelens, M.; De Kimpe, N. *Tetrahedron Lett.* **2008**, *49*, 6039-6042.
- ³² Johnson, C. R.; Marren, T. J. *Tetrahedron Lett.* **1987**, *28*, 27-30.
- ³³ Mukopadhyay, T.; Seebach, D. *Helv. Chim. Acta* **1982**, *65*, 385-391.
- ³⁴ Knochel, P.; Chou, T.-S.; Jubert, C.; Rajagopal, D. *J. Org. Chem.* **1993**, *58*, 588-599.
- ³⁵ Noyori, R.; Murata, S.; Suzuki, M. *Tetrahedron* **1981**, *37*, 3899-3910.
- ³⁶ Egger, M.; Pellett, P.; Nickl, K.; Geiger, S.; Graetz, S.; Seifert, R.; Heilmann, J.; König, B. *Chem. Eur. J.* **2008**, *14*, 10978-10984.
- ³⁷ Marcantoni, E.; Nobili, F.; Bartoli, G.; Bosco, M.; Sambri, L. *J. Org. Chem.* **1997**, *62*, 4183-4184.
- ³⁸ Majumdar, S.; Bhattacharjya, A. *J. Org. Chem.* **1999**, *64*, 5682-5685.
- ³⁹ Hagiwara, H.; Uda, H. *J. Chem. Soc., Chem. Commun.* **1987**, 1351-1353.
- ⁴⁰ Babler, J. H.; Malek, N. C.; Coghlan, M. J. *J. Org. Chem.* **1978**, *43*, 1821-1823.
- ⁴¹ Walborsky, H. M.; Davis, R. H.; Howton, D. R. *J. Am. Chem. Soc.* **1951**, *73*, 2590-2594.
- ⁴² Barton, D. H. R.; Magnus, P. D.; Smith, G.; Zurr, D. *J. Chem. Soc. D, Chem. Commun.* **1971**, 861-863.
- ⁴³ Balme, G.; Goré, J. *J. Org. Chem.* **1983**, *48*, 3336-3338.
- ⁴⁴ Johnstone, C.; Kerr, W. J.; Scott, J. S. *Chem. Commun.* **1996**, 341-342.
- ⁴⁵ Ireland, R. E.; Liu, L. *J. Org. Chem.* **1993**, *58*, 2899.

-
- ⁴⁶ Brubaker, A. N.; Colley, Jr., M. *J. Med. Chem.* **1986**, *29*, 1528-1531.
- ⁴⁷ Frigerio, M.; Santagostino, M.; Sputore, S. *J. Org. Chem.* **1999**, *64*, 4537-4538.
- ⁴⁸ Pour, M.; Špulák, M.; Balšánek, V.; Kuneš, J.; Kubanová, P.; Buchta, V. *Bioorg. Med. Chem.* **2003**, *11*, 2843-2866.
- ⁴⁹ Huo, X.; Quan, M.; Yang, G.; Zhao, X.; Liu, D.; Liu, Y.; Zhang, W. *Org. Lett.* **2014**, *16*, 1570-1573.
- ⁵⁰ Joosten, A.; Lambert, É.; Vasse, J.-L.; Szymoniak, J. *Org. Lett.* **2010**, *12*, 5128-5131.
- ⁵¹ Armarego, W. L. F.; Chai, C. L. L. *Purification of Laboratory Chemicals*, 6th ed.; Elsevier Inc. Burlington, 2009.
- ⁵² Korenaga, T.; Ko, A.; Shimada, K. *J. Org. Chem.* **2013**, *78*, 9975-9980.
- ⁵³ Crandall, K. J.; Arrington, J. P.; Watkins, R. J. *J. Chem. Soc., Chem. Commun.* **1967**, 1052.
- ⁵⁴ Mukopadhyay, T.; Seebach, D. *Helv. Chim. Acta* **1982**, *65*, 385-391.
- ⁵⁵ Mash, E. A.; Hemperly, S. B. *J. Org. Chem.* **1990**, *55*, 2055-2060.
- ⁵⁶ Smith, M. B.; March, J. *March's Advanced Organic Chemistry*, 6th Ed. 2007, John Wiley and Sons, Hoboken, NJ, pp 1523-1525.
- ⁵⁷ Kärnä, M. K.; Lahtinen, M. K.; Valkonen, J. U. *J. Chem. Eng. Data* **2013**, *58*, 1893-1908.
- ⁵⁸ (a) Tsuji, T.; Beck, L. W.; Davis, M. E. *Microporous and Mesoporous Materials* **1999**, *28*, 519-530, (b) Kore, R.; Sridharkrishna, R.; Srivastava, R. *RSC Adv.* **2013**, *3*, 1317-1322.
- ⁵⁹ Ahamed, P.; Haque, M. A.; Ishimoto, M.; Parvez, M. M.; Haraguchi, N.; Itsuno, H. *Tetrahedron* **2013**, *69*, 3978-3983.
- ⁶⁰ Maruoka, K. *Pure Appl. Chem.* **2012**, *84*, 1575-1585.
- ⁶¹ (a) Mizuta, H.; Naruto, S.; Suzuki, T.; Nagamoto, N.; Uno, H.; Nishimura, H. *Eur. J. Med. Chem.* **1987**, *22*, 209-212, (b) Graulich, A.; Mercier, F.; Scuvée-Moreau, J.; Seutin, V.; Liégeois,

J.-F. *Bioorg. Med. Chem.* **2005**, *13*, 1201-1209, (c) Dega-Szafran, Z.; Dulewicz, E.; Brycki, B. *ARKIVOC* **2007**, *6*, 90-102, (d) Lukáč, M.; Mojžiš, J.; Mojžišová, G.; Mrva, M.; Ondriska, F.; Valentová, J.; Lacko, I.; Bukovský, M.; Devínsky, F.; Karlovská, J. *Eur. J. Med. Chem.* **2009**, *44*, 4970-4977, (e) Jin, Q.; Davis, R. S.; Bullion, A. M.; Jin, J.; Wang, Y.; Widdowson, K. L.; Palovich, M. R.; Foley, J. J.; Schmidt, D. B.; Buckley, P. T.; Webb, E. F.; Salmon, M.; Belmonte, K. E.; Sarau, H. M.; Busch-Petersen, J. *Bioorg. Med. Chem. Lett.* **2012**, *22*, 7087-7091, (f) Lainé, D. I.; Yan, H.; Xie, H.; Davis, R. S.; Dufour, J.; Widdowson, K. L.; Palovich, M. R.; Wan, Z.; Foley, J. J.; Schmidt, D. B.; Hunsberger, G. E.; Burman, M.; Bacon, A. M.; Webb, E. F.; Luttmann, M. A.; Salmon, M.; Sarau, H. M.; Umbrecht, S. T.; Landis, P. S.; Peck, B. J.; Busch-Petersen, J. *Bioorg. Med. Chem. Lett.* **2012**, *22*, 3366-3369.

⁶² McKenna, J. *Top. Stereochem.* **1970**, *5*, 275-308.

⁶³ Lambert, J. B. *Top. Stereochem.* **1971**, *6*, 19-105.

⁶⁴ Crowley, P. J.; Robinson, M. J. T.; Ward, M. G. *J. Chem. Soc. Chem. Comm.* **1974**, 825-826.

⁶⁵ Kawazoe, Y.; Tsuda, M. *Chem. Pharm. Bull.* **1967**, *15*, 1405-1410.

⁶⁶ (a) Curtin, D. Y. *Rec. Chem. Prog.* **1954**, *15*, 111-128, (b) Seeman, J. I. *Chem. Rev.* **1983**, *83*, 83-134.

⁶⁷ Belostoskii, A. M.; Gottlieb, H. E.; Aped, P.; Hassner, A. *Chem. Eur. J.* **1999**, *5*, 449-455 and references therein.

⁶⁸ Bottini, A. T. *Sel. Org. Transform.* **1970**, *1*, 89-142 and references therein.

⁶⁹ (a) Fedeli, W.; Mazza, F.; Vaciago, A. *J. Chem. Soc. B* **1970**, 1218-1223, (b) R. Brettle, D. R. Brown, J. McKenna, and R. Mason, *J. Chem. Soc. D* **1969**, 339.

⁷⁰ Bare, T. M.; Hershey, N. D.; House, H. O.; Swain, C. G. *J. Org. Chem.* **1972**, *37*, 997-1002.

⁷¹ House, H. O.; Tefertiller, B. A.; Pitt, C. G. *J. Org. Chem.* **1966**, *31*, 1073-1079.

-
- ⁷² Baker, V. J.; Blackburne, I. D.; Katritzky, A. R.; Kolinski, R. A.; Takeuchi, Y. *J. Chem. Soc. Perkin Trans II* **1974**, 1563-1568.
- ⁷³ Brown, D. R.; McKenna, J.; McKenna, J. M. *Chem. Commun.* **1969**, 186.
- ⁷⁴ Baker, V. J.; Blackburne, I. J.; Katritzky, A. R. *J. Chem. Soc. Perkin Trans II* **1974**, 1557-1561.
- ⁷⁵ Bottini, A. T.; O'Rell, M. K. *Tetrahedron Lett.* **1967**, 423-428.
- ⁷⁶ Duke, R. P.; Jones, R. A. Y.; Katritzky, A. R. *J. Chem. Soc. Perkin Trans II* **1973**, 1553-1557.
- ⁷⁷ Vedejs, E.; Arco, M. J.; Powell, D. W.; Renga, J. M.; Singer, S. P. *J. Org. Chem.* **1978**, *43*, 4831-4837.
- ⁷⁸ Gawley, R. E.; Moon, K. *Org. Lett.* **2007**, *9*, 3093-3096.
- ⁷⁹ Smith, R. V.; Benz, F. W.; Long, J. P. *Can. J. Chem.* **1973**, *51*, 171-176.
- ⁸⁰ Jones, R. A. Y.; Katritzky, A. R.; Mente, P. G. *J. Chem. Soc. B* **1970**, 1210-1217.
- ⁸¹ Nakano, H.; Yamamoto, T. *J. Chem. Theor. Comput.* **2013**, *9*, 188-203 and references therein.
- ⁸² (a) Becke, A. D. *J. Chem. Phys.* **1993**, *98*, 5648-5652, (b) Lee, C.; Yang, W.; Parr, R. G. *Phys. Rev. B* **1988**, *37*, 785-789.
- ⁸³ Zhao, Y.; Truhlar, D. G. *Theor. Chem. Acc.* **2008**, *120*, 215-241.
- ⁸⁴ Adamo, C.; Barone, V. *J. Chem. Phys.* **1998**, *108*, 664-675.
- ⁸⁵ Frisch, M. J.; Trucks, G. W.; Schlegel, H. B.; Scuseria, G. E.; Robb, M. A.; Cheeseman, J. R.; Scalmani, G.; Barone, V.; Mennucci, B.; Petersson, G. A.; Nakatsuji, H.; Caricato, M.; Li, X.; Hratchian, H. P.; Izmaylov, A. F.; Bloino, J.; Zheng, G.; Sonnenberg, J. L.; Hada, M.; Ehara, M.; Toyota, K.; Fukuda, R.; Hasegawa, J.; Ishida, M.; Nakajima, T.; Honda, Y.; Kitao, O.; Nakai, H.; Vreven, T.; Montgomery Jr., J. A.; Peralta, J. E.; Ogliaro, F.; Bearpark, M.; Heyd, J. J.; Brothers, E.; Kudin, K. N.; Staroverov, V. N.; Keith, T.; Kobayashi, R.; Normand, J.; Raghavachari, K.;

Rendell, A.; Burant, J. C.; Iyengar, S. S.; Tomasi, J.; Cossi, M.; Rega, N.; Millam, J. M.; Klene, M.; Knox, J. E.; Cross, J. B.; Bakken, V.; Adamo, C.; Jaramillo, J.; Gomperts, R.; Stratmann, R. E.; Yazyev, O.; Austin, A. J.; Cammi, R.; Pomelli, C.; Ochterski, J. W.; Martin, R. L.; Morokuma, K.; Zakrzewski, V. G.; Voth, G. A.; Salvador, P.; Dannenberg, J. J.; Dapprich, S.; Daniels, A. D.; Farkas, O.; Foresman, J. B.; Ortiz, J. V.; Cioslowski, J.; Fox, D. J. *Gaussian 09*, Gaussian, Inc., Wallingford CT, **2013**, Revision D.01.

⁸⁶ Head-Gordon, M.; Pople, J. A.; Frisch, M. J. *Chem. Phys. Lett.* **1988**, *153*, 503-506.

⁸⁷ (a) Martin, J. M. L.; Sundermann, A. *J. Chem. Phys.* **2001**, *114*, 3408-3420, (b) Basis set obtained from the EMSL Basis Set Exchange: Schuchardt, K.L.; Didier, B.T.; Elsethagen, T.; Sun, L.; Gurumoorthi, V.; Chase, J.; Li, J.; Windus, T.L. *J. Chem. Inf. Model.* **2007**, *47*, 1045-1052.

⁸⁸ Dolg, M.; Wedig, U.; Stoll, H.; Preuss, H. *J. Chem. Phys.* **1987**, *86*, 866-872.

⁸⁹ Wilson, A. K.; Woon, D. E.; Peterson, K. A.; Dunning, Jr., T. H. *J. Chem. Phys.* **1999**, *110*, 7667-7676.

⁹⁰ Fukui, K. *J. Phys. Chem.* **1970**, *74*, 4161-4163.

⁹¹ (a) Tomasi, J.; Persico, M. *Chem. Rev.* **1994**, *94*, 2027-2033, (b) Simkin, B. Y.; Sheikhet, I. *Quantum Chemical and Statistical Theory of Solutions-A Computational Approach*; Ellis Horwood: London, 1995.

⁹² Leah J. Miedema performed the alkylations on the hydroxyl-substituted piperidines.

⁹³ Carey, F. A.; Sundberg, R. J. *Advanced Organic Chemistry Part A: Structure and Mechanisms*, 5th ed.; Springer: New York, 2007; p 360.

⁹⁴ For a general discussion of the relationship between solvation and nucleophilicity, see: Anslyn, E. V.; Dougherty, D. A. Nucleophilicity and Nucleofugality. In *Modern Physical Organic Chemistry*; University Science Books: Sausalito, 2006; pp 458-461.

⁹⁵ (a) London, F. *J. Phys. Radium* **1937**, *8*, 397-409, (b) McWeeny, R. *Phys. Rev.* **1962**, *126*, 1028-1034, (c) Ditchfield, R. *Mol. Phys.* **1974**, *27*, 789-807, (e) Wolinski, K.; Hilton, J. F.; Pulay, P. *J. Am. Chem. Soc.* **1990**, *112*, 8251-8260, (f) Cheeseman, J. R.; Trucks, G. W.; Keith, T. A.; Frisch, M. J. *J. Chem. Phys.* **1996**, *104*, 5497-5509.

⁹⁶ (a) Lodewyk, M. W.; Soldi, C.; Jones, P. B.; Olmstead, M. M.; Rita, J.; Shaw, J. T.; Tantillo, D. J. *J. Am. Chem. Soc.* **2012**, *134*, 18550–18553, (b) Lodewyk, M. W.; Siebert, M. R.; Tantillo, D. J. *Chem. Rev.* **2012**, *112*, 1839-1862, (c) Tantillo, D. J. CHESHIRE Chemical Shift Repository, 2013. cheshirenmr.info (accessed July 1, 2014).

⁹⁷ Marenich, A. V.; Cramer, C. J.; Truhlar, D. G. *J. Phys. Chem. B* **2009**, *113*, 6378-6396.

⁹⁸ For a perspective article detailing CH-O non-classical hydrogen bonding in organic reactions, see: Johnston, R. C.; Cheong, P. H.-Y. *Org. Biomol. Chem.* **2013**, *11*, 5057-5064.

⁹⁹ Eliel, E. L. *J. Chem. Educ.* **1960**, *37*, 126-133.

¹⁰⁰ Jensen, H. H.; Lyngbye, L.; Jensen, A.; Bols, M. *Chem. Eur. J.* **2002**, *8*, 1218-1226.

¹⁰¹ See Chapter 3, Section 3.2.

¹⁰² Crystallographic data provided by Dr. R. MacDonald at the University of Alberta.

¹⁰³ Computational details for this work are the same as those in Section 4.3.1. Note that 15 conformers of each diastereomer were located, with four conformers of **173-D1** and six conformers of **173-D2** contributing significantly (greater than 1% of the conformer population) based on computed free energies at the B3LYP/6-31+G(d,p) level of theory.

¹⁰⁴ Computational details for this work are the same as those in Section 4.4.1.

-
- ¹⁰⁵ Lacheretz, R.; Pardo, D. G.; Cossy, J. *Org. Lett.* **2009**, *11*, 1245-1248.
- ¹⁰⁶ For recent reviews, see: (a) West, F. G.; Scadeng, O.; Wu, Y.-K.; Fradette, R. J.; Joy, S. In *Comprehensive Organic Synthesis, 2nd Edition*, Molander, G. A., Knochel, P., Eds.; Vol. 5, Elsevier: Oxford, 2014; pp. 827–866, (b) Tius, M. A. *Chem Soc. Rev.* **2014**, *43*, 2979–3002, (c) Spencer, W. T.; Vaidya, T.; Frontier, A. J. *Eur. J. Org. Chem.*, **2013**, 3621–3633, (d) Shimada, N.; Stewart, C.; Tius, M. A. *Tetrahedron* **2011**, *67*, 5851–5870, (e) Vaidya, T.; Eisenberg, R.; Frontier, A. J. *ChemCatChem* **2011**, *3*, 1531–1548, (f) Davis, R. L.; Tantillo, D. J. *Curr. Org. Chem.* **2010**, *14*, 1561-1577, (g) Nakanishi, W.; West, F. G. *Curr. Opin. Drug Discov. Dev.* **2009**, *12*, 732–751.
- ¹⁰⁷ Grant, T. N.; Reider, C. J.; West, F. G. *Chem. Commun.* **2009**, 5676–5688.
- ¹⁰⁸ (a) Wu, Y.-K. PhD Dissertation, University of Alberta, 2013, (b) Wu, Y.-K.; Dunbar, C. R.; McDonald, R.; Ferguson, M.; West, F. G. *J. Am. Chem. Soc.* **2014**, *136*, 14903-14911.
- ¹⁰⁹ (a) Hoffman, H. M. R. *Angew. Chem., Int. Ed. Engl.* **1973**, *12*, 819–835. (b) Hoffman, H. M. R. *Angew. Chem., Int. Ed. Engl.* **1984**, *23*, 1–88. (c) Cramer, C. J.; Barrows, S. E. *J. Org. Chem.* **1998**, *63*, 5523–5532.
- ¹¹⁰ For a recent account discussing stereoselectivity of reactions controlled by aromatic rings, see: Krenske, E. H.; Houk, K. N. *Acc. Chem. Res.* **2013**, *46*, 979-989.
- ¹¹¹ Nishio, M. *Phys. Chem. Chem. Phys.* **2011**, *13*, 13873–13900.
- ¹¹² Anderson, C. D.; Dudding, T.; Gordillo, R.; Houk, K. N. *Org. Lett.* **2008**, *10*, 2749–2752.
- ¹¹³ Zhao, Y.; Truhlar, D. G. *Chem. Phys. Lett.* **2011**, *502*, 1–13.
- ¹¹⁴ Antoline, J. E.; Krenske, E. H.; Lohse, A. G.; Houk, K. N.; Hsung, R. P. *J. Am. Chem. Soc.* **2011**, *133*, 14443–14451.

-
- ¹¹⁵ For a recent mini review concerning this effect: Wang, H.; Houk, K. N. *Chem. Sci.* **2014**, *5*, 462–470.
- ¹¹⁶ Cramer, C. J.; Barrows, S. E. *J. Phys. Org. Chem.* **2000**, *13*, 176–186.
- ¹¹⁷ Domingo, L. R.; Pérez, P.; Ortega, D. E. *J. Org. Chem.* **2013**, *78*, 2462–2471.
- ¹¹⁸ Fernández, I.; Cossío, F. P.; de Cozár, A.; Lledós, A.; Mascareñas, J. L. *Chem. Eur. J.* **2010**, *16*, 12147–12157.
- ¹¹⁹ Visualization in Molden 5.1: Schaftenaar, G.; Noordik, J. H. *J. Comput.-Aided Mol. Design*, **2000**, *14*, 123–134.
- ¹²⁰ (a) Domnin, N. A. *Journal of General Chemistry USSR (English Translation)* **1945**, *15*, 461, (b) Domin, N. A. *Journal of General Chemistry USSR (English Translation)* **1940**, *10*, 1939, (c) Wittig, G.; Fritze, P. *Angew. Chem. Int. Ed.* **1966**, *5*, 846, (d) Wittig, G.; Fritze, P. *Liebigs Ann. Chem.* **1968**, *711*, 82–87, (e) Christl, M. In *Modern Allene Chemistry*; Krause, N.; Hashmi, A. S. K., Eds.; Wiley-VCH, 2004; Vol. 1, pp. 243–357, (f) Johnson, R. P. *Chem. Rev.* **1989**, *89*, 1111–1124, (g) Balci, M.; Taskesenligil, Y. In *Advances in Strained and Interesting Organic Molecules*; Halton, B., Ed.; JAI Press: Stamford, Connecticut, 1999; Vol. 8, pp. 43–82, (h) McMahon, R. J.; Abelt, C. J.; Chapman, O. L.; Johnson, J. W.; Kreil, C. L.; LeRoux, J.-P.; Mooring, A. M.; West, P. R. *J. Am. Chem. Soc.* **1987**, *109*, 2456–2469.
- ¹²¹ Lofstrand, V. A.; West, F. G. *Manuscript in preparation*.
- ¹²² Skraba, S. L.; Johnson, R. P. *J. Org. Chem.* **2012**, *77*, 11096–11100.
- ¹²³ Bottini, A. T.; Cabral, L. J. *Tetrahedron Lett.* **1977**, *7*, 615–618.
- ¹²⁴ Lofstrand, V. A. *Unpublished results*.
- ¹²⁵ Hujo, W.; Grimme, S. *J. Chem. Theory Comput.* **2013**, *9*, 308–315.
- ¹²⁶ Halgren, T. A. *J. Comp. Chem.* **1996**, *17*, 490–519.

¹²⁷ MarvinSketch 5.12.0, ChemAxon Ltd., Hungary, Budapest, **2013**.